UNIVERSIDAD DE CHILE

FACULTAD DE CIENCIAS FÍSICAS Y MATEMÁTICAS

DEPARTAMENTO DE GEOLOGÍA

PETROGÉNESIS Y GEOCRONOLOGÍA $^{40}Ar/^{39}Ar$ DEL VOLCANISMO INTRAPLACA DE LA DORSAL DE JUAN FERNÁNDEZ, PLACA DE NAZCA, PACIFICO SE

TESIS PARA OPTAR AL GRADO DE DOCTOR EN

CIENCIAS MENCIÓN GEOLOGÍA

JAVIER ANTONIO REYES VIZCARRA

PROFESOR GUÍA:

DIEGO MORATA CÉSPEDES

PROFESOR CO-GUÍA:

LUIS LARA PULGAR

MIEMBROS DE LA COMISIÓN:

MIGUEL ÁNGEL PARADA REYES

ÁNGELO CASTRUCCIO ÁLVAREZ

SANTIAGO DE CHILE

2018

RESUMEN DE LA TESIS PARA OPTAR AL GRADO DE: Doctor en Ciencias mención Geología
POR: Javier Antonio Reyes Vizcarra
FECHA: 14/08/2018
PROFESOR GUÍA: Diego Morata Céspedes
PROFESOR CO-GUÍA: Luis Lara Pulgar

PETROGÉNESIS Y GEOCRONOLOGÍA $^{40}Ar/^{39}Ar$ DEL VOLCANISMO INTRAPLACA DE LA DORSAL DE JUAN FERNÁNDEZ, PLACA DE NAZCA, PACIFICO SE

La Dorsal de Juan Fernández (JFR) es una cadena volcánica (~ 800 km) de intraplaca emplazada sobre la Placa de Nazca en el Pacífico SE alejada de márgenes activos. Mediante datos de geoquímica (roca total y mineral), isotópicos (Sr-Nd-Pb) y geocronológicos ($^{40}Ar/^{39}Ar$) se busca comprender los procesos petrogenéticos implicados en la generación del volcanismo y en la evolución magmática de JFR.

Se determina que los 4 edificios volcánicos más volumétricos de JFR: O'Higgins (~ 9.26 – 8.41 Ma), Alpha (~ 4.63 – 4.58 Ma), Robinson Crusoe (~ 4.10 – 3.40 Ma) y Alejandro Selkirk (~ 0.94 – 0.83 Ma); satisfacen una progresión de edades más joven hacia el W coherente con la teoría de plumas mantélicas.

La fase de construcción del escudo representa casi la totalidad del volumen de los edificios estudiados, se compone principalmente de basaltos con signatura geoquímica (e.g., alto contenido de TiO_2, alto FC3MS y anomalía TITAN) e isotópica (FOZO-A con participación adicional de DM) que sugiere la presencia de piroxenita (formada a partir de corteza oceánica reciclada) como heterogeneidad en una fuente mantélica peridotítica. Dicha presencia es confirmada mediante un modelo petrogénetico para la pluma que indica una baja temperatura potencial (rango de 1290 – 1322 °C para Robinson Crusoe vs. 1312 – 1362 °C en Alejandro Selkirk), presión de término de fusión (2.34 – 2.54 vs. 2.24 – 2.52 GPa) probablemente relacionado al límite litósfera-astenosfera, y una similar participación en el melt final de fundidos provenientes de piroxenita (38.6 – 56.4 vs. 35.8 – 55.6 wt%) pese a su baja presencia en la pluma (4 – 8 vs. 6 – 12 wt%). Las variaciones composicionales internas se explican por fraccionamiento de olivino + clinopiroxeno ± plagioclasa, mezcla y/o recarga magmática y acumulación de cristales de olivino en una cámara magmática somera (~ 1 a 3 kbar) donde la temperatura de los magmas puede descender hasta 1156 – 1181 °C, y las variaciones entre volcanes se explica por variaciones temporales en la temperatura potencial y tasa de fusión parcial de la pluma mantélica.

O'Higgins y Robinson Crusoe también muestran una fase de volcanismo rejuvenecido formada por coladas de lava basanítica eruptadas tras un periodo de inactividad máximo de ~ 0.25 Ma en O'Higgins, y ~ 1.73 Ma en Robinson Crusoe. Su mayor enriquecimiento geoquímico y signatura isotópica relativamente similar al escudo confirman que también se origina a partir de una pluma mantélica, pero posiblemente con sutiles variaciones en la proporción de sus constituyentes (peridotita y piroxenita), temperatura y grado de fusión parcial (ambas menores a la etapa de escudo). Estos magmas ascienden de manera directa (> 1300 °C), capturando xenocristales, con cristalización polibárica y poca diferenciación, ya que solo algunas son almacenadas por breves periodos en pequeños reservorios someros (a ~ 1256 – 1295 °C).

A Magaly y Hugo, mis padres
A Vanessa, mi compañera de vida
A Claudia e Ignacio, mis hermanos

Agradecimientos

Quiero partir agradeciendo a mi profesor guía, Diego Morata, por su colaboración y apoyo brindado durante estos años. A mi profesor co-guía, Luis Lara, por introducirme al estudio del hermoso y apasionante mundo de las islas oceánicas. Gracias por la constante enseñanza, ayuda y confianza. Y a los miembros de la Comisión, Miguel Ángel Parada y Ángelo Castruccio, por sus importantes aportes y comentarios que sin duda enriquecieron la discusión, y permitieron mejorar este trabajo.

Nada de esto sería posible sin mi familia. En particular agradezco a Magaly y Hugo, mis padres, por el esfuerzo, amor y apoyo incondicional durante toda mi vida. Y a Claudia e Ignacio, mis hermanos, por su alegría, cariño y apoyo.

A Vanessa, mi compañera de tantos años, gracias por tu amor, comprensión, paciencia y aliento. Gracias por caminar a mi lado y construir juntos nuestra historia.

Todos estos años de trabajo en la U fueron amenizados por mucha gente. Un especial agradecimiento a los siempre optimistas miembros del RAP: Seba, Pablo, Atax, Javier, Italo, Ivan y Bascu; a los destacados deportistas y dirigentes del CSDyC Journal of Freestyle con quienes compartimos tantas GeoChampions, acabados estudios científicos, y amenas charlas técnicas; a Mary, Babi, Chino, Rayen, Naty, Ore, Coni, Feña, Vale, Ale, Berni, Kari, Pelao, Claudio, etc., y a los distintos integrantes de la sala de postgrado en el tiempo. Con todos disfruté momentos de alegría y distracción (e incluso ocasionales discusiones geológicas) durante estos largos años. También a los amigos de mi primera etapa en la Universidad, agrupados en La Cofradía y en mis compañeros de generación de Geología.

A los amigos de la vida, del colegio y del barrio, por largas jornadas de conversaciones sobre la vida, fútbol, acontecer nacional y otros, bajo la compañía refrescante de una que otra bebida. Reuniones que sin duda alegraron mis años de estudio (y lo continúan haciendo).

También se agradece a las personas e instituciones que han colaborado de manera directa durante el desarrollo de este estudio (apoyo en campañas de terreno, facilitación de muestras de montes submarinos, apoyo en análisis y discusión, etc): Kaj Hoernle, Folkmar Hauff, Daniel Sellés, Jean-Louis Paquette, Suzanne Kay, Oliver Cooper, Gabriel Orozco, Valentina Astudillo, Mirella Piña, Pablo Sepúlveda, Hernán Vergara, Fernando Barra, SCRIPPS Institution of Oceanography, CONAF, DIFROL y Armada de Chile.

Finalmente quiero agradecer al cuerpo de académicos y funcionarios del Departamento de Geología, especialmente a Blanca y Maritza, por su constante ayuda, sobretodo en trámites habitualmente realizados a última hora.

Muchas gracias a todos.

Esta tesis fue financiada por la Beca de Doctorado Nacional CONICYT 21120781, y los proyectos FONDECYT 1110966, FONDECYT 1141303, y FONDAP-CEGA 15090013.

Tabla de contenido

Capítulo I

Introducción

La generación de magmas en la Tierra ocurre principalmente en zonas de contacto entre placas tectónicas, ya sea en ambientes divergentes (con formación de dorsales midoceánicas) o convergentes (con desarrollo de subducción). Sin embargo, al interior de estas placas suelen generarse conjuntos volcánicos de intraplaca, cuyo origen, formación, y evolución son temas de debate dentro del ámbito de las ciencias de la Tierra.

Si esta actividad volcánica ocurre dentro de una placa tectónica oceánica, se manifiesta mediante la formación de islas oceánicas y montes submarinos, con volcanes tipo escudo capaces de alcanzar grandes volúmenes, ampliamente superiores a los estratovolcanes típicos de ambientes de subducción (Schmincke, 2004). En ocasiones, estos edificios volcánicos forman notables alineamientos a lo largo de las placas oceánicas, conocidos como ridges o dorsales asísmicas. Se ha considerado que el magmatismo intraplaca, en particular el generado en ambientes oceánicos, representa una ventana hacia el manto terrestre, dada la poca influencia de agentes externos (e.g., ausencia de fluidos provenientes del slab, manto en general sin notables empobrecimientos, escasa contaminación cortical) en la evolución de sus productos magmáticos, generalmente basaltos toleíticos o alcalinos.

El origen de este volcanismo es un tema controversial en ciencias de la Tierra. En trabajos pioneros, Morgan (1971, 1972) propone al ascenso de plumas mantélicas fijas al manto, con material enriquecido y anomalías térmicas, que, mediante descompresión adiabática, son capaces de fundirse parcialmente para dar origen a los típicos magmas basálticos observados en diversas islas. La amplia aceptación de esta teoría, conocida como ‘hotspot’ explica la amplia utilización de este término genérico como denominativo común para este tipo de volcanismo. En este contexto, la formación de cadenas volcánicas subparalelas, con desarrollo de progresión de edades concordantes con la tasa de movimiento de la placa sobre la cual se emplazan, se explica por el supuesto anclaje de la pluma al manto astenosférico, generándose un movimiento independiente de la litosfera por sobre ella. Luego, dicha progresión es una característica necesaria para la validez de la hipótesis de hostspot, en particular para placas oceánicas de desplazamiento rápido.

Trabajos compilatorios basados en aplicación de técnicas multidisciplinarias (Clouard y Bonneville, 2001; Courtillot et al., 2003; French y Romanowicz, 2015; Jackson et al., 2017), concluyen que un número limitado de conjuntos pueden ser explicados a partir de una pluma mantélica ascendente fija al manto. Dicha afirmación va en línea con propuestas que incorporan variaciones en el modelo de plumas para explicar el volcanismo intraplaca, por ejemplo, plumas no fijas capaces de moverse sutilmente (Steinberger y O"Connell, 1998), plumas húmedas o ricas en volátiles, con o sin, temperaturas elevadas (Bonatti, 1990; Nichols et al, 2002), o derechamente ausencia de plumas. En este último grupo se pueden mencionar diversos modelos, por ejemplo, hidrofracturas magmáticas en zonas de máxima tensión flexural (Hieronymus y Bercovici, 2000), variaciones normales en el marco de la tectónica de placas en presencia de fracturas, ridges, rifts, etc. (Anderson, 2000, 2001) y convecciones sublitosféricas a pequeña escala (Ballmer et al, 2007).

El magmatismo tipo OIB (ocean island basalts) está comúnmente caracterizado por un marcado enriquecimiento geoquímico e isotópico con respecto al manto empobrecido característico de dorsales midoceánicas (e.g., Sun y McDonough, 1989). La importante variación en la magnitud de estos enriquecimientos presente entre distintos conjuntos volcánicos sugiere la presencia de heterogeneidades mantélicas, con diferencias que pueden ser composicionales, isotópicas y/o mineralógicas (Zindler y Hart, 1986 y referencias en él).

Además, en varias islas oceánicas se han reconocido diversas etapas de actividad volcánica, caracterizadas principalmente por variaciones en la geoquímica de sus productos, y por el volumen de material emanado. Por ejemplo, para el caso arquetípico a nivel mundial, el archipiélago de Hawaii, se reconocen tres periodos consecutivos de actividad: pre-escudo (volcanismo submarino de afinidad alcalina), escudo (voluminoso volcanismo toleítico, submarino y subaereo) y postescudo (pulsos de afinidad alcalina), seguidos por un periodo variable de inactividad volcánica. Posteriormente se desarrolla la etapa rejuvenecida o post-erosional, consistente en volcanismo marcadamente alcalino y poco volumétrico (e.g., Ozawa et al., 2005; Garcia et al., 2010). Cada conjunto de islas puede, o no, desarrollar cada una de estas etapas, exhibiendo variaciones en las características química, petrografías y en los volúmenes emitidos caso a caso.

La Dorsal de Juan Fernández (JFR) representa un clásico ejemplo de magmatismo intraplaca con productos del tipo OIB formado sobre una placa oceánica de movimiento rápido (Nazca) lejos de márgenes extensivos, y que posteriormente subducta bajo la placa Sudamericana, lo que ofrece una oportunidad única para estudiar las características del manto en el Pacífico SE, y su eventual influencia en el margen continental. Pese a ello, aspectos relacionados a su mecanismo de generación y ascenso magmático, junto a la evolución magmática de JFR han sido escasamente investigados. Esta tesis busca comprender los principales procesos petrogenéticos implicados en la generación del volcanismo y en la evolución magmática de JFR.

Mediante análisis geoquímicos (en roca total y en cristales de olivino/clinoproxeno), isotópicos (Sr-Nd-Pb), petrográficos (SEM) y geocronológicos ($^{40}Ar/^{39}Ar$), se busca determinar el origen del magmatismo intraplaca de JFR; inferir las características de la fuente mantélica implicada en su génesis, cuantificar los parámetros asociados a la fusión parcial de ella, comprender las diferencias entre las distintas etapas del volcanismo en JFR, y establecer un modelo de ascenso y almacenamiento magmático para las distintas rocas volcánicas de JFR; lo que permitirá aumentar el conocimiento sobre las características genéticas del volcanismo intraplaca a nivel global, y alimentar el debate actual sobre su origen y evolución.

Para ello, esta tesis está conformada por capítulos de Introducción, Discusión y Conclusión generales (en español) en base a cinco capítulos principales (en inglés): dos artículos científicos, uno publicado en Journal of Volcanology and Geothermal Research (Capítulo II, ‘Contrasting P-T paths of shield and rejuvenated volcanism at Robinson Crusoe Island, Juan Fernández Ridge, SE Pacific’), y otro sometido en Geochimica et Cosmochimica Acta (Capítulo V, ‘Petrogenesis of the shield volcanism in Juan Fernández Ridge, SE Pacific: melting from a low temperature pyroxenite-bearing mantle plume’); junto a tres abstract extendidos (Capítulo III, ‘Ascent and storage model for the shield and rejuvenated volcanism of Robinson Crusoe extended to other

volcanoes of Juan Fernández Ridge'; Capítulo IV, 'Mantle plume beneath Juan Fernández Ridge: 40Ar/39Ar plateau ages progression consistent with the Nazca plate movement'; Capítulo VI, 'Geochemistry and isotopic features of the rejuvenated volcanism in Juan Fernández Ridge, SE Pacific') cuyo objetivo es contextualizar ciertos aspectos de los artículos mencionados, y que, en algunos casos pretender transformarse en publicaciones en el mediano plazo. Como dichos capítulos buscan ser independientes entre sí, por lo que cada capítulo tiene su propia introducción y desarrollo de temas, por lo mismo, es común que a lo largo del texto existan citas cruzadas entre ellos.

Las publicaciones y presentaciones en congresos científicos asociados a esta tesis se detallan a continuación:

Publicaciones

Reyes, J.; Lara, L.E.; Morata, D. 2017. Contrasting P-T paths of shield and rejuvenated volcanism at Robinson Crusoe Island, Juan Fernández Ridge, SE Pacific. Journal of Volcanology and Geothermal Research 341, 242–252.

Reyes, J.; Lara, L.E.; Hauff, F.; Hoernle, K.; Morata, D.; Selles, D.; Cooper, O. Paquette, J.L. Petrogenesis of the shield volcanism in Juan Fernández Ridge, SE Pacific: melting from a low temperature pyroxenite-bearing mantle plume. Submitted to Geochimica et Cosmochimica Acta.

Lara, L.E., Díaz-Naveas, J., **Reyes, J.**, Jicha, B., Orozco, G., Kay, S.M., 2018a. Unraveling short-lived rejuvenated volcanism and a rapid transition from shield stage at O ' Higgins guyot , Juan Fernández Ridge , Pacific SE. Submitted to Deep Sea Research Part I.

Lara, L.E., **Reyes, J.**, Jicha, B., Díaz-Naveas, J. 2018b. 40Ar/39Ar constraints for the age progression along the Juan Fernández Ridge, SE Pacific: insights into deep mantle processes. Submitted to Frontiers in Volcanology.

Congresos

Lara, L.E.; **Reyes, J.**; Orozco, G.; Díaz-Naveas, J. 2017. Rapid transition from shield to post-erosional volcanism at O'Higgins guyot, Juan Fernández Ridge, Pacific SE. AGU (American Geophysical Union) Chapman conference on submarine volcanism: new approaches and research frontiers, Hobart, Tasmania, Australia.

Reyes, J.; Orozco, G.; Lara, L.E.; Morata, D. 2016. Shield vs post-erosional volcanism in Juan Fernandez Ridge (Nazca plate): insights for magma transport and storage. IAVCEI (International Association of Volcanology and Chemistry of the Earth's Interior) Cities on Volcanoes IX, 2016, Puerto Varas, Chile.

Reyes, J.; Lara, L.E.; Orozco, G.; Astudillo, V. 2016. Outcrops of „post-erosional" volcanism on Juan Fernandez Archipelago as geosites. IAVCEI (International Association of Volcanology and Chemistry of the Earth's Interior) Cities on Volcanoes IX, 2016, Puerto Varas, Chile.

Reyes, J.; Lara, L.E.; Morata, D. 2015. Petrogénesis, evolución magmática y geocronología 40Ar/39Ar de la isla Robinson Crusoe, Dorsal de Juan Fernández,

Pacifico SE. XIV Congreso Geológico Chileno, Geología Para el Sigo XXI, 2015, La Serena, Chile.

Lara, L.E.; Rodrigo, C.; **Reyes, J.**; Orozco, G. 2014. Evolution of the western segment of Juan Fernández Ridge (Nazca Plate): plume vs. plate tectonic processes. EGU (European Geosciences Union) General Assembly 2014, Viena, Austria.

Reyes, J.; Lara, L.E.; Piña-Gauthier, M.; Orozco, G. 2013. Magmatic evolution and age progression of the Juan Fernández Ridge (Nazca Plate, SE Pacific). GeoSur, International Geological Congress on the Southern Hemisphere 2013, Viña del Mar, Chile.

Lara, L.E.; **Reyes, J.**; Piña-Gauthier, M.; Orozco, G. 2013. Geological evidence of a post-shield stage at the Juan Fernández Ridge (Nazca Plate). IAVCEI (International Association of Volcanology and Chemistry of the Earth´s Interior) Scientific Assembly 2013, Kagoshima, Japón.

Reyes, J.; Lara, L.E. 2013. Petrology and thermochronology of the Juan Fernández Ridge (Nazca Plate). IAVCEI (International Association of Volcanology and Chemistry of the Earth's Interior) Scientific Assembly 2013, Kagoshima, Japón.

Lara, L.E.; **Reyes, J.**; Piña-Gauthier, M.; Díaz, J.; Orozco, G. 2012. Es la Dorsal de Juan Fernández resultado de un hotspot clásico?: análisis de la progresión de edades radiométricas. Congreso Geológico Chileno 13, Antofagasta, Chile.

Reyes, J.; Lara, L.E. 2012. Evolución magmática de la isla Robinson Crusoe, Dorsal de Juan Fernández, Chile: resultados preliminares. Congreso Geológico Chileno 13, Antofagasta, Chile.

Reyes, J.; Lara, L.E. 2012. Juan Fernández Ridge (Nazca Plate): petrology and thermochronology of a rejuvenated hot spot trail. EGU (European Geosciences Union) General Assembly 2012, Viena, Austria.

Bibliografía

Anderson, D.L., 2000. The thermal state of the upper mantle; no role for mantle plumes. Geophys. Res. Lett. 27, 3623–3626. doi:10.1029/2000GL011533

Anderson, D.L., 2001. Top-down tectonics? Science 293, 2016–2018. doi:10.1126/science.1065448

Ballmer, M.D., van Hunen, J., Ito, G., Tackley, P.J., Bianco, T. a., 2007. Non-hotspot volcano chains originating from small-scale sublithospheric convection. Geophys. Res. Lett. 34. doi:10.1029/2007GL031636

Bonatti, E., 1990. Not So hot “hot spots” in the oceanic mantle. Science 250 (4977), 107–111. doi.org/10.1126/science.250.4977.107

Clouard, V., Bonneville, A., 2001. How many Pacific hotspots are fed by deep-mantle plumes? Geology 29(8), 695–698. doi:10.1130/0091-7613(2001)029<0695:HMPHAF>2.0.CO;2

Courtillot, V., Davaille, A., Besse, J., Stock, J., 2003. Three distinct types of hotspots in the Earth’s mantle. Earth Planet. Sci. Lett. 205, 295–308. doi.org/10.1016/S0012-821X(02)01048-8

French, S.W., Romanowicz, B., 2015. Broad plumes rooted at the base of the Earth’s mantle beneath major hotspots. Nature 525, 95–99. doi.org/10.1038/nature14876

Garcia, M.O., Swinnard, L., Weis, D., Greene, a. R., Tagami, T., Sano, H., Gandy, C.E., 2010. Petrology, geochemistry and geochronology of Kaua’i lavas over 4-5 Myr: Implications for the origin of rejuvenated volcanism and the evolution of the Hawaiian plume. J. Petrol. 51, 1507–1540. doi:10.1093/petrology/egq027

Hieronymus, C.F., Bercovici, D., 2000. Non-hot spot formation of volcanic chains: Controls of tectonic stresses on magma transport. Earth Planet. Sci. Lett. 181, 539–554. doi:10.1016/S0012-821X(00)00227-2

Jackson, M.G., Konter, J.G., Becker, T.W., 2017. Primordial helium entrained by the hottest mantle plumes. Nature 542, 340–343. doi.org/10.1038/nature21023

Morgan, W.J., 1971. Convection plumes in the lower mantle. Nature 230, 42–43. doi.org/10.1038/230042a0

Morgan, W.J., 1972. Deep mantle convection plumes and plate motions. Am. Assoc. Pet. Geol. Bull. 56, 203–213. doi.org/10.1306/819A3E50-16C5-11D7-8645000102C1865D

Nichols, A.R.L., Carroll, M.R., Höskuldsson, Á., 2002. Is the Iceland hot spot also wet? Evidence from the water contents of undegassed submarine and subglacial pillow basalts. Earth Planet. Sci. Lett. 202, 77–87. doi.org/10.1016/S0012-821X(02)00758-6

Ozawa, A., Tagami, T., Garcia, M.O., 2005. Unspiked K–Ar dating of the Honolulu rejuvenated and Koʻolau shield volcanism on Oʻahu, Hawaiʻi. Earth and Planetary Science Letters 232, 1–11. doi:10.1016/j.epsl.2005.01.021

Schmincke, H.-U. 2004. Volcanism. 1st edition. Springer Berlin Heidelberg 324 p.

Steinberger, B., O’Connell, R.J., 1998. Advection of plumes in mantle flow: implications for hotspot motion, mantle viscosity and plume distribution. Geophys. J. Int. 132, 412–434. doi.org/10.1046/j.1365-246x.1998.00447.x

Sun, S., McDonough, W.F., 1989. Chemical and isotopic systematics of oceanic basalts: implications for mantle composition and processes. Geol. Soc. London, Spec. Publ. 42, 313–345. doi.org/10.1144/GSL.SP.1989.042.01.19

Zindler, A., Hart, S., 1986. Chemical Geodynamics. Annu. Rev. Earth Planet. Sci. 14, 493–571. doi.org/10.1146/annurev.earth.14.1.493

Capítulo II

Contrasting P-T paths of shield and rejuvenated volcanism at Robinson Crusoe Island, Juan Fernández Ridge, SE Pacific

Abstract

A remarkable expression of intraplate volcanism is the occurrence of evolutionary stages with important variations of magmatic processes and products. Plumbing systems and storage conditions seem to be different for shield and rejuvenated volcanism, two classical stages notably preserved in Robinson Crusoe Island, Juan Fernández Ridge in the SE Pacific Ocean. We here present first order geochemical features for rocks from both shield and rejuvenated stages and through geothermobarometry and textural analysis we unravel their contrasting ascent and storage history. The shield stage (~ 3.8 Ma) is represented by a ~ 900 m thick sequence of basalt, picrobasalt and picrite lava flows forming subsets according their chemistry and mineralogy: 'differentiated', 'near-primitive' and 'olivine-rich' lavas. Pressure estimates for in equilibrium assemblages are < 3.2 kbar, and temperature ranges around 1321 °C for the 'near-primitive' and 1156–1181 °C for the 'differentiated' groups. Volcanic rocks from the rejuvenated stage (~ 0.9 Ma) fill the eroded morphology of the shield pile with basanite and picrite lava flows with two compositional varieties: the primitive 'high-Mg' group that crystallized clinopyroxene at pressures < 3.7 kbar and olivine at temperatures in the range 1316–1354 °C; and the 'low-Mg' group that carries notably zoned crystals formed at a wide range of pressures (0–10.8 kbar) and temperatures (1256–1295 °C). This allows us to infer contrasting patterns of ascent and storage during these archetypical stages in Robinson Crusoe Island, which also controlled volcanic processes on surface and finally shaped the island. We propose the existence of shallow magmatic reservoirs in the shield stage, where the ascending magmas would have been stored and differentiated. On the other hand, rejuvenated magmas experimented rapid ascent with polybaric crystallization and sometimes short-time storage in low-volume reservoirs. Similar conditions have been proposed in other oceanic islands suggesting that shallow reservoirs in the shield stage and deeper crystallization of more alkaline magmas in the rejuvenated stage seems to describe a global pattern.

II.1. Introduction

Intraplate volcanoes are related to primary mantle plumes (e.g., Courtillot et al., 2003) and serve as virtual windows to the deep Earth's mantle. Pioneering work by Morgan (1971, 1972a, 1972b) introduced the hypothesis of fixed mantle plumes, hot and enriched, able to melt by decompression. One of the most evident results of such an origin is the observed age progression of volcanic rocks from oceanic islands and/or seamounts along a chain. However, a number of volcanic alignments do not satisfy this condition, as observed by Clouard and Bonneville (2001) for the Pacific Ocean basin. Alternative ideas have been proposed as non-fixed plumes (Steinberger and O'Connell, 1988) or tectonically-controlled decompression related to magmatic hydrofracture driven by flexural stresses in presence of a volcanic load (Hieronymus and Bercovici, 2000). More frequent processes as subduction cooling, continental insulation, small-scale convection in presence of ridges, rifts and fracture zones (Anderson, 2000, 2001) or small-scale sublithospheric convections (Ballmer et al., 2007) could also explain the array of hotspot volcanoes on oceanic plates.

‘Wet’ or volatile-rich plumes without high temperatures have also been proposed (Bonatti, 1990; Nichols et al., 2002), which fuels the controversy about the source and P-T conditions for intraplate volcanism.

The archetypical evolutionary model of oceanic islands (based on the Hawaiian case, e.g., García et al., 2015) includes the pre-shield (alkaline submarine volcanism), shield (voluminous tholeiitic submarine and subaerial volcanism) and post-shield stages (alkaline pulses). The geochemical and isotopic differences for those three stages are usually explained by variations in the degree of partial melting and some changes in the mantle source composition (Frey et al., 1990). Sometimes, after a period of quiescence, a rejuvenated stage (Ozawa et al., 2005) is recognized, consisting in a small volume of alkaline magmatism. The origin of this late stage of volcanism is still controversial, despite the growing amount of occurrences, first recognized at Hawaii (Macdonald et al., 1983; García et al., 2010) and then in Samoa (Wright and White, 1987; Konter et al., 2012), Marquesas (Woodhead, 1992), Canary Islands (Hoernle and Schmincke, 1993), Society (White and Duncan, 1996), Kerguelen (Weis et al., 1998), Madeira (Geldmacher and Hoernle, 2000), Mauritius (Paul et al., 2005) and Fieberling-Guadalupe (Konter et al., 2009).

A number of models have been proposed for the origin of the rejuvenated stage: (1) thermal effect of a mantle plume that melts the surrounding oceanic lithosphere (e.g., Gurriet, 1987); (2) secondary melting zone in the plume as a result of internal convection and lateral spreading beneath the lithosphere (e.g., Ribe and Christensen, 1999); (3) decompression melting of the plume due to a flexure of the oceanic plate generated by the construction of new shield volcanoes on top (e.g., Bianco et al., 2005); and (4) small-scale sublithospheric convection in the ambient mantle and spreading plume (Ballmer et al., 2011). Each oceanic hotspot may (or may not) develop the volcanic stages described (pre-shield, shield, postshield and rejuvenated) displaying variations in the chemistry, petrography, and erupted volume.

The magmatic plumbing and storage for shield and post-shield stages have an extended effect on both eruptive style and morphological evolution of oceanic islands and seamounts. P-T paths retrieved from mineral chemistry can track the ascent and storage history. For example, shallow reservoirs have been inferred (and independently tested by geophysical tools) in Hawaii for the shield stage (Ryan, 1988; Poland et al., 2014; Tilling et al., 2014; Pietruszka et al., 2015), but a deeper storage region was inferred for the post-shield stage (Frey et al., 1990), either in the mantle (Chatterjee et al., 2005) or within the crust (Hammer et al., 2016).

Rejuvenated volcanism seems to be more complex in origin implying different sources and ascent pathways. Here we characterize first order geochemical features of both shield and rejuvenated stages in Robinson Crusoe Island. Through geothermobarometry and textural analysis we unravel their ascent and storage history.

II.2. Juan Fernández Ridge

An outstanding yet still poorly studied example of intraplate volcanism is the Juan Fernández Ridge (JFR), an aseismic ridge running for ca. 800 km over the Nazca Plate in the Southeast Pacific. The JFR obliquely converges (N80ºE) with the South American margin at 33.4ºS (Fig. II.1) and is mostly built on top of a ca. 22–37 Ma old Nazca Plate

(Rodrigo and Lara, 2014). Because of the isolation from active spreading ridges, it is a suitable target for understanding mantle signatures of the Southeast Pacific and general evolution of oceanic island/seamounts on a relatively fast moving plate (70.53 mm/yr eastward at present according to GEODVEL 2010 model; Argus et al., 2010).

Around 15 volcanoes comprise the Juan Fernández Ridge: Robinson Crusoe, Santa Clara, Alejandro Selkirk islands and at least 12 seamounts (> 1000 m above the ocean floor, Fig. II.1). The most important seamounts (from E to W) are O'Higgins, O'Higgins guyot (Vergara and Morales, 1985), Alpha (Farley et al., 1993) Beta, Gamma, Duke, Cinque Ports, Dresden (Rodrigo and Lara, 2014), Friday (Farley et al., 1993) and Domingo (Devey et al., 2000). Ar-Ar total fusion age for O'Higgins (~ 8.50 Ma; Von Huene et al., 1997) and K-Ar for Robinson Crusoe (~ 3.10–5.80 Ma) and Alejandro Selkirk (0.85–1.30 Ma; Booker et al., 1967; Stuessy et al., 1984) define a general age progression for shield stages and thus a fixed primary mantle plume would be implied.

Some geological studies were carried out in the past decades in Juan Fernández archipelago. The pioneer geological description of Robinson Crusoe and Alejandro Selkirk islands by Quensel (1920) (who reported some curiosities like the presence of trachytes and olivine-rich lavas called 'masafuerites' in reference to the former name 'Más Afuera' for Alejandro Selkirk Island) was followed by the geological reconnaissance of Robinson Crusoe Island by Morales (1987). A narrow field for $^{87}Sr/^{86}Sr$ and $^{143}Nd/^{144}Nd$ ratios was interpreted to indicate the involvement of a limited range of mantle components (Gerlach et al., 1986). Baker et al. (1987) and Farley et al. (1993) identified two different lithologies, basalts and basanites, as shield and post-shield units. The geochemical and isotopic ($^{3}He/^{4}He$ in olivine phenocrysts) differences were explained by transition from a typical plume for the first stage to a MORB-like source in the second one (Farley et al., 1993). Natland (2003) studied the morphology of olivine crystals and their capture of He concluding the existence of mixing between low and high temperature (olivine-charged) magmas. Furthermore, Devey et al. (2000) studied Friday and Domingo seamounts, which correspond to the westernmost volcanoes in JFR, reporting the presence of vesicular basalts, basanites and basaltic trachyandesites interpreted as products of metasomatic reactions between mantle harzburgites and a CO_2-bearing plume.

Geochronological data for Robinson Crusoe is scarce and based on imprecise K-Ar ages of 3.5 ± 0.8, 3.1 ± 0.9 (Booker et al., 1967) and 3.8 ± 0.2, 4.2 ± 0.2, 5.8 ± 2.1 (Stuessy et al., 1984). A sharp unconformity separates both the shield and rejuvenated units and is an evidence of erosion and volcanic quiescence in between.

II.3. Methods and analytical procedures

From the geological map and field reconnaissance, the main sequences or volcanic units were recognized and sampling sites chosen where sharp unconformity separates both the shield and post-shield units. Fresh whole-rocks were crushed to 250–180 μm grain sizes and handy-picked for extract major phenocrysts or weathered surfaces. Single aliquots were analyzed by incremental heating with a CO_2 laser at Servicio Nacional de Geología y Minería, Chile (SERNAGEOMIN). Clean samples were first placed in a disk of high purity aluminium together with a monitor grain of Fish Canyon sanidine (28.03 ± 0.1 Ma; Renne et al., 1994). Sealed disc was sent for irradiation to La Reina nuclear reactor (Chile), operated by the Comisión Chilena de Energía Nuclear.

Both samples LL240711-1 and JR160913-2 were irradiated 21,95 h. Once the samples were received from the reactor, individual total fusion analyses were performed for all the monitors from the disk, and J factors are calculated for each grain, which represents an individual position in the disc. The distribution of J in 2 dimensions across the disc is modeled by a 2-dimensional quadratic fit to the data, resulting in a 'J surface' for the disc (e.g., Lara et al., 2006). Individual J factors for each sample are thus calculated depending upon the coordinates of the sample. The samples were analyzed by successive heating with increments of temperature by increases in the power of the laser using an integrative lens, which allows even heating of a plane of 6×6 mm (each sample hole has a diameter of 5 mm). The CO_2 laser has a maximum power of 30 W. Following each three heating steps a line blank was analyzed. Then, the noble gases were separated from the other evolved ones by means of a cold trap at ~ 133 °C and a ST101 getter operated at 2.2 A. Once purified the noble gases were introduced into a high resolution MAP 215-50 mass spectrometer in electron multiplier mode. The isotopes ^{36}Ar, ^{37}Ar, ^{38}Ar, ^{39}Ar and ^{40}Ar were analyzed in 10 cycles, and the $^{36}Ar/^{40}Ar$, $^{37}Ar/^{40}Ar$, $^{38}Ar/^{40}Ar$ and $^{39}Ar/^{40}Ar$ ratios were calculated for time zero to eliminate the effects of isotope fractionation during the analysis. The baseline was analyzed at the beginning and the end of the analysis, for each step, and subtracted from the peak heights. Spectrometer bias was corrected using periodic analyses of air samples, from which a correction factor (discrimination factor) was calculated. Two reproducible results were obtained from the step heating experiments. Each apparent age considers the corrections corresponding to isotopes of Ar associated with atmospheric argon, and argon that results from the irradiation of K, Ca and Cl. Plateaus were defined using the approach of Fleck et al. (1977). For a plateau to be valid, it must comprise three or more serial steps containing at least 50% of the total liberated ^{39}Ar, and the 2σ errors of these steps must overlap. When ^{40}Ar excess was detected, the isochrone age was preferred. When concordant plateau and isochrone ages were obtained, the plateau age was preferred because of its low uncertainty (Table II.S.1).

Petrographic analysis was made by optical microscopy and scanning electron microscopy (SEM FEI Quanta 250) at the Centro de Excelencia en Geotermia de Los Andes (CEGA) facilities of Universidad de Chile and SERNAGEOMIN. Modal count (500 points) was performed in 20 samples (results in Table II.1). Whole rock major element and Ni chemistry (55 samples) was analyzed at AcmeLabs, Vancouver, Canada. The rock chips crushed from field hand samples were fused with lithium metaborate/tetraborate and a dilute nitric acid digestion prior to major element analysis by ICP-ES. In addition a separate split was digested in Aqua Regia and analyzed by ICP-MS to report the Ni content. Loss on ignition (LOI) is by weigh difference after ignition at 1000 °C. Table II.2 provides the analytical detection limits for each element used in this study. Precision and accuracy of the analyses were monitored by analysis of: recognized geochemical standards, split duplicate samples and AcmeLabs internal standards.

Olivine and clinopyroxene chemistry (20 samples) was measured by electronic microprobe (EPMA JEOL JXA 8230 equipped with three wavelength-dispersive spectrometers) at Laboratorio de Microscopía Electrónica y Análisis de Rayos X (LAMARX), Universidad Nacional de Córdoba, Argentina. Crystals used for the analysis were: TAP (Na, Mg, Al and Si), PET (Ca and Ti) and LiF (Cr, Mn, Fe and Ni) with an accelerating potential of 15.0 kV and electron beam current of 20 nA in 5 µm circles.

Counting times were 10 s for peak and 5 s at each background position. Data reduction was performed using the ZAF correction method. Based on repeated analyses of standards, concentrations for major elements are accurate to within 1.5% (relative) for elements that exceed 10 wt%, about 5% for those between 10 and 1 wt%, and about 20% for those below 1 wt%. Precision is better than 0.6, 2 and 9% (relative), respectively. Tables II.S.3 and II.S.4 provides the analytical detection limits for each element used in this study. These are typical measurement conditions used in literature considered as 'routine analysis' and do not show high precision results (Sobolev et al., 2007) reflected in an error of 0.26 in olivine forsterite content and 0.24 in clinopyroxene wollastonite content.

II.4. Results

II.4.1 Geological overview of shield and rejuvenated exposures

Shield stage in Robinson Crusoe Island forms a ca. 900 m thick sequence, with outstanding exposures in the sea cliffs. The island is built on a submarine pedestal (> 2000 m high) probably formed by pre-shield and shield volcanic rocks. Baker et al. (1987) proposed a scheme with central and peripheral vents but early reconnaissance by Morales (1987) and our more detailed field mapping favor a central structure with a gently dipping shield sequence cross cut by dyke complexes (Fig. II.2a), which in turn is covered with unconformity by the rejuvenated unit (Fig. II.2b). The latter is defined by several small and isolated vents with related lavas and pyroclastic beds (Fig. II.1). Feeder dykes for the shield stage are clustered in areas with expression as ridges below sea level (Orozco, 2016).

The shield unit (locally 'Punta Larga' and 'Puerto Inglés' sequences) is formed by basaltic, picrobasaltic and picritic lavas (Tables II.2 and II.S.2, Fig. II.3) with breccia layers and a few interbedded tephra horizons. The most common lithology carries olivine, plagioclase and clinopyroxene phenocrysts embedded in intersertal to intergranular groundmass (plagioclase, clinopyroxene, Fe-Ti oxides and rare olivine). Some rocks have abundant olivine (> 20% vol, Table II.1) with resorption rims in a subophitic groundmass. Vesicles are common (Table II.1) and in some samples they are partially filled by a secondary mineralogy (mainly Fe-Ti oxides) also visible in glass. In some places this unit is characterized by the presence of basaltic dike swarms (Fig. II.2a). A dike in the shield pile contains plagioclase-bearing dunite xenoliths that show a hetero-cumulate texture. Basaltic lava from the shield unit sampled at the present sea level gave an age of 3.83 ± 0.03 Ma ($^{40}Ar/^{39}Ar$ isochron in groundmass) (location in Fig. II.1, data in Table II.S.1).

Rejuvenated volcanism is represented by the locally named 'Bahía del Padre' sequence, which fill the eroded morphology of the shield stage unit (Fig. II.2b). This unit represents volcanic products erupted from minor eruptive centers, usually forming succesions of pyroclastic deposits that contain juvenile basanite material embedded in a yellow palagonitic matrix, covered by vesicle-poor (Table II.1) basanite, and occasionally picrite (Tables II.2 and II.S.2, Fig. II.3) lava flows (~ 3 m thickness). Their mineralogy consists of olivine and zoned clinopyroxene phenocrysts with a groundmass that also contains plagioclase, Fe-Ti oxides, analcime and natrolite. Few samples show moderate alteration to Fe-Ti oxides in glass and veins. The $^{40}Ar/^{39}Ar$ age (step-heating in groundmass) of a basanite from this unit gave 0.90 ± 0.03 Ma (location in Fig. II.1, data

in Table II.S.1). Rocks from this unit rarely carry spinel lherzolite xenoliths that contain glassy vesicular veins with reaction rims around them.

II.4.2 Whole rock major element geochemistry

The shield unit contains transitional basalts, picrobasalts (Fig. II.3) and picrites with SiO_2 contents ranging between 42.6 and 49.9 wt% (Tables II.2 and II.S.2, all data normalized to 100% without LOI) and Mg-number (Mg# = $Mg^{2+}/[Mg^{2+}+Fe^{2+}]$ between 40.8 and 79.4 assuming 90% of total iron is ferrous in all samples (a reasonable estimate used in other oceanic islands like Hawaii, e.g., García, 1996). Based on Mg#, Ni, and olivine content the shield lavas are grouped in: (1) 'differentiated' basalts (Mg# < 58.1, Ni < 111 ppm, low olivine); (2) primitive or 'near primitive' basalts (59.7 < Mg# < 68.1, 158 < Ni < 266 ppm, high olivine); (3) 'olivine-rich' basalts, similar to 'masafuerites' as defined by Quensel (1920) in Alexander Selkirk island (Mg# > 69.4, Ni > 514 ppm, very abundant olivine) (Fig. II.4). Some chemical differences arise between these groups: the 'differentiated' group displays the highest contents of TiO_2, Al_2O_3 and CaO (3.1–4.4 / 13.9–16.6 / 8.2–12.9 wt%) with classical characteristics of fractional crystallization (e.g., clinopyroxene) (Fig. II.5); the 'olivine-rich' group shows the lowest values (1.6–3.1 / 6.5–11.4 / 5.0–9.3 wt%) as a result of olivine accumulation (Fig. II.5); and the 'near-primitive' group covers an intermediate range (2.5–3.4 / 12.1–14.9 / 7.2–13.1 wt%) (Fig. II.5), probably due to mixing between primitive (high-T) and differentiated melts (low-T) as suggested by Natland (2003). Variations in mobile elements (as Na_2O in Fig. II.5) can be explained as an effect of alteration. These groups do not have a clear geographic or stratigraphic distribution.

The rejuvenated unit is composed by basanite and picrite lavas (Fig. II.3). Their SiO_2 and Mg# contents range between 41.6 and 45.4 wt% (Tables II.2 and II.S.2) and 55.9–69.9, respectively. Other remarkable compositional differences (major elements) between the units are visible in the MnO (shield/rejuvenated ratio: 0.12–0.20 / 0.19–0.24 wt%), Na_2O (1.3–3.5 / 1.8–4.7 wt%), K_2O (0.05–1.35 / 0.54–2.17 wt%) and P_2O_5 (0.18–0.65 / 0.45–0.97 wt%) content (Na_2O and P_2O_5 in Fig. II.5). These differences would be explained by changes in the source and/or variations in degree of partial melting, although a detailed analysis of the source is beyond the scope of this study. According to their major elements geochemistry and Mg#, two compositional groups can be established in this unit: a 'high-Mg' group formed by primitive lavas (Mg# > 68), and a 'low-Mg' group with slightly differentiated basanites (Fig. II.4). Other chemical differences between both groups are subtle, and only slight differences in the Fe_2O_3, MnO and P_2O_5 contents are appreciable. In fact, the 'low-Mg' shows the highest values of these oxides (Fe_2O_3: 12.1–15.0 / MnO: 0.20–0.24 / P_2O_5: 0.57–0.97 wt%) compared to the 'high-Mg' group (12.1–13.6 / 0.19–0.20 / 0.45–0.69 wt%) (P_2O_5 in Fig. II.5). Internal variations in rejuvenated lavas can be thus related to fractional crystallization (olivine and clinopyroxene), magmatic recharge (generating some mixing) or alteration (in mobile elements).

II.4.3 Mineral chemistry and geothermobarometry

II.4.3.1 Methodology

Pressure conditions were estimated using clinopyroxene EPMA data and the structural geobarometer of Nimis and Ulmer (1998) for anhydrous basalts. The standard error of

this method (anhydrous basalts) is ± 1.7 kbar, but the presence of water in the system increases the pressure in ~ 1.0 kbar per 1wt% H_2O content. Only for reference, according to their Ce content, parental magmas in JFR would have 0.8–1.0 wt% H_2O in the shield stage, and 1.5–2.0 wt% in rejuvenated volcanism (Dixon et al. (2002) as estimated for Pacific FOZO magmas [H_2O/Ce=200]). The possible presence of water increases the error, but we prefer this method instead of Nimis and Ulmer (1998) for hydrous basalts, Nimis (1999), Putirka et al. (2003) and Putirka (2008a), which need clinopyroxene temperature estimation. The latter is difficult to obtain without orthopyroxene, and/or liquid-crystal equilibrium, absent in most samples of Robinson Crusoe Island, especially in rejuvenated magmas, considering $^{Cpx\text{-}Liq}Kd$ value ($^{Cpx\text{-}Liq}Kd = X_{FeO}^{Oliv} * X_{MgO}^{Liq} / X_{FeO}^{Liq} * X_{MgO}^{Oliv}$) of 0.27 ± 0.03 representative of equilibrium conditions (e.g., Putirka et al., 2003) (Table II.S.3). We do not use olivine-liquid temperatures as input of T-dependent geobarometers because they cannot be assumed as clinopyroxene temperatures. Given the high error of the method, the results are relevant from a qualitative point of view, as they represent major trends in a group of samples, or significant variations in individual crystals. A pressure estimate of 0.0 kbar (or slightly < 0.0 kbar) represents shallow conditions of crystallization (Nimis, 2014 in ResearchGate web). Structural formula and Fe^{3+} contents for clinopyroxene were calculated through charge balance (Papike et al., 1974) according to the methodology by Nimis and UImer (1998) (CpxBar software). Wollastonite content (Wo) was calculated as Wo = 100*(Ca/[Ca + Mg + Fe]), where Mg and Fe are molar concentrations.

Crystallization temperatures were estimated using the olivine-liquid geothermometer of Herzberg and O'Hara (2002) modified from Beattie (1993). Their standard error is ±31 °C. Olivine composition was measured by EPMA and major elements geochemistry were considered as representative of the liquid composition (we used only phenocrysts-poor samples: < 13 vol% considering also microphenocrysts, see Table II.1). Canonical $^{Ol\text{-}Liq}Kd$ values ($^{Ol\text{-}Liq}Kd = X_{FeO}^{Oliv} * X_{MgO}^{Liq} / X_{FeO}^{Liq} * X_{MgO}^{Oliv}$) of 0.30 ± 0.03 were considered in olivine-liquid equilibrium (Roeder and Emslie, 1970) (Fig. II.6). Given the estimated pressures for the shield and rejuvenated magmas (Table II.3, described in sections 4.3.2 and 4.3.3), and in order to make valid comparisons, we fix the pressure value as input for geothermometer in 2.0 kbar for all units, which is the most frequent value obtained (excluding values near to 0.0 that represent shallow crystallization, see histograms in Fig. II.11). Note that a pressure increase of 1.0 kbar generates an increase of ~ 5 °C in the temperature estimation. All Fe in olivine is considered as Fe^{2+} and forsterite content (Fo) was calculated as Fo = 100*(Mg/[Mg + Fe^{2+}]), where Mg and Fe are molar concentrations. For the shield stage we also estimated clinopyroxene-liquid temperatures (2σ standard deviation of ±33 °C) considering $^{Cpx\text{-}Liq}Kd$ values 0.24–0.30 representative of equilibrium conditions (Putirka et al., 2003) using the pressure from Nimis and Ulmer (1998) anhydrous basalts as input.

II.4.3.2 Pressure and temperature for the shield stage

Clinopyroxene is common in the shield lavas, although not always as phenocryst in all samples. Usually they are eu- to subhedral homogeneous crystals, isolated or in a glomeroporphiric texture with olivine and plagioclase. In general, their diameter is < 0.7 mm with a variable composition in the range of $Wo_{42\text{-}47}En_{39\text{-}48}Fs_{8\text{-}17}$, Na_2O: 0.16–0.54 and TiO_2: 0.80–3.61 wt% (Fig. II.7 and Table II.S.3). Clinopyroxene composition is the same in 'differentiated', 'near-primitive' and 'olivine-rich' groups. Pressure conditions estimated for the shield lavas are 0.0–3.2 kbar (Table II.3, most samples between 1.0

and 2.0 kbar, see histogram in Fig. II.11). The latter also supports the choice of pressure input of 2.0 kbar for olivine-liquid geothermometer.

The olivine phenocrysts in the shield unit are eu- to subhedral, with diameter up to 1.8 mm with an iddingsite altered rim (Fig. II.8a) (of variable width, sometimes obliterating the whole crystal). Their chemical composition ranges between Fo_{76-88} and Ni: 196–2695 ppm commonly with normal zonation (Figs. II.8a and II.10a). In the 'olivine-rich' and 'near-primitive' groups there is an abundance of high Fo values (Fo_{84-88}) (Table II.S.4). Estimates of crystallization temperature in one sample of 'near-primitive' group are 1321 °C (Tables II.3 and II.S.4), but the analyzed lava of 'olivine-rich' group do not show chemical equilibrium with liquid (Fig. II.6). In the 'differentiated' group some rims of zoned crystals are in textural and chemical equilibrium with liquid (Fig. II.6) giving temperatures in the range 1156–1181 °C (Tables II.3 and II.S.4). Olivine-liquid temperature of the 'differentiated' lavas are well correlated with those obtained by the clinopyroxene-liquid equilibrium geothermometer, which varies between 1162 and 1194 °C (Tables II.3 and II.S.3). This does not occur in 'near-primitive' group where clinopyroxene-liquid temperature is 1205–1221 °C (Tables II.3 and II.S.3) (but in a sample with Mg# of 59.7 in contrast of 67.6 in the sample measured with olivine-liquid geothermometer).

II.4.3.3 Pressure and temperature for the rejuvenated stage

The rejuvenated lavas contain clinopyroxene as a ubiquitous phase, generally visible as phenocrysts (up to 1.6 mm in diameter) and in the groundmass. The main compositional differences respect to shield unit are the higher contents of Wo component and Na_2O (Fig. II.7 and Table II.S.3). According to their mineral chemistry and pressure estimation, the 'high-Mg' and 'low-Mg' groups can be analyzed separately.

The 'high-Mg' group is characterized by the presence of subhedral microphenocrysts of clinopyroxene with diameter < 0.3 mm. Generally they exhibit oscillatory zonation and have compositions in the range of $Wo_{44-51}En_{36-44}Fs_{8-17}$, Na_2O: 0.29–0.64 and TiO_2: 1.69–3.49 wt% (Table II.S.3). Resorption rims are absent and their crystallization pressure was estimated between 0 and 3.7 kbar (Table II.3 and II.S.3). On the other hand, the 'low-Mg' group shows a more complex compositional and textural pattern. In general, Na-enriched cores (< 1.1 mm in diameter) are visible with composition in the range of $Wo_{46-48}En_{38-45}Fs_{8-15}$, Na_2O: 0.69–1.25 and TiO_2: 1.23–2.51 wt% (Fig. II.7) that usually show evidences of resorption (sinuous and irregular rims), without zonation and occasionally 'spongy' texture. The formation pressure of these Na-enriched clinopyroxene cores was estimated in the range 3.7–10.8 kbar (Table II.S.3) (most of the estimates are > 5.0 kbar, see histogram in Fig. II.11), the highest values for Robinson Crusoe Island lavas. Around the cores there are rims (< 0.25 mm in diameter) that develop oscillatory zonation with chemical ($Wo_{46-50}En_{34-48}Fs_{5-16}$, Na_2O: 0.38–0.66 and TiO_2: 0.32–4.26 wt%) and textural characteristics very similar to the 'high-Mg' clinopyroxenes (Fig. II.7). The pressure estimated for the rims was 0–5.2 kbar (Table II.S.3) (most of the data < 3.0 kbar, see histogram in Fig. II.11) generating important variations (e.g., 1.7–10.3 kbar) in single crystals from the 'low-Mg' group (Fig. II.9a). Compositional outliers (in clinopyroxene crystals with notable resorption rims) are scarcely recognizable in one sample of the 'low-Mg' group, with diameter < 0.6 mm and $Wo_{49}En_{30-31}Fs_{20-21}$, Na_2O: 1.52–1.70 and TiO_2: 2.19–2.45 wt% (Figs. II.7 and II.9b), but their pressure conditions cannot be estimated because of the low Mg# of the crystals for

the Nimis and Ulmer (1998) geobarometer. Then, the rejuvenated volcanism is characterized by the formation of clinopyroxene with high-pressure Na-rich cores (only in 'low-Mg' group and occasionally around anomalous compositions) followed by low-pressure rims (in both groups).

Olivine is a ubiquitous phenocryst in lavas of the rejuvenated volcanism, with diameter up to 4.0 mm and a notably thinner iddingsite rim than those from the shield unit. They are characterized by the presence of Mg-rich cores (< 1.6 mm in diameter, Fo_{85-90}, most of the samples around Fo_{88} and Ni: 534–2617 ppm) (Fig. II.10a and Table II.S.4) sometimes in equilibrium with the mantle and melts derived from it (Fo > 88). Mg-rich cores compose the whole crystals in the 'high-Mg' group (Fig. II.8b) and are in chemical and textural equilibrium with the liquid (Fig. II.6). This allow us to estimate the olivine-liquid equilibrium temperature for the 'high-Mg' group between 1316 and 1354 °C (Tables II.3 and II.S.4), the highest values in Robinson Crusoe Island. But in the 'low-Mg' group, the Mg-rich cores show resorption rims with chemical disequilibrium (Table S.4) and are surrounded by more differentiated rims (diameter < 0.1 mm, Fo_{80-84}, Ni: ~ 0–1658 ppm) (Fig. II.8c) in equilibrium with the liquid (Fig. II.6). Then, the temperature for the 'low-Mg' group was estimated in the range 1256–1295 °C (Tables II.3 and II.S.4). Some olivines from both groups have cores with anomalous compositions (different to Mg-rich cores) that can be interpreted as xenocrysts remnants. Most of olivine xenocrysts are characterized by low Ca (< 700 ppm) and high Fo_{84-90} contents (Fig. II.10b) and might be interpreted as mantle olivines (discussed in section 5.1). These olivines do not display significant differences respect to the typical Mg-rich cores of the rejuvenated unit, which make them indistinguishable in absence of EPMA data. In the 'high-Mg' group these xenocrysts are in chemical and textural equilibrium with the liquid (Table II.S.4), but in the 'low-Mg' group they show resorption evidences and are surrounded by the characteristic Fo_{80-84} rims. Another set of xenocrysts is scarcely visible only in the 'low-Mg' group. These correspond to the lowest values of Fo in the rejuvenated unit (Fo_{78-84}) with crystals showing notable resorption rims. The classical pattern of 'low-Mg' olivine (Mg-rich cores and differentiated rims) is visible around these anomalous xenocrysts (Fig. II.8d). In summary, the olivine evolution consist in the formation on Mg-rich cores (Fo_{85-90}, T: 1316–1354 °C), occasionally around xenocrysts (Fo_{84-90} or Fo_{78-84}) (in both groups), surrounded by more differentiated rims (Fo_{80-84}, T: 1256–1295 °C) only in the 'low-Mg' group.

II.4.3.4 Xenoliths

Plagioclase-bearing dunite xenoliths are recognized in a dyke of the rejuvenated unit with hetero-cumulate texture that suggests their origin from cumulated ultramafic intrusive. In fact, their mineralogy (see Table II.1) (plagioclase presence implies shallow crystallization) and olivine chemistry (Fo < 82.7, Ni < ~ 2000 ppm and Ca > 1000 ppm) (Table II.S.4) discard a mantle origin. Olivines are very similar to those from shield stage lavas, which suggest that xenoliths are carried out from intrusive bodies probably formed by olivine accumulation from shield-like magmas. In the rejuvenated unit it is also possible to recognize xenolithic fragments that consist of spinel lherzolites in basanite dykes and lavas. Their mineralogical (Table II.1) and textural characteristics (e.g., glass veins and reaction rims on minerals in contact with them) admit an origin in the mantle. The olivine chemistry (Fo_{88-89}, Ni > 2200 ppm and Ca < 650 ppm) (Table II.S.4) confirms their mantle origin (e.g., Simkin and Smith, 1970). Pressure conditions in clinopyroxene

were estimated between 8.9 and 11.0 kbar (Table II.S.3) (Nimis and Ulmer, 1998), depth associated with lithospheric mantle (i.e., > ~ 32 km depth).

II.5. Discussion

II.5.1 Heterogeneous crystal origin

Clinopyroxenes and olivines in the shield lavas show compositional features interpretable as phenocrysts origin (defined as phases that are in equilibrium with the liquid), crystallized from a liquid affected by shallow fractional crystallization (Fig. II.10a). The possibility that the cores in zoned crystal correspond to antecrysts (defined as crystals that did not crystallized directly from the host melt but maintain a genetic relationship with the same system; e.g., Davidson et al., 2007) is plausible but difficult to confirm. According to the olivine Fo and Ni content (Fig. II.10a), the shield magmatism has an origin in a peridotitic source probably similar to Hawaiian tholeiitic melt source (based on crystallization trend from Wang and Gaetani, 2008). Minor participation of pyroxenite (according to a crystallization trend from peridotite and pyroxenite source from Ruprecht and Plank, 2013) cannot be discarded but olivines from the shield stage do not show classical features considered as pyroxenite signature (e.g., high contents of Ni, after Sobolev et al., 2005). Although Herzberg and O'Hara (2002) geothermometer was calibrated in primary magmas from peridotite source, they discussed that the presence of pyroxenite/eclogite is a problem only if they exist as a distinct lithology (e.g., as veins) and not as source of chemical metasomatism. We do not have evidences of pyroxenite/eclogite veins in Robinson Crusoe.

In the rejuvenated lavas there are clinopyroxenes cores with chemical compositions interpretable as phenocrysts, xenocrysts or antecrysts crystallized at different conditions. An important feature of the clinopyroxenes in the 'low-Mg' group is the presence of Na-rich cores that yields the higher pressures estimates, which could be interpreted as an origin in the mantle. However, from a comparison with mantle clinopyroxenes (data from spinel lherzolites as xenoliths in 'low-Mg' group) notable differences arise, (e.g., TiO_2, Al_2O_3 and Cr_2O_3 contents) (TiO_2 in Fig. II.7), which suggests that Na-rich cores are not evident mantle xenocrysts. In addition, Robinson Crusoe lavas do not show any composition similar to these Na-rich cores, which allow us to discard them to be considered as xenocrysts originated at shield stage. We interpret these Na-rich clinopyroxene cores as antecrysts and the chemical differences as a result of crystallization from a liquid more primitive than the rims-equilibrated melts, which explain their presence only in 'low-Mg' group (no primitive compositions). Same situation has been observed in rocks of other oceanic islands, e.g., the post-shield lavas at Hawaii (Welsch et al., 2016). Only the Na-rich cores formed at pressures ~ 10 kbar could be mantle xenocrysts (those chemically similar to spinel lherzolites). Rare cores highly enriched in FeO^T and Na_2O in one sample of 'low-Mg' group are considered xenocrysts of enigmatic origin due to their anomalous composition (Fig. II.7), different to any composition (lavas, dunite or lherzolite) in Robinson Crusoe Island.

The olivines from the rejuvenated magmas show cores with different compositions (up to three in one sample). Most of them are formed directly from magmas in equilibrium (or near-equilibrium) with the mantle (according their Fo and Ca content) and correspond to phenocrysts in 'high-Mg' group and antecrysts in 'low-Mg' lavas. According to their chemical composition they come from a peridotitic source, apparently with minor or null

participation of pyroxenite or eclogite derived melts (Fig. II.10a). Two sets of cores have an enigmatic origin. The first one has major element geochemistry identical to phenocrysts (Fo_{84-90}) but strong variations in some trace elements (Ni > 2000 ppm and Ca < 700 ppm). These features have been assigned to mantle olivines (e.g., Simkin and Smith, 1970; Boudier, 1991; Hirano et al., 2004; Rohrbach et al., 2005). However, recent studies indicate that such compositions may also be generated from non-mantle conditions (e.g., Kamenetsky et al., 2006; Li et al., 2012). In this case, the remarkable compositional similarity of these crystals with olivines from spinel lherzolites (mantle xenoliths) (Fig. II.10b) allows to interpret their origin as mantle xenocrysts. The second set has the lowest Fo values of the rejuvenated unit (Fo_{78-84} and Ca > 800 ppm) and shows evident chemical similarities with olivines of dunite cumulates in the shield unit (Fig. II.10b). Then, their origin is interpreted as xenocrysts from shield-like magmas.

The rims of olivine and clinopyroxene are in textural (and chemical for olivines, Fig. II.6) equilibrium with the liquid and we interpret that they are formed directly from the magma as phenocrysts. The evolution trend of both mineral rims follows the classic shallow fractional crystallization trend (Fig. II.10a for olivine).

II.5.2 Contrasting magma ascent and storage paths

II.5.2.1 Shield volcanism

The estimated pressure-temperature pre-eruptive conditions for the shield volcanism, their chemical features (abundant differentiated and cumulated rocks) and xenolith content (only from shallow origin) allow us to infer the existence of shallow magmatic reservoirs, where the ascending magmas would have been stored, crystallized and sometimes differentiated. These reservoirs were located at depth between ~ 3 and 11 km (1–3 kbar, Fig. II.11), and probably had a considerable size due to the volume of erupted material. Inside of this shallow reservoir the three types of magmas defined for the shield stage resided, but undergone a different evolutionary history. The ‘differentiated’ group is formed by magmas that were stored and differentiated in the reservoir (shallow fractional crystallization and magmatic recharge). During the chamber evolution the magmatic differentiation would have caused a significant temperature decrease to ~ 1156–1181 °C. These temperatures are well correlated with Kilauea geothermometer (Helz and Thornber, 1987) estimations of Natland (2003). This group represents the largest volume of magma erupted in Robinson Crusoe Island.

The ‘near-primitive’ group is composed by basaltic magmas with high content of olivine that undergone little (or no) differentiation and were partially mixed with magmas from the ‘differentiated’ group. Their olivines were formed at ~ 1321 °C and thus the whole rock chemistry closely reflects the primitive composition of the shield magmatism in Robinson Crusoe Island. Differences in the degree of magma mixing explain the clinopyroxene-liquid temperatures of 1205–1221 obtained in a more evolved sample of this group. Natland (2003) also recognized the mixing processes between cold magmas and hotter olivine-bearing magmas.

Finally, we interpret the formation of the ‘olivine-rich’ group as a result of fractional crystallization and gravitational settling in the reservoir or pick-up of primitive antecrysts. The olivine accumulation also explains the formation of plagioclase-bearing dunites cumulates at shallow conditions carried in one dyke of the shield unit.

Putirka et al., (2008b) estimated an average olivine-liquid temperature of 1517 °C for primitive magmas in Juan Fernández Ridge. We cannot evaluate this estimation because samples details were not provided (taken from GEOROC database that contains both shield and rejuvenated samples together with olivine-cumulated rocks).

II.5.2.2 Rejuvenated volcanism

Magma ascent and storage conditions for the rejuvenated volcanism are different when compared to the shield stage. Fractional crystallization in shallow reservoirs was replaced by high-pressure crystallization, direct ascent and only occasional short-time storage in low-volume reservoirs (Fig. II.11).

Basanites of 'high-Mg' group represent primitive magmas in equilibrium with the mantle. Clinopyroxene began to crystallize at shallow depth < 15 km (< 4 kbar) without evidence of polybaric ascent (absence of high-pressure cores and chemical signs of fractionation). Olivine was formed at temperatures about 1316–1354 °C, probably starting from deep regions ~ 33–41 km (9–11 kbar) where xenocrysts were captured (only distinguishable by trace elements). There is no evidence of storage in shallow reservoirs for this group.

For the 'low-Mg' group we interpret a complex storage and ascent history. First, xenocrysts of olivine and lherzolite xenoliths were incorporated at ~ 33–41 km depth (9–11 kbar). Probably a coeval polybaric crystallization of high-pressure clinopyroxene started at ~ 40 km ending at ~ 18 km (~ 5–11 kbar, with a few cases at ~ 13 km or ~ 3.5 kbar). After that, magmas ascended quickly (preserving xenoliths) and formed resorption rims in the cores (probably due to magma mixing or recharge that changed the magma chemistry). Finally we suggest the magma storage occurred at low-volume shallow reservoirs (depth < ~ 18 km or ~ 5 kbar) where the rims of both olivine and clinoyroxene formed at temperatures between ~ 1256–1295 °C. The preservation of zonation in olivine (preventing elemental diffusion) suggests short-time residence in the reservoir (e.g., Ruprecht and Plank, 2013).

II.5.3 Robinson Crusoe storage system in hotspot global view

Our model suggests the existence of shallow reservoirs at the shield stage in Robinson Crusoe (< 10 km, Fig. II.11). Similar models have been proposed for other oceanic islands using different techniques. Based on geophysical data (Ryan et al., 1988; Poland et al., 2014; Tilling et al., 2014), geochemical-geological observations (Clague, 1987) and high-precision Pb isotope analysis (Pietruzka et al., 2015), one or several shallow magma reservoirs (< 7 km depth) have been recognized for the shield stage in Hawaii. In addition, for Réunion shield stage Fisk et al. (1988) identified reservoirs between 5 and 8 kbar (from melting and recrystallization experiments at pressure from 1 atm to 20 kbar) and Peltier et al. (2009) proposed storage regions at 2.3, 7.5 and 15 km based on geophysical data. These data support the idea that shield stage volcanism is fueled from shallow magmatic reservoirs.

For rejuvenated volcanism in Hawaii, Clague (1987) proposed the absence of shallow or intermediate reservoirs based on xenoliths occurrence and chemical primitive features of the alkaline magmas. Rejuvenated magmas in Robinson Crusoe bring also mantle xenoliths (spinel lherzolite) with primitive chemistry (confirmed by Mg# and olivine-liquid temperatures), and our pressure estimations indicate a deep origin (within the mantle). Similar conditions have been proposed for other alkaline rocks from oceanic islands. For

Hawaii postshield stage, Chatterjee et al. (2005) identified reservoirs in the mantle and Hammer et al. (2016) recognized crystallization in mantle conditions, although some shallow reservoirs in crustal levels as well. High depths (within the mantle) up to 9.5 kbar have also been estimated for the reservoir of postshield alkali rocks from Canary Islands (Hasteen et al., 1998).

Thus, shallow reservoirs for shield stage and deeper P conditions for rejuvenated volcanism seems to be a global pattern, despite the regional geodynamical features that control long-term evolution of hotspot volcanoes.

II.6. Conclusions

Contrasting patterns of ascent and storage have been recognized for shield and rejuvenated volcanism in Robinson Crusoe Island, a classical example of intraplate magmatism fed by a primary mantle plume. In fact, whole rock and mineral chemistry (P-T estimations) allow us to infer shallow storage conditions (~ 3–11 km) for the shield stage (dated in ~ 3.83 Ma) and rapid ascent with polybaric crystallization (started at ~ 40 km) for the rejuvenated stage (dated ~ 0.90 Ma). Shallow (and probably large) magma chambers during the shield stage control the low-pressure differentiation and might be responsible for the high growing rate of the central volcano now represented by the ca. 2000 thick volcanic pile and related dyke swarms. On the other hand, direct ascent of small magma batches extracted during the rejuvenated stage well explains the distributed occurrence of minor eruptive centers feeding low volume eruptions. These findings provide a framework for the long-term volcanic evolution of the island and point to a characteristic behavior also proposed in other oceanic islands as Hawaii or Réunion.

Acknowledgments

This research was supported by FONDECYT 1110966, 1141303 (both granted to L. E. Lara) and FONDAP 15090013 projects. Main results presented in this manuscript are part of the first author's doctoral thesis also supported by a CONICYT fellowship. Authors are grateful to Michael Garcia and Jasper Konter for providing constructive reviews that improved this paper. We also acknowledge LAMARX – Universidad Nacional de Córdoba staff, who provided us assistance with the microprobe. Gabriel Orozco, Valentina Astudillo, and Oliver Cooper are thanked for their assistance in the field and further discussion. CONAF authorized scientific research in this protected area and DIFROL provided logistical support during the 2013 field campaign.

Supplementary data

Supplementary data associated with this article (Tables II.S.1, II.S.2, II.S.3 and II.S.4) can be found in the online version, at doi: http://dx.doi.org/10.1016/j.jvolgeores.2017.05.035.

Bibliography

Anderson, D.L., 2000. The thermal state of the upper mantle; no role for mantle plumes. Geophys. Res. Lett. 27, 3623–3626. doi:10.1029/2000GL011533

Anderson, D.L., 2001. Top-down tectonics? Science 293, 2016–2018. doi:10.1126/science.1065448

Argus, D.F., Gordon, R.G., Heflin, M.B., Ma, C., Eanes, R.J., Willis, P., Peltier, W.R., Owen, S.E., 2010. The angular velocities of the plates and the velocity of Earth's centre from space geodesy. Geophysical Journal International 180, 913–960. doi:10.1111/j.1365-246X.2009.04463.x

Baker, P.E., Gledhill, a., Harvey, P.K., Hawkesworth, C.J., 1987. Geochemical evolution of the Juan Fernandez Islands, SE Pacific. J. Geol. Soc. London. 144, 933–944. doi:10.1144/gsjgs.144.6.0933

Ballmer, M.D., van Hunen, J., Ito, G., Tackley, P.J., Bianco, T. a., 2007. Non-hotspot volcano chains originating from small-scale sublithospheric convection. Geophys. Res. Lett. 34. doi:10.1029/2007GL031636

Ballmer, M.D., Ito, G., van Hunen, J., Tackley, P.J., 2011. Spatial and temporal variability in Hawaiian hotspot volcanism induced by small-scale convection. Nat. Geosci. 4, 457–460. doi:10.1038/ngeo1187

Beattie, P., 1993. Olivine-melt and orthopyroxene-melt equilibria. Contrib. to Mineral. Petrol. 115, 103–111. doi:10.1007/BF00712982

Bianco, T.A., Ito, G., Becker, J.M., Garcia, M.O., 2005. Secondary Hawaiian volcanism formed by flexural arch decompression. Geochemistry, Geophys. Geosystems 6, 1–24. doi:10.1029/2005GC000945

Bonatti, E., 1990. Not so hot "hot spots" in the oceanic mantle. Science 250, 107–111. doi:10.1126/science.250.4977.107

Booker, J., Bullard, E.C., Grasty, R.L., 1967. Palaeomagnetism and age of rocks from Easter Island and Juan Fernandez. Geophys. J. Int. 12, 469–471. doi:10.1111/j.1365-246X.1967.tb03127.x

Boudier, F., 1991. Olivine xenocrysts in picritic magmas - An experimental and microstructural study. Contrib. to Mineral. Petrol. 109, 114–123. doi:10.1007/BF00687204

Chatterjee, N., Bhattacharji, S., Fein, C., 2005. Depth of alkalic magma reservoirs below Kolekole cinder cone, Southwest rift zone, East Maui, Hawaii. J. Volcanol. Geotherm. Res. 145, 1–22. doi:10.1016/j.jvolgeores.2005.01.001

Clague, D.A., 1987. Hawaiian xenolith populations, magma supply rates, and development of magma chambers. Bulletin of Volcanology 49, 577–587. doi:10.1007/BF01079963

Clouard, V., Bonneville, A., 2001. How many Pacific hotspots are fed by deep-mantle plumes? Geology 29(8), 695–698. doi:10.1130/0091-7613(2001)029<0695:HMPHAF>2.0.CO;2

Courtillot, V., Davaille, A., Besse, J., Stock, J., 2003. Three distinct types of hotspots I the Earth's mantle. Earth Planet. Sci. Lett. 205, 295–308. doi.org/10.1016/S0012-821X(02)01048-8

Davidson, J.P., Morgan, D.J., Charlier, B.L.A., Harlou, R., Hora, J.M., 2007. Microsampling and Isotopic Analysis of Igneous Rocks: Implications for the Study of Magmatic Systems. Annual Review of Earth and Planetary Sciences 35, 273–311. doi:10.1146/annurev.earth.35.031306.140211

Devey, C.W., Hemond, C., Stoffers, P., 2000. Metasomatic reactions between carbonated plume melts and mantle harzburgite: the evidence from Friday and Domingo Seamounts (Juan Fernandez chain, SE Pacific). Contrib. to Mineral. Petrol. 139, 68–84. doi:10.1007/s004100050574

Dixon, J.E., Leist, L., Langmuir, C., Schilling, J.-G., 2002. Recycled dehydrated lithosphere observed in plume-influenced mid-ocean-ridge basalt. Nature 420, 385–389. doi:10.1038/nature01215

Farley, K.A., Basu, A.R., Craig, H., 1993. He, Sr and Nd isotopic variations in lavas from the Juan Fernandez Archipelago, SE Pacific. Contrib. to Mineral. Petrol. 115, 75–87. doi:10.1007/BF00712980

Fisk, M.R., Upton, B.G.J., Ford, C.E., White, W.M., 1988. Geochemical and experimental study of the genesis of magmas of Reunion Island, Indian Ocean. Journal of Geophysical Research: Solid Earth 93, 4933–4950. doi:10.1029/JB093iB05p04933

Fleck, R.J., Sutter, J.F., Elliot, D.H., 1977. Interpretation of discordant 40Ar/39Ar age-spectra of mesozoic tholeiites from antarctica. Geochimica et Cosmochimica Acta 41, 15–32. doi:10.1016/0016-7037(77)90184-3

Frey, F.A., Wise, W.S., Garcia, M.O., West, H., -T, K.S., Kennedy, A., 1990. Evolution of Mauna Kea volcano, Hawaii: Petrologic and geochemical constraints on postshield volcanism. J. Geophys. Res. 95, 1271–1300. doi:10.1029/JB095iB02p01271

Garcia, M.O., 1996. Petrography and olivine and glass chemistry of lavas from the Hawaii Scientific Drilling Project. Journal of Geophysical Research: Solid Earth 101, 11701–11713. doi:10.1029/95JB03846

Garcia, M.O., Swinnard, L., Weis, D., Greene, a. R., Tagami, T., Sano, H., Gandy, C.E., 2010. Petrology, geochemistry and geochronology of Kaua'i lavas over 4-5 Myr: Implications for the origin of rejuvenated volcanism and the evolution of the Hawaiian plume. J. Petrol. 51, 1507–1540. doi:10.1093/petrology/egq027

Garcia, M.O., Smith, J.R., Tree, J.P., Weis, D., Harrison, L., Jicha, B.R., 2015. Petrology, geochemistry, and ages of lavas from Northwest Hawaiian Ridge volcanoes. Geological Society of America Special Papers 511 . doi:10.1130/2015.2511(01)

Geldmacher, J., Hoernle, K., 2000. The 72 Ma geochemical evolution of the Madeira hotspot (eastern North Atlantic): Recycling of Paleozoic (<500 Ma) oceanic lithosphere. Earth Planet. Sci. Lett. 183, 73–92. doi:10.1016/S0012-821X(00)00266-1

Gerlach, D.C., Hart, S.R., Morales, V.W.J., Palacios, C., 1986. Mantle heterogeneity beneath the Nazca plate: San Felix and Juan Fernandez islands. Nature 322, 165–169. doi:10.1038/322165a0

Gurriet, P., 1987. A thermal model for the origin of post-erosional alkalic lava, Hawaii. Earth Planet. Sci. Lett. 82, 153–158. doi:10.1016/0012-821X(87)90115-4

Hammer, J., Jacob, S., Welsch, B., Hellebrand, E., Sinton, J., 2016. Clinopyroxene in postshield Haleakala ankaramite: 1. Efficacy of thermobarometry. Contrib. to Mineral. Petrol. 171, 1–23. doi:10.1007/s00410-015-1212-x

Hansteen, T.H., Klügel, A., Schmincke, H.-U., 1998. Multi-stage magma ascent beneath the Canary Islands: evidence from fluid inclusions. Contributions to Mineralogy and Petrology 132, 48–64. doi:10.1007/s004100050404

Helz, R.T., Thornber, C.R., 1987. Geothermometry of Kilauea Iki lava lake, Hawaii. Bulletin of Volcanology 49, 651–668. doi:10.1007/BF01080357

Herzberg, C., O'Hara, M.J., 2002. Plume-associated ultramafic magmas of Phanerozoic age. J. Petrol. 43, 1857–1883. doi:10.1093/petrology/43.10.1857

Hieronymus, C.F., Bercovici, D., 2000. Non-hot spot formation of volcanic chains: Controls of tectonic stresses on magma transport. Earth Planet. Sci. Lett. 181, 539–554. doi:10.1016/S0012-821X(00)00227-2

Hirano, N., Yamamoto, J., Kagi, H., Ishii, T., 2004. Young, olivine xenocryst-bearing alkali-basalt from the oceanward slope of the Japan Trench. Contrib. to Mineral. Petrol. 148, 47–54. doi:10.1007/s00410-004-0593-z

Hoernle, K., Schmincke, H.U., 1993. The petrology of the tholeiites through melilite nephelinites on Gran Canaria, Canary Islands: Crystal fractionation, accumulation, and depths of melting. J. Petrol. 34, 573–597. doi:10.1093/petrology/34.3.573

Irvine, T.N., Baragar, R.A., 1971. A guide to the chemical classification of the common volcanic rocks. Can. J. Earth Sci. 8 (5), 523–548. doi:10.1139/e71-055

Kamenetsky, V.S., Elburg, M., Arculus, R., Thomas, R., 2006. Magmatic origin of low-Ca olivine in subduction-related magmas: Co-existence of contrasting magmas. Chem. Geol. 233, 346–357. doi:10.1016/j.chemgeo.2006.03.010

Konter, J.G., Staudigel, H., Blichert-Toft, J., Hanan, B.B., Polvé, M., Davies, G.R., Shimizu, N., Schiffman, P., 2009. Geochemical stages at Jasper seamount and the origin of intraplate volcanoes. Geochemistry, Geophys. Geosystems 10. doi:10.1029/2008GC002236

Konter, J.G., Jackson, M.G., 2012. Large volumes of rejuvenated volcanism in Samoa: Evidence supporting a tectonic influence on late-stage volcanism. Geochemistry, Geophys. Geosystems 13. doi:10.1029/2011GC003974

Lara, L.E., Moreno, H., Naranjo, J.A., Matthews, S., Pérez de Arce, C., 2006. Magmatic evolution of the Puyehue–Cordón Caulle Volcanic Complex (40° S), Southern Andean Volcanic Zone: From shield to unusual rhyolitic fissure volcanism. Journal of Volcanology and Geothermal Research 157, 343–366. doi:10.1016/j.jvolgeores.2006.04.010

Le Maitre, R.W., 2002. Igneous rocks – a classification and glossary of terms. Cambridge University Press, Cambridge (236 pp.). doi:10.1017/CBO9780511535581

Li, C., Thakurta, J., Ripley, E.M., 2012. Low-Ca contents and kink-banded textures are not unique to mantle olivine: Evidence from the Duke Island Complex, Alaska. Mineral. Petrol. 104, 147–153. doi:10.1007/s00710-011-0188-0

Macdonald, G.A., Abbott, A.T., Peterson, F.L., 1983. Volcanoes in the Sea: The Geology of Hawaii. University of Hawaii Press, Honolulu (544 pp.).

Morales, A.J., 1987. Geología de las islas Robinson Crusoe y Santa Clara, Archipiélago Juan Fernández, V Región, Chile, Universidad Católica del Norte (103 pp.).

Morgan, W.J., 1971. Convection plumes in the lower mantle. Nature 230, 42–43. doi:10.1038/230042a0

Morgan, W.J., 1972a. Deep mantle convection plumes and plate motions. Am. Assoc. Pet. Geol. Bull: 56(2), 203–213. doi:10.1306/819A3E50-16C5-11D7-8645000102C1865D

Morgan, W.J., 1972b. Plate motions and deep mantle convection. Geol. Soc. Am. Mem. 132, 7–22. doi:10.1130/MEM132-p7

Natland, J.H., 2003. Capture of helium and other volatiles during the growth of olivine phenocrysts in picritic basalts from the Juan Fernandez Islands. J. Petrol. 44, 421–456. doi:10.1093/petrology/44.3.421

Nichols, A.R.L., Carroll, M.R., Höskuldsson, Á., 2002. Is the Iceland hot spot also wet? Evidence from the water contents of undegassed submarine and subglacial pillow basalts. Earth Planet. Sci. Lett. 202, 77–87. doi:10.1016/S0012-821X(02)00758-6

Nimis, P., Ulmer, P., 1998. Clinopyroxene geobarometry of magmatic rocks Part 1: An expanded structural geobarometer for anhydrous and hydrous, basic and ultrabasic systems. Contrib. to Mineral. Petrol. 133, 122–135. doi:10.1007/s004100050442

Nimis, P., 1999. Clinopyroxene geobarometry of magmatic rocks. Part 2. Structural geobarometers for basic to acid, tholeiitic and mildly alkaline magmatic systems. Contrib. to Mineral. Petrol. 135, 62–74. doi:10.1007/s004100050498

Nimis, P., 2014. ResearchGate web. May 30, 2014. Last access May 2017. www.researchgate.net/post/Is_there_a_recent_model_for_pressure_estimates_from_clinopyroxene2

Orozco, G., 2016. Evolución estructural y tectónica de la isla Robinson Crusoe, Dorsal de Juan Fernández. Universidad de Chile (94 pp.).

Ozawa, A., Tagami, T., Garcia, M.O., 2005. Unspiked K–Ar dating of the Honolulu rejuvenated and Ko‘olau shield volcanism on O‘ahu, Hawai‘i. Earth and Planetary Science Letters 232, 1–11. doi:10.1016/j.epsl.2005.01.021

Papike, J.J., Cameron K.L., Baldwin, K., 1974. Amphiboles and pyroxenes; characterization of other than quadrilateral components and estimates of ferric iron from microprobe data. Geol .Soc. Amer. Abs. Prog. 6, 1053–1054.

Paul, D., White, W.M., Blichert-Toft, J., 2005. Geochemistry of Mauritius and the origin of rejuvenescent volcanism on oceanic island volcanoes. Geochemistry, Geophys. Geosystems 6. doi:10.1029/2004GC000883

Peltier, A., Bachèlery, P., Staudacher, T., 2009. Magma transport and storage at Piton de La Fournaise (La Réunion) between 1972 and 2007: A review of geophysical and geochemical data. Journal of Volcanology and Geothermal Research 184, 93–108. doi:10.1016/j.jvolgeores.2008.12.008

Pietruszka, A.J., Heaton, D.E., Marske, J.P., Garcia, M.O., 2015. Two magma bodies beneath the summit of Kilauea Volcano unveiled by isotopically distinct melt deliveries from the mantle. Earth Planet. Sci. Lett. 413, 90–100. doi:10.1016/j.epsl.2014.12.040

Poland, M.P., Miklius, A., Montgomery-Brown, E.K., 2014. Magma supply, storage, and transport at shield-stage Hawaiian volcanoes: Chapter 5 in Characteristics of Hawaiian volcanoes (RPRT), Professional Paper. Reston, VA. doi:10.3133/pp18015

Putirka, K.D., Mikaelian, H., Ryerson, F., Shaw, H. 2003. New clinopyroxene-liquid thermobarometers for mafic, evolved, and volatile-bearing lava compositions, with applications to lavas from Tibet and the Snake River Plain, Idaho. Am. Mineral. 88, 1542–1554. doi:10.2138/am-2003-1017

Putirka, K.D., 2008a. Thermometers and barometers for volcanic systems. Rev. Mineral. Geochemistry 69, 61–120. doi:10.2138/rmg.2008.69.3

Putirka, K., 2008b. Excess temperatures at ocean islands: Implications for mantle layering and convection. Geology 36, 283–286. doi:10.1130/G24615A.1

Quensel, P., 1920. Additional comments on the geology of the Juan Fernandez Islands, in: Skottsberg, C. (Ed.), The Natural History of Juan Fernandez and Easter Island. v. 1. Geography, Geology, Origin of Island Life. pp. 37–88.

Renne, P.R., Deino, A.L., Walter, R.C., Turrin, B.D., Swisher, C.C., Becker, T.A., Curtis, G.H., Sharp, W.D., Jaouni, A.-R., 1994. Intercalibration of astronomical and radioisotopic time. Geology 22 , 783–786. doi:10.1130/0091-7613(1994)022<0783:IOAART>2.3.CO;2

Ribe, N.M., Christensen, U.R., 1999. The dynamical origin of Hawaiian volcanism. Earth Planet. Sci. Lett. 171, 517–531. doi:10.1016/S0012-821X(99)00179-X

Rodrigo, C., Lara, L., 2014. Plate tectonics and the origin of the Juan Fernández Ridge: Analysis of bathymetry and magnetic patterns. Lat. Am. J. Aquat. Res 42(4), 907–917. doi:10.3856/vol42-issue4-fulltext-15

Roeder, P.L., Emslie, R.F., 1970. Olivine-liquid equilibrium. Contrib. to Mineral. Petrol. v. 29, 275–289. doi:10.1007/BF00371276

Rohrbach, A., Schuth, S., Ballhaus, C., Münker, C., Matveev, S., Qopoto, C., 2005. Petrological constraints on the origin of arc picrites, New Georgia Group, Solomon Islands. Contrib. to Mineral. Petrol. 149, 685–698. doi:10.1007/s00410-005-0675-6

Ruprecth, P., Plank, T., 2013. Feeding andesitic eruptions with a high-speed connection from the mantle. Nature 500, 68–72. doi:10.1038/nature12342

Ryan, M.P., 1988. The mechanics and three-dimensional internal structure of active magmatic systems: Kilaue volcano, Hawaii. J. Geophys. Res. 93, 4213–4248. doi: 10.1029/JB093iB05p04213

Simkin, T.O.M., Smith, J. V, 1970. Minor-element distribution in olivine. J. Geol. 78, 304–325. doi:10.1086/627519

Sobolev, A. V, Hofmann, A.W., Sobolev, S. V, Nikogosian, I.K., 2005. An olivine-free mantle source of Hawaiian shield basalts. Nature 434, 590–597. doi:10.1038/nature03411

Sobolev, A. V, Hofmann, A.W., Kuzmin, D. V, Yaxley, G.M., Arndt, N.T., Chung, S.-L., Danyushevsky, L. V, Elliott, T., Frey, F.A., Garcia, M.O., Gurenko, A.A., Kamenetsky, V.S., Kerr, A.C., Krivolutskaya, N.A., Matvienkov, V. V, Nikogosian, I.K., Rocholl, A., Sigurdsson, I.A., Sushchevskaya, N.M., Teklay, M., 2007. The Amount of Recycled Crust in Sources of Mantle-Derived Melts. Science 316, 412–417. doi:10.1126/science. 1138113

Steinberger, B., O'Connell, R.J., 1998. Advection of plumes in mantle flow: Implications for hotspot motion, mantle viscosity and plume distribution. Geophys. J. Int. 132, 412–434. doi:10.1046/j.1365-246x.1998.00447.x

Straub, S.M., Gomez-Tuena, A., Stuart, F.M., Zellmer, G.F., Espinasa-Perena, R., Cai, Y., Iizuka, Y., 2011. Formation of hybrid arc andesites beneath thick continental crust. Earth Planet. Sci. Lett. 303, 337–347. doi:10.1016/j.epsl.2011.01.013

Stuessy, T.F., Foland, K.A., Sutter, J.F., Sanders, R.W., Silva, M., 1984. Botanical and geological significance of potassium-argon dates from the Juan Fernandez Islands. Science (80-.). 225, 49–51. doi:10.1126/science.225.4657.49

Tilling, R.I., Kauahikaua, J.P., Brantley, S.R., Neal, C.A., 2014. The Hawaiian Volcano Observatory: a natural laboratory for studying basaltic volcanism: Chapter 1 in Characteristics of Hawaiian volcanoes (RPRT), Professional Paper. Reston, VA. doi:10.3133/pp18011

Vergara, H., Morales, E., 1985. Morofología submarina del segmento central del cordón asísimico Juan Fernández. In: Arana, P. (ed), Investigaciones marinas en el archipiélago de Juan Fernández. Universidad Católica de Valparaíso, Valparaíso, 25–34.

Von Huene, R., Corvalán, J., Flueh, E.R., Hinz, K., Korstgard, J., Ranero, C.R., Weinrebe, W., 1997. Tectonic control of the subducting Juan Fernández Ridge on the Andean margin near Valparaiso, Chile. Tectonics 16, 474–488. doi:10.1029/96TC03703

Wang, Z., Gaetani, G.A., 2008. Partitioning of Ni between olivine and siliceous eclogite partial melt: experimental constraints on the mantle source of Hawaiian basalts. Contributions to Mineralogy and Petrology 156, 661–678. doi:10.1007/s00410-008-0308-y

Weis, D., Frey, F.A., Giret, A., Cantagrel, J.M., 1998. Geochemical characteristics of the youngest volcano (Mount Ross) in the Kerguelen Archipelago: Inferences for magma flux, lithosphere assimilation and composition of the Kerguelen plume. J. Petrol. 39, 973–994. doi:10.1093/petroj/39.5.973

Welsch, B., Hammer, J., Baronnet, A., Jacob, S., Hellebrand, E., Sinton, J., 2016. Clinopyroxene in postshield Haleakala ankaramite: 2. Texture, compositional zoning and supersaturation in the magma. Contrib. to Mineral. Petrol. 171, 1–19. doi:10.1007/s00410-015-1213-9

White, W.M., Duncan, R.A., 1996. Geochemistry and geochronology of the Society Islands: New evidence for deep mantle recycling, in: Earth Processes: Reading the Isotopic Code. American Geophysical Union, pp. 183–206. doi:10.1029/GM095p0183

Woodhead, J.D., 1992. Temporal geochemical evolution in oceanic intra-plate volcanics: A case study from the Marquesas (French Polynesia) and comparison with other hotspots. Contrib. to Mineral. Petrol. 111, 458–467. doi:10.1007/BF00320901

Wright, E., White, W.M., 1987. The origin of Samoa: New evidence from Sr, Nd, and Pb isotopes. Earth Planet. Sci. Lett. 81, 151–162. doi:10.1016/0012-821X(87)90152-X

Table II.1. Petrography of Robinson Crusoe samples utilized in geothermobarometry estimations based on 500 point modes. Mineralogy reported as vesicle-free volume percent only for pheno and microphenocrysts (>0.2 mm in diameter). All samples used in clinopyroxene geobarometry. (O) used in olivine-liquid and (C) in clinopyroxene-liquid geothermometry. Rock type according mineralogy and chemistry. GM: groundmass. Ves: vesicles content.

		GM	Mineralogy				Ves
Sample	Rock type	(%)	Oli	Cpx	Plg	Op	(%)
Shield 'differentiated'							
LL230711-7 (*)	tholeiitic basalt	70	-	6	15	-	2
LL250711-1 (C)	alkali basalt	64	5	10	21	-	4
LL260711-3	tholeiitic basalt	80	6	4	10	-	13
JR160913-13 (C)	tholeiitic basalt	99	-	1	-	-	1
LL220112-3 (O)(C)	tholeiitic basalt	94	2	2	2	-	5
LL240711-1 (O)(C)	alkali basalt	98	<1	<1	2	-	12
LL250711-9 (C)	tholeiitic basalt	98	<1	1	1	-	4
Shield 'differentiated'							
LL250711-7 (C)	tholeiitic basalt	92	6	1	1	-	5
JR290513-2 (O)	tholeiitic basalt	92	7	-	-	1	-
JR290513-5	alkali basalt	93	2	3	2	-	3
Shield 'differentiated'							
LL250711-5	tholeiitic basalt	75	25	-	-	-	
Rejuvenated 'high-Mg'							
JR220112-3 (O)	basanite	88	12	<1	-	-	3
JR250112-3 (O)	picrite	87	12	1	-	-	2
Rejuvenated 'low-Mg'							
LL230711-2	basanite	81	10	9	-	<1	<1
JR020613-3	basanite	93	5	1	-	1	2
JR160913-2 (O)	basanite	87	6	7	-	-	2
LL010213-6 (O)	basanite	94	6	<1	-	<1	-
LL220112-4 (O)	basanite	90	8	2	-	-	-
Xenoliths							
LL240711-5C	dunite	-	96	-	2	2	-
		Oli	Cpx	Opx	Sp	Gl	
JF-2A	lherzolite	47	21	28	3	1	

Table II.2. Major element (wt%) and Ni (ppm) concentrations of Robinson Crusoe Island lavas. $Fe_2O_3^T$: total iron as ferric. Loss-on-ignition (LOI) (wt%) is included.

Sample	SiO_2	TiO_2	Al_2O_3	$Fe_2O_3^T$	MgO	MnO	CaO	Na_2O	K_2O	P_2O_5	Ni	LOI	Sum
Det. limit	*0.01*	*0.01*	*0.01*	*0.04*	*0.01*	*0.01*	*0.01*	*0.01*	*0.01*	*0.01*	*0.1*	*0.1*	
Shield 'differentiated'													
LL230711-7	45.98	3.57	14.34	11.88	4.88	0.18	12.38	2.35	0.33	0.43	30.8	3.4	99.72
LL230112-1	46.03	3.28	14.97	11.31	6.77	0.15	9.49	2.90	1.05	0.48	67.9	3.1	99.53
JR300513-3	46.07	3.25	13.83	12.49	6.27	0.19	10.40	2.63	0.95	0.44	66.4	3.1	99.62
LL240711-1	47.03	3.61	14.56	12.67	5.77	0.17	10.24	2.98	1.00	0.50	31.7	1.1	99.63
LL240711-2	46.98	3.14	14.57	12.49	6.13	0.16	10.47	3.00	0.86	0.41	46.6	1.4	99.61
LL240711-6	46.58	3.58	15.38	12.24	5.40	0.15	10.01	3.06	0.91	0.51	39.9	1.8	99.62
LL260711-2	47.56	3.60	14.75	12.39	5.67	0.16	10.26	3.11	1.01	0.49	39.1	0.6	99.60
JR270513-1	45.18	3.77	16.01	13.69	5.55	0.16	8.10	2.72	0.85	0.56	79.5	3.0	99.59
LL250711-1	45.60	3.58	14.88	12.29	5.69	0.15	10.41	2.69	1.00	0.58	84.5	2.7	99.57
LL250711-3	45.97	3.76	15.33	12.95	5.13	0.15	8.99	3.19	1.17	0.63	105.2	2.3	99.57
LL220112-2	47.28	3.73	15.64	12.63	4.19	0.12	9.00	3.12	0.91	0.47	45.1	2.6	99.69
LL220112-3	47.53	3.35	14.21	12.58	6.75	0.16	10.40	2.79	0.88	0.43	80.7	0.6	99.68
LL220112-5	46.60	3.65	16.04	12.62	5.78	0.17	9.37	3.29	1.08	0.50	41.0	0.5	99.60
JR220112-2	46.94	3.36	14.26	12.53	5.63	0.16	10.11	3.12	1.03	0.47	35.8	2.1	99.71
JR250513-2	47.93	3.04	15.51	11.83	5.84	0.18	10.07	2.61	0.82	0.35	64.3	1.5	99.68
JR250513-4	48.59	3.23	15.28	11.50	6.15	0.16	10.51	2.92	0.93	0.41	49.9	0.0	99.68
JR250513-5	47.09	3.91	15.74	12.40	5.67	0.16	8.88	3.42	1.34	0.63	72.9	0.4	99.64
JR160913-1	46.44	3.38	14.79	12.50	5.39	0.12	9.59	2.49	0.66	0.41	84.6	3.4	99.17
JR160913-10	49.20	3.17	14.56	10.99	5.53	0.14	11.12	2.90	0.69	0.38	31.8	1.0	99.68
JR160913-13	47.87	3.51	14.69	11.39	5.18	0.14	11.08	3.04	0.90	0.42	35.8	1.4	99.62
LL250711-8	46.22	3.64	15.28	12.71	5.94	0.18	9.58	2.66	0.95	0.47	33.6	2.0	99.63
LL250711-9	47.18	3.42	14.78	12.48	6.24	0.17	10.56	2.76	0.80	0.39	34.8	0.9	99.68
LL250711-4	46.77	3.80	14.73	13.22	5.33	0.17	9.23	3.15	1.04	0.59	46.4	1.6	99.63
MP270112-4	45.41	3.79	15.32	13.65	6.70	0.16	9.02	2.86	1.10	0.54	110.6	1.1	99.65
Shield 'near-primitive'													
JR290513-5	45.42	3.31	13.43	12.06	9.11	0.17	9.28	2.68	1.31	0.42	265.5	2.4	99.59
JR290513-2	45.65	2.48	12.80	12.66	12.04	0.19	9.49	2.28	0.60	0.30	158.3	0.9	99.39
LL250711-7	45.89	2.96	13.38	12.48	8.42	0.15	9.70	2.60	0.64	0.34	193.9	3.0	99.56
LL300113-1	46.31	2.88	13.45	12.87	9.91	0.17	9.98	2.22	0.68	0.36	186.4	0.8	99.63
Shield 'olivine-rich'													
JR270513-2	45.07	3.05	10.98	14.36	14.82	0.18	7.14	2.52	0.93	0.41	558.4	-0.1	99.36
LL250711-5	45.46	1.83	10.37	13.66	17.47	0.17	7.20	2.02	0.34	0.20	583.4	0.6	99.32
JR250513-1	43.75	2.01	8.37	15.55	20.51	0.15	4.84	1.34	0.52	0.26	1098.6	1.8	99.10
LL040213-2	45.83	2.46	11.04	12.28	14.23	0.17	8.56	2.01	0.58	0.28	514.1	2.1	99.54
Rejuvenated 'high-Mg'													
JR250112-3	42.42	2.79	12.43	12.09	12.20	0.18	11.35	2.32	0.52	0.54	261.4	2.6	99.44
LL230112-2	41.32	2.73	12.58	12.75	13.31	0.19	10.31	2.43	1.33	0.58	273.1	1.7	99.23
LL230112-4	43.00	2.80	12.91	11.74	11.45	0.18	11.51	2.42	0.55	0.53	257.5	2.2	99.29
JR220112-3	42.62	2.75	12.66	12.40	13.09	0.19	10.92	3.40	0.70	0.48	250.9	0.2	99.41
Rejuvenated 'low-Mg'													
LL230711-2	42.15	2.80	13.77	12.30	10.22	0.21	10.58	2.83	0.59	0.62	182.1	3.3	99.37
LL230711-8	42.14	3.20	13.04	12.81	11.16	0.20	10.59	3.79	0.80	0.68	225.5	1.0	99.41
JR250112-2	42.02	3.08	13.06	13.15	10.81	0.20	10.08	3.45	0.56	0.64	233.7	2.4	99.45
LL060213-1	43.09	3.04	13.72	12.37	8.72	0.19	10.86	2.84	0.77	0.59	219.0	3.4	99.59
LL060213-3	41.69	3.18	13.95	13.17	8.86	0.21	10.50	2.39	1.18	0.89	148.9	3.4	99.42
LL060213-4	43.82	2.71	14.57	11.90	8.37	0.21	10.55	3.68	1.78	0.63	129.0	1.3	99.52
JR230112-1	42.19	3.18	13.10	13.10	11.04	0.20	10.78	3.88	0.78	0.61	172.5	0.6	99.46
JR230112-2	41.42	3.34	13.62	13.69	8.66	0.21	10.77	3.93	0.68	0.61	154.2	2.6	99.53
JR230112-3	42.99	2.91	13.43	13.77	9.52	0.23	9.81	3.79	1.70	0.91	142.4	0.4	99.46
JR160913-2	42.66	3.06	14.32	12.98	8.96	0.22	10.28	3.37	0.99	0.72	132.9	1.9	99.46
MP270112-3	44.59	2.63	13.42	12.51	9.94	0.23	9.28	3.74	1.71	0.74	224.4	0.6	99.39
JR020613-3	43.66	2.70	14.15	12.60	9.65	0.22	9.03	3.44	1.66	0.73	234.5	1.6	99.44
LL010213-6	43.81	3.18	14.10	13.87	8.54	0.22	9.51	3.53	1.83	0.78	135.2	0.2	99.57
JR220112-4A	44.06	3.07	14.17	12.92	8.43	0.21	10.03	4.16	0.92	0.65	141.7	0.9	99.52
LL220112-1	42.86	3.11	13.25	12.50	10.58	0.20	11.21	2.80	1.37	0.63	171.7	0.9	99.41
JR250513-3	41.99	3.07	13.91	13.27	10.22	0.21	10.57	1.76	0.75	0.68	207.1	3.0	99.43
LL220112-4	44.14	2.79	14.30	12.72	9.10	0.23	9.18	3.96	1.84	0.69	147.9	0.5	99.45
JR250513-9	43.69	2.85	13.98	13.57	9.72	0.23	8.00	2.82	1.87	0.95	245.4	1.7	99.38
LL020213-1	41.06	3.02	14.01	13.24	10.81	0.21	10.41	1.98	0.95	0.68	206.8	3.2	99.57

Table II.3. Pressure and temperature calculated from clinopyroxene and olivine crystals from Robinson Crusoe Island, n indicates the number of samples considered in each compositional group.

Geological unit	Compositional groups	n	Cpx_{an} P (kbar)[A]	n	Ol-Liq T (°C)[B]	n	Cpx-Liq T (°C)[C]
Shield							
	olivine-rich	0	-	0	-		-
	near-primitive	2	0.0-2.9	1	1321	1	1205-1221
	differentiated	7	0.0-3.2	2	1156-1181	5	1162-1194
Rejuvenated							
	high-Mg	2	0.0-3.7	2	1316-1354		-
	low-Mg	5	0.0-10.8	3	1256-1295		-

(A) Clinopyroxene pressure in anhydrous basalts from Nimis and Ulmer, 1989 (±1.7 kbar + ca. 1 kbar per 1wt% H_2O in melt).
(B) Olivine-liquid temperature from Herzberg and O'Hara, 2002 (±31 °C).
(C) Clinopyroxene-liquid temperature from Putirka et al., 2003 (±33 °C).

Supplementary data

Table II.S.1. Summary of $^{40}Ar/^{39}Ar$ incremental heating experiments. Preferred ages in bold (see section 3 for explanation). All uncertainties reported at 2σ precision. Samples analyzed at SERNAGEOMIN (Servicio Nacional de Geología y Minería. Chile) were calculated relative to 28.03 Ma Fish Canyon sanidine (Renne et al., 1994). GM: groundmass material free of phenocrysts.

				Step-heating			**Isochron**		
Sample	**Geological unit**		^{39}Ar	Age (Ma)			Age (Ma)	$^{40}Ar/^{36}Ar_i$	
Experiment	Lat/Long (º)	material	(%)	± 2σ	MSWD	N	± 2σ	± 2σ	MSWD
LL240711-1	*Shield stage*								
12870-01	*Puerto Inglés Seq.*	GM	100	3.79 ± 0.04	1.17	7 of 7	3.79 ± 0.04	296.0 ± 3.0	1.40
12870-02	33°37.85'S/78°49.74'W	GM	100	3.85 ± 0.03	0.63	7 of 7	3.85 ± 0.04	294.0 ± 2.0	0.62
				Combined isochron:		14 of 14	**3.83 ± 0.03**	294.8 ± 1.7	1.20
JR160913-2	*Rejuvenated stage*								
13354-01	*Bahía del Padre unit* 33°42.09'S/78°56.72'W	GM	100	**0.90 ± 0.03**	0.2	7 of 7	0.89 ± 0.06	298.0 ± 12.0	0.2

Table II.S.2. Major element concentrations (wt%) of Robinson Crusoe Island lavas from previous work (1) Gerlach et al., (1986); (2) Baker et al., (1987); (3) Farley et al., (1993). $Fe_2O_3^T$: total iron as ferric. Loss-on-ignition (LOI) (wt%) is included.

	Sample	SiO_2	TiO_2	Al_2O_3	$Fe_2O_3^T$	MgO	MnO	CaO	Na_2O	K_2O	P_2O_5	LOI
	Shield 'differentiated'											
(1)	32MT0182	47.68	3.19	13.98	14.41	7.38	0.17	9.10	2.97	0.74	0.38	2.66
(1)	14MT0182	47.46	3.52	15.70	14.12	5.41	0.15	9.93	2.81	0.49	0.41	1.70
(1)	59MT0282-B-3	47.13	3.34	15.15	13.22	6.64	0.17	9.94	3.30	0.73	0.39	0.65
(1)	28MT0182-A	45.17	3.70	15.10	14.55	7.45	0.19	9.08	3.15	1.09	0.54	0.70
(1)	11MT0182	46.33	3.75	15.25	14.42	6.28	0.19	9.76	2.83	0.74	0.45	1.74
(1)	5MT0283	47.62	3.68	15.07	13.72	5.41	0.18	9.32	3.46	1.02	0.52	0.64
(2)	17982	48.13	3.97	14.98	13.25	5.33	0.17	8.90	3.38	1.29	0.61	0.55
(2)	17814	48.37	4.45	15.12	14.09	4.42	0.17	8.25	3.30	1.23	0.61	0.80
(2)	17986	48.35	3.62	16.30	12.93	5.29	0.18	9.90	2.51	0.50	0.41	0.00
(2)	18018	48.75	3.45	14.65	13.79	5.17	0.16	9.80	3.02	0.80	0.40	0.33
(2)	18017	45.87	3.99	14.87	13.55	7.47	0.17	9.10	3.38	1.07	0.52	0.00
(2)	17906	48.39	4.16	14.08	13.47	5.36	0.18	9.67	3.24	0.95	0.51	0.00
(2)	18012	45.85	4.01	14.85	13.97	7.52	0.17	9.13	2.94	1.05	0.51	0.00
(3)	PV-2	46.39	2.74	14.86	10.04	8.77	0.15	13.14	2.91	0.64	0.36	-
(3)	PF-2	46.11	2.74	12.14	12.87	12.50	0.18	9.25	2.95	0.85	0.42	-
(3)	PF-3	46.11	2.45	11.40	12.72	14.53	0.17	9.29	2.54	0.46	0.33	-
(3)	PF-5	46.98	2.83	12.92	12.49	10.50	-	9.81	3.19	0.89	0.40	-
(3)	KF-18	45.68	3.07	11.27	14.12	14.70	-	7.29	2.62	0.84	0.40	-
(3)	KF-19	46.46	3.11	13.93	12.75	8.03	-	10.77	3.43	0.76	0.42	-
(3)	PIN-6	43.62	2.11	10.22	14.74	20.10	0.19	6.75	1.95	0.09	0.22	-
	Shield 'near-primitive'											
(1)	30MT0182	46.12	2.65	13.30	13.20	11.79	0.17	9.17	2.50	0.75	0.35	1.15
(1)	59 MT0282-A-7	46.47	2.93	13.30	14.47	10.55	0.16	8.64	2.71	0.47	0.30	0.97
(1)	10MT0283	45.36	2.93	13.92	14.86	11.28	0.17	7.23	2.92	0.89	0.45	1.75
(3)	PF-22	46.54	2.83	12.60	12.57	11.30	0.16	9.44	3.21	0.90	0.44	-
	Shield 'olivine-rich'											
(1)	68 MT0282	42.61	1.56	6.53	15.28	26.84	0.18	5.14	1.27	0.40	0.19	0.71
(3)	PIN-8	43.97	1.89	9.71	13.90	21.04	-	7.75	1.51	0.05	0.18	-
(3)	VER,NO,16	44.14	1.98	8.59	13.99	21.86	0.16	6.79	1.70	0.53	0.25	-
(3)	PF-10	45.95	2.42	10.78	13.19	15.53	0.17	8.96	2.07	0.62	0.31	-
(3)	PIN-12	44.73	1.96	9.62	13.61	19.81	0.17	7.97	1.65	0.26	0.22	-
	Rejuvenated 'high-Mg'											
(1)	40MT0383	41.62	3.51	12.97	14.95	10.05	0.22	10.80	4.30	0.87	0.72	1.29
(3)	PF-21	42.99	2.92	12.81	13.20	11.85	0.22	9.68	3.88	1.74	0.71	-
	Rejuvenated 'low-Mg'											
(2)	18003	43.46	2.93	13.85	12.70	9.88	0.24	10.29	3.72	2.17	0.75	0.00
(2)	17975	44.20	2.86	13.46	12.34	9.78	0.22	11.12	4.54	0.79	0.69	1.24
(2)	17920	45.36	2.67	13.52	12.35	9.84	0.23	9.36	4.13	1.75	0.78	0.00
(2)	17910	43.82	2.99	13.73	12.50	9.83	0.22	10.51	3.99	1.68	0.73	0.00
(2)	18022	43.97	3.19	13.88	14.35	8.29	0.21	9.72	3.92	1.69	0.78	0.08
(3)	PV-1	44.93	2.58	13.37	12.94	10.58	-	9.49	3.57	1.81	0.74	-
(3)	PF-6	42.88	2.81	12.99	12.94	11.49	0.20	10.71	4.68	0.70	0.60	-
(3)	PF-7	43.83	2.99	13.12	13.05	11.89	0.21	9.88	2.75	1.55	0.72	-
(3)	PF-9	42.17	2.72	13.07	13.26	11.70	0.21	10.65	4.36	1.30	0.57	-
(3)	PF-16	43.42	2.40	12.61	13.57	13.52	0.20	9.41	3.17	1.22	0.48	-
(3)	PF-17	43.47	2.91	12.87	12.56	12.42	0.20	9.52	3.71	1.65	0.69	-
(3)	PF-19	43.65	2.36	12.60	13.03	13.67	0.20	9.64	3.20	1.20	0.45	-
(3)	PF-20	43.41	2.63	13.48	13.33	11.26	0.21	9.94	3.47	1.53	0.73	-

Table II.S.3. EPMA data (wt%) of clinopyroxene in Robinson Crusoe Island. Only clinopyroxenes with good structural formula are considered (cations equal to 4.00 ± 0.02), except for anomalous cores in 'low-Mg' group (on italics) reported despite their bas structural formula due to their rare composition. (A) Clinopyroxene pressure in anhydrous basalts from Nimis and Ulmer, 1989 (±1.7 kbar + ca. 1 kbar per 1wt% H_2O in the melt). (B) $^{Cpx\text{-}Liq}Kd$ calculated assuming 90% of total iron is ferrous in the liquid (whole rock). (C) Clinopyroxene-liquid temperature from Putirka et al., 2003 (±33 °C). (*) Negatives pressures (slightly < 0.0 kbar) are considered as 0.0 (see section 4.3.1 for details).

Sample	Spot	SiO_2	TiO_2	Al_2O_3	FeO^T	MgO	MnO	CaO	Na_2O	Cr_2O_3	Sum	Wo	Cpx_{an}	Cpx-Liq	
Det. limit		*0.02*	*0.03*	*0.01*	*0.02*	*0.01*	*0.02*	*0.01*	*0.01*	*0.02*			P(kbar)[A]	Kd[B]	T (°C)[C]
Shield 'differentiated'															
LL230711-7	Cpx-1	51.58	0.83	3.27	4.73	16.64	0.07	21.47	0.30	0.91	99.79	44.4	1.4	0.12	
	Cpx-2	50.58	1.27	4.26	5.16	15.76	0.11	21.41	0.29	0.89	99.73	45.1	1.8	0.15	
	Cpx-3	51.03	1.18	4.06	5.11	16.30	0.15	20.94	0.33	0.92	100.02	43.9	2.3	0.15	
	Cpx-4	51.04	1.21	3.10	5.84	16.30	0.17	21.17	0.29	0.16	99.27	43.6	0.0	0.15	
	Cpx-5	51.52	1.11	2.63	6.59	16.32	0.18	20.75	0.26	0.09	99.46	42.6	0.0(*)	0.18	
	Cpx-6	50.26	1.11	4.99	5.28	15.88	0.11	21.18	0.28	0.42	99.50	44.6	3.2	0.14	
	Cpx-7	50.89	1.15	3.94	5.31	16.04	0.11	21.39	0.30	0.79	99.94	44.6	1.5	0.15	
LL250711-1	Cpx-1	48.95	2.23	5.16	6.45	14.40	0.11	21.90	0.42	0.55	100.18	46.5	0.4	0.21	
	Cpx-2	48.77	2.20	5.42	6.28	14.46	0.08	21.83	0.39	0.63	100.05	46.5	0.9	0.20	
	Cpx-3	50.87	1.90	3.12	7.09	14.89	0.11	21.40	0.33	0.17	99.89	44.8	0.0(*)	0.27	1162
	Cpx-4	49.78	2.01	4.20	6.40	14.89	0.15	21.79	0.37	0.50	100.09	45.8	0.0(*)	0.21	
	Cpx-5	49.48	1.84	5.08	6.16	14.76	0.12	21.94	0.42	0.87	100.67	46.3	1.0	0.19	
	Cpx-6	46.27	3.61	7.24	7.44	12.90	0.17	21.47	0.54	0.17	99.80	47.3	1.1	0.27	1194
	Cpx-7	49.17	1.96	5.26	6.08	14.52	0.10	21.96	0.33	0.65	100.02	46.7	1.0	0.21	
LL260711-3	Cpx-1	49.78	1.88	4.54	6.23	15.11	0.14	21.08	0.37	1.08	100.20	44.8	1.0	0.17	
	Cpx-2	51.73	1.34	2.81	6.00	16.20	0.16	21.36	0.32	0.63	100.54	43.9	0.0(*)	0.15	
	Cpx-3	52.12	1.26	3.00	5.92	16.13	0.11	21.37	0.36	0.77	101.04	44.0	0.2	0.16	
	Cpx-4	51.97	1.42	2.50	6.25	15.80	0.17	21.25	0.31	0.26	99.92	44.0	0.0(*)	0.18	
	Cpx-5	51.86	1.21	2.80	5.98	15.69	0.15	21.48	0.29	0.46	99.93	44.7	0.0(*)	0.17	
	Cpx-6	51.07	1.56	3.33	5.91	15.09	0.14	21.63	0.31	0.45	99.50	45.7	0.0(*)	0.17	
	Cpx-7	51.83	1.23	2.59	6.22	15.74	0.11	20.87	0.32	0.34	99.24	43.7	0.0	0.18	
	Cpx-8	51.42	1.39	2.86	5.74	15.62	0.13	21.16	0.33	0.72	99.38	44.6	0.0	0.16	
	Cpx-9	51.72	0.98	2.65	5.95	15.76	0.16	20.92	0.28	0.50	98.90	43.9	0.3	0.17	
	Cpx-10	50.80	1.16	2.94	5.83	15.50	0.14	21.02	0.27	0.79	98.45	44.5	0.0(*)	0.17	
	Cpx-11	50.92	1.87	4.11	5.88	15.14	0.14	21.42	0.38	0.66	100.52	45.4	1.0	0.17	
	Cpx-12	52.16	1.25	2.80	5.76	15.97	0.15	21.40	0.29	0.39	100.16	44.4	0.1	0.16	
JR160913-13	Cpx-1	52.03	1.11	2.96	5.17	16.13	0.09	21.62	0.26	0.53	99.88	44.9	0.5	0.18	
	Cpx-2	49.42	1.95	5.15	5.55	14.74	0.09	21.55	0.29	0.80	99.54	46.4	1.7	0.21	
	Cpx-3	50.02	1.59	4.60	5.44	14.85	0.12	21.84	0.32	0.79	99.57	46.6	1.2	0.20	
	Cpx-4	51.97	1.38	2.71	6.30	16.32	0.14	20.61	0.23	0.30	99.94	42.6	0.1	0.22	
	Cpx-5	48.55	2.35	5.85	6.13	14.38	0.13	21.27	0.24	0.71	99.61	46.1	1.8	0.24	1167
	Cpx-6	51.37	1.46	3.27	6.48	16.47	0.17	20.13	0.16	0.31	99.81	41.7	0.7	0.22	
	Cpx-7	51.57	1.08	3.04	5.06	16.15	0.11	21.64	0.32	0.59	99.55	45.0	0.5	0.16	
	Cpx-8	48.86	1.79	5.30	5.64	14.69	0.09	21.64	0.29	0.96	99.25	46.5	1.6	0.19	
	Cpx-9	48.56	2.30	5.98	6.31	14.22	0.13	21.16	0.37	0.49	99.52	46.0	2.3	0.24	1182
	Cpx-10	49.93	1.40	4.77	5.44	14.95	0.11	21.67	0.32	0.74	99.32	46.3	1.9	0.19	
	Cpx-11	49.70	1.81	5.39	5.82	14.84	0.17	21.51	0.25	0.59	100.07	45.9	2.1	0.22	
	Cpx-12	50.95	1.34	3.63	5.54	16.04	0.20	21.09	0.24	0.53	99.56	44.0	0.9	0.19	
	Cpx-13	52.15	1.12	2.99	5.08	16.35	0.14	21.33	0.30	0.60	100.04	44.3	1.0	0.17	
	Cpx-14	48.96	2.14	5.47	5.74	14.77	0.14	21.53	0.36	1.02	100.12	46.1	1.7	0.19	
	Cpx-15	49.64	2.17	5.42	5.78	14.88	0.09	21.31	0.31	0.84	100.44	45.7	2.2	0.22	
	Cpx-16	50.34	1.39	4.47	5.30	15.05	0.08	21.86	0.27	0.85	99.61	46.5	1.4	0.20	
	Cpx-17	48.33	2.72	6.22	6.42	14.03	0.12	21.23	0.32	0.62	100.01	46.3	1.9	0.26	1177
	Cpx-18	48.83	2.39	4.59	9.69	13.09	0.22	20.72	0.50	0.03	100.04	44.4	0.0(*)	0.37	
LL220112-3	Cpx-1	49.84	1.51	4.11	6.09	15.11	0.12	21.57	0.27	0.47	99.08	45.5	0.2	0.24	1184
	Cpx-2	50.04	1.35	4.21	6.34	15.30	0.15	21.32	0.32	0.23	99.26	44.7	0.8	0.23	
	Cpx-3	49.76	1.65	3.40	8.64	14.78	0.20	20.01	0.33	0.06	98.84	42.1	0.0(*)	0.35	
	Cpx-4	51.42	1.36	4.26	5.23	15.70	0.12	21.72	0.32	0.94	101.06	45.5	1.8	0.22	
	Cpx-5	51.86	1.16	3.09	6.07	15.92	0.13	21.53	0.27	0.15	100.18	44.4	0.0(*)	0.24	1182
	Cpx-6	51.29	1.02	3.08	6.16	16.10	0.14	21.39	0.32	0.21	99.70	43.9	0.0(*)	0.21	
	Cpx-7	50.11	1.30	4.24	6.36	15.24	0.16	21.66	0.28	0.27	99.61	45.2	0.4	0.23	

	Cpx-8	52.48	1.20	3.10	6.08	15.94	0.19	21.40	0.27	0.21	100.87	44.2	0.6	0.25	1184
	Cpx-9	51.80	1.44	2.92	8.09	15.52	0.19	20.22	0.39	0.00	100.57	41.9	0.0(*)	0.33	
	Cpx-10	49.69	2.31	4.60	8.54	13.97	0.14	20.34	0.37	0.13	100.08	43.7	0.0(*)	0.41	
	Cpx-11	47.73	2.76	6.87	7.23	14.18	0.17	20.50	0.25	0.69	100.38	44.6	2.6	0.32	
LL240711-1	Cpx-1	49.87	1.49	4.38	5.84	14.91	0.16	21.36	0.27	0.46	98.74	45.7	1.1	0.21	
	Cpx-2	50.22	1.45	4.68	5.95	15.24	0.14	20.92	0.30	0.45	99.34	44.6	2.2	0.22	
	Cpx-3	48.56	2.18	5.82	7.02	14.28	0.13	20.52	0.30	0.22	99.03	44.6	2.3	0.27	1177
	Cpx-5	46.44	2.94	6.94	7.44	13.23	0.14	20.63	0.36	0.40	98.52	45.9	2.0	0.29	1185
	Cpx-6	46.53	3.01	7.05	7.57	13.49	0.17	20.60	0.41	0.38	99.21	45.4	2.1	0.27	1190
	Cpx-8	47.72	2.35	5.86	7.70	13.48	0.14	21.02	0.36	0.14	98.77	45.8	0.8	0.28	1179
	Cpx-9	49.32	1.83	5.23	6.17	14.84	0.16	21.12	0.32	0.38	99.36	45.2	1.9	0.22	
	Cpx-10	50.22	1.55	4.50	5.90	15.05	0.14	21.47	0.29	0.42	99.53	45.6	1.2	0.21	
	Cpx-11	51.79	1.10	3.37	5.65	15.95	0.15	21.12	0.31	0.41	99.84	44.2	1.3	0.20	
	Cpx-12	48.84	2.24	5.90	7.01	14.20	0.13	20.89	0.36	0.24	99.80	45.2	2.2	0.26	1182
	Cpx-13	51.68	1.20	3.17	5.47	16.02	0.16	21.23	0.30	0.36	99.59	44.3	0.7	0.19	
	Cpx-14	50.00	2.00	4.74	5.96	15.38	0.15	21.49	0.34	0.51	100.56	45.1	1.0	0.19	
	Cpx-15	48.84	1.94	5.76	7.01	14.58	0.15	20.58	0.34	0.15	99.36	44.3	2.5	0.25	1181
LL250711-9	Cpx-1	50.03	1.46	4.99	5.94	15.25	0.14	21.19	0.33	0.73	100.06	44.9	2.3	0.22	
	Cpx-2	50.12	1.76	4.95	5.68	14.99	0.03	21.26	0.32	0.77	99.88	45.6	2.4	0.23	
	Cpx-3	50.72	1.48	4.24	5.46	15.59	0.08	21.32	0.30	0.71	99.89	45.0	1.6	0.21	
	Cpx-4	51.33	1.11	2.82	5.56	16.19	0.09	21.13	0.29	0.46	98.98	44.0	0.1	0.20	
	Cpx-5	49.69	1.77	4.66	5.87	14.96	0.14	21.66	0.29	0.76	99.80	45.9	0.8	0.22	
	Cpx-6	51.59	1.14	2.86	5.52	16.12	0.12	20.92	0.26	0.52	99.04	43.8	0.6	0.21	
	Cpx-7	49.13	1.62	4.95	5.92	15.05	0.11	21.58	0.27	0.75	99.37	45.7	1.1	0.20	
	Cpx-8	50.93	0.98	3.10	5.47	15.88	0.12	21.74	0.29	0.47	98.97	45.1	0.0(*)	0.18	
	Cpx-9	50.18	1.37	4.14	5.57	15.19	0.09	21.85	0.35	0.68	99.41	46.1	0.8	0.20	
	Cpx-10	51.69	0.80	2.74	5.55	16.26	0.09	20.94	0.35	0.40	98.81	43.7	0.8	0.20	
	Cpx-11	50.65	1.79	3.25	7.32	14.80	0.19	21.26	0.30	0.13	99.67	44.6	0.0(*)	0.30	1174
Shield 'near-primitive'															
LL250711-7	Cpx-1	52.24	0.83	2.69	5.88	16.34	0.13	20.80	0.23	0.26	99.40	43.1	0.8	0.30	1205
	Cpx-2	50.34	1.41	4.08	6.16	15.44	0.12	20.78	0.24	0.38	98.94	44.1	1.2	0.33	
	Cpx-3	51.05	1.11	3.57	5.93	15.84	0.14	20.73	0.30	0.36	99.03	43.6	1.4	0.30	1217
	Cpx-5	51.10	1.20	3.93	5.60	15.65	0.16	20.99	0.32	0.80	99.74	44.4	1.9	0.30	1221
	Cpx-6	50.61	1.25	3.89	6.02	15.46	0.15	20.88	0.30	0.51	99.07	44.2	1.3	0.31	
	Cpx-7	50.97	0.96	3.93	5.45	15.68	0.13	21.15	0.29	0.92	99.48	44.7	1.9	0.28	1217
	Cpx-8	51.98	0.84	3.09	5.67	16.09	0.13	21.12	0.25	0.41	99.58	44.0	1.1	0.29	1207
	Cpx-9	51.58	1.16	3.56	6.08	15.95	0.15	20.89	0.30	0.28	99.96	43.6	1.3	0.31	
	Cpx-10	49.23	1.90	5.46	6.98	15.02	0.17	19.91	0.32	0.36	99.35	42.9	2.9	0.37	
	Cpx-11	51.65	1.12	2.76	5.94	16.35	0.11	20.55	0.24	0.28	98.99	42.8	0.5	0.30	1206
JR290513-5	Cpx-1	49.99	2.02	4.56	6.46	14.49	0.11	21.72	0.44	0.67	100.46	46.2	0.3	0.39	
	Cpx-2	50.15	1.73	4.40	6.22	14.58	0.13	21.91	0.33	0.70	100.15	46.5	0.2	0.38	
	Cpx-3	50.07	2.10	4.09	6.71	14.31	0.12	21.77	0.39	0.49	100.04	46.3	0.0(*)	0.43	
	Cpx-4	51.54	1.34	2.85	6.09	15.35	0.17	21.45	0.35	0.53	99.67	45.0	0.0(*)	0.37	
	Cpx-5	49.98	2.19	4.08	6.94	14.17	0.10	21.62	0.36	0.29	99.73	46.2	0.0(*)	0.46	
	Cpx-6	51.13	1.84	3.43	6.63	14.92	0.13	21.55	0.33	0.39	100.35	45.3	0.0(*)	0.41	
	Cpx-7	50.54	1.98	4.31	6.64	14.65	0.14	21.30	0.38	0.43	100.37	45.3	0.6	0.42	
	Cpx-8	49.47	2.11	5.01	6.15	14.16	0.15	21.99	0.36	0.78	100.16	47.2	0.5	0.39	
	Cpx-9	49.22	2.01	5.02	6.24	14.24	0.12	21.85	0.33	0.50	99.53	46.9	0.6	0.38	
Rejuvenated 'high-Mg'															
JR220112-3	Cpx-1	50.10	1.92	5.14	7.46	15.03	0.12	20.74	0.40	0.55	101.45	43.6	1.6	0.58	
	Cpx-3	48.22	2.56	7.19	6.04	13.43	0.10	23.39	0.31	0.16	101.39	49.9	1.5	0.49	
	Cpx-5	48.95	2.48	5.27	8.18	14.07	0.15	21.38	0.29	0.17	100.93	45.0	0.0(*)	0.67	
	Cpx-7	45.47	3.49	9.96	7.23	11.53	0.12	22.85	0.43	0.05	101.14	51.2	3.7	0.69	
	Cpx-10	48.04	2.92	7.09	7.26	12.29	0.18	22.91	0.64	0.02	101.34	50.0	1.1	0.65	
JR250112-3	Cpx-1	45.74	3.28	9.09	6.32	12.31	0.09	23.11	0.40	0.30	100.63	51.1	3.0	0.49	
	Cpx-3	45.65	3.42	8.89	6.42	12.38	0.08	23.12	0.40	0.28	100.64	50.9	2.4	0.48	
	Cpx-4	49.82	2.03	5.33	5.92	14.45	0.11	22.99	0.31	0.14	101.09	48.1	0.3	0.43	
	Cpx-5	50.49	1.69	4.55	5.18	15.02	0.13	23.22	0.33	0.56	101.17	48.1	0.0	0.34	
Rejuvenated 'low-Mg'															
LL230711-2	Cpx-2	49.07	1.52	5.04	5.63	14.47	0.12	22.03	0.49	0.35	98.72	47.2	1.7	0.30	
	Cpx-3	49.01	1.48	5.26	5.44	14.58	0.10	21.79	0.52	0.33	98.50	47.0	2.5	0.29	
	Cpx-4	47.17	1.85	8.33	6.56	13.29	0.15	19.81	0.95	0.05	98.15	45.5	8.5	0.40	
	Cpx-5	46.37	2.24	9.94	6.69	12.95	0.16	19.75	0.95	0.07	99.12	45.8	10.3	0.41	
	Cpx-6	47.32	2.15	7.84	5.73	13.59	0.12	21.74	0.56	0.13	99.17	48.1	5.2	0.33	
	Cpx-7	48.28	1.67	7.38	5.26	14.00	0.15	21.51	0.70	0.45	99.40	47.6	6.2	0.29	
	Cpx-8	49.32	1.62	4.82	5.49	14.62	0.17	22.18	0.49	0.33	99.03	47.3	1.3	0.29	
	Cpx-10	46.41	2.51	9.53	6.01	13.04	0.13	19.72	0.93	0.05	98.33	46.2	10.0	0.41	

	Cpx-11	47.61	1.54	8.90	6.00	13.40	0.17	19.98	1.11	0.28	98.97	46.0	10.4	0.33
	Cpx-12	47.56	1.47	8.97	5.92	13.20	0.13	19.85	1.04	0.18	98.31	46.2	10.8	0.38
JR020613-3	Cpx-2	51.26	1.62	4.17	5.86	14.60	0.14	23.08	0.45	0.29	101.47	48.0	0.0(*)	0.34
	Cpx-7	45.21	4.26	8.30	9.02	10.83	0.23	22.15	0.66	0.02	100.66	49.8	0.0(*)	0.66
	Cpx-8	48.90	2.12	6.03	6.82	13.65	0.13	22.90	0.48	0.23	101.26	48.4	0.7	0.35
	Cpx-9	52.98	0.32	4.49	3.25	16.57	0.07	22.68	0.43	0.89	101.69	46.9	4.5	0.17
	Cpx-10	50.80	1.71	4.23	6.23	14.62	0.14	22.65	0.38	0.27	101.02	47.2	0.0(*)	0.36
	Cpx-12	50.99	1.23	7.02	4.68	14.36	0.12	20.78	1.25	0.63	101.06	46.7	9.5	0.28
	Cpx-14	49.66	2.03	4.99	6.95	13.90	0.18	22.91	0.41	0.15	101.18	47.9	0.0(*)	0.38
JR160913-2	Cpx-1	47.56	2.15	9.29	8.40	11.98	0.13	20.50	1.06	0.00	101.07	46.8	8.0	0.49
	Cpx-2	51.20	1.13	5.31	5.70	15.09	0.12	21.40	0.57	0.51	101.03	45.6	4.2	0.30
	Cpx-4	49.15	1.61	7.75	6.57	13.61	0.19	21.38	0.77	0.04	101.06	46.9	6.5	0.34
	Cpx-5	**46.66**	**2.19**	**8.89**	**11.19**	**8.94**	**0.35**	**20.63**	**1.70**	**0.00**	**100.54**	**49.0**	**-**	**0.81**
	Cpx-7	49.09	1.52	7.89	5.93	13.83	0.14	21.35	0.78	0.69	101.23	47.1	7.2	0.30
	Cpx-8	46.72	2.42	8.32	6.51	12.60	0.16	22.06	0.61	0.60	100.00	49.2	4.5	0.34
	Cpx-10	49.12	1.54	7.44	6.31	13.54	0.17	21.52	0.75	0.01	100.41	47.4	6.1	0.33
	Cpx-11	**46.75**	**2.45**	**9.41**	**10.64**	**9.32**	**0.29**	**20.63**	**1.52**	**0.00**	**101.02**	**49.0**	**-**	**0.79**
	Cpx-12	49.22	1.45	7.98	5.99	13.79	0.13	20.96	0.84	0.76	101.13	46.7	8.0	0.32
	Cpx-15	50.00	1.69	5.20	6.46	14.11	0.09	22.40	0.48	0.16	100.58	47.5	1.1	0.34
	Cpx-16	49.39	1.58	6.91	5.94	14.05	0.14	21.31	0.69	0.60	100.61	46.7	5.6	0.31
	Cpx-18	48.25	1.51	7.67	5.85	13.50	0.11	21.15	0.86	0.73	99.64	47.4	7.1	0.28
LL010213-6	Cpx-4	49.24	2.14	5.29	7.22	13.74	0.21	22.11	0.48	0.01	100.45	47.0	0.2	0.34
	Cpx-6	48.91	2.22	5.40	7.36	13.58	0.15	22.42	0.53	0.01	100.58	47.5	0.0(*)	0.32
	Cpx-8	49.01	2.20	5.52	7.48	13.65	0.15	22.21	0.47	0.01	100.70	47.1	0.1	0.34
LL220112-4	Cpx-1	47.15	2.05	7.69	6.80	12.50	0.18	21.28	0.69	0.24	98.59	48.2	5.0	0.41
	Cpx-2	47.67	2.16	7.39	7.18	12.89	0.12	21.72	0.69	0.32	100.12	47.9	3.7	0.38
	Cpx-3	47.10	2.48	7.76	6.71	12.60	0.10	21.97	0.61	0.56	99.88	49.0	3.6	0.39
	Cpx-4	50.81	1.35	4.13	6.56	14.73	0.19	21.94	0.50	0.20	100.41	46.0	0.6	0.33
	Cpx-5	50.12	1.60	4.64	6.71	14.30	0.17	22.04	0.47	0.05	100.11	46.6	0.5	0.36
	Cpx-6	49.25	1.73	4.55	6.73	14.01	0.16	22.24	0.43	0.09	99.20	47.2	0.0(*)	0.34
	Cpx-7	45.74	3.33	8.80	8.18	11.58	0.17	22.26	0.55	0.01	100.62	49.6	2.3	0.50
	Cpx-12	50.46	1.59	4.37	6.36	14.38	0.19	21.95	0.52	0.28	100.08	46.6	0.7	0.35
	Cpx-15	50.75	1.53	4.04	6.49	14.44	0.12	22.13	0.42	0.25	100.15	46.7	0.0(*)	0.37
	Cpx-19	49.49	1.70	5.01	7.20	14.17	0.16	21.75	0.57	0.17	100.21	46.1	0.9	0.35
	Cpx-20	49.61	1.65	4.44	6.63	14.31	0.15	22.24	0.42	0.13	99.58	46.9	0.0(*)	0.33
	Cpx-21	48.20	2.30	5.65	8.05	13.03	0.17	22.10	0.38	0.01	99.88	47.4	0.0(*)	0.46
	Cpx-22	49.45	1.93	4.53	6.86	13.94	0.16	22.55	0.47	0.01	99.90	47.5	0.0(*)	0.34
	Cpx-26	50.81	1.52	4.07	6.45	14.64	0.17	22.09	0.56	0.31	100.62	46.4	0.3	0.33
	Cpx-27	48.41	2.11	5.23	7.50	13.42	0.13	22.16	0.45	0.02	99.44	47.4	0.0(*)	0.39
	Cpx-29	49.98	1.48	4.57	6.57	14.66	0.12	21.60	0.53	0.31	99.82	45.7	1.2	0.32
	Cpx-30	49.68	1.83	4.37	6.81	13.84	0.21	22.47	0.42	0.04	99.66	47.6	0.0(*)	0.38
Spinel lherzolite														
JF-2A	Cpx-1	51.22	0.68	6.88	3.48	14.97	0.12	20.73	1.36	0.73	100.17	46.9	11.0	
	Cpx-2	51.58	0.62	6.54	3.44	15.04	0.12	20.55	1.35	0.78	99.99	47.3	10.9	
	Cpx-3	52.67	0.37	5.49	3.30	15.79	0.07	21.08	1.27	0.61	100.64	48.1	9.3	
	Cpx-4	52.38	0.29	5.39	3.24	15.68	0.11	21.01	1.23	0.61	99.94	48.0	9.2	
	Cpx-6	52.37	0.42	5.63	3.26	15.66	0.07	20.85	1.27	0.68	100.19	48.2	9.7	
	Cpx-7	52.54	0.26	5.38	3.16	15.69	0.11	21.19	1.12	0.68	100.12	47.9	8.9	
	Cpx-8	50.83	0.93	6.38	3.63	15.37	0.11	20.50	1.13	0.66	99.53	47.7	9.5	
	Cpx-9	51.34	0.72	6.18	3.71	15.65	0.09	20.47	1.08	0.65	99.88	48.2	9.4	
	Cpx-10	51.47	0.59	5.89	3.73	15.85	0.05	20.18	1.07	0.71	99.53	48.8	9.4	
	Cpx-11	50.94	0.69	6.17	3.66	15.67	0.11	20.57	1.12	0.64	99.56	48.1	9.2	
	Cpx-12	50.98	0.70	6.05	3.59	15.57	0.09	20.60	1.10	0.73	99.41	48.0	9.1	
	Cpx-13	51.93	0.42	5.81	3.68	15.74	0.09	20.50	1.09	0.75	100.00	48.3	9.4	

Table II.S.4. EPMA data (wt%) of olivine in Robinson Crusoe Island. Only olivines with good structural formula are considered (cations equal to 3.00 ± 0.02). For rejuvenated unit; c: core; r: rim; m: mantle xenocryst; s: shield-like xenocryst. (A) $^{Ol\text{-}Liq}$Kd calculated assuming 90% of total iron is ferrous in the liquid (whole rock). (B) Olivine-liquid temperature from Herzberg and O'Hara, 2002 (±31 °C). (*) Temperatures in low-Mg cores (in textural disequilibrium) are not considered. (**) Temperatures in xenoliths are not considered despite their chemical equilibrium according $^{Ol\text{-}Liq}$Kd.

Sample	Spot	SiO_2	FeO^T	MgO	MnO	CaO	NiO	Sum	Fo	Ol-Liq	
Det. limit		*0.02*	*0.02*	*0.01*	*0.02*	*0.01*	*0.02*			$K_D^{(A)}$	T (°C)$^{(B)}$
Shield 'differentiated'											
LL260711-3	Ol-1	38.45	15.93	44.59	0.24	0.24	0.27	99.71	83.3	0.16	
	Ol-2	38.68	15.93	44.49	0.24	0.25	0.23	99.83	83.3	0.16	
	Ol-3	38.93	16.31	44.15	0.25	0.26	0.22	100.13	82.8	0.16	
	Ol-4	38.37	16.02	44.05	0.19	0.33	0.15	99.11	83.1	0.16	
	Ol-5	38.74	13.95	45.16	0.17	0.31	0.24	98.55	85.2	0.14	
	Ol-6	38.75	14.27	45.33	0.20	0.29	0.30	99.14	85.0	0.14	
	Ol-7	39.20	19.55	41.20	0.29	0.38	0.14	100.76	79.0	0.21	
LL220112-3	Ol-1	39.36	12.55	47.05	0.22	0.24	0.27	99.69	87.0	0.18	
	Ol-2	39.25	13.09	46.52	0.21	0.26	0.34	99.66	86.4	0.19	
	Ol-3	39.13	14.99	45.32	0.25	0.29	0.26	100.23	84.3	0.22	
	Ol-4	38.48	17.56	43.29	0.21	0.29	0.14	99.97	81.5	0.27	1179
	Ol-5	38.49	17.37	43.35	0.18	0.34	0.14	99.88	81.7	0.27	1179
	Ol-6	38.76	17.83	43.51	0.32	0.32	0.23	100.96	81.3	0.27	1180
	Ol-7	38.48	17.40	43.35	0.26	0.31	0.17	99.98	81.6	0.27	1179
	Ol-8	38.90	16.25	44.63	0.26	0.34	0.19	100.56	83.0	0.24	
	Ol-9	39.25	13.89	46.23	0.25	0.25	0.21	100.08	85.6	0.20	
	Ol-10	39.15	13.82	46.05	0.19	0.32	0.22	99.74	85.6	0.20	
	Ol-11	39.00	15.86	44.47	0.19	0.30	0.19	100.00	83.3	0.24	
	Ol-12	38.46	16.38	43.47	0.23	0.26	0.24	99.04	82.5	0.25	
	Ol-13	38.65	17.71	43.04	0.26	0.24	0.18	100.07	81.2	0.27	1181
	Ol-14	38.64	17.72	43.07	0.26	0.29	0.12	100.09	81.2	0.27	1181
	Ol-15	39.10	13.89	46.42	0.16	0.25	0.23	100.05	85.6	0.20	
	Ol-16	39.11	14.49	45.84	0.22	0.30	0.23	100.18	84.9	0.21	
LL240711-1	Ol-1	38.36	19.12	41.56	0.28	0.26	0.11	99.69	79.5	0.26	
	Ol-2	38.43	17.07	43.30	0.22	0.28	0.10	99.40	81.9	0.22	
	Ol-3	38.38	17.91	42.51	0.26	0.28	0.14	99.47	80.9	0.24	
	Ol-4	38.18	18.86	41.81	0.28	0.28	0.07	99.48	79.8	0.25	
	Ol-5	37.63	20.31	40.60	0.31	0.25	0.09	99.18	78.1	0.28	1156
	Ol-6	38.40	17.65	43.10	0.25	0.26	0.10	99.77	81.3	0.23	
	Ol-7	38.30	17.76	43.25	0.25	0.24	0.12	99.93	81.3	0.23	
	Ol-8	38.29	18.05	42.67	0.28	0.26	0.14	99.69	80.8	0.24	
	Ol-9	38.28	17.65	42.85	0.24	0.24	0.10	99.35	81.2	0.23	
	Ol-10	38.10	17.40	43.09	0.27	0.26	0.10	99.22	81.5	0.23	
	Ol-11	38.17	18.02	42.95	0.25	0.31	0.09	99.79	80.9	0.24	
LL250711-9	Ol-1	38.69	16.66	43.60	0.24	0.29	0.03	99.51	82.3	0.24	
	Ol-2	37.98	17.96	42.67	0.26	0.30	0.14	99.32	80.9	0.26	
	Ol-3	38.01	17.40	42.37	0.28	0.30	0.13	98.48	81.3	0.25	
Shield 'near-primitive'											
LL250711-7	Ol-1	38.97	13.04	46.35	0.22	0.23	0.30	99.11	86.4	0.23	
	Ol-2	38.60	13.08	45.94	0.20	0.22	0.26	98.31	86.2	0.24	
	Ol-3	39.05	13.54	45.61	0.19	0.25	0.27	98.91	85.7	0.25	
	Ol-4	39.11	13.76	45.84	0.23	0.27	0.25	99.45	85.6	0.25	
	Ol-5	39.05	12.87	46.59	0.21	0.26	0.29	99.27	86.6	0.23	
	Ol-6	38.72	12.88	46.48	0.18	0.23	0.21	98.70	86.5	0.23	
	Ol-7	39.09	12.81	46.13	0.20	0.23	0.19	98.65	86.5	0.23	
JR290513-2	Ol-1	39.09	13.76	46.07	0.17	0.33	0.23	99.66	85.6	0.35	
	Ol-2	39.66	13.03	47.22	0.20	0.26	0.25	100.61	86.6	0.32	1321
	Ol-3	38.87	15.33	45.20	0.20	0.33	0.23	100.15	84.0	0.40	
	Ol-4	39.06	15.41	45.37	0.21	0.28	0.26	100.58	84.0	0.40	
	Ol-5	38.73	14.80	45.21	0.18	0.28	0.25	99.44	84.5	0.38	
	Ol-6	38.95	14.74	45.68	0.23	0.28	0.23	100.10	84.7	0.38	
	Ol-7	39.17	14.55	45.49	0.23	0.30	0.19	99.94	84.8	0.38	
	Ol-8	38.70	14.47	45.28	0.21	0.29	0.22	99.17	84.8	0.38	

	Ol-9		39.26	14.86	45.52	0.22	0.29	0.19	100.34	84.5	0.38	
	Ol-10		38.71	16.25	44.55	0.27	0.31	0.24	100.31	83.0	0.43	
	Ol-11		39.40	13.71	46.27	0.21	0.25	0.28	100.11	85.7	0.35	
	Ol-12		39.00	15.71	44.93	0.23	0.32	0.22	100.42	83.6	0.41	
JR290513-5	Ol-1		39.27	12.57	47.12	0.11	0.27	0.24	99.58	87.0	0.25	
	Ol-2		38.02	21.04	40.56	0.28	0.30	0.16	100.35	77.5	0.48	
	Ol-3		38.11	20.59	40.92	0.33	0.35	0.18	100.47	78.0	0.47	
	Ol-4		37.64	22.32	39.64	0.37	0.36	0.13	100.47	76.0	0.53	
	Ol-5		37.90	19.87	41.37	0.31	0.36	0.13	99.94	78.8	0.45	
	Ol-6		37.99	20.65	40.13	0.28	0.36	0.17	99.58	77.6	0.48	
	Ol-7		37.75	21.25	40.22	0.34	0.37	0.17	100.10	77.1	0.49	
	Ol-9		37.73	21.07	39.86	0.25	0.35	0.19	99.45	77.1	0.49	
	Ol-10		37.80	21.18	40.39	0.29	0.28	0.18	100.13	77.3	0.49	
	Ol-11		37.60	20.81	39.98	0.34	0.32	0.16	99.20	77.4	0.49	
Shield 'olivine-rich'												
LL250711-5	Ol-2		39.43	12.11	47.98	0.18	0.23	0.28	100.22	87.6	0.40	
	Ol-4		38.93	12.34	47.07	0.24	0.24	0.34	99.16	87.2	0.41	
	Ol-5		38.78	13.15	46.28	0.20	0.27	0.30	98.97	86.3	0.45	
Rejuvenated 'high-Mg'												
JR220112-3	Ol-1	s	38.59	15.54	45.14	0.17	0.16	-	99.60	83.8	0.45	
	Ol-2	c	39.32	12.91	47.34	0.21	0.26	0.07	100.11	86.7	0.36	
	Ol-4	c	39.81	11.34	48.50	0.17	0.23	0.25	100.29	88.4	0.30	1351
	Ol-5	c	39.71	10.56	49.24	0.13	0.19	0.31	100.14	89.3	0.28	1346
	Ol-6	c	39.31	12.50	47.35	0.18	0.35	0.23	99.91	87.1	0.34	
	Ol-7	c	39.38	11.91	47.90	0.19	0.25	0.25	99.88	87.8	0.32	1353
	Ol-8	c	39.33	12.11	47.94	0.16	0.28	0.24	100.06	87.6	0.33	1354
	Ol-9	c	39.76	10.81	49.03	0.15	0.24	0.33	100.31	89.0	0.29	1348
	Ol-10	c	39.11	13.03	46.82	0.24	0.27	0.19	99.65	86.5	0.36	
	Ol-11	c	39.42	10.90	48.63	0.17	0.22	0.25	99.59	88.8	0.29	1348
	Ol-12	c	39.40	12.01	48.09	0.19	0.25	0.20	100.15	87.7	0.33	1353
	Ol-14	m	38.99	14.04	46.27	0.22	0.05	0.29	99.85	85.5	0.40	
	Ol-15	c	40.23	11.30	49.22	0.20	0.25	0.24	101.44	88.6	0.30	1350
	Ol-16	c	39.56	13.67	47.34	0.25	0.36	0.17	101.36	86.1	0.38	
	Ol-17	c	39.67	12.12	48.34	0.22	0.30	0.19	100.84	87.7	0.33	1353
	Ol-18	c	39.90	10.97	49.16	0.14	0.18	0.29	100.64	88.9	0.29	1348
JR250112-3	Ol-1	c	38.94	14.50	46.00	0.23	0.28	0.14	100.07	85.0	0.39	
	Ol-2	c	39.45	13.47	47.11	0.28	0.30	0.23	100.83	86.2	0.36	
	Ol-3	c	39.34	11.59	48.14	0.20	0.26	0.23	99.75	88.1	0.30	1321
	Ol-4	c	39.59	12.27	47.96	0.21	0.26	0.26	100.55	87.5	0.32	1325
	Ol-5	c	39.64	12.26	47.88	0.18	0.25	0.28	100.47	87.4	0.32	1324
	Ol-6	c	39.08	11.42	48.07	0.19	0.28	0.28	99.30	88.2	0.30	1320
	Ol-8	c	39.29	12.70	47.31	0.25	0.34	0.22	100.11	86.9	0.33	1326
	Ol-9	c	39.46	12.95	47.13	0.20	0.29	0.13	100.16	86.6	0.34	
	Ol-10	c	39.85	12.03	48.75	0.20	0.30	0.16	101.30	87.8	0.31	1322
	Ol-11	c	39.94	12.98	47.41	0.20	0.29	0.18	100.99	86.7	0.34	
	Ol-12	c	40.18	10.61	49.53	0.18	0.22	0.24	100.95	89.3	0.27	1316
	Ol-13	c	40.11	11.73	48.85	0.21	0.28	0.22	101.39	88.1	0.30	1321
	Ol-14	c	39.88	11.56	48.82	0.17	0.27	0.16	100.85	88.3	0.30	1320
	Ol-15	c	40.13	11.47	48.44	0.15	0.27	0.21	100.68	88.3	0.29	1322
	Ol-16	c	40.18	11.15	48.84	0.15	0.23	0.31	100.86	88.6	0.28	1320
Rejuvenated 'low-Mg'												
LL230711-2	Ol-1	s	38.17	18.35	42.63	0.28	0.13	0.06	99.62	80.6	0.44	
	Ol-2	s	38.02	18.28	42.13	0.26	0.12	0.09	98.92	80.4	0.45	
	Ol-3	c	39.46	11.37	47.69	0.17	0.26	0.23	99.18	88.2	0.24	
	Ol-4	r	38.82	15.61	44.71	0.30	0.28	0.14	99.86	83.6	0.36	
	Ol-6	r	38.45	15.76	44.42	0.33	0.33	0.06	99.35	83.4	0.36	
	Ol-7	c	38.83	14.22	45.75	0.18	0.22	0.23	99.43	85.1	0.32	(*)
	Ol-8	c	39.05	12.95	46.22	0.16	0.24	0.16	98.77	86.4	0.29	(*)
	Ol-10	c	39.30	10.05	48.69	0.15	0.22	0.33	98.74	89.6	0.21	
	Ol-11	c	39.33	10.21	48.69	0.12	0.21	0.30	98.85	89.5	0.22	
	Ol-12	r	38.54	15.03	44.48	0.36	0.26	0.17	98.84	84.1	0.35	
	Ol-13	c	39.28	11.19	47.60	0.17	0.24	0.23	98.71	88.3	0.24	
	Ol-14	c	39.16	11.16	47.72	0.15	0.26	0.23	98.67	88.4	0.24	
JR020613-3	Ol-1	c	39.78	10.11	49.15	0.17	0.24	0.32	99.77	89.7	0.19	
	Ol-3	m	40.06	10.40	48.85	0.11	0.08	0.33	99.82	89.3	0.20	
	Ol-5	c	40.19	10.36	48.49	0.19	0.27	0.33	99.81	89.3	0.20	
	Ol-6	c	40.37	10.13	48.86	0.12	0.22	0.31	100.01	89.6	0.20	

	Ol-7	m	40.57	9.88	49.55	0.16	0.02	0.42	100.59	89.9	0.19	
	Ol-8	m	39.85	10.28	49.83	0.13	0.08	0.33	100.50	89.6	0.20	
	Ol-9	r	38.75	16.35	44.70	0.29	0.23	0.16	100.48	83.0	0.35	
	Ol-10	c	40.23	10.15	49.72	0.16	0.25	0.23	100.74	89.7	0.19	
	Ol-11	r	38.87	16.85	44.40	0.40	0.28	0.21	101.02	82.4	0.36	
	Ol-13	m	40.12	10.79	49.06	0.16	0.07	0.29	100.50	89.0	0.21	
JR160913-2	Ol-1	c	39.16	13.64	46.08	0.19	0.23	0.23	99.53	85.8	0.25	
	Ol-2	r	38.92	17.27	43.79	0.37	0.27	0.13	100.75	81.9	0.34	
	Ol-3	c	39.42	13.10	46.93	0.27	0.25	0.20	100.15	86.5	0.24	
	Ol-4	r	38.53	18.69	42.13	0.38	0.34	0.05	100.12	80.1	0.38	
	Ol-5	r	38.64	16.87	43.74	0.28	0.28	0.16	99.97	82.2	0.33	1270
	Ol-6	c	39.90	10.24	49.03	0.14	0.25	0.24	99.79	89.5	0.18	
	Ol-7	c	39.57	11.13	48.44	0.15	0.23	0.29	99.80	88.6	0.20	
	Ol-8	r	38.53	18.24	42.96	0.35	0.29	0.05	100.43	80.8	0.36	
	Ol-9	c	39.82	10.01	49.14	0.19	0.21	0.33	99.70	89.7	0.17	
	Ol-10	r	38.27	17.69	43.15	0.33	0.32	0.10	99.85	81.3	0.35	
	Ol-11	c	39.98	10.12	48.70	0.18	0.21	0.29	99.49	89.6	0.18	
	Ol-12	r	38.57	16.79	43.64	0.30	0.23	0.12	99.64	82.2	0.33	1270
	Ol-13	c	39.78	10.10	48.97	0.12	0.23	0.31	99.50	89.6	0.18	
	Ol-14	r	38.52	16.58	43.72	0.33	0.26	0.13	99.54	82.5	0.32	1269
	Ol-15	r	38.99	16.83	44.22	0.32	0.21	0.19	100.74	82.4	0.32	1269
LL010213-6	Ol-1	c	39.37	11.24	47.85	0.17	0.23	0.33	99.19	88.4	0.18	
	Ol-3	r	39.88	15.91	43.71	0.34	0.31	0.12	100.27	83.0	0.28	1263
	Ol-4	c	40.22	11.46	46.64	0.10	0.24	0.26	98.92	87.9	0.19	
	Ol-5	r	39.40	17.12	42.44	0.32	0.32	0.11	99.70	81.5	0.31	1269
	Ol-6	c	40.56	11.18	48.08	0.13	0.21	0.31	100.47	88.5	0.18	
	Ol-7	c	39.82	11.70	48.27	0.18	0.23	0.28	100.48	88.0	0.18	
	Ol-8	r	39.17	15.79	44.78	0.30	0.31	0.13	100.48	83.5	0.27	1257
	Ol-9	c	39.67	11.90	47.77	0.16	0.23	0.23	99.96	87.7	0.19	
	Ol-10	r	38.89	17.09	43.05	0.30	0.38	0.12	99.83	81.8	0.30	1266
	Ol-11	c	39.63	12.94	47.54	0.14	0.20	0.10	100.55	86.8	0.21	
	Ol-12	c	39.87	12.98	47.29	0.16	0.26	0.13	100.69	86.7	0.21	
	Ol-13	r	38.54	18.12	43.00	0.40	0.32	0.09	100.48	80.9	0.32	1267
	Ol-14	r	38.85	15.97	44.03	0.32	0.34	0.18	99.69	83.1	0.28	1259
	Ol-15	r	39.15	16.00	45.27	0.34	0.31	0.18	101.25	83.5	0.27	1256
	Ol-16	r	38.74	15.89	44.32	0.29	0.31	0.15	99.69	83.3	0.27	1257
	Ol-17	r	38.60	18.03	42.78	0.34	0.37	-	100.11	80.9	0.32	1267
LL220112-4	Ol-1	r	39.06	15.10	43.97	0.19	0.25	0.07	98.65	83.8	0.30	1284
	Ol-2	r	38.28	16.61	43.12	0.29	0.26	0.12	98.69	82.2	0.34	
	Ol-3	s	40.18	15.15	45.40	0.26	0.17	0.15	101.31	84.2	0.29	(**)
	Ol-4	r	39.35	16.69	43.61	0.34	0.25	0.13	100.37	82.3	0.34	
	Ol-5	c	39.72	14.27	45.59	0.21	0.22	0.19	100.19	85.1	0.28	1279
	Ol-7	s	39.44	20.38	41.21	0.22	0.15	-	101.41	78.3	0.44	
	Ol-8	r	39.89	15.06	44.85	0.24	0.21	0.20	100.44	84.2	0.30	1284
	Ol-9	r	40.15	15.91	43.17	0.30	0.29	0.14	99.95	82.9	0.33	1295
	Ol-10	s	39.20	19.35	41.46	0.22	0.13	-	100.36	79.2	0.41	
	Ol-11	r	39.93	16.06	44.28	0.31	0.25	0.14	100.98	83.1	0.32	1289
	Ol-12	c	40.45	12.91	46.94	0.22	0.22	0.27	100.99	86.6	0.24	
	Ol-13	s	39.99	15.84	44.55	0.28	0.19	0.25	101.10	83.4	0.31	(**)
	Ol-14	r	39.68	17.78	43.33	0.36	0.33	0.02	101.49	81.3	0.36	
	Ol-15	c	40.67	11.96	47.61	0.15	0.23	0.26	100.87	87.6	0.22	
	Ol-16	r	39.81	16.42	44.31	0.33	0.24	0.19	101.31	82.8	0.33	1289
	Ol-17	s	39.76	16.41	44.06	0.18	0.14	0.24	100.78	82.7	0.33	(**)
	Ol-20	c	40.32	12.83	46.66	0.20	0.21	0.22	100.43	86.6	0.24	
	Ol-21	r	39.91	16.01	44.27	0.32	0.24	0.10	100.85	83.1	0.32	1288
	Ol-22	s	40.03	15.81	44.78	0.21	0.16	0.15	101.13	83.5	0.31	(**)
	Ol-23	c	40.62	12.34	47.10	0.17	0.20	0.26	100.68	87.2	0.23	
	Ol-25	c	39.18	12.35	47.32	0.18	0.21	0.21	99.45	87.2	0.23	
Plagioclase-bearing dunite												
LL240711-5C	Ol-2		38.16	16.50	43.82	0.22	0.16	0.26	99.11	82.6		
	Ol-4		38.06	16.30	43.44	0.22	0.17	0.17	98.36	82.6		
	Ol-5		37.86	16.94	43.21	0.24	0.16	0.17	98.58	82.0		
Spinel lherzolite												
JF-2A	Ol-1		39.33	10.88	48.33	0.17	0.04	0.38	99.13	88.8		
	Ol-2		39.56	11.06	48.86	0.14	0.04	0.39	100.06	88.7		
	Ol-3		39.29	10.94	48.45	0.19	0.05	0.34	99.26	88.8		
	Ol-4		39.50	11.41	48.45	0.16	0.07	0.31	99.89	88.3		
	Ol-7		39.32	11.64	48.18	0.17	0.09	0.29	99.67	88.1		

Ol-8	39.26	11.21	47.98	0.20	0.07	0.35	99.07	88.4
Ol-9	39.54	11.10	48.23	0.14	0.07	0.32	99.39	88.6
Ol-10	39.36	11.29	48.27	0.14	0.03	0.32	99.39	88.4
Ol-11	39.31	11.24	48.15	0.18	0.06	0.38	99.32	88.4
Ol-12	39.38	11.03	48.43	0.20	0.06	0.49	99.59	88.7
Ol-13	39.22	11.44	47.92	0.15	0.06	0.37	99.15	88.2

Figure II.1. Simplified geological map of Robinson Crusoe and Santa Clara Islands (modified from Morales, 1987) with main units as presented in the text. Dip/strike in shield sequence, vents of rejuvenated stage and $^{40}Ar/^{39}Ar$ age sites are showed. Inset shows the regional topography and bathymetry around the Juan Fernández Ridge.

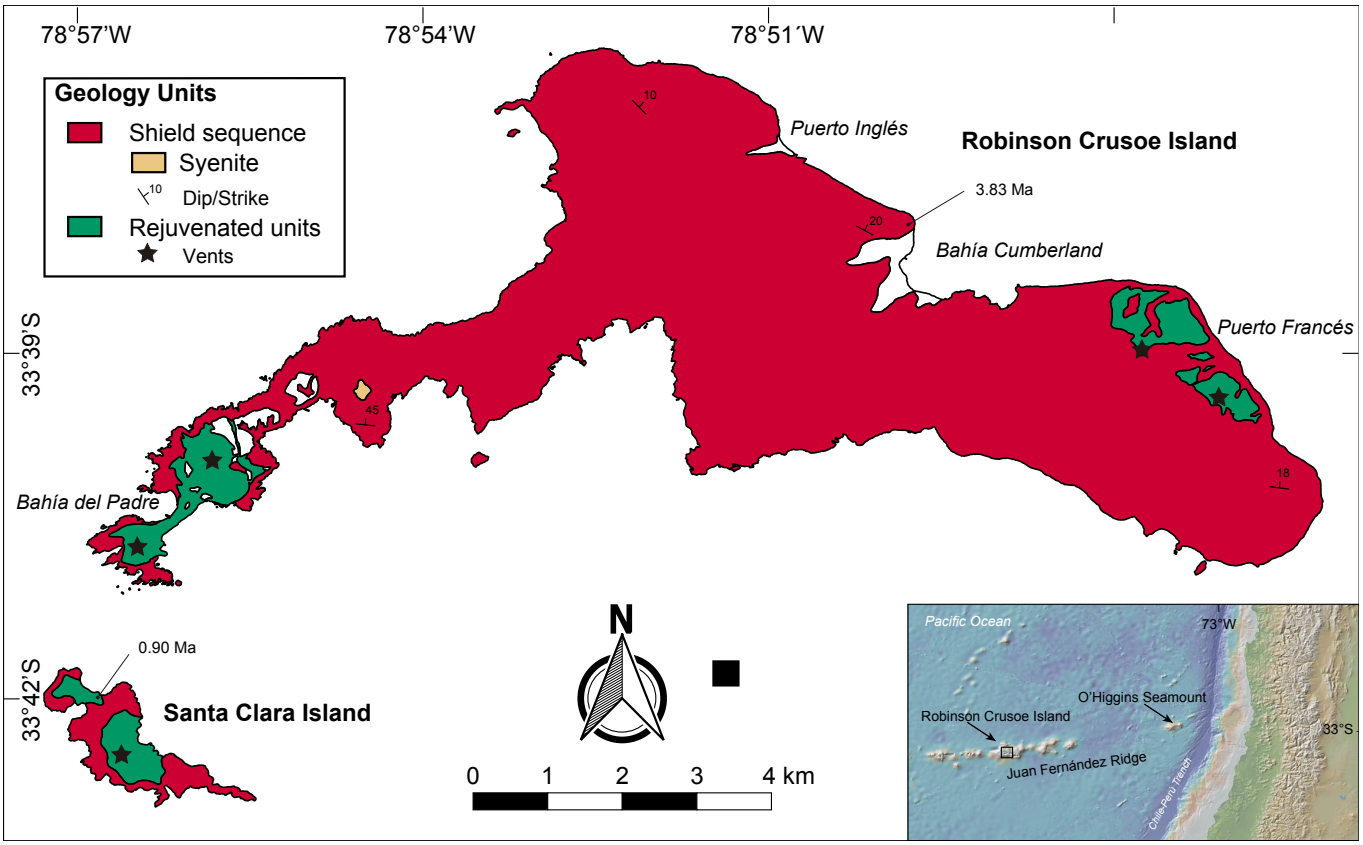

Figure II.2. Field photographs of Robinson Crusoe Island. a) Basaltic dike swarms in the shield unit (located in Puerto Inglés, Robinson Crusoe Island). b) A pile representing the rejuvenated volcanism (~ 0.90 Ma) filling with unconformity (dashed line) the eroded morphology of the shield unit (~ 3.83 Ma, NW of Puerto Francés).

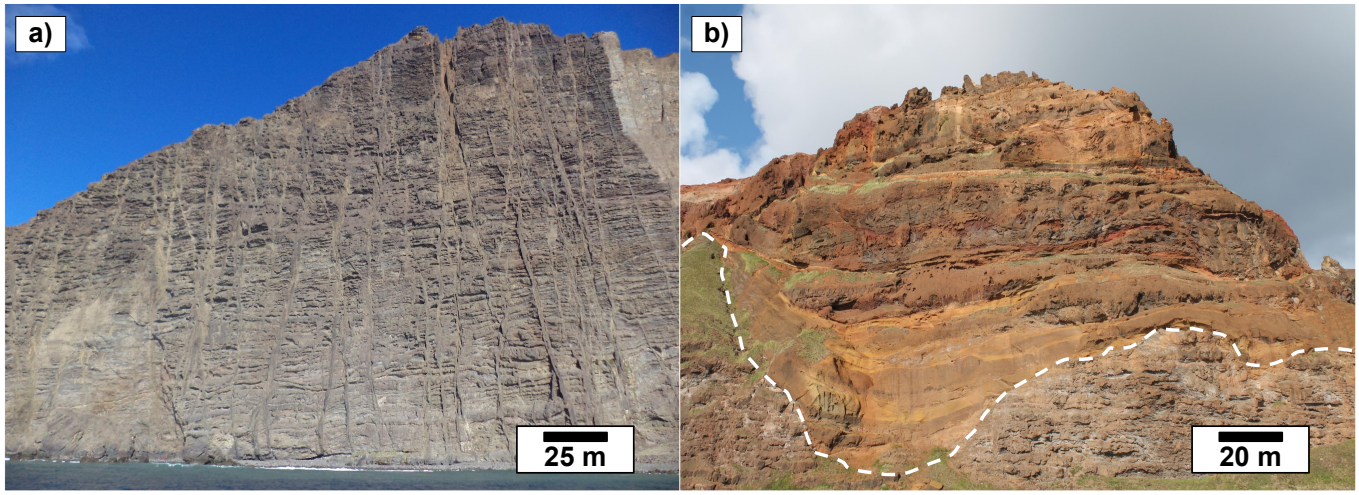

Figure II.3. Total-alkali vs. silica (TAS) classification diagram for the Robinson Crusoe Island lavas (after Le Maitre, 2002; alkali-subalkali boundary is from Irvine and Baragar, 1971). Previous data (Table II.S.2) from Gerlach et al., (1986); Baker et al., (1987) and Farley et al., (1993) are included.

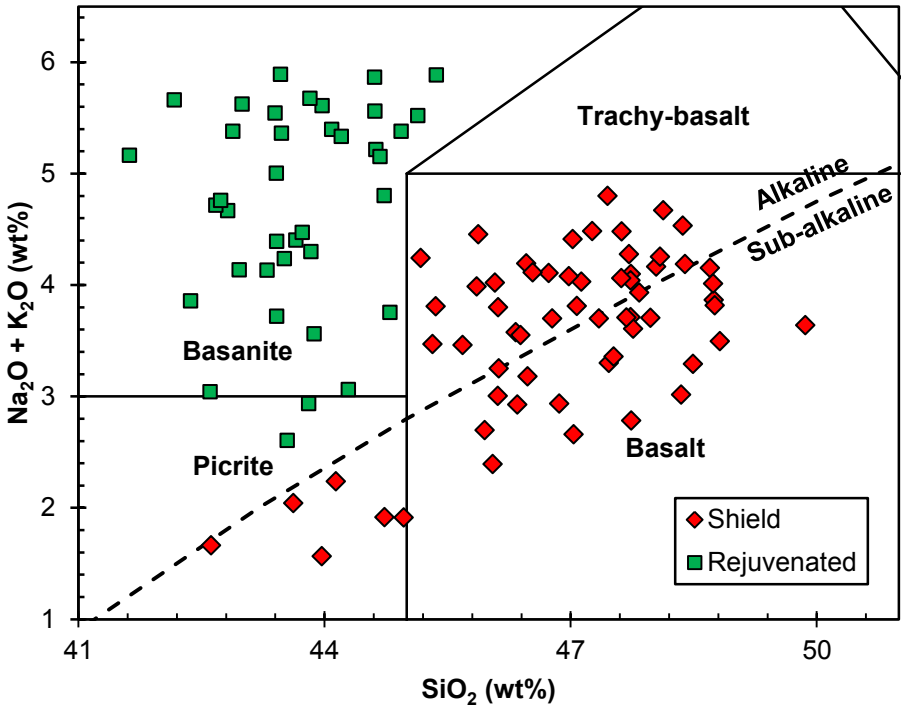

Figure II.4. Mg# vs. Ni content diagram and compositional classification of shield and rejuvenated lavas from Robinson Crusoe Island. Only high-precision Ni data (ICP-MS) are included (previous work data excluded).

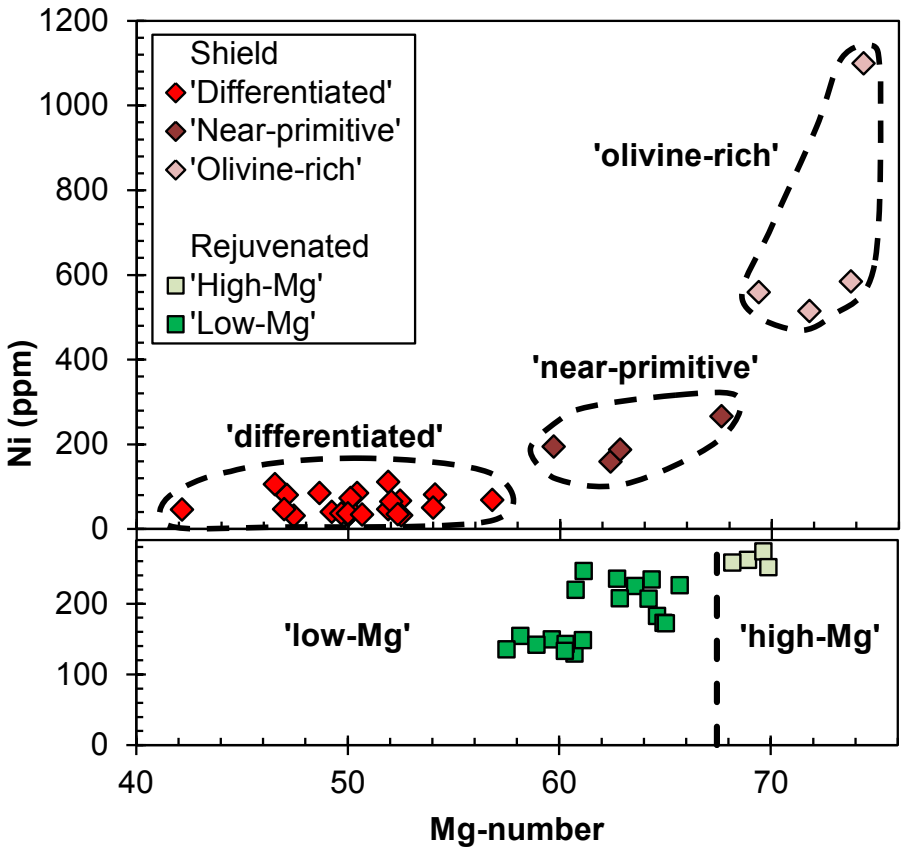

Figure II.5. Mg# variations vs. major elements (Al_2O_3, Na_2O, CaO and P_2O_5 in wt%) plots for lavas from Robinson Crusoe Island. Dashed line indicates possible primitive compositions (Mg# > 68).

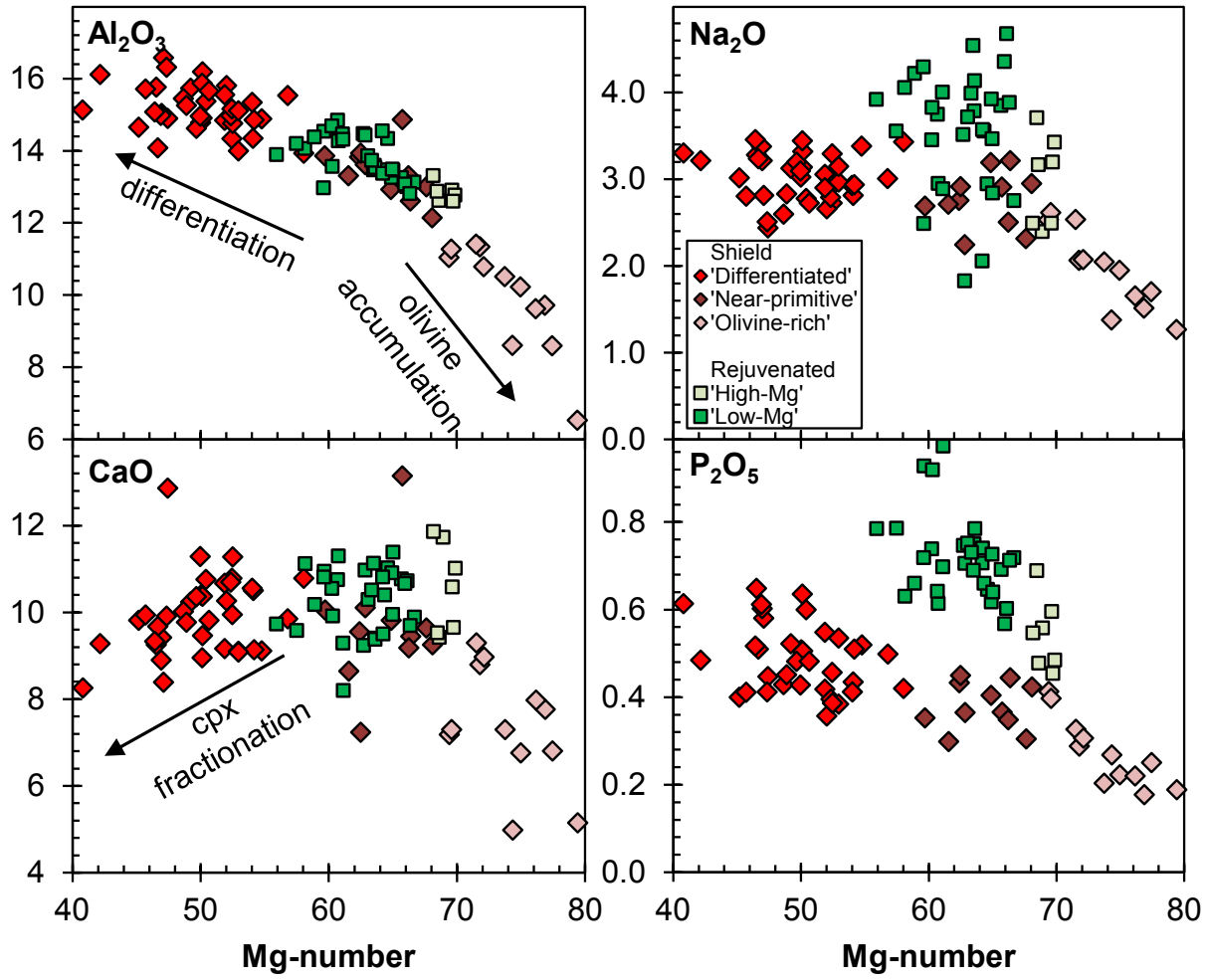

Figure II.6. Olivine Fo content vs. whole-rock Mg# for Robinson Crusoe Island lavas. Olivine-liquid equilibrium field after Roeder and Emslie (1970) using a $^{Ol\text{-}Liq}Kd$ of 0.30 ± 0.03.

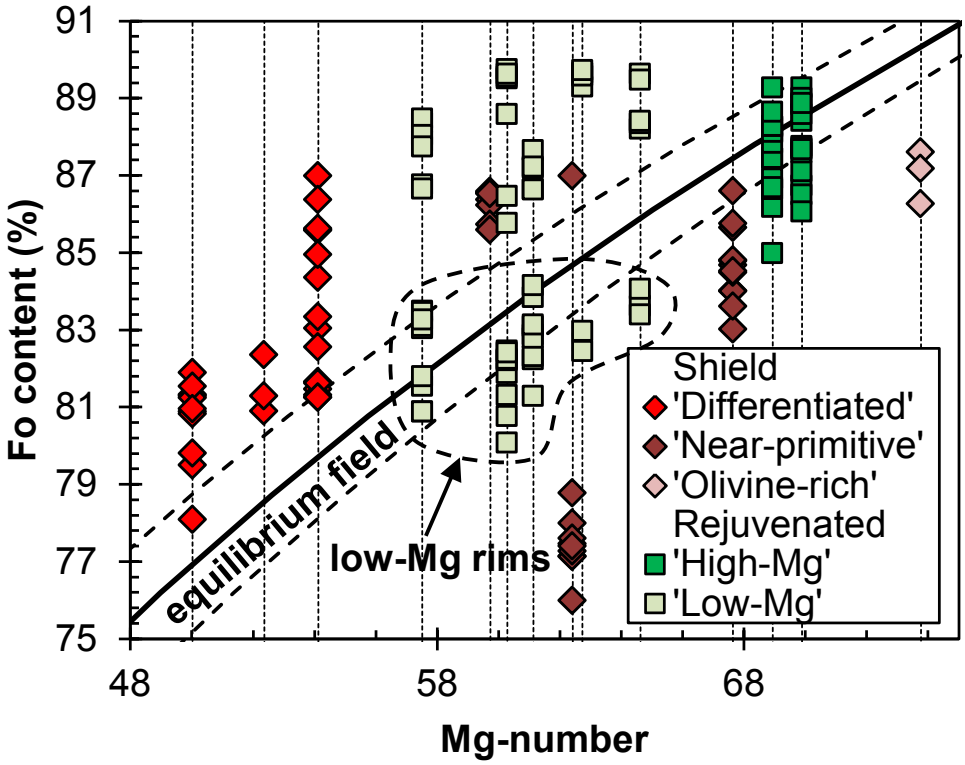

Figure II.7. Clinopyroxene composition, Na_2O and TiO_2(wt%) vs. Wo content in Robinson Crusoe Island. Dashed lines enclose 'low-Mg' cores compositions (described in text). Spinel lherzolite xenoliths data is also included showing differences respect to rejuvenated (Na-enriched) cores that suggest differences in their origin. Error bars reflect the mean of the SD(%) values reported by microprobe.

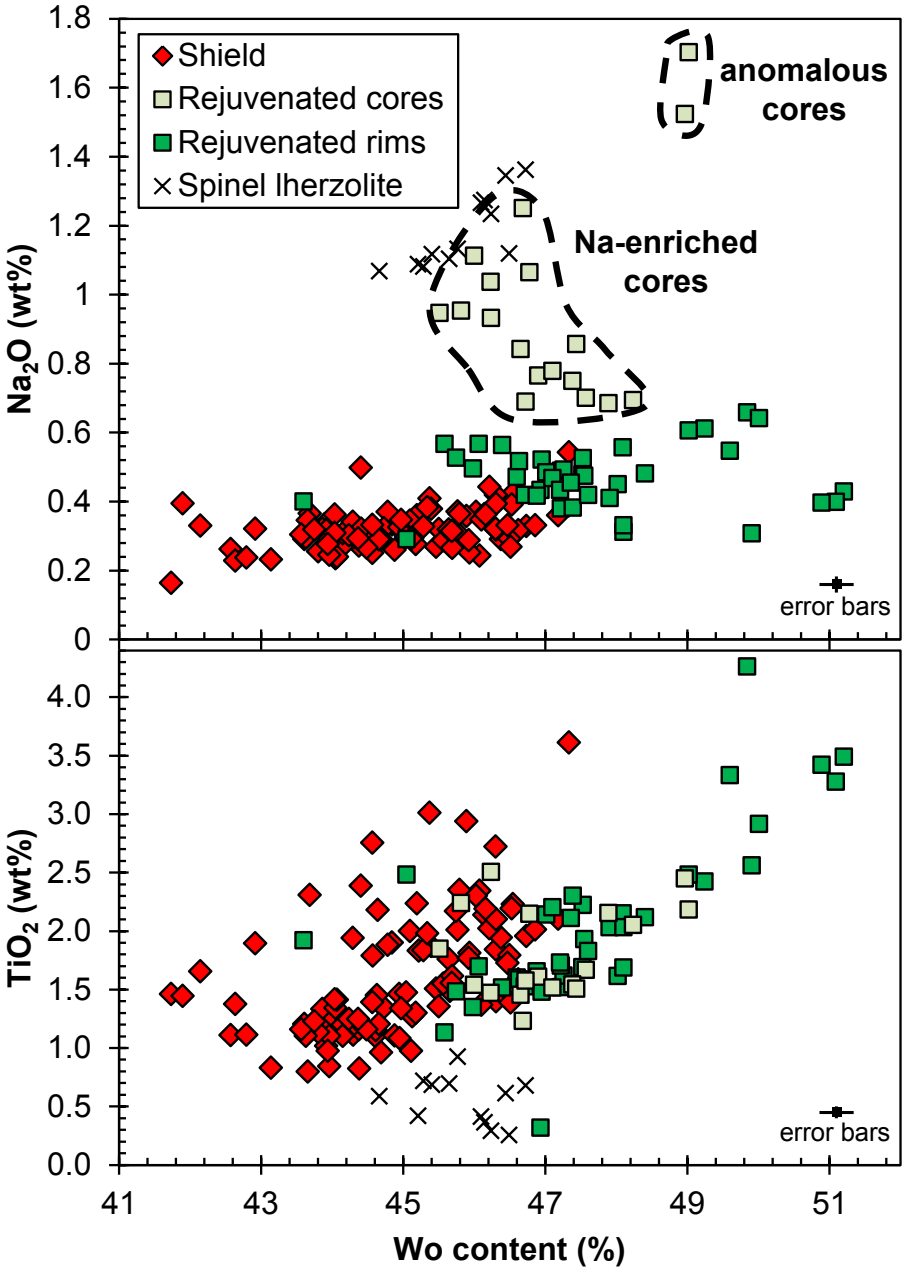

Figure II.8. SEM microphotographs of olivine. Fo content is indicated. a) Typical phenocryst with normal zonation of 'differentiated' group in shield unit. b) High-Fo compositions of 'high-Mg' group in rejuvenated unit. c) Classical 'low-Mg' group pattern: high-Fo cores (antecrysts) and differentiated rims in the rejuvenated unit. d) Anomalous cores (xenocrysts) in rejuvenated unit surrounded by typical 'low-Mg' compositions (described in c).

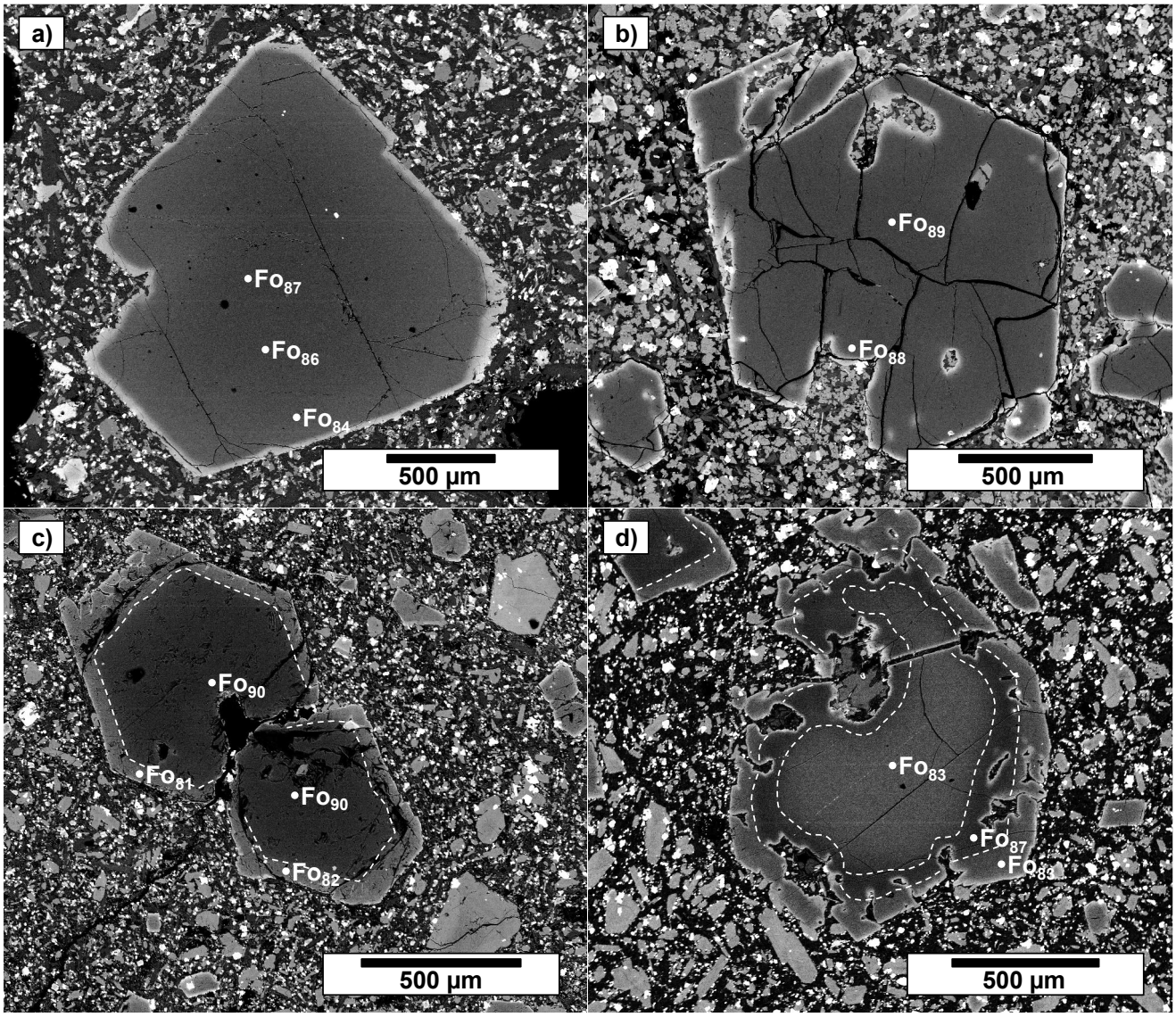

Figure II.9. SEM microphotographs of clinopyroxene in rejuvenated lavas. Pressure estimations (kbar) are indicated. a) Classical pattern in 'low-Mg' group: Na-enriched cores (antecrysts formed at high-pressure) with polybaric crystallization and more differentiated rims (low-pressure phenocrysts). b) Na-enriched cores (antecrysts) and differentiated rims (phenocrysts) surrounding anomalous cores (unknown origin xenocrysts) with resorption rims in one sample of 'low-Mg' group.

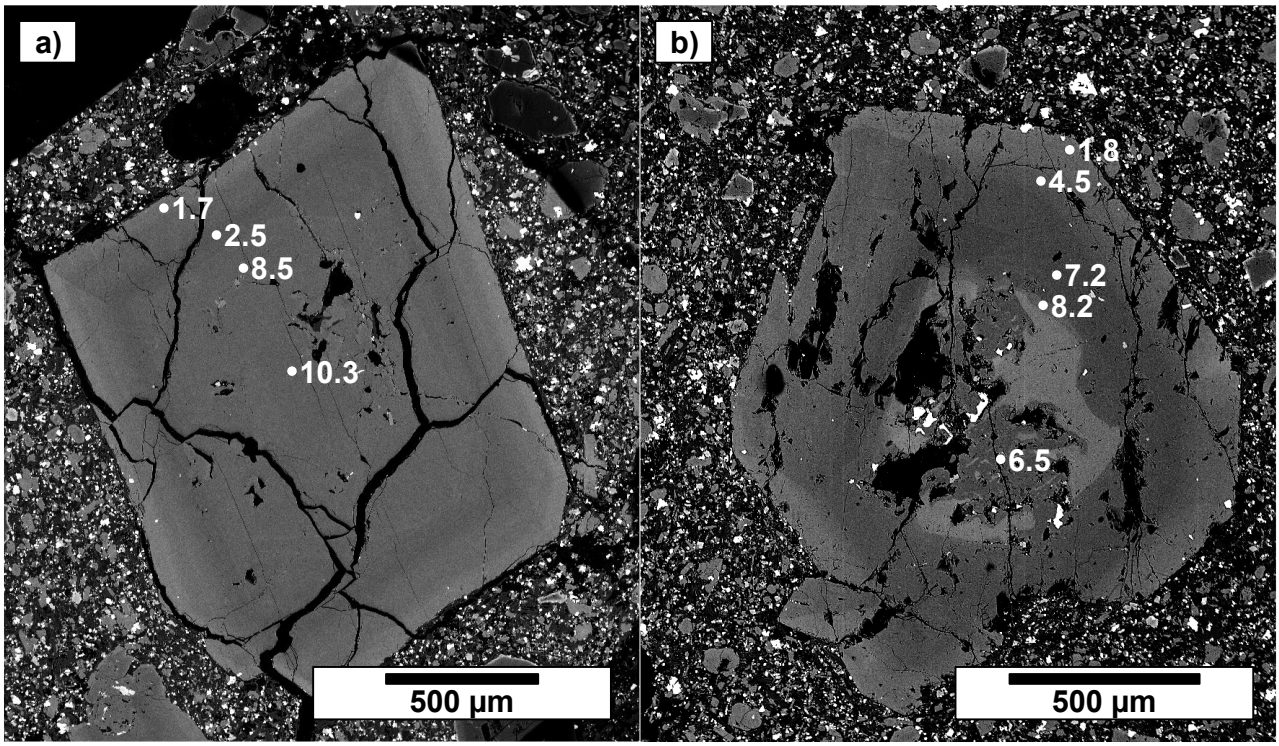

Figure II.10. Olivine composition in Robinson Crusoe Island. a) Ni (ppm) vs. Fo content. Crystallization trends for different primary melts are provided: (1) and (2) fractional of primitive magma from peridotite and pyroxenite source respectively, arrow indicates shallow crystallization trend (Ruprecht and Plank, 2013; sources from Straub et al., 2011), (3) batch (dashed line) and fractional (solid line) of primitive Hawaiian tholeiitic melt without eclogite partial melt (Wang and Gaetani, 2008). b) Ca (ppm) vs. Fo content, spinel lherzolite and dunite cumulate data is showed and allows to interpret the origin of rejuvenated xenocrysts (dashed curves enclose mantle or shield-like compositions). Error bars reflect the mean of the SD(%) values reported by microprobe.

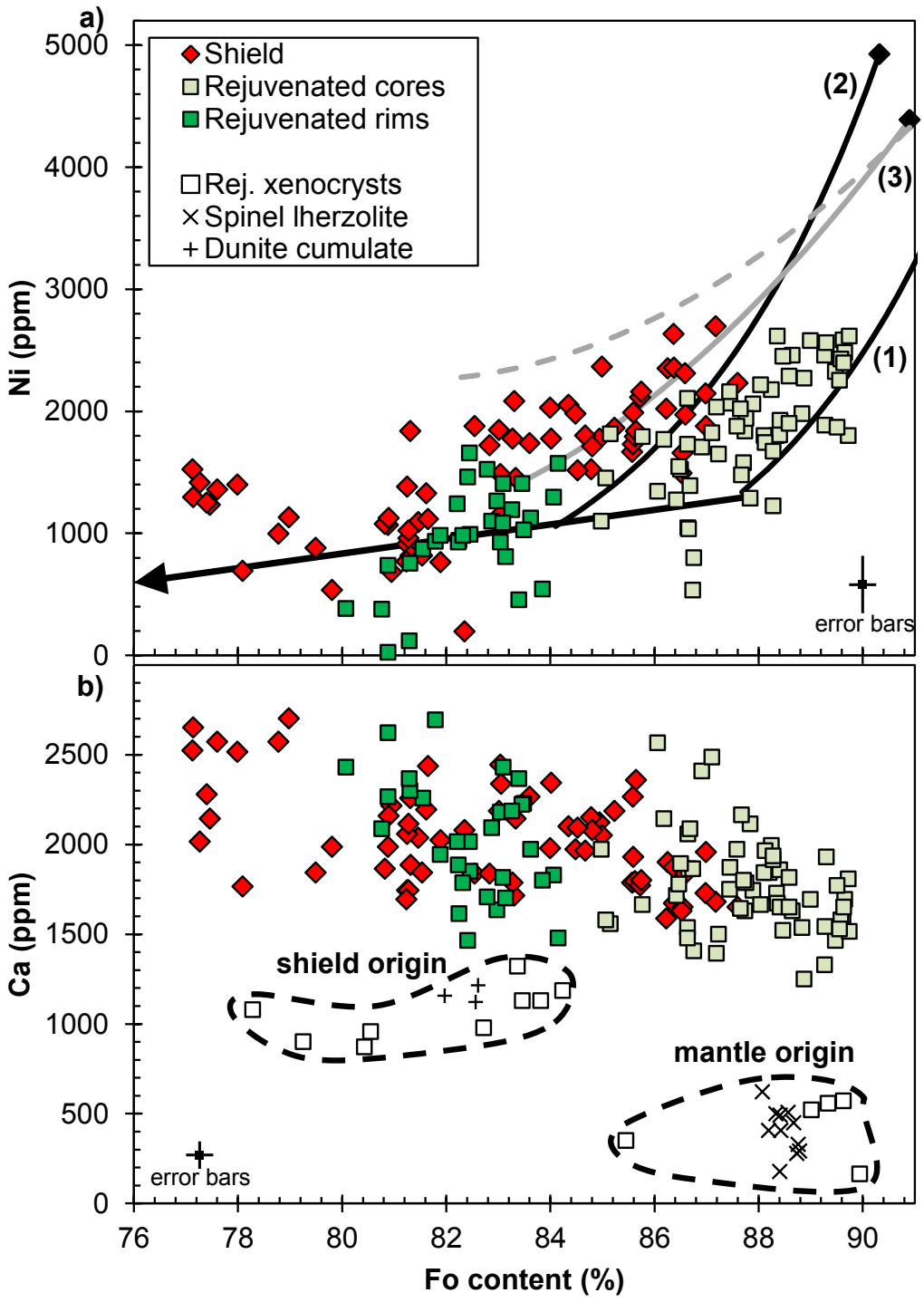

Figure II.11. Schematic model of the magmatic ascent and storage in Robinson Crusoe Island showing the contrasting pattern for shield and rejuvenated volcanism: storage in shallow reservoirs for shield and rapid ascent with polybaric crystallization for the rejuvenated stage (details in section 5.2). Qualitative differences in depth (from pressure estimations of clinopyroxene geobarometer from Nimis and Ulmer, 1998) and temperature conditions (according olivine-liquid geothermometer from Herzberg and O'Hara, 2002) of each compositional group are also shown. Pressure conditions estimated are showed in histograms for both units.

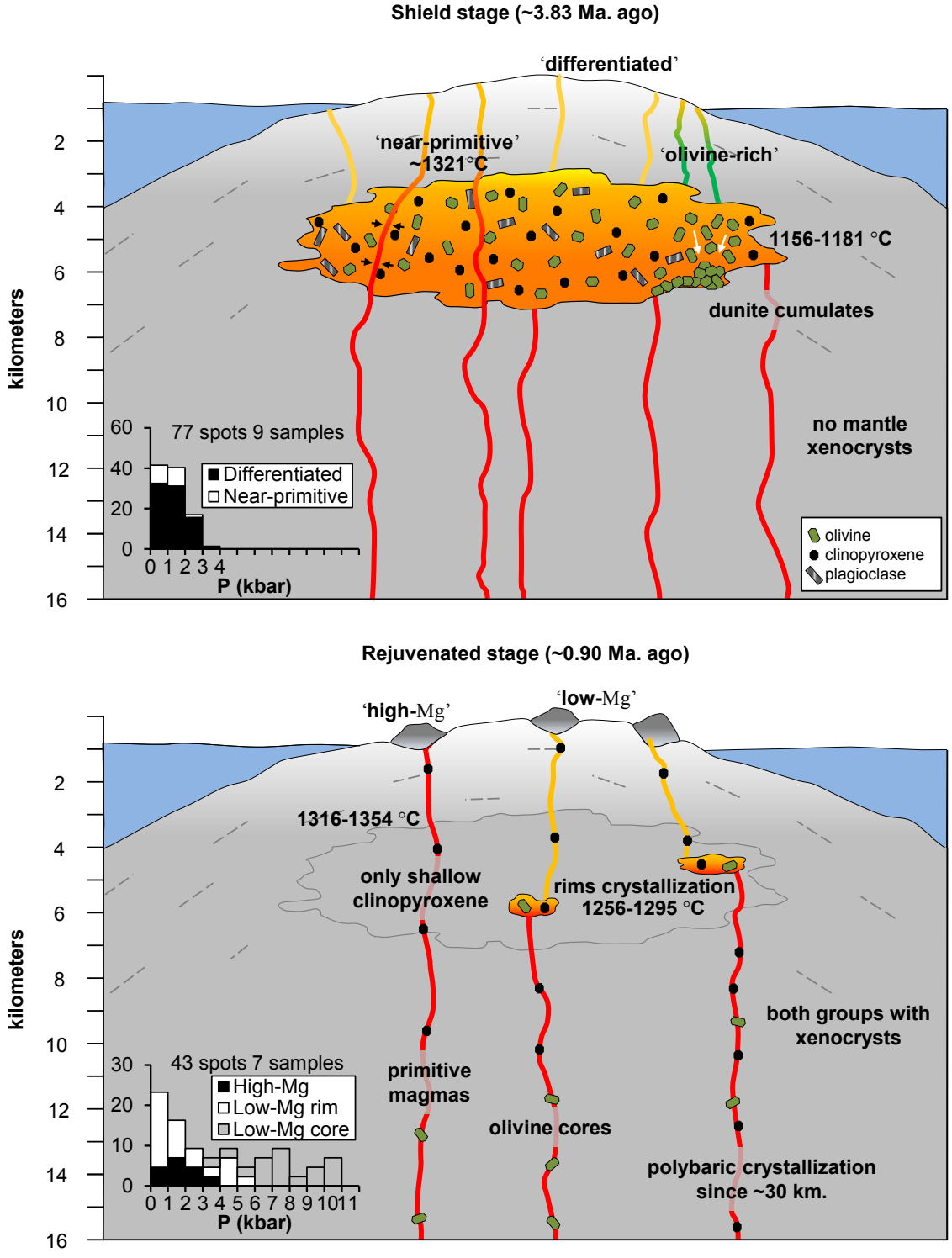

Capítulo III

Ascent and storage model for the shield and rejuvenated volcanism of Robinson Crusoe extended to other volcanoes of Juan Fernández Ridge

III.1. Introduction

The intraplate volcanism of the Juan Fernández Ridge (JFR), an aseismic ridge built on top of the Nazca Plate in Pacific SE (Rodrigo and Lara, 2014), is characterized by the presence of shield-building and rejuvenated volcanism. In fact, the shield stage has been recognized at least in (E to W) O'Higgins guyot, Alpha seamount, Robinson Crusoe and Alejandro Selkirk islands, and the rejuvenated stage in O'Higgins and Robinson Crusoe (Baker et al., 1987; Farley et al., 1993; Reyes et al., 2017; Truong et al., 2018; Lara et al., submitted) (see Figure V.1 of Chapter V for the location of these volcanoes).

A model for the magmatic plumbing and storage was proposed for Robinson Crusoe Island (the main volcanic center in JFR), establishing the existence of shallow magmatic reservoirs in the shield stage, and rapid ascent with polybaric crystallization and short-time storage in the rejuvenated stage (Reyes et al., 2017). In this chapter we present whole-rock geochemistry, textural analysis and chemical data of olivine and clinopyroxene for O'Higgins, Alpha and Alejandro Selkirk, to extend the Robinson Crusoe ascent and storage model to more volcanoes of JFR.

III.2. Methods and analytical procedures

Petrographic analysis was made by optical microscopy and scanning electron microscopy (SEM FEI Quanta 250) at the Andean Geothermal Center of Excellence (CEGA) facilities of Universidad de Chile. Modal count (500 points) was performed in 12 representative samples using JMicroVision 1.2.7 software (Table III.1). Whole-rock major element and Ni chemistry (57 samples) was analyzed at AcmeLabs, Vancouver, Canada (major elements by ICP-ES and Ni by ICP-MS) (analytical detection limits and provided in Table V.2 of Chapter V). Olivine and clinopyroxene chemistry (12 samples) was measured by electronic microprobe (EPMA JEOL JXA 8230 equipped with three wavelength-dispersive spectrometers) at Laboratorio de Microscopía Electrónica y Análisis de Rayos X (LAMARX), Universidad Nacional de Córdoba, Argentina with typical measurement conditions used in literature considered as "routine analysis" and do not show high precision results (Sobolev et al., 2007) reflected in an error of 0.26 in olivine forsterite content and 0.24 in clinopyroxene wollastonite content (analytical detection limits for each element used in showed in Table III.2 and Table III.3). Details of measurement conditions of ICP-ES, ICP-MS and EPMA are given in Reyes et al. (2017).

III.3. Geochemical and petrographic main features

The shield stage in O'Higgins, Alpha and Alejandro Selkirk is formed by great sequences (O'Higgins guyot has a total height of ~ 3450 mt, Alpha seamount reaches to 322 mbsl, and Alejandro Selkirk an exposed sequence of ~ 1300 m high) of vesicular lavas (ranging from 0 to 18%) (Table III.1) with transitional basalts (tholeiitic and alkali), trachy-basalts and picrites (including dykes, hereinafter referred simply as lavas). Few

trachy-basalts, basaltic trachy-andesites and basanites are also present (Figure III.1). The SiO_2 content (normalized to 100% without LOI) is in the range 43.6 – 50.5 wt%, and Mg# (considering FeO/Fe_2O_3: 0.9) in 42.2 – 80.3. According to Ni content and Mg#, the compositional groups ('olivine-rich', 'near-primitive' and 'differentiated') of Robinson Crusoe (Reyes et al., 2017) can be extended to this study. In effect, O'Higgins has samples with 'olivine-rich' and 'differentiated' features (data in Lara et al., submitted, available in Table A.1), basalts of Alpha belong only to 'differentiated' group, and Alejandro Selkirk shows compositions of the three groups (Figure III.2) (geochemical data in Table V.2 of Chapter V). Mineralogically these lavas are characterized by the presence of olivine, clinopyroxene and plagioclase phenocrysts embedded in a groundmass of clinopyroxene, plagioclase, Fe-Ti oxides and sometimes olivine. The olivine is the most common phenocrysts with a broad range of content (< 1 – 7 in 'differentiated', 6 – 13 in 'near-primitive' and 17 – 47 vol% in 'olivine-rich' considering the analyzed representative samples), clinopyroxene and plagioclase phenocrysts are scarce in 'olivine-rich' (0 – 1 vol%) and variable in 'near-primitive' and 'differentiated' groups (mainly between 0 and 4, but with some exceptions of up to 21 vol% of plagioclase in differentiated basalts) (Table III.1).

In addition to Robinson Crusoe Island, the O'Higgins guyot also shows rejuvenated volcanism represented by basanitic flows apparently fed by a low relief volcanic vent at the top of the guyot (Lara et al., submitted), with ~ 42.8 wt% of SiO_2 (Figure III.1) and Mg# of 57.5 – 58.9 (data in Lara et al., submitted, available in Table A.1) correlated with the 'low-Mg' group of Robinson Crusoe (Reyes et al., 2017) (Figure III.2). These vesicular basanites (1 to 7 vol% of vesicles) contain 5 – 6 vol% of olivine phenocrysts and ~ 1 vol% of clinopyroxene in a groundmass with clinopyroxene, plagioclase, Fe-Ti oxides and olivine. Ultramafic xenoliths fragments are also recognized (up to 6 vol%).

III.4. Mineral chemistry, geothermobarometry and crystals origin

The methodology used is the same detailed in Reyes et al. (2017). In brief, pressure conditions were estimated using clinopyroxene EPMA data and the structural geobarometer of Nimis and Ulmer (1998) for anhydrous basalts (standard error of ± 1.7 kbar plus ~ 1.0 kbar per 1 wt% of H_2O, probably around 0.8 wt% in JFR shield; see Chapter II for details), and crystallization temperatures were estimated using the olivine-liquid geothermometer of Herzberg and O'Hara (2002) modified from Beattie (1993) (standard error of ± 31 °C, considering a $^{Ol\text{-}Liq}Kd$ of 0.30 ± 0.03 in equilibrium and a pressure value of 2.0 kbar as input) and the clinopyroxene-liquid geothermometer of Putirka et al. (2003) (standard error of ± 33 °C, considering $^{Cpx\text{-}liq}Kd$ of 0.027 ± 0.03 in equilibrium and the pressure estimated from Nimis and Ulmer [1998] as input).

In the shield unit, the clinopyroxene is visible as eu- to subhedral homogeneous crystals (sometimes with a thin differentiated rim) (Figure III.3) with a variable composition in the range of $Wo_{38\text{-}47}En_{40\text{-}49}Fs_{8\text{-}16}$, Na_2O of 0.22 – 0.44 wt% and TiO_2 of 0.81 – 3.44 wt% (Figure III.4) (Table III.2) interpretable as phenocrysts. There are no big differences between compositional groups, different volcanoes or individual crystals (Figure III.3), so the estimated pressure conditions for all shield lavas are between 0.0 and 2.4 kbar (Table III.3). Clinopyroxene-liquid temperature estimations for the 'differentiated' group (Alpha and Alejandro Selkirk) are between 1141 and 1192 °C (Table III.3).

Olivine is a ubiquitous mineral in shield unit ranging between Fo_{77-88} and Ni: 338 – 2727 ppm (Table III.4) with homogeneous crystals or normally zoned, except in 'near-primitive' group of Alejandro Selkirk that also shows reverse zoning (Figure III.5). Crystallization temperatures were estimated between 1150 and 1153 °C for rims in the 'differentiated' group (Alejandro Selkirk) (Table III.3); the other groups, 'near-primitive' and 'olivine-rich', do not show olivine-liquid equilibrium impeding temperature estimations (Figure III.6) because their crystals really represent antecrysts. The temperatures estimated using clinopyroxene and olivine are well correlated (the range of olivine is within clinopyroxene values) and similar to pressure-temperature conditions obtained by Reyes et al. (2017) for the shield-building stage in Robinson Crusoe Island (0.0 to 3.2 kbar and 1156 – 1194 °C).

On the other hand, in the basanites of the rejuvenated volcanism, the clinopyroxene is a very scarce phenocrysts, and often with clear evidence of a xenolitic origin. Is possible to identify two groups separated by their Na_2O content: the low-Na group (individual crystals or rims) has compositions in the range $Wo_{47-51}En_{35-41}Fs_{11-14}$, Na_2O: 0.41 – 0.65 and TiO_2: 2.46 – 4.85; and the high-Na (individual crystals or cores) in $Wo_{42-48}En_{39-44}Fs_{11-17}$, Na_2O: 1.05 – 1.51 and TiO_2: 0.99 – 2.04 wt% (Figure III.4). These changes are reflected in pressure estimations of 0.0 – 1.6 kbar for the low-Na group formed by individual crystals or rims, and 6.6 – 12.0 kbar for the high-Na group (Table III.3) composed by individual crystals (with resorption rims) or cores (Figure III.3). The origin of the cores, also reported in Robinson Crusoe (Reyes et al., 2017), is enigmatic, but in this case, the xenolitic origin (probably from mantle) appears to be more realistic (due to their low Wo and high Na_2O content like spinel lherzolite from Robinson Crusoe), and the antecrysts option is only valid for composition relatively enriched in TiO_2 (Figure III.3).

Olivines in the rejuvenated stage are characterized by the limited presence of Mg-rich 'cores' (Fo_{85-88}, Ni: 542 – 2224 ppm) in some crystals, more 'primitive' than their rims and the abundant rest of crystals (Fo_{81-84}, Ni: 0 – 1532 ppm; hereinafter called 'rims') (Figure III.5). These 'rims' are in chemical equilibrium with the liquid (not observed in 'cores') (Figure III.6) allowing the estimations of temperatures between 1266 and 1287 °C (Table III.3). Some 'rims' crystallize around anomalous compositions interpreted as xenocrysts with an unknown (Fo_{78-80}, Ni: 0 - 1589) or mantle (Fo_{86}, Ni: 2122 - 3073) origin based on their Fo and Ca content (e.g., Simkin and Smith, 1970, Rohrbach et al., 2005) (Figure III.7). Then, the clinopyroxene and olivine from O'Higgins rejuvenated stage are formed by slightly differentiated compositions (phenocrysts) occasionally around more primitive cores (antecrysts and/or xenocrysts).

III.5. Magma ascent and storage in Juan Fernández Ridge

The whole-rock chemistry (Figure III.1) (Figure III.2), EPMA data for clinopyroxene (Figure III.4) and olivine (Figure III.7), and textural features (Figure III.3) (Figure III.5) of shield and rejuvenated stages analyzed in this study allow to extend the ascent and storage model of Robinson Crusoe (Reyes et al., 2017) to O'Higgins, Alpha and Alejandro Selkirk volcanoes, implying a volcanic evolution with common processes in JFR.

Then, the JFR shield stage is built by basalts stored in a shallow magmatic chamber where melts can be differentiated (even forming basaltic trachy-andesites) implying a

temperature descent below 1200 °C and normal zonation (‘differentiated’ group) or being affected by olivine accumulation (‘olivine-rich’). Some melts would be extruded quickly suffering some mixing with differentiated compositions, or alternatively, differentiated melts are affected by magmatic recharge, generating lavas with primary signature of the ‘near-primitive’ group (explaining reverse zonation of some olivines in this group).

On the other hand, the JFR rejuvenated stage is characterized by rapid ascent of primary basanitic melts with polybaric crystallization and occasionally short-time storage in a shallow reservoir where slightly differentiated ‘rims’ crystallize at temperatures above 1250 °C in new grains or around antecrysts/xenocrysts.

Bibliography

Baker, P.E., Gledhill, A., Harvey, P.K., Hawkesworth, C.J., 1987. Geochemical evolution of the Juan Fernandez Islands, SE Pacific. J. Geol. Soc. London. 144, 933–944. doi.org/10.1144/gsjgs.144.6.0933

Beattie, P., 1993. Olivine-melt and orthopyroxene-melt equilibria. Contrib. to Mineral. Petrol. 115, 103–111. doi:10.1007/BF00712982

Farley, K.A., Basu, A.R., Craig, H., 1993. He, Sr and Nd isotopic variations in lavas from the Juan Fernandez Archipelago, SE Pacific. Contrib. to Mineral. Petrol. 115, 75–87. doi.org/10.1007/BF00712980

Herzberg, C., O'Hara, M.J., 2002. Plume-associated ultramafic magmas of Phanerozoic age. J. Petrol. 43, 1857–1883. doi:10.1093/petrology/43.10.1857

Irvine, T.N., Baragar, R.A., 1971. A guide to the chemical classification of the common volcanic rocks. Can. J. Earth Sci. 8 (5), 523–548. doi:10.1139/e71-055

Lara, L.E., Díaz-Naveas, J., Reyes, J., Jicha, B., Orozco, G., Kay, S.M., submitted. Unraveling short-lived rejuvenated volcanism and a rapid transition from shield stage at O' Higgins guyot , Juan Fernández Ridge , Pacific SE.

Le Maitre, R.W., 2002. Igneous rocks – a classification and glossary of terms. Cambridge University Press, Cambridge (236 pp.). doi:10.1017/CBO9780511535581

Nimis, P., Ulmer, P., 1998. Clinopyroxene geobarometry of magmatic rocks Part 1: An expanded structural geobarometer for anhydrous and hydrous, basic and ultrabasic systems. Contrib. to Mineral. Petrol. 133, 122–135. doi:10.1007/s004100050442

Putirka, K.D., Mikaelian, H., Ryerson, F., Shaw, H. 2003. New clinopyroxene-liquid thermobarometers for mafic, evolved, and volatile-bearing lava compositions, with applications to lavas from Tibet and the Snake River Plain, Idaho. Am. Mineral. 88, 1542–1554. doi:10.2138/am-2003-1017

Reyes, J., Lara, L.E., Morata, D., 2017. Contrasting P-T paths of shield and rejuvenated volcanism at Robinson Crusoe Island, Juan Fernández Ridge, SE Pacific. J. Volcanol. Geotherm. Res. 341, 242–254. doi.org/10.1016/j.jvolgeores.2017.05.035

Rodrigo, C., Lara, L.E., 2014. Plate tectonics and the origin of the Juan Fernandez Ridge: analysis of bathymetry and magnetic patterns. Lat. Am. J. Aquat. Res. 42, 907–917. doi.org/10.3856/vol42-issue4-fulltext-15

Roeder, P.L., Emslie, R.F., 1970. Olivine-liquid equilibrium. Contrib. to Mineral. Petrol. v. 29, 275–289. doi:10.1007/BF00371276

Rohrbach, A., Schuth, S., Ballhaus, C., Münker, C., Matveev, S., Qopoto, C., 2005. Petrological constraints on the origin of arc picrites, New Georgia Group, Solomon Islands. Contrib. to Mineral. Petrol. 149, 685–698. doi:10.1007/s00410-005-0675-6

Simkin, T.O.M., Smith, J. V, 1970. Minor-element distribution in olivine. J. Geol. 78, 304–325. doi:10.1086/627519

Sobolev, A. V, Hofmann, A.W., Kuzmin, D. V, Yaxley, G.M., Arndt, N.T., Chung, S.-L., Danyushevsky, L. V, Elliott, T., Frey, F.A., Garcia, M.O., Gurenko, A.A., Kamenetsky, V.S., Kerr, A.C., Krivolutskaya, N.A., Matvienkov, V. V, Nikogosian, I.K., Rocholl, A., Sigurdsson, I.A., Sushchevskaya, N.M., Teklay, M., 2007. The Amount of Recycled

Crust in Sources of Mantle-Derived Melts. Science 316 (5823), 412–417. doi.org/10.1126/science. 1138113

Truong, T.B., Castillo, P.R., Hilton, D.R., Day, J.M.D., 2018. The trace element and Sr-Nd-Pb isotope geochemistry of Juan Fernandez lavas reveal variable contributions from a high- $^{3}He/^{4}He$ mantle plume. Chem. Geol. 476 280–291. doi.org/10.1016/j.chemgeo.2017.11.024

Table III.1. Petrography of representative samples from O'Higgins, Alpha and Alejandro Selkirk based on 500 points count using JMicroVision 1.2.7 software. Mineralogy reported as vesicle-free volume percent for pheno- and microphenocrysts (>0.2 mm in diameter). Rock type according mineralogy and chemistry. GM: groundmass. Ves: vesicle content. Xen: xenoliths content.

			GM	Mineralogy				Ves	Xen
Sample		Rock type	(%)	Oli	Cpx	Plg	Op	(%)	(%)
O'Higgins guyot shield									
'olivine-rich'	D10-5	picrite	70	29	-	<1	<1	-	-
'differentiated'	D10-42	alkali basalt	92	7	-	1	-	18	-
Alpha seamount shield									
'differentiated'	D11-12	alkali basalt	97	<1	-	3	-	6	-
	D11-14	alkali basalt	93	2	4	1	-	4	-
Alejandro Selkirk Island shield									
'olivine-rich'	JR170913-4	picrite	52	47	<<1	-	1	-	-
	MF-6	tholeiitic basalt	82	17	<<1	1	-	17	-
'near-primitive'	JR170913-5	tholeiitic basalt	80	13	4	3	-	11	-
	JR170913-16	tholeiitic basalt	90	6	-	4	-	4	-
'differentiated'	LL250112-1	alkali basalt	75	4	<<1	21	-	4	-
	LL260112-4	alkali basalt	99	<1	-	1	-	1	-
O'Higgins guyot rejuvenated									
'low-Mg'	2D-1	basanite	94	6	<1	-	-	7	
	2D-2	basanite	94	5	1	-	-	1	5

Table III.2. EPMA data (wt%) of clinopyroxene in lavas from O'Higgins, Alpha and Alejandro Selkirk volcanoes. Only measures with acceptable structural formula are considered (cations equal to 4.00 ± 0.02). (A) Clinopyroxene pressure in anhydrous basalts from Nimis and Ulmer, 1998 (±1.7 kbar + ca. 1 kbar per 1wt% H_2O in the melt). (B) $^{Cpx-Liq}Kd$ calculated assuming 90% of total iron is ferrous in the liquid (whole rock). (C) Clinopyroxene-liquid temperature from Putirka et al., 2003 (±33 °C). (*) Negatives pressures (slightly < 0.0 kbar) are considered as 0.0 (see section 4 of Chapter II for details).

Sample	Spot	SiO_2	TiO_2	Al_2O_3	FeO^T	MgO	MnO	CaO	Na_2O	Cr_2O_3	Sum	Wo	Cpx_{an}	Cpx-Liq	
Det. limit		*0.02*	*0.03*	*0.01*	*0.02*	*0.01*	*0.02*	*0.01*	*0.01*	*0.02*			P(kbar)[A]	Kd[B]	T (°C)[C]
O'Higgins guyot rejuvenated															
'low-Mg'															
2D-1	Cpx-1	48.36	2.92	5.89	6.98	13.53	0.13	22.25	0.47	0.04	100.54	47.7	0.0 (*)	0.34	
	Cpx-2	48.59	2.94	5.86	6.86	13.49	0.11	22.52	0.48	0.01	100.77	48.2	0.0 (*)	0.34	
	Cpx-3	48.69	2.79	5.49	7.28	13.63	0.12	22.20	0.47	0.00	100.68	47.3	0.0	0.35	
	Cpx-4	44.14	4.77	9.20	7.49	11.45	0.12	22.16	0.53	0.00	99.84	50.3	1.3	0.42	
	Cpx-5	49.14	2.47	4.99	6.52	13.90	0.13	22.25	0.41	0.00	99.83	47.6	0.0 (*)	0.32	
	Cpx-6	48.94	2.46	5.12	6.69	13.74	0.15	22.33	0.45	0.04	99.99	47.7	0.0 (*)	0.32	
	Cpx-7	43.86	4.72	9.21	7.16	11.14	0.20	22.14	0.59	0.00	99.09	51.0	1.6	0.41	
	Cpx-8	49.09	2.04	7.42	6.38	13.10	0.12	20.70	1.18	0.14	100.14	47.1	7.3	0.32	
	Cpx-9	48.96	2.03	7.34	6.64	12.96	0.17	20.48	1.05	0.14	99.73	46.7	6.9	0.36	
	Cpx-10	49.04	1.73	6.80	7.51	12.02	0.20	20.60	1.47	0.10	99.43	47.5	6.5	0.38	
	Cpx-11	50.51	1.04	7.57	5.68	13.57	0.13	19.13	1.51	0.88	100.09	45.0	12.0	0.31	
	Cpx-12	45.75	4.14	7.91	6.88	11.95	0.14	22.45	0.65	0.04	99.88	50.4	1.0	0.37	
2D-2	Cpx-1	50.84	0.99	6.30	9.15	12.31	0.25	18.96	1.32	0.10	100.29	43.7	7.5	0.59	
	Cpx-2	44.08	4.85	8.87	7.47	11.06	0.17	22.44	0.62	0.02	99.59	51.2	0.5	0.45	
	Cpx-3	49.67	1.20	7.71	9.31	12.66	0.19	18.42	1.29	0.23	100.72	42.4	9.5	0.54	
	Cpx-4	50.00	1.15	7.31	8.52	12.61	0.24	19.10	1.36	0.16	100.45	43.9	9.0	0.49	
	Cpx-5	50.25	1.04	7.11	8.69	12.93	0.18	19.11	1.34	0.18	100.90	43.4	8.7	0.47	
	Cpx-6	48.19	2.85	5.45	7.46	13.36	0.12	22.16	0.41	0.01	100.00	47.5	0.0	0.39	
	Cpx-7	48.87	2.60	5.26	7.23	13.48	0.20	22.25	0.42	0.00	100.26	47.5	0.0	0.39	
Alpha seamount shield															
'differentiated'															
D11-12	Cpx-1	51.44	1.32	2.58	6.69	16.24	0.15	20.55	0.27	0.16	99.37	42.4	0.0 (*)	0.23	
	Cpx-2	47.82	2.33	5.58	6.48	14.10	0.15	21.52	0.33	0.67	99.06	46.5	0.6	0.23	
	Cpx-3	46.43	3.44	6.91	7.42	13.21	0.15	21.49	0.41	0.30	99.82	46.9	0.5	0.28	1180
	Cpx-4	46.80	3.18	6.22	7.56	13.51	0.13	20.99	0.44	0.36	99.18	45.8	0.4	0.28	1183
	Cpx-5	47.07	2.90	6.19	7.17	14.12	0.17	21.08	0.33	0.58	99.66	45.4	0.6	0.25	1174
D11-14	Cpx-1	51.14	1.15	3.99	5.31	15.61	0.11	21.41	0.27	0.83	99.86	45.2	1.8	0.23	
	Cpx-2	52.34	0.81	2.74	5.36	16.83	0.12	21.00	0.26	0.51	100.00	43.1	0.9	0.21	
	Cpx-3	52.43	0.86	2.99	5.14	17.09	0.12	20.79	0.26	0.71	100.41	42.7	1.6	0.20	
	Cpx-4	50.45	1.73	3.14	8.69	14.76	0.22	20.14	0.36	0.05	99.60	42.3	0.0 (*)	0.38	
	Cpx-5	51.37	1.30	4.23	5.75	15.74	0.13	21.37	0.28	0.60	100.82	44.7	1.7	0.25	1179
	Cpx-6	51.09	1.01	3.95	5.00	16.04	0.12	21.23	0.25	0.94	99.67	44.6	2.1	0.21	
	Cpx-7	51.23	1.11	4.14	4.89	15.71	0.10	21.66	0.27	0.83	99.93	45.7	2.2	0.21	
	Cpx-8	48.74	2.26	4.84	6.61	14.71	0.15	20.90	0.41	0.56	99.16	44.8	0.7	0.27	1192
	Cpx-9	50.66	1.71	3.70	6.53	15.12	0.13	21.34	0.33	0.18	99.71	44.9	0.0 (*)	0.29	1179
	Cpx-10	50.91	1.63	3.32	8.13	14.98	0.15	20.48	0.32	0.15	100.09	42.9	0.0 (*)	0.36	
	Cpx-11	49.71	1.41	4.65	5.93	15.40	0.09	21.14	0.33	0.51	99.19	44.7	1.8	0.22	
	Cpx-12	51.76	0.95	2.74	5.55	16.55	0.11	20.83	0.27	0.36	99.17	43.1	0.6	0.22	
	Cpx-13	50.98	1.47	4.55	5.97	15.47	0.17	21.06	0.32	0.46	100.43	44.5	2.2	0.27	1185
	Cpx-14	50.26	1.47	4.94	6.10	15.24	0.12	21.06	0.33	0.48	99.97	44.7	2.4	0.26	1188
	Cpx-15	52.35	0.99	2.60	5.76	16.72	0.17	20.80	0.28	0.32	100.01	42.7	0.5	0.23	
	Cpx-16	50.30	1.50	4.48	5.96	15.51	0.14	21.48	0.29	0.38	100.07	44.9	1.2	0.23	
	Cpx-17	52.54	0.86	2.56	6.07	16.85	0.16	20.87	0.31	0.20	100.44	42.4	0.4	0.22	
Alejandro Selkirk Island shield															
'olivine-rich'															
JR170913-4	Cpx-1	51.56	1.31	2.14	8.42	16.80	0.20	18.39	0.26	0.11	99.26	37.9	0.0 (*)	1.09	
	Cpx-2	49.77	2.30	3.41	9.41	14.52	0.19	19.56	0.35	0.05	99.53	41.4	0.0 (*)	1.42	
MF-6	Cpx-1	52.06	0.99	2.97	6.16	16.18	0.11	20.70	0.31	0.51	100.02	43.0	0.9	0.53	
	Cpx-2	52.75	0.96	2.22	6.62	16.56	0.17	20.07	0.26	0.35	99.97	41.5	0.6	0.55	
	Cpx-3	51.40	1.37	3.14	6.34	15.80	0.14	20.72	0.30	0.46	99.67	43.4	0.3	0.55	
	Cpx-4	51.13	1.18	3.34	6.58	15.75	0.11	20.55	0.35	0.50	99.49	43.1	0.8	0.55	
'near-															

primitive'															
JR170913-5	Cpx-1	51.71	1.22	3.43	5.32	16.25	0.09	21.63	0.31	0.86	100.83	44.6	0.7	0.34	
	Cpx-2	51.79	0.98	3.46	5.21	16.17	0.10	21.36	0.28	0.88	100.22	44.5	1.4	0.36	
	Cpx-3	50.69	1.83	4.13	6.58	15.49	0.15	21.15	0.34	0.26	100.59	44.1	0.5	0.44	
	Cpx-4	51.63	1.29	3.63	5.67	15.95	0.14	21.23	0.30	0.73	100.55	44.3	1.2	0.40	
	Cpx-5	50.26	1.67	4.26	6.74	15.65	0.15	20.90	0.36	0.31	100.23	43.5	0.8	0.41	
	Cpx-6	51.79	0.99	3.46	5.21	16.14	0.12	21.47	0.32	0.90	100.43	44.7	1.3	0.35	
	Cpx-7	51.25	1.08	3.96	6.64	15.86	0.15	20.97	0.27	0.37	100.53	43.4	1.2	0.43	
	Cpx-8	52.00	1.13	2.93	5.43	16.23	0.16	21.42	0.25	0.44	99.95	44.3	0.3	0.38	
	Cpx-9	51.32	1.55	3.64	6.69	15.61	0.14	20.97	0.32	0.17	100.42	43.7	0.4	0.47	
	Cpx-10	52.93	0.94	2.27	6.48	16.72	0.14	20.42	0.28	0.14	100.35	41.8	0.3	0.44	
	Cpx-11	51.33	1.42	3.67	6.72	15.60	0.12	20.95	0.26	0.20	100.33	43.6	0.4	0.48	
	Cpx-12	52.69	1.05	2.20	6.47	16.65	0.14	20.73	0.29	0.11	100.32	42.3	0.0 (*)	0.43	
	Cpx-13	51.22	1.43	3.71	6.55	15.53	0.13	21.16	0.35	0.16	100.18	44.1	0.5	0.45	
	Cpx-14	51.00	1.83	3.71	6.78	15.48	0.14	21.12	0.32	0.18	100.51	43.9	0.0 (*)	0.47	
	Cpx-15	51.88	1.11	3.20	5.50	16.05	0.13	21.53	0.31	0.43	100.12	44.6	0.6	0.38	
	Cpx-16	51.79	1.10	3.45	5.26	16.15	0.14	21.48	0.33	0.87	100.52	44.6	1.2	0.35	
	Cpx-17	51.64	0.87	3.36	4.99	15.95	0.11	21.54	0.31	0.81	99.56	45.2	1.4	0.35	
	Cpx-18	51.01	1.70	3.87	7.15	15.55	0.16	20.28	0.39	0.24	100.37	42.6	1.0	0.51	
	Cpx-19	53.31	1.16	2.04	6.95	16.86	0.19	19.88	0.25	0.13	100.70	40.6	0.5	0.47	
	Cpx-20	50.77	1.61	4.09	7.17	15.54	0.17	20.43	0.32	0.18	100.24	42.8	1.0	0.50	
	Cpx-21	50.18	1.56	4.09	7.25	15.36	0.19	20.15	0.38	0.15	99.26	42.6	1.2	0.49	
	Cpx-22	50.92	1.67	3.79	7.05	15.58	0.17	20.80	0.29	0.20	100.43	43.2	0.2	0.48	
	Cpx-23	50.66	1.80	4.02	7.27	15.49	0.21	20.68	0.30	0.16	100.57	43.0	0.2	0.49	
	Cpx-24	51.08	1.47	3.84	6.94	15.35	0.16	21.08	0.35	0.18	100.40	43.9	0.4	0.48	
	Cpx-25	51.57	1.62	3.46	6.70	15.54	0.17	21.06	0.31	0.19	100.58	43.8	0.1	0.49	
	Cpx-26	51.00	1.59	3.95	7.02	15.38	0.16	20.80	0.29	0.19	100.39	43.5	0.6	0.51	
	Cpx-27	51.11	1.48	3.89	6.73	15.45	0.10	20.66	0.35	0.38	100.21	43.5	1.2	0.49	
'differentiated'															
LL250112-1	Cpx-1	51.30	1.82	3.78	5.94	15.04	0.09	21.40	0.36	0.64	100.42	45.5	1.1	0.24	1159
	Cpx-2	52.56	1.00	2.63	6.16	15.95	0.12	20.80	0.37	0.53	100.06	43.4	1.0	0.23	
	Cpx-3	52.55	1.32	2.71	5.92	15.65	0.09	21.06	0.37	0.54	100.18	44.3	1.1	0.23	
	Cpx-4	52.74	1.41	2.30	7.64	15.62	0.18	20.00	0.28	0.16	100.28	41.8	0.4	0.29	1152
	Cpx-5	52.00	1.60	2.35	7.88	15.57	0.19	20.29	0.33	0.15	100.32	42.1	0.0 (*)	0.30	1149
	Cpx-6	51.94	1.72	2.29	8.46	15.06	0.14	20.24	0.26	0.03	100.14	42.3	0.0 (*)	0.34	
	Cpx-7	51.79	1.37	2.47	8.00	15.06	0.17	20.52	0.27	0.11	99.77	42.9	0.0 (*)	0.32	
	Cpx-8	52.30	1.75	2.37	8.27	14.82	0.16	20.49	0.30	0.07	100.48	43.0	0.0 (*)	0.33	
	Cpx-9	52.34	1.24	2.79	5.94	15.87	0.14	21.29	0.36	0.70	100.67	44.3	0.3	0.22	
	Cpx-10	50.95	1.47	4.13	6.09	15.04	0.13	21.51	0.35	0.88	100.56	45.5	1.0	0.24	1158
	Cpx-11	50.41	2.49	4.08	7.72	14.26	0.17	21.22	0.39	0.17	100.90	44.9	0.0 (*)	0.32	
	Cpx-12	51.95	1.30	3.12	5.86	15.68	0.17	21.31	0.36	0.67	100.43	44.6	0.5	0.22	
	Cpx-13	51.77	1.34	3.58	5.81	15.59	0.17	21.47	0.37	0.73	100.84	44.9	0.9	0.22	
	Cpx-14	51.82	1.10	3.47	5.88	15.50	0.11	21.53	0.39	0.79	100.59	45.1	0.9	0.22	
	Cpx-15	50.73	1.49	3.94	6.00	15.26	0.15	21.59	0.37	0.70	100.19	45.3	0.5	0.22	
	Cpx-16	52.08	1.16	3.01	6.00	15.79	0.15	21.73	0.38	0.58	100.88	44.8	0.0 (*)	0.21	
	Cpx-17	52.24	1.14	2.93	5.93	15.59	0.12	21.34	0.34	0.58	100.20	44.7	0.7	0.23	
	Cpx-18	50.78	1.67	4.22	6.25	15.12	0.11	21.28	0.39	0.70	100.53	45.0	1.0	0.24	1163
	Cpx-19	51.23	1.72	3.84	6.07	15.07	0.11	21.54	0.34	0.82	100.65	45.5	0.7	0.24	1157
	Cpx-20	51.80	1.36	2.73	5.97	15.97	0.16	21.08	0.35	0.66	100.07	43.8	0.0 (*)	0.22	
	Cpx-21	50.77	1.86	3.88	6.40	14.69	0.10	21.51	0.37	0.60	100.15	45.8	0.2	0.26	1158
	Cpx-22	50.67	1.77	3.91	6.53	14.66	0.11	21.59	0.42	0.56	100.23	45.8	0.0 (*)	0.26	1161
	Cpx-23	51.06	1.59	3.77	6.34	14.92	0.10	21.42	0.37	0.64	100.17	45.4	0.5	0.25	1159
	Cpx-24	49.60	2.52	4.52	8.20	13.93	0.16	20.91	0.41	0.22	100.38	44.7	0.0 (*)	0.34	
	Cpx-25	50.62	2.15	3.80	7.66	14.26	0.14	21.42	0.39	0.14	100.52	45.3	0.0 (*)	0.32	
	Cpx-26	52.53	1.23	2.93	5.87	15.70	0.18	21.65	0.32	0.55	100.91	44.9	0.3	0.22	
	Cpx-27	50.58	1.66	4.26	6.18	14.86	0.11	21.49	0.44	0.80	100.37	45.6	1.0	0.24	1166
	Cpx-28	52.20	1.17	2.70	5.79	15.62	0.14	21.66	0.35	0.55	100.18	45.1	0.0 (*)	0.22	
	Cpx-29	52.82	1.48	2.13	7.79	15.93	0.17	20.48	0.22	0.18	101.20	41.9	0.0 (*)	0.29	1141
	Cpx-30	52.38	1.31	2.10	7.09	15.36	0.16	21.07	0.34	0.22	99.94	43.8	0.0 (*)	0.28	1152

Table III.3. Pressure and temperature conditions estimated from clinopyroxene and olivine EPMA data in lavas from O'Higgins, Alpha and Alejandro Selkirk volcanoes. n indicates the number of samples considered in each case.

Geological unit	Volcanic center	Compositional groups	n	Cpx_{an} P (kbar)[A]	n	Ol-Liq T (°C)[B]	n	Cpx-Liq T (°C)[C]
Shield	O'Higgins							
		olivine-rich		-		-		-
		differentiated		-		-		-
	Alpha							
		differentiated	2	0.0 - 2.4		-	2	1174 - 1192
	Alejandro Selkirk							
		olivine-rich	2	0.0 - 0.9		-		-
		near-primitive	1	0.0 - 1.4		-		-
		differentiated	1	0.0 - 1.1	1	1150 - 1153	2	1141 . 1166
Rejuvenated	O'Higgins							
		low-Mg (all)	2	0.0 - 12.0	2	1266 - 1287		-
		(high Na_2O)	2	6.5 - 12.0		-		-
		(low Na_2O)	2	0.0 - 1.6		-		-

(A) Clinopyroxene pressure in anhydrous basalts from Nimis and Ulmer, 1989 (±1.7 kbar + ca. 1 kbar per 1wt% H_2O in melt).
(B) Olivine-liquid temperature from Herzberg and O'Hara, 2002 (±31 °C).
(C) Clinopyroxene-liquid temperature from Putirka et al., 2003 (±33 °C).

Table III.4. EPMA data (wt%) of olivine in lavas from O'Higgins, Alpha and Alejandro Selkirk volcanoes. Only measures with acceptable structural formula are considered (cations equal to 3.00 ± 0.02). For rejuvenated unit; c: core; r: rim; m: mantle xenocryst; x: unknown origin xenocryst. (A) $^{Ol\text{-}Liq}$Kd calculated assuming 90% of total iron is ferrous in the liquid (whole rock). (B) Olivine-liquid temperature from Herzberg and O'Hara, 2002 (±31 °C).

Sample	Spot		SiO_2	FeO^T	MgO	MnO	CaO	NiO	Sum	Fo	Ol-Liq	
Det. limit			*0.02*	*0.02*	*0.01*	*0.02*	*0.01*	*0.02*			$K_D^{(A)}$	T (°C)$^{(B)}$
O'Higgins guyot shield 'olivine-rich'												
D10-5	Ol-1		38.74	13.36	46.03	0.21	0.28	0.29	99.09	86.0	0.47	
	Ol-2	c	39.10	13.33	46.99	0.19	0.24	0.22	100.25	86.3	0.46	
	Ol-3	c	38.48	14.44	45.37	0.25	0.28	0.35	99.45	84.8	0.51	
	Ol-4	c	38.83	14.24	45.59	0.17	0.26	0.25	99.56	85.1	0.51	
	Ol-5	c	38.86	13.74	46.18	0.22	0.26	0.26	99.64	85.7	0.48	
	Ol-6	c	38.89	13.68	46.29	0.19	0.25	0.32	99.80	85.8	0.48	
	Ol-7	c	39.17	13.46	46.68	0.20	0.26	0.26	100.20	86.1	0.47	
O'Higgins guyot rejuvenated 'low-Mg'												
2D-1	Ol-1	r	38.84	16.42	44.60	0.23	0.19	0.14	100.56	82.9	0.28	1267
	Ol-2	r	38.37	17.20	42.94	0.27	0.23	0.11	99.18	81.7	0.30	1274
	Ol-3	r	38.57	16.34	44.42	0.20	0.20	0.16	99.97	82.9	0.28	1267
	Ol-4	r	38.33	17.24	43.22	0.24	0.21	0.04	99.42	81.7	0.30	1273
	Ol-5	r	38.20	18.08	42.39	0.36	0.30	0.15	99.59	80.7	0.32	1278
	Ol-6	r	38.03	17.55	42.60	0.29	0.23	0.11	98.92	81.2	0.31	1275
	Ol-7	r	38.62	15.87	44.54	0.19	0.21	0.14	99.74	83.3	0.27	1266
	Ol-8	r	38.53	16.52	43.79	0.26	0.20	0.14	99.55	82.5	0.29	1269
	Ol-9	r	38.85	16.37	44.40	0.19	0.17	0.14	100.18	82.9	0.28	1268
	Ol-10	r	38.30	16.95	43.15	0.27	0.20	0.14	99.14	81.9	0.30	1272
2D-2	Ol-1	x	38.04	18.85	42.19	0.26	0.18	0.00	99.58	80.0	0.36	
	Ol-2	r	38.41	17.51	43.73	0.15	0.22	0.00	100.12	81.7	0.32	1283
	Ol-3	r	39.00	16.03	45.17	0.17	0.22	0.01	100.69	83.4	0.29	1276
	Ol-4	r	39.05	17.10	44.13	0.26	0.28	0.14	101.09	82.1	0.31	1283
	Ol-5	r	39.20	15.76	45.49	0.13	0.17	0.17	101.04	83.7	0.28	1275
	Ol-6	r	38.55	17.29	43.15	0.25	0.28	0.10	99.73	81.6	0.32	1286
	Ol-7	r	38.73	15.39	44.43	0.21	0.20	0.14	99.17	83.7	0.28	1277
	Ol-8	r	38.57	17.30	43.46	0.25	0.26	0.09	100.04	81.7	0.32	1285
	Ol-9	c	39.02	13.82	46.21	0.11	0.23	0.07	99.60	85.6	0.24	
	Ol-10	r	38.27	17.73	42.92	0.26	0.27	0.09	99.65	81.2	0.33	1287
	Ol-11	c	39.74	11.58	48.00	0.17	0.20	0.28	100.11	88.1	0.19	
	Ol-12	c	39.26	14.43	45.75	0.17	0.21	0.17	100.09	85.0	0.25	
	Ol-13	r	38.78	17.21	43.52	0.26	0.28	0.09	100.21	81.8	0.32	1285
	Ol-14	x	38.18	20.30	41.62	0.37	0.02	0.17	100.67	78.5	0.39	
	Ol-15	x	38.09	20.20	41.38	0.31	0.07	0.20	100.29	78.5	0.39	
	Ol-16	r	39.18	15.41	45.00	0.18	0.21	0.20	100.30	83.9	0.28	1276
	Ol-17	r	38.17	17.37	43.36	0.28	0.22	0.14	99.66	81.6	0.32	1284
	Ol-21	m	39.06	13.30	46.46	0.18	0.05	0.39	99.41	86.2	0.23	
	Ol-22	m	39.66	13.20	47.43	0.18	0.05	0.27	100.80	86.5	0.22	
Alpha seamount shield 'differentiated'												
D11-12	Ol-1		38.21	17.25	43.42	0.27	0.28	0.13	99.60	81.8	0.24	
	Ol-2		38.36	17.48	43.31	0.28	0.26	0.12	99.89	81.5	0.25	
	Ol-3		38.30	17.50	43.27	0.25	0.28	0.13	99.77	81.5	0.25	
	Ol-4		38.34	17.58	43.44	0.24	0.27	0.13	100.05	81.5	0.25	
	Ol-5		38.46	17.36	43.55	0.28	0.25	0.16	100.13	81.7	0.24	
	Ol-6		38.40	17.23	43.19	0.31	0.25	0.14	99.65	81.7	0.24	
	Ol-7		38.19	17.41	43.12	0.25	0.27	0.17	99.44	81.5	0.25	
	Ol-8		38.20	17.48	43.20	0.30	0.26	0.14	99.66	81.5	0.25	
	Ol-9		38.25	17.39	43.25	0.24	0.27	0.16	99.59	81.6	0.25	
D11-14	Ol-1		38.41	14.99	44.49	0.27	0.30	0.25	98.74	84.1	0.23	
	Ol-2		38.98	15.15	45.40	0.23	0.24	0.17	100.23	84.2	0.23	
	Ol-3		38.88	15.08	45.05	0.20	0.28	0.15	99.72	84.2	0.23	
	Ol-4		39.13	14.49	45.51	0.24	0.27	0.22	99.92	84.8	0.22	

	Ol-5	39.32	12.75	47.10	0.17	0.21	0.30	99.98	86.8	0.19
	Ol-6	39.41	13.11	47.35	0.20	0.24	0.27	100.66	86.6	0.19
	Ol-7	40.28	12.36	45.75	0.22	0.24	0.26	99.18	86.8	0.19
Alejandro Selkirk Island shield										
'olivine-rich'										
JR170913-4	Ol-1	38.52	15.25	44.67	0.21	0.27	0.28	99.30	83.9	0.78
	Ol-2	38.56	15.12	44.54	0.21	0.24	0.24	99.13	84.0	0.78
	Ol-3	38.43	15.34	44.71	0.25	0.23	0.24	99.39	83.9	0.78
	Ol-4	38.23	15.07	44.49	0.25	0.23	0.27	98.63	84.0	0.77
	Ol-5	38.50	15.27	44.65	0.20	0.20	0.27	99.27	83.9	0.78
	Ol-6	38.26	14.96	44.71	0.21	0.19	0.26	98.76	84.2	0.76
	Ol-7	38.69	14.72	44.81	0.20	0.24	0.29	99.09	84.4	0.75
	Ol-8	38.50	14.30	44.61	0.25	0.23	0.27	98.31	84.8	0.73
	Ol-9	38.60	14.37	45.24	0.20	0.23	0.24	99.01	84.9	0.73
	Ol-10	38.41	14.83	44.58	0.18	0.25	0.22	98.53	84.3	0.76
	Ol-11	38.50	14.93	44.47	0.26	0.23	0.24	98.67	84.1	0.77
	Ol-12	38.53	14.80	44.12	0.23	0.25	0.29	98.34	84.2	0.77
	Ol-13	38.66	15.01	44.57	0.22	0.23	0.21	99.00	84.1	0.77
	Ol-14	38.55	15.13	44.66	0.19	0.25	0.24	99.15	84.0	0.77
MF-6	Ol-1	38.87	16.09	44.61	0.24	0.28	0.23	100.49	83.2	0.50
	Ol-2	38.57	15.21	44.63	0.23	0.23	0.26	99.25	83.9	0.47
	Ol-3	39.07	15.71	44.73	0.20	0.25	0.22	100.25	83.5	0.48
	Ol-4	38.52	15.48	44.38	0.21	0.26	0.21	99.24	83.6	0.48
	Ol-5	38.70	15.29	44.63	0.17	0.28	0.24	99.51	83.9	0.47
	Ol-6	38.42	15.35	44.54	0.16	0.25	0.28	99.04	83.8	0.48
	Ol-7	38.86	15.34	44.72	0.22	0.22	0.21	99.75	83.9	0.47
	Ol-8	38.74	15.44	44.94	0.23	0.25	0.28	99.97	83.8	0.47
	Ol-9	38.87	15.49	44.79	0.23	0.24	0.26	99.98	83.8	0.48
	Ol-10	38.71	15.69	44.97	0.18	0.25	0.27	100.16	83.6	0.48
	Ol-11	38.92	15.12	45.06	0.20	0.21	0.25	99.79	84.2	0.46
	Ol-12	38.72	15.49	44.70	0.22	0.31	0.23	99.69	83.7	0.48
	Ol-13	38.68	15.59	44.97	0.18	0.24	0.21	99.79	83.7	0.48
	Ol-14	38.73	15.43	45.00	0.21	0.24	0.22	99.90	83.9	0.47
	Ol-15	38.93	15.47	44.78	0.20	0.24	0.27	99.98	83.8	0.48
	Ol-16	38.53	15.36	44.70	0.18	0.24	0.18	99.33	83.8	0.47
	Ol-17	38.77	15.56	44.78	0.22	0.28	0.26	99.91	83.7	0.48
	Ol-18	38.76	15.29	45.02	0.21	0.26	0.21	99.89	84.0	0.47
	Ol-19	38.77	16.13	44.48	0.25	0.27	0.21	100.30	83.1	0.50
	Ol-20	38.67	15.65	44.37	0.17	0.24	0.22	99.44	83.5	0.49
	Ol-21	38.75	15.65	44.64	0.21	0.27	0.22	99.86	83.6	0.48
	Ol-22	39.04	15.70	44.99	0.18	0.24	0.24	100.43	83.6	0.48
	Ol-23	38.83	15.31	44.96	0.24	0.24	0.25	99.95	84.0	0.47
	Ol-24	38.98	15.66	44.68	0.23	0.28	0.27	100.15	83.6	0.48
'near-primitive'										
JR170913-5	Ol-1	39.13	15.58	45.07	0.20	0.26	0.30	100.49	83.8	0.39
	Ol-2	38.98	15.53	45.06	0.18	0.25	0.20	100.39	83.8	0.39
	Ol-3	38.75	15.47	44.81	0.22	0.24	0.28	99.87	83.8	0.39
	Ol-4	38.97	15.56	45.22	0.23	0.25	0.21	100.47	83.8	0.39
	Ol-5	39.02	15.81	44.93	0.24	0.26	0.22	100.65	83.5	0.40
	Ol-6	39.21	15.58	45.04	0.20	0.24	0.29	100.62	83.8	0.39
	Ol-7	38.87	15.56	45.26	0.20	0.24	0.29	100.52	83.8	0.39
	Ol-8	38.66	16.71	44.23	0.27	0.27	0.18	100.36	82.5	0.43
	Ol-9	39.32	15.63	45.35	0.22	0.23	0.22	101.11	83.8	0.39
	Ol-10	39.27	15.63	44.96	0.23	0.23	0.25	100.63	83.7	0.39
	Ol-11	39.18	15.51	45.24	0.26	0.25	0.29	100.71	83.9	0.39
	Ol-12	38.91	15.68	45.15	0.25	0.27	0.31	100.69	83.7	0.39
	Ol-13	39.04	15.80	45.40	0.22	0.26	0.29	101.17	83.7	0.39
	Ol-14	39.14	16.00	44.97	0.20	0.27	0.24	100.73	83.4	0.40
	Ol-15	38.51	15.86	44.58	0.24	0.23	0.18	99.58	83.4	0.40
	Ol-16	38.57	15.92	44.69	0.20	0.24	0.26	99.93	83.3	0.40
	Ol-17	38.92	16.51	44.20	0.27	0.25	0.18	100.29	82.7	0.42
	Ol-18	38.82	15.94	44.72	0.28	0.21	0.23	100.27	83.3	0.40
JR170913-16	Ol-1	38.47	18.14	43.10	0.21	0.18	0.27	100.39	80.9	0.40
	Ol-2	38.71	18.26	43.25	0.22	0.20	0.19	100.89	80.8	0.40
	Ol-3	38.73	18.21	43.15	0.26	0.23	0.19	100.94	80.9	0.40
	Ol-4	38.55	18.53	42.78	0.19	0.22	0.20	100.52	80.4	0.41
	Ol-5	38.81	18.46	43.00	0.24	0.24	0.20	101.02	80.6	0.41
	Ol-6	38.61	18.18	43.13	0.23	0.26	0.22	100.70	80.9	0.40

	Ol-7	38.21	19.30	42.17	0.24	0.19	0.10	100.34	79.6	0.43	
	Ol-8	38.46	19.28	42.31	0.24	0.17	0.16	100.85	79.6	0.43	
	Ol-9	38.49	19.41	42.27	0.25	0.16	0.15	100.79	79.5	0.44	
	Ol-10	38.33	18.41	42.86	0.23	0.20	0.22	100.28	80.6	0.41	
	Ol-11	38.60	18.01	43.36	0.21	0.19	0.17	100.52	81.1	0.39	
	Ol-12	38.88	17.88	43.37	0.22	0.17	0.11	100.79	81.2	0.39	
	Ol-13	38.44	17.94	43.26	0.22	0.21	0.19	100.33	81.1	0.39	
	Ol-14	38.12	18.09	42.83	0.27	0.23	0.19	99.84	80.8	0.40	
	Ol-15	38.36	18.25	42.66	0.23	0.26	0.20	100.11	80.6	0.41	
	Ol-16	38.30	17.93	43.13	0.20	0.24	0.22	100.17	81.1	0.39	
JR170913-21	Ol-1	38.22	18.69	41.99	0.26	0.23	0.26	99.68	80.0	0.55	
	Ol-2	38.64	16.50	43.53	0.25	0.19	0.20	99.36	82.5	0.46	
	Ol-3	38.61	16.42	43.84	0.27	0.30	0.27	99.90	82.6	0.46	
	Ol-4	38.68	17.09	43.67	0.23	0.28	0.21	100.15	82.0	0.48	
	Ol-5	38.10	19.17	41.58	0.22	0.25	0.18	99.50	79.4	0.56	
	Ol-6	38.64	16.63	43.83	0.24	0.24	0.28	100.08	82.4	0.46	
	Ol-7	38.23	19.20	41.76	0.24	0.24	0.18	99.89	79.5	0.56	
	Ol-8	38.30	19.49	41.72	0.21	0.23	0.22	100.33	79.2	0.57	
	Ol-9	38.18	17.48	42.99	0.22	0.24	0.25	99.53	81.4	0.50	
	Ol-10	38.56	16.50	44.14	0.22	0.24	0.17	99.93	82.7	0.46	
	Ol-11	38.49	17.09	43.89	0.20	0.25	0.25	100.18	82.1	0.48	
	Ol-12	38.50	17.21	43.39	0.26	0.29	0.21	99.96	81.8	0.49	
	Ol-13	38.44	16.88	43.94	0.24	0.27	0.29	100.19	82.3	0.47	
	Ol-14	38.64	16.90	43.59	0.22	0.27	0.27	99.99	82.1	0.48	
	Ol-15	38.56	16.67	43.93	0.24	0.24	0.21	99.93	82.4	0.46	
	Ol-16	38.74	17.17	43.92	0.20	0.26	0.24	100.54	82.0	0.48	
'differentiated'											
LL250112-1	Ol-1	37.97	20.98	40.41	0.35	0.33	0.08	100.14	77.4	0.31	1152
	Ol-3	38.12	21.31	40.57	0.29	0.35	0.11	100.68	77.2	0.31	1153
	Ol-4	37.77	20.96	40.48	0.31	0.34	0.14	100.01	77.5	0.31	1151
	Ol-5	38.18	20.66	40.45	0.26	0.49	0.04	100.28	77.7	0.31	1152
	Ol-6	38.11	20.95	40.92	0.23	0.34	0.05	100.64	77.7	0.31	1150
	Ol-7	38.11	20.92	41.13	0.29	0.38	0.13	101.06	77.8	0.30	1150
	Ol-8	37.91	20.99	40.79	0.27	0.37	0.09	100.48	77.6	0.31	1151
	Ol-9	37.66	20.90	40.61	0.30	0.32	0.14	100.04	77.6	0.31	1151
	Ol-10	37.86	21.32	40.72	0.29	0.36	0.13	100.65	77.3	0.31	1152
	Ol-11	38.06	21.38	40.40	0.31	0.35	0.14	100.73	77.1	0.32	1153
	Ol-12	37.93	20.93	40.64	0.29	0.33	0.19	100.28	77.6	0.31	1151
	Ol-13	38.08	20.89	40.95	0.32	0.31	0.10	100.68	77.7	0.30	1150
	Ol-14	37.98	21.06	40.56	0.32	0.33	0.14	100.62	77.4	0.31	1152
	Ol-15	38.18	21.36	40.57	0.32	0.33	0.11	100.99	77.2	0.31	1153
LL260112-4	Ol-2	38.00	18.96	42.17	0.24	0.22	0.17	99.82	79.9	0.26	
	Ol-3	38.17	19.01	42.33	0.23	0.21	0.20	100.18	79.9	0.26	

Figure III.1. Total-alkali vs. silica (TAS) classification diagram for lavas and dykes from O'Higgins, Alpha and Alejandro Selkirk volcanoes (after Le Maitre, 2002; alkali-subalkali boundary is from Irvine and Baragar, 1971).

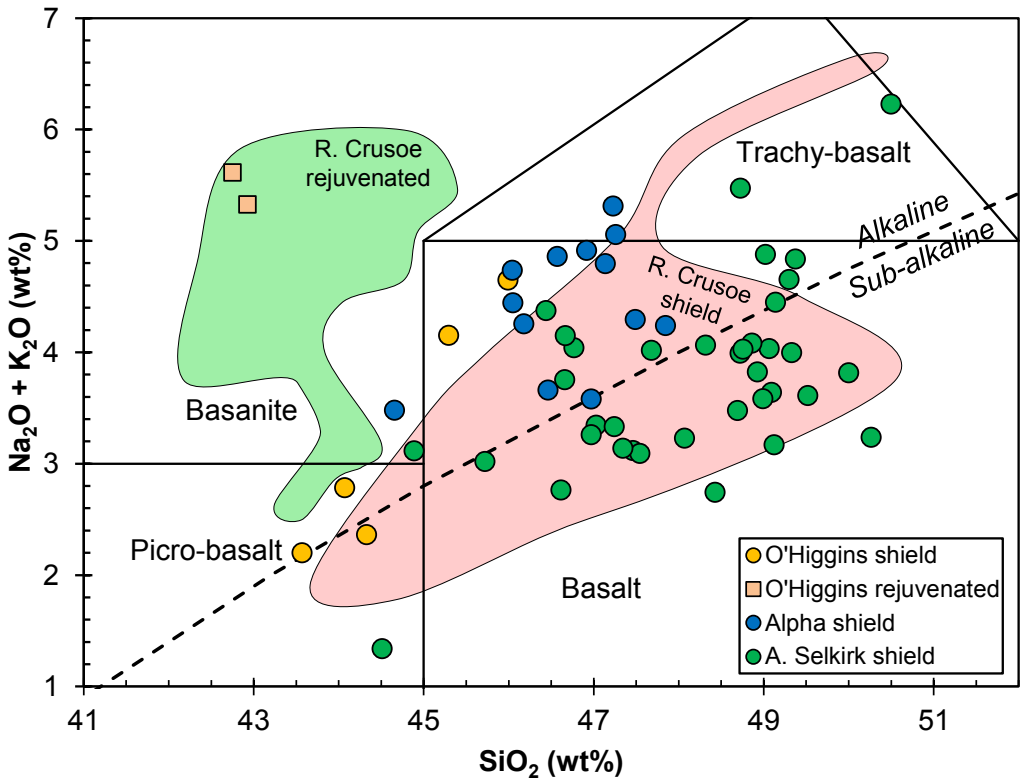

Figure III.2. Mg-number (Mg#) vs. Ni content diagram for shield and rejuvenated lavas from O'Higgins, Alpha and Alejandro Selkirk volcanoes. Compositional groups of Robinson Crusoe are showed.

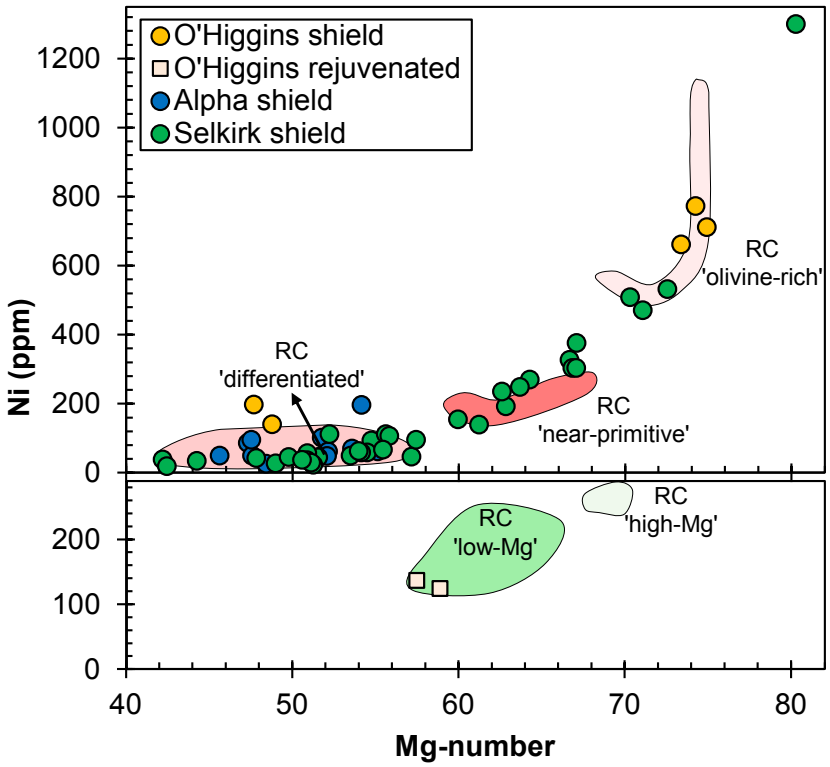

Figure III.3. SEM microphotographs of clinopyroxene in JFR. Pressure estimations (kbar) are indicated. a), b) and c) Phenocrysts formed at low pressure in lavas from shield stage of Alpha seamount (a: D11-14), 'near-primitive' (b: JR170913-5) and 'differentiated' (c: LL50112-1) groups of Alejandro Selkirk Island. d) Phenocrysts formed at low pressures (low-Na) in rejuvenated volcanism (2D-1) of O'Higgins. e) Low-Na rims around high-Na core (xenocryst) in rejuvenated basanite (2D-2) from O'Higgins. f) Antecryst formed at high pressures showing resorption texture in O'Higgins rejuvenated stage. (*) Negatives pressures (slightly < 0.0 kbar) are considered as 0.0 (see section 4 of Chapter II for details).

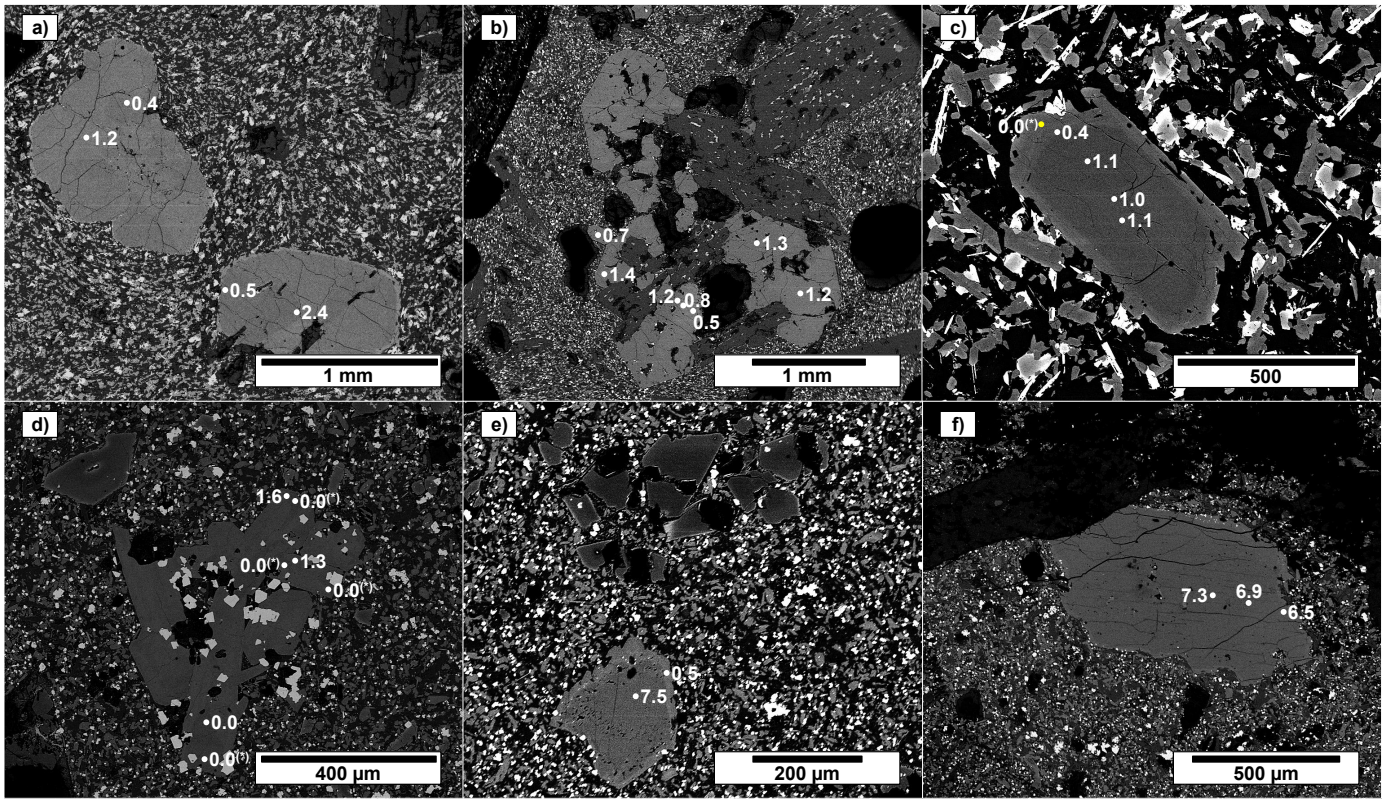

Figure III.4. Clinopyroxene composition, Na2O and TiO2 (wt%) vs. wollastonite content (Wo) in lavas from O´Higgins, Alpha and Alejandro Selkirk volcanoes. Fields of Robinson Crusoe data and error bars are also showed.

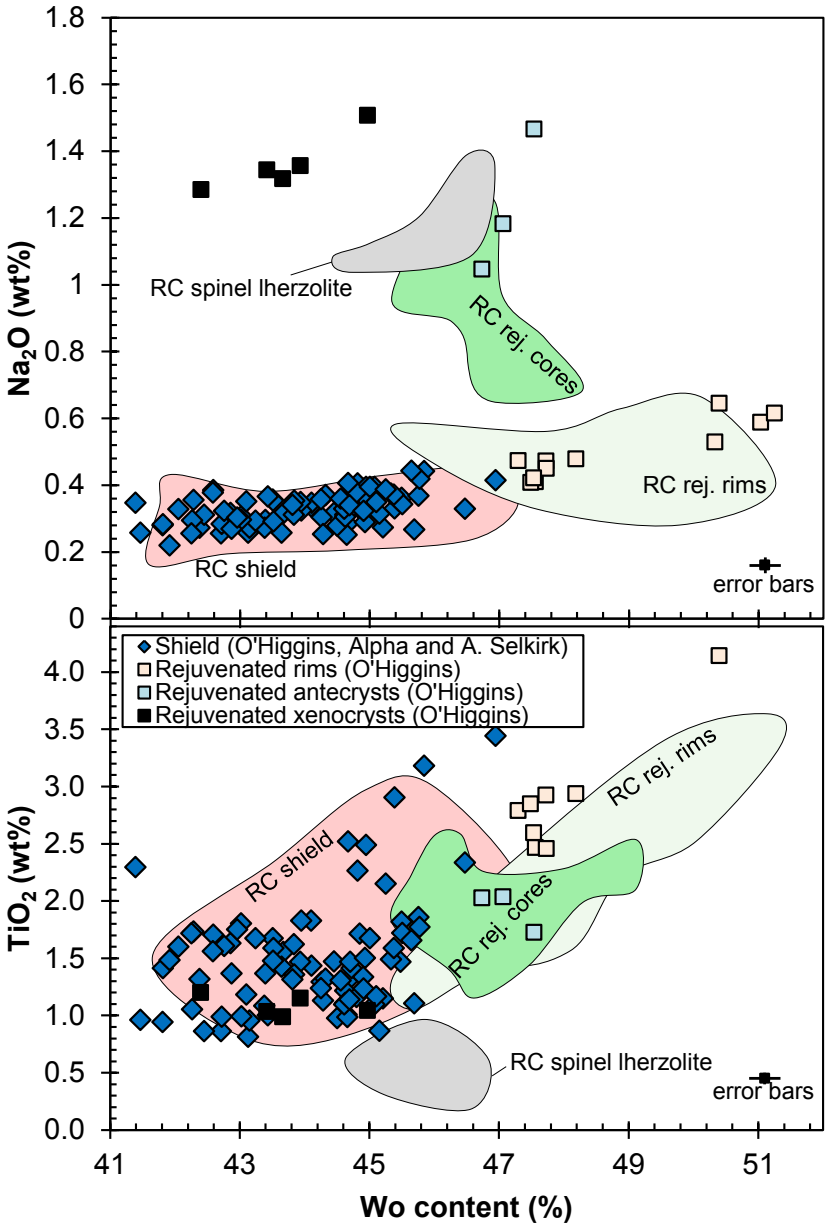

Figure III.5. SEM microphotographs of olivine in JFR, forsterite content (Fo) is indicated. a) Phenocrysts in picrite (D10-5) from 'olivine-rich' group in O'Higgins guyot. b) Two phenocrysts with iddingsite rims in shield basalt (D11-14) from Alpha seamount. c) Crystals with spinel inclusions of 'olivine-rich' group (MF-6) in Alejandro Selkirk shield stage. d) Subtle reverse zoning in basalt (JR170913-16) of 'near-primitive' group from Alejandro Selkirk shield volcanism. e) Normally zoned crystal with iddingsite rims from 'differentiated' group (LL250112-1) of Alejandro Selkirk shield. f) Classical pattern for the rejuvenated stage: differentiated rims (low-Fo content) around high-Fo cores (antecrysts) in basanites (2D-1) from O'Higgins guyot.

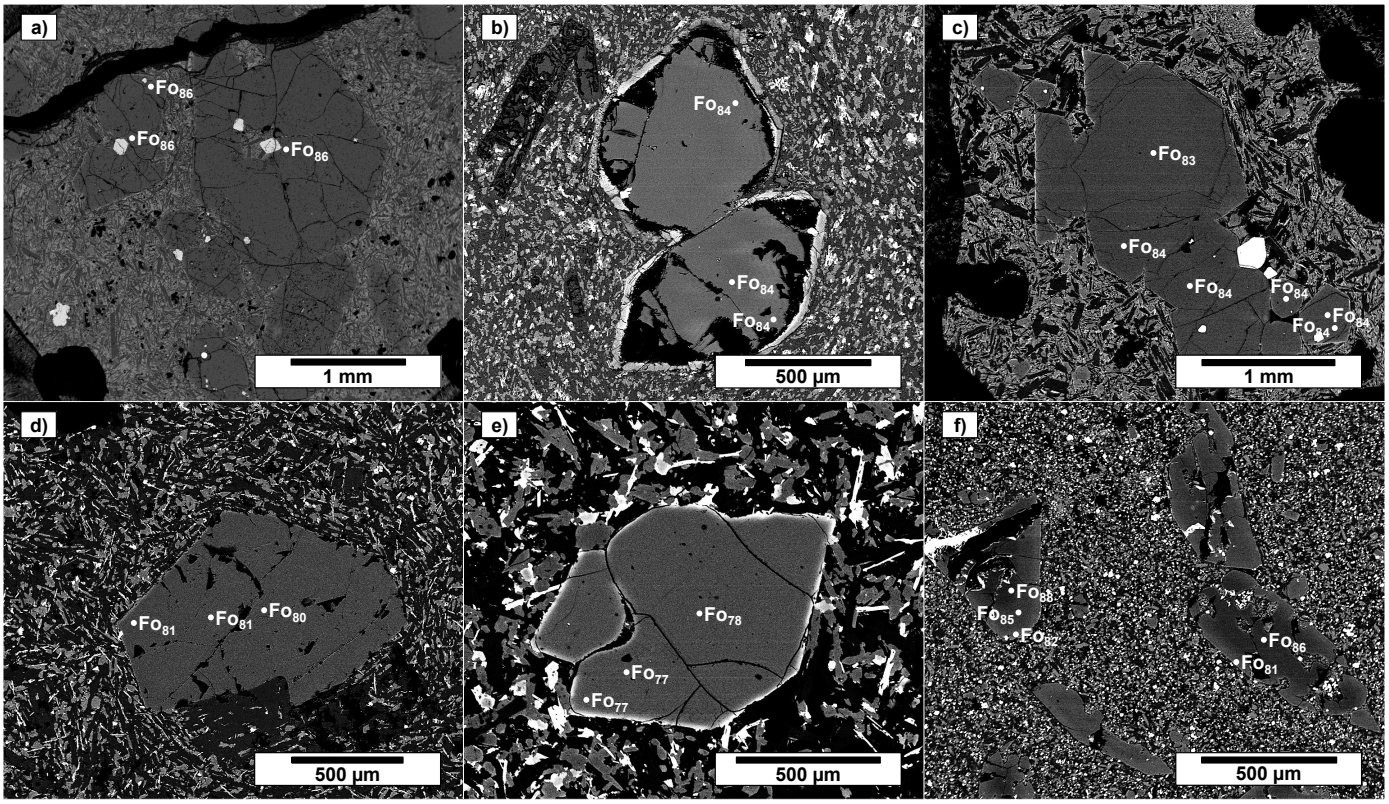

Figure III.6. Olivine Fo content vs. whole-rock Mg# in lavas from O'Higgins, Alpha and Alejandro Selkirk lavas. Olivine-liquid equilibrium field after Roeder and Emslie (1970) using a $^{Ol\text{-}Liq}Kd$ of 0.30 ± 0.03.

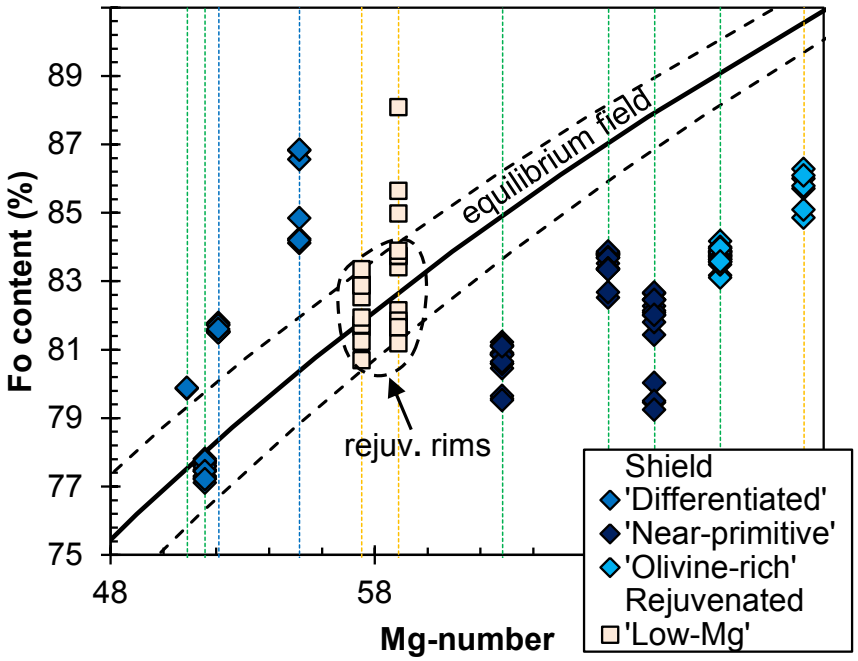

Figure III.7. Olivine composition, Ni and Ca (ppm) vs. Fo content in lavas from O'Higgins, Alpha and Alejandro Selkirk volcanoes. Fields of Robinson Crusoe data, origin of xenocrysts and error bars are also showed.

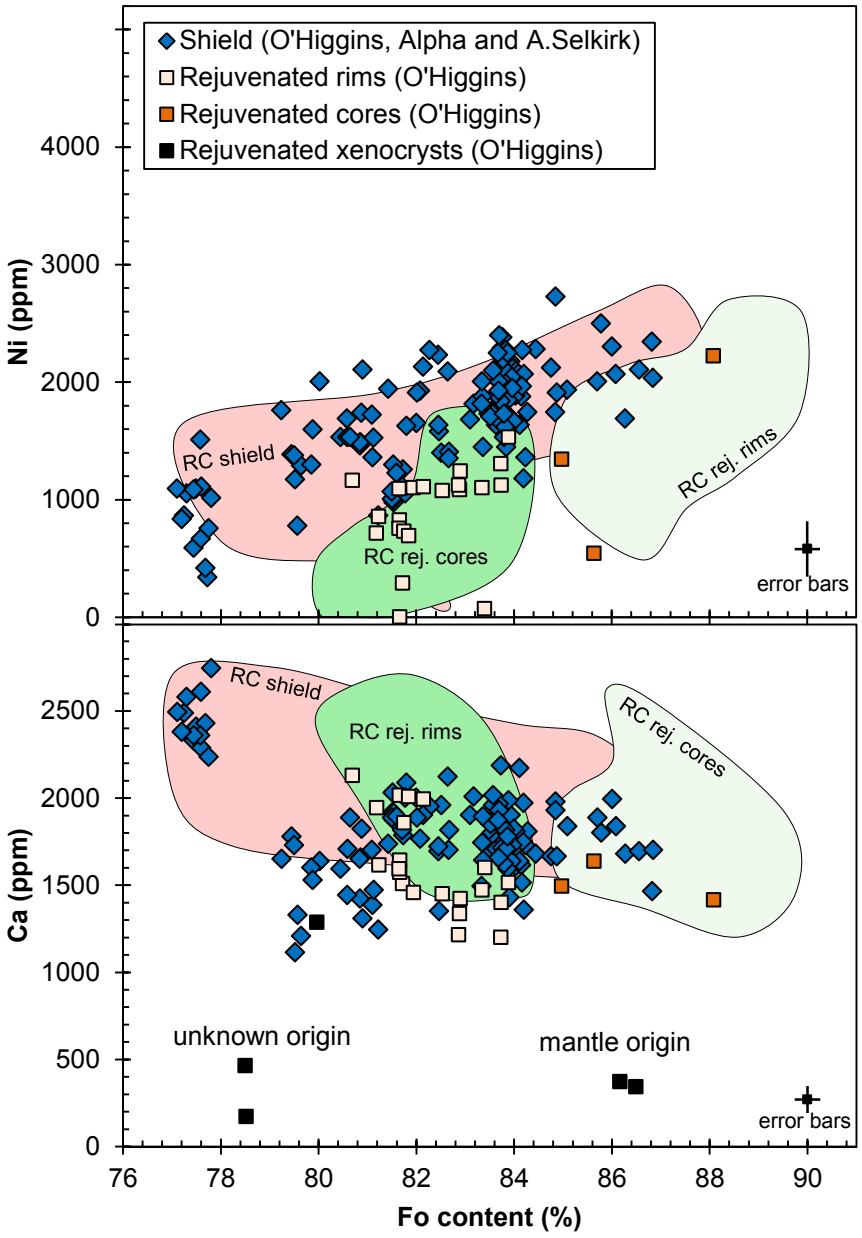

Capítulo IV

Mantle plume beneath Juan Fernández Ridge: $^{40}Ar/^{39}Ar$ plateau ages progression consistent with the Nazca plate movement

IV.1. Introduction

The Juan Fernández Ridge (JFR) is an aseismic ridge (c.a. 800 km) located in the Nazca Plate (SE Pacific) as reflect of oceanic intraplate volcanism. It formation (based on isotopic or geophysical observations) has been associated to the ascent of a mantle plume based mainly in their high $^{3}He/^{4}He$ ratios (Farley et al., 1993; Devey et al., 2000; Courtillot et al., 2003; Montelli et al., 2006; French and Romanowicz, 2015; Jackson et al., 2017; Truong et al., 2018). An important aspect according to the classical theory (e.g., Morgan, 1971; 1972) is the age progression of the chain concordant to plate movement (the lithosphere moves over the fixed to asthenosphere plume). Despite this, geochronological data of JFR is still scarce and only a few anchor points are available to test the hypothesis, mainly K-Ar ages (Booker et al., 1967; Stuessy et al., 1984), three $^{40}Ar/^{39}Ar$ ages of O'Higgins (~ 9.3, ~ 8.4 Ma; Lara et al., submitted; ~ 8.5 Ma; von Heune et al., 1997) and two of Robinson Crusoe (~ 3.8 and ~ 0.9 Ma for shield and rejuvenated volcanism; Reyes et al., 2017). This contribution shows new $^{40}Ar/^{39}Ar$ geochronological data along the chain (O'Higgins guyot, Alpha seamount, Robinson Crusoe and Alejandro Selkirk islands, see Figure III.1 of Chapter III) including the different volcanic stages recognized in JFR (shield and rejuvenated, Reyes et al., 2017; Lara et al., submitted).

IV.2. $^{40}Ar/^{39}Ar$ geochronology of JFR

From field reconnaissance and dredging locations, strategic sites were sampled to obtain new $^{40}Ar/^{39}Ar$ geochronological data. 16 samples was analyzed at Servicio Nacional de Geología y Minería, Chile (SERNAGEOMIN) with a MAP 215-50 mass spectrometer following the procedure described in Reyes et al (2017). Additionally, 14 samples were analyzed at WiscAr Geochronology Laborarory also used a MAP 215-50 (see procedure details in Lara et al., submitted). Results are detailed in Table 1 and show plateau ages between 9.26 ± 0.28 (in O'Higgins guyot) and 0.77 ± 0.14 (in Robinson Crusoe).

IV.3. Recognizing the rejuvenated volcanism in JFR

The rejuvenated volcanism (previously called post-erosional) is a stage of magmatism after the building of shield volcano that does not satisfy the principle of age progression (e.g., Hoernle and Schmincke, 1993; Garcia et al., 2010; Konter and Jackson, 2012) recognized in two volcanoes of JFR: O'Higgins guyot and Robinson Crusoe Island. So, it is necessary to distinguish this volcanism from the shield stage to discard it from the plume analysis. In Robinson Crusoe, the field expression of rejuvenated volcanism is clear, principally filling paleo-relief depressions (Figure IV.1) with basanites considerably younger than shield basalts (Figure IV.2) (Table IV.1). In O'Higgins, the high resolution bathymetry shows the rejuvenated lavas as a fresh morphology just on top of the guyot (Figure 3, taken from Lara et al., 2017). Furthermore, geochemical and isotopic features (associated to petrogenetic changes between stages, see chapter 6) as enrichments in Nb/Zr and $^{207}Pb/^{204}Pb$ ratios (Figure IV.4, data in Tables V.3 and V.4 from Chapter V)

facilitate the recognition. From the data is possible to establish a minimum (because the top of the shield is eroded) hiatus of ~ 1.73 Ma between shield and rejuvenated volcanism in Robinson Crusoe, and ~ 0.25 Ma in O'Higgins.

IV.4. Age progression in the shield volcanism

If is true that JFR is a result of the ascent of a mantle plume in the classic sense, is possible to estimate the movement of the oceanic plate considering the available ages and the distance between the volcanoes. Figure IV.5 shows the shield ages of O'Higgins, Alpha, Robinson Crusoe and Alejandro Selkirk vs. their distance (great circle distance) from Domingo seamount (the westernmost known volcano of JFR). The linear trend (r^2: 0.96) indicates a velocity of 81.18 mm/yr, very closer to the NUVEL 1A model (82.11 mm/yr; Gripp and Gordon, 1990; DeMets et al., 1994), and only 6% higher than MORVEL 2010 (76.65 mm/yr; DeMets et al., 2010) and 14% than GEODVEL 2010 (70.53 mm/yr; Argus et al., 2010). These data allow validating the mantle plume theory from the point of view of the hotspot track, which adds a new check to Courtillot et al. (2003) catalogue (the other checks are high values of $^3He/^4He$ and buoyancy), raising JFR to the category of primary mantle plume. The available data also implies a fast eruption rate in Robinson Crusoe. In fact, the volcanic pile of the island (915 m high) was formed in ~ 0.70 Ma. Other observations are that the best fit crosses the x-axis in -23.27, suggesting that the actual position of the plume would be located ~ 120 km to west of Alejandro Selkirk, relatively close to Friday and Domingo, two seamounts considering as part of JFR (Devey et al., 2000), the activity occurred simultaneously in two volcanoes: Robinson Crusoe (in the rejuvenated stage) and Alejandro Selkirk (in the voluminous shield-building stage), and the notorious volcanic gap (based in bathymetry) between O'Higgins and the closest seamount to the E (Figure III.1 of Chapter III).

IV.5. U-Pb zircon ages in syenites of Robinson Crusoe

Most of the rocks in the JFR correspond to basic lavas and hypabyssal intrusives. However, in Robinson Crusoe, there are outcrops of coarse grained rocks that bear syenites with clinopyroxene and adcumulate texture. Two U-Pb zircon ages (Centro de Excelencia en Geotermia de Los Andes, CEGA; see Leisen et al., 2015 for analytical details) yielded values which correlate well with the shield stage of volcanism in Robinson Crusoe. In detail, the sample LL270711-1 has a TuffZirc age (Ludwig, 2003) of 3.71 (+0.07 -0.05) Ma (n= 15 of 21), and the sample LL270711-2, an age of 3.89 (+0.05 -0.04) Ma (n= 11 of 19) (Figure IV.6). These ages are clearly within the range of shield volcanism in Robinson Crusoe (~4.10 – 3.40 Ma), and consistent with the age progression of the JFR, suggesting a bimodal character of magmatism in the island. Four crystals have less representative ages between 23 and 27 Ma, and thus, they are interpreted as inherited zircons, probably related to the formation of the Nazca Plate seafloor.

Bibliography

Argus, D.F., Gordon, R.G., Heflin, M.B., Ma, C., Eanes, R.J., Willis, P., Peltier, W.R., Owen, S.E., 2010. The angular velocities of the plates and the velocity of Earth's centre from space geodesy. Geophys. J. Int. 180, 913–960. doi.org/10.1111/j.1365-246X.2009.04463.x

Booker, J., Bullard, E.C., Grasty, R.L., 1967. Palaeomagnetism and age of rocks from Easter Island and Juan Fernandez. Geophys. J. Int. 12, 469–471. doi.org/10.1111/j.1365-246X.1967.tb03127.x

Courtillot, V., Davaille, A., Besse, J., Stock, J., 2003. Three distinct types of hotspots in the Earth's mantle. Earth Planet. Sci. Lett. 205, 295–308. doi.org/10.1016/S0012-821X(02)01048-8

DeMets, C., Gordon, R.G., Argus, D.F., Stein, S., 1994. Effects of recent revision to the geomagnetic reversal timescale on estimates of current plate motion. Geophys. Res. Lett. 21, 2191–2194.

DeMets, C., Gordon, R.G., Argus, D.F., 2010. Geologically current plate motions. Geophys. J. Int. 181, 1–80. doi:10.1111/j.1365-246X.2009.04491.x

Devey, C.W., Hémond, C., Stoffers, P., 2000. Metasomatic reactions between carbonated plume melts and mantle harzburgite: the evidence from Friday and Domingo Seamounts (Juan Fernandez chain, SE Pacific). Contrib. to Mineral. Petrol. 139, 68–84. doi.org/10.1007/s004100050574

Farley, K.A., Basu, A.R., Craig, H., 1993. He, Sr and Nd isotopic variations in lavas from the Juan Fernandez Archipelago, SE Pacific. Contrib. to Mineral. Petrol. 115, 75–87. doi.org/10.1007/BF00712980

French, S.W., Romanowicz, B., 2015. Broad plumes rooted at the base of the Earth's mantle beneath major hotspots. Nature 525, 95–99. doi.org/10.1038/nature14876

Garcia, M.O., Swinnard, L., Weis, D., Greene, A.R., Gami, T., Sano, H., Gandy, C.E., 2010. Petrology, geochemistry and geochronology of Kaua'i lavas over 4·5Myr: Implications for the origin of rejuvenated volcanism and the evolution of the Hawaiian plume. J. Petrol. 51, 1507–1540. doi:10.1093/petrology/egq027

Gripp, A.E., Gordon, R.G., 1990. Current plate velocities relative to the hotspots incorporating the NUVEL-1 global plate motion model. Geophys. Res. Lett. 17, 1109–1112. doi:10.1029/GL017i008p01109

Hoernle, K., Schmincke, H.-U., 1993. The petrology of the tholeiites through melilite nephelinites on Gran Canaria, Canary Islands: crystal fractionation, accumulation, and depths of melting. J. Petrol. 34, 573–597. doi:10.1093/petrology/34.3.573

Jackson, M.G., Konter, J.G., Becker, T.W., 2017. Primordial helium entrained by the hottest mantle plumes. Nature 542, 340–343. doi.org/10.1038/nature21023

Konter, J.G., Jackson, M.G., 2012. Large volumes of rejuvenated volcanism in Samoa: Evidence supporting a tectonic influence on late-stage volcanism. Geochemistry, Geophys. Geosystems 13, n/a-n/a. doi:10.1029/2011GC003974

Lara, L.E., Reyes, J., Orozco, G., Díaz-Naveas, J. 2017. Rapid transition from shield to post-erosional volcanism at O'Higgins guyot , Juan Fernández Ridge , Pacific SE, in:

AGU (American Geophysical Union) Chapman Conference on Submarine Volcanism: New Approaches and Research Frontiers. Hobart, Tasmania, Australia.

Lara, L.E., Díaz-Naveas, J., Reyes, J., Jicha, B., Orozco, G., Kay, S.M., submitted. Unraveling short-lived rejuvenated volcanism and a rapid transition from shield stage at O ' Higgins guyot , Juan Fernández Ridge , Pacific SE.

Leisen, M.; Barra, F.; Romero, R.; Morata, D.; Reich, M. 2015. Geocronología U-Pb de Circones Mediante Ablación Láser Acoplado a un ICP-MS Multicolector: Metodología Utilizada en el Laboratorio de Geoquímica Isotópica del Centro Fondap CEGA, Universidad de Chile. XIV Congreso Geológico Chileno: La Serena, Chile.

Ludwig, K.R. 2003. Isoplot／Ex 3.00. A geochronological toolkit for Microsoft Excel. Berkeley Geochronological Center (Berkeley, CA, USA), 70p.

Montelli, R., Nolet, G., Dahlen, F.A., Masters, G., 2006. A catalogue of deep mantle plumes: New results from finite-frequency tomography. Geochemistry, Geophys. Geosystems 7, Q11007. doi.org/10.1029/2006GC001248

Morgan, W.J., 1971. Convection plumes in the lower mantle. Nature 230, 42–43. doi.org/10.1038/230042a0

Morgan, W.J., 1972. Deep mantle convection plumes and plate motions. Am. Assoc. Pet. Geol. Bull. 56, 203–213. doi.org/10.1306/819A3E50-16C5-11D7-8645000102C1865D

Reyes, J., Lara, L.E., Morata, D., 2017. Contrasting P-T paths of shield and rejuvenated volcanism at Robinson Crusoe Island, Juan Fernández Ridge, SE Pacific. J. Volcanol. Geotherm. Res. 341, 242–254. doi.org/10.1016/j.jvolgeores.2017.05.035

Stuessy, T.F., Foland, K.A., Sutter, J.F., Sanders, R.W., Silva., M., 1984. Botanical and geological significance of potassium-argon dates from the Juan Fernandez Islands. Science 225 (4657), 49–51. doi.org/10.1126/science.225.4657.49

Truong, T.B., Castillo, P.R., Hilton, D.R., Day, J.M.D., 2018. The trace element and Sr-Nd-Pb isotope geochemistry of Juan Fernandez lavas reveal variable contributions from a high- $^{3}He/^{4}He$ mantle plume. Chem. Geol. 476 280–291. doi.org/10.1016/j.chemgeo.2017.11.024

von Huene, R., Corvalán, J., Flueh, E.R., Hinz, K., Korstgard, J., Ranero, C.R., Weinrebe, W., 1997. Tectonic control of the subducting Juan Fernández Ridge on the Andean margin near Valparaiso, Chile. Tectonics 16, 474–488. doi.org/10.1029/96TC03703

Table IV.1. Summary of $^{40}Ar/^{39}Ar$ geochronological data for the Juan Fernández Ridge volcanoes. The stage of volcanism, material dated (GM: groundmass, PLG: plagioclase; WR: whole rock) and laboratory are also indicated (1: SERNAGEOMIN; 2: WiscAr).

Sample	Material	Age plateau ± 2σ (Ma)	Laboratory
O'Higgins guyot shield			
D10-2	GM	8.41 ± 0.07	(1)
D10-7	GM	9.26 ± 0.28	(2)
O'Higgins guyot rejuvenated			
2D	GM	8.16 ± 0.04	(2)
Alpha seamount shield			
D11-03	GM	4.58 ± 0.06	(1)
D11-04	GM	4.63 ± 0.06	(2)
Robinson Crusoe Island shield			
MP270112-4		3.70 ± 0.05	(2)
JR220112-2	GM	3.81 ± 0.04	(2)
LL240711-1		3.83 ± 0.04	(1)
LL230112-1		3.85 ± 0.15	(2)
MP260112-1		3.87 ± 0.05	(2)
LL250711-8		3.88 ± 0.04	(1)
LL260711-2		3.95 ± 0.02	(1)
JR220112-1	PLG	3.40 ± 0.30	(1)
LL250711-5		3.80 ± 0.08	(2)
LL270711-5		4.10 ± 0.09	(2)
Robinson Crusoe Island rejuvenated			
JR220112-3	GM	1.30 ± 0.03	(2)
JR250112-3	GM	1.38 ± 0.05	(2)
LL230112-4	WR	1.25 ± 0.03	(1)
LL230711-2		0.77 ± 0.14	(1)
LL230711-8		0.90 ± 0.04	(1)
JR230112-1	GM	1.17 ± 0.04	(2)
LL220112-1	GM	1.30 ± 0.03	(2)
JR020613-3	GM	1.55 ± 0.02	(1)
LL010213-6	GM	1.67 ± 0.02	(1)
JR160913-2	GM	0.90 ± 0.03	(1)
LL020213-1	GM	1.52 ± 0.02	(1)
Alejandro Selkirk Island shield			
LL270112-2		0.94 ± 0.07	(2)
JR170913-16	GM	0.83 ± 0.03	(1)
LL260112-4	GM	0.93 ± 0.02	(2)
JR180913-1	GM	0.87 ± 0.01	(1)
JR170913-7	WR	0.93 ± 0.02	(1)

Figure IV.1. Field pictures of Robinson Crusoe Island showing rejuvenated lavas filling paleo-reliefs in the shield basalts with unconformities (dashed lines). The stars indicate locations of samples detailed in Figure 2.

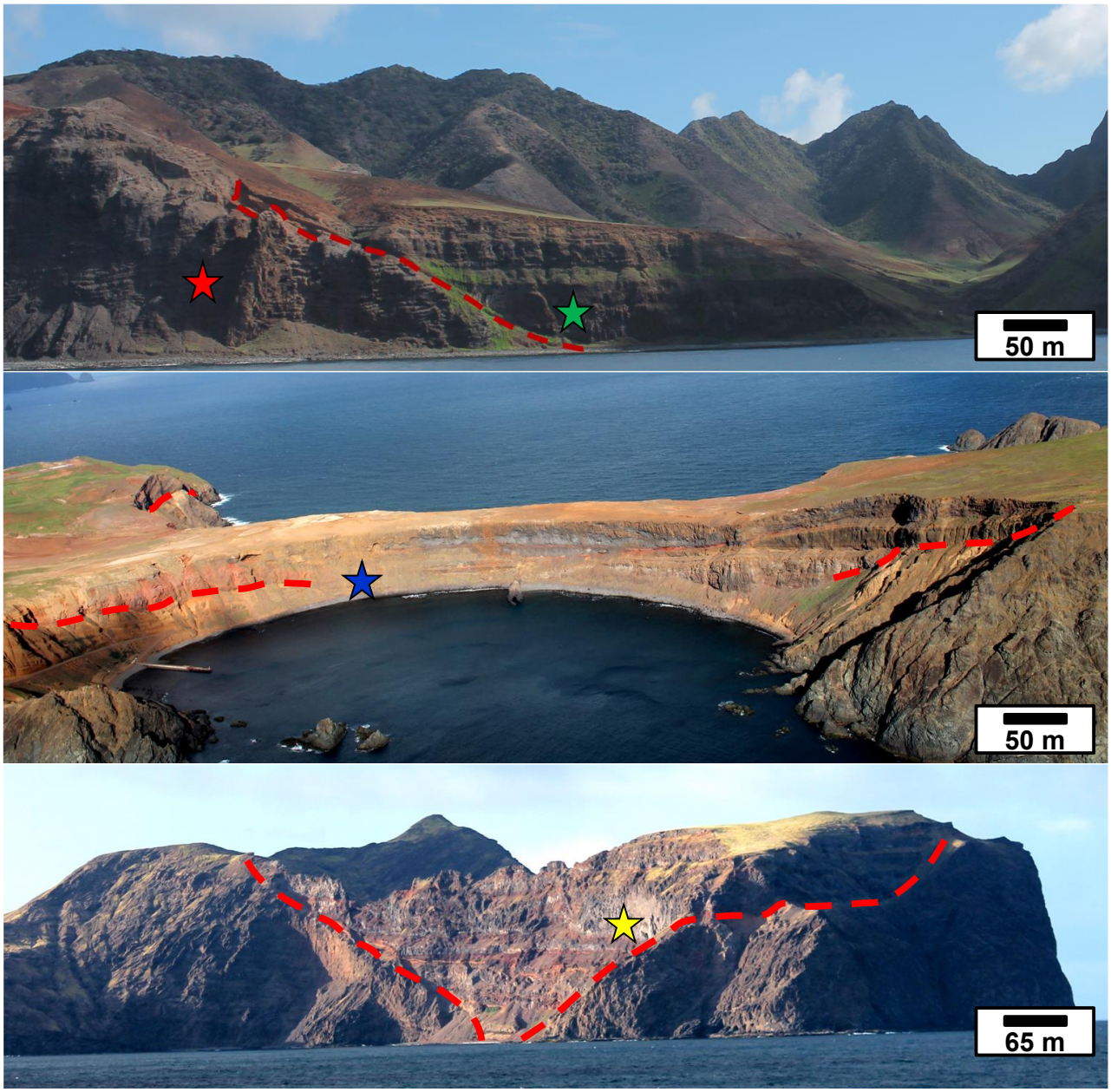

Figure IV.2. Step-heating $^{40}Ar/^{39}Ar$ age spectra for samples of Robinson Crusoe Island. The stars indicate location of each sample (detailed in Figure 1).

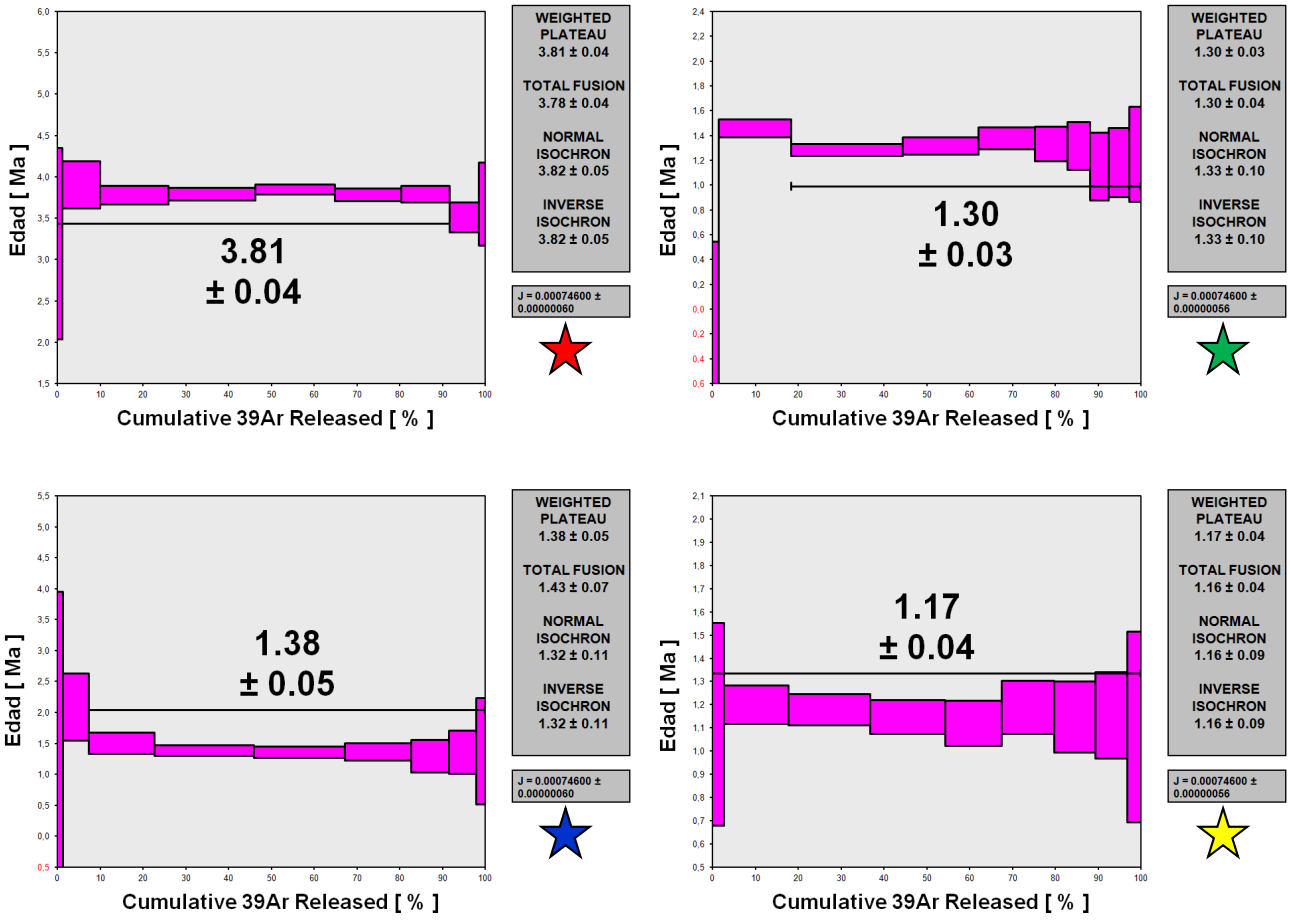

Figure IV.3. Bathymetric map of O'Higgins guyot showing the fresh morphology (basanite flows) representative of rejuvenated volcanism at the top of the guyot.

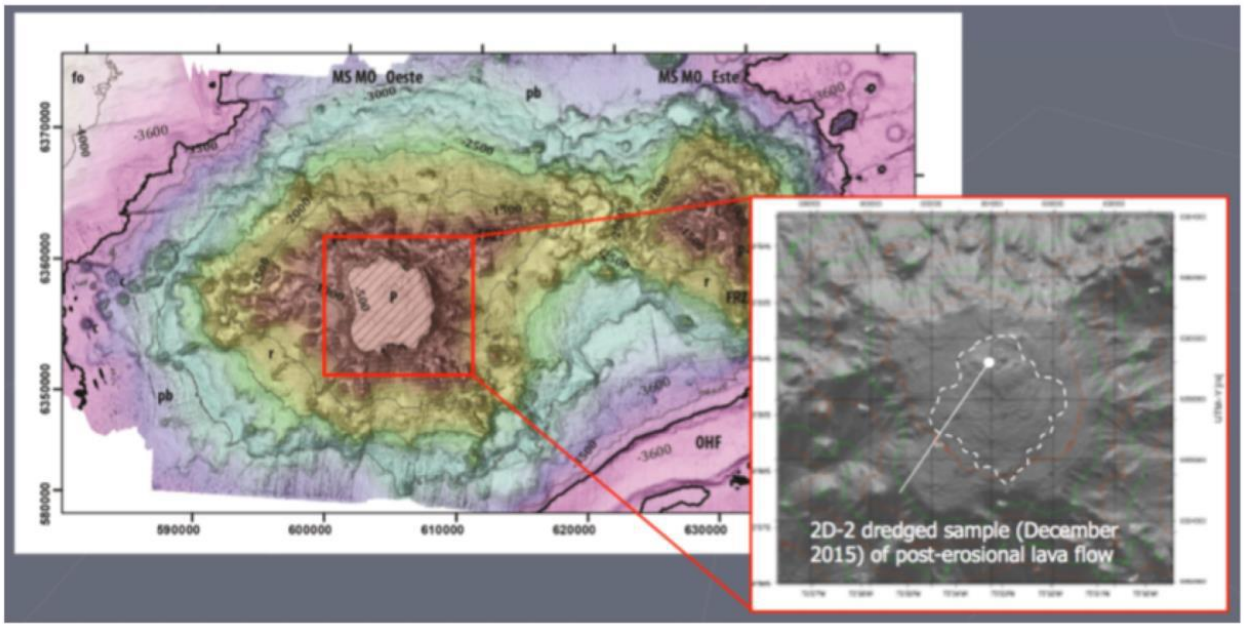

Figure IV.4. Geochemical (Nb/Zr) and isotopic ratios ($^{207}Pb/^{204}Pb$) vs. $^{40}Ar/^{39}Ar$ plateau age (Ma) as discriminant between shield and rejuvenated volcanism in JFR.

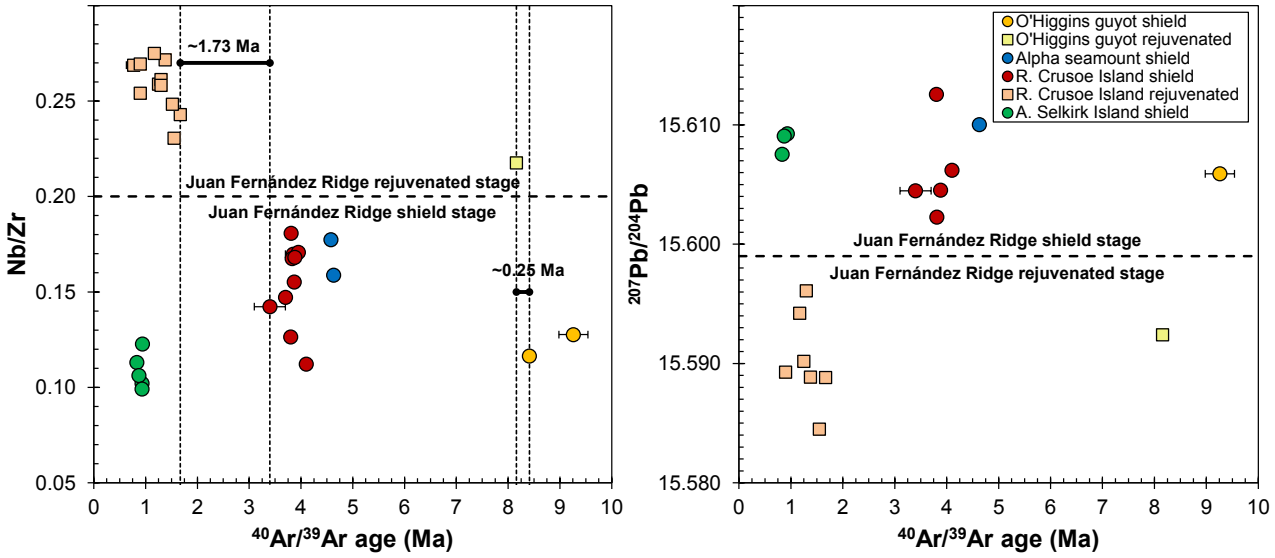

Figure IV.5. $^{40}Ar/^{39}Ar$ plateau ages vs. distance from Alejandro Selkirk Island (km). The linear trend between shield-building samples satisfies the classical mantle plume theory in the age progression sense. Models of Nazca plate movement are showed. OH: O'Higgins, AL: Alpha, RC: Robinson Crusoe, AS: Alejandro Selkirk, FR: Friday.

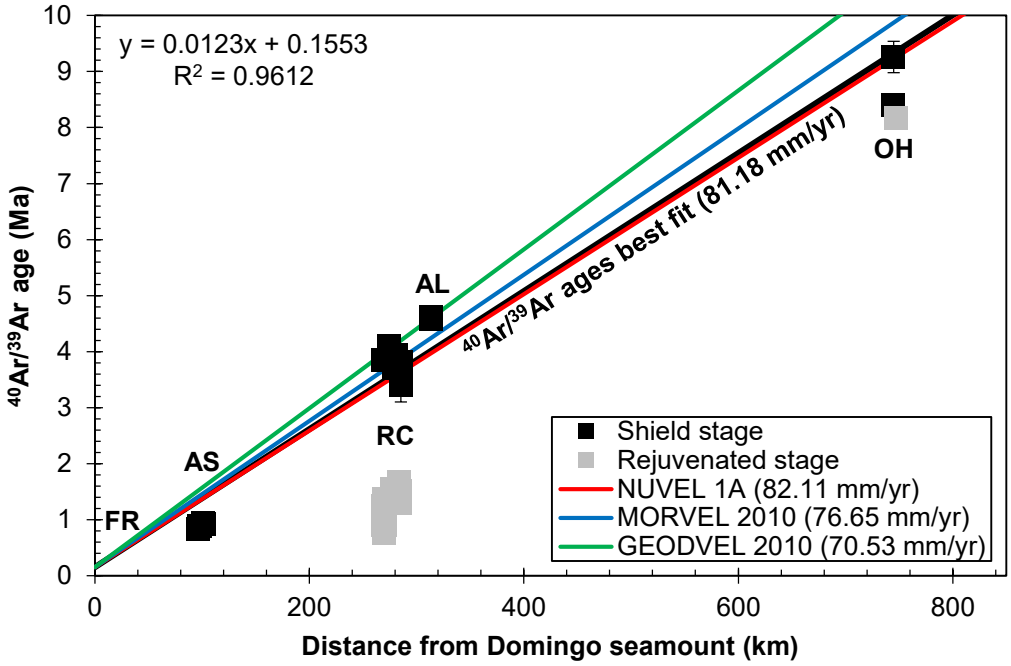

Figure IV.6. U-Pb zircon ages for syenites in Robinson Crusoe Island. A) and B) Wetherill and Tera-Wasserburg concordia plots for sample LL270711-1. C) and D) Tera-Wasserburg concordia plots of more abundant data (n= 19 of 23) and > 20 Ma ages (n= 4 of 23) for sample LL270711-2. E) TuffZirc age (Ludwig, 2003) (more probable) for each sample of syenite.

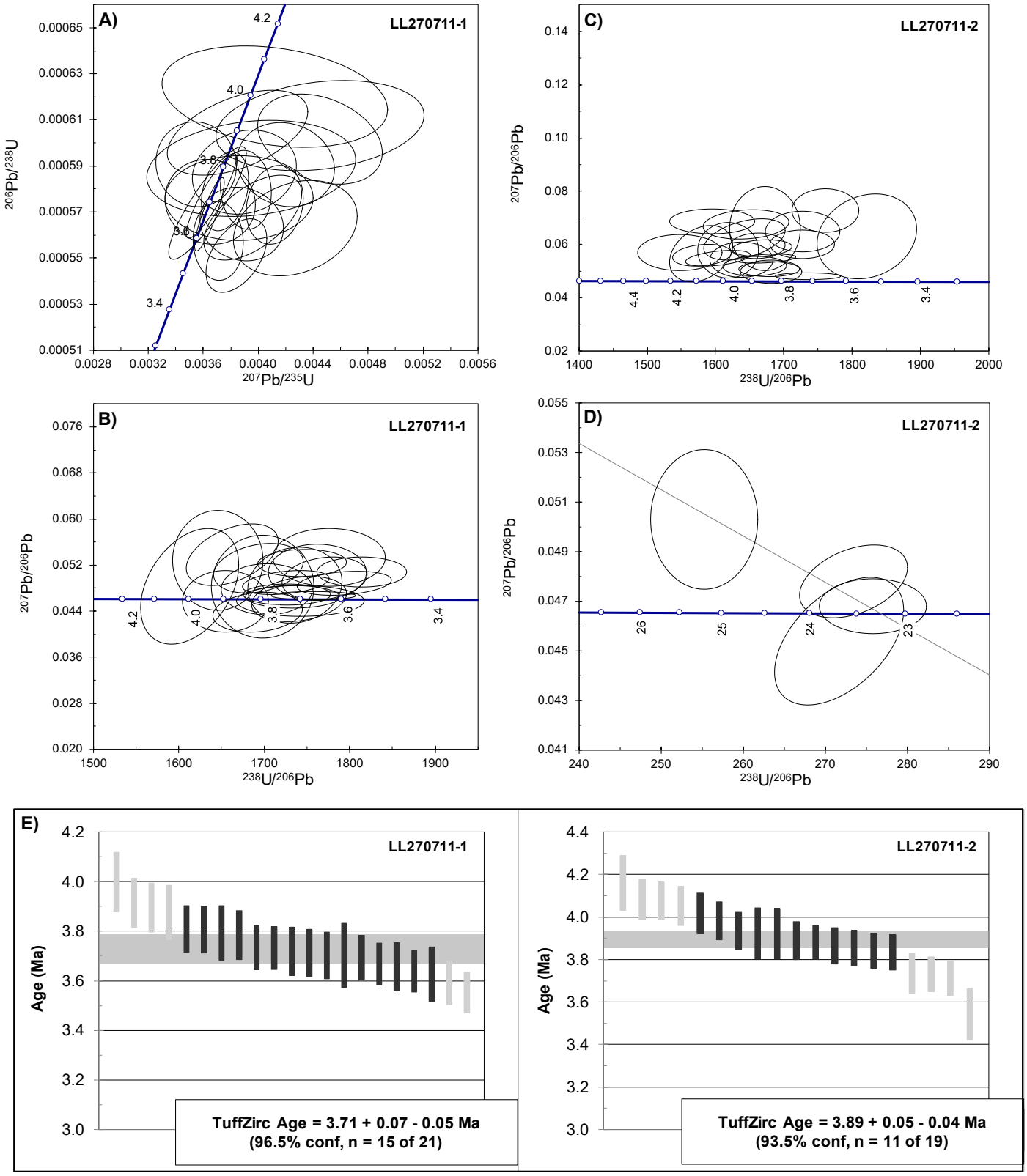

Capítulo V

Petrogenesis of the shield volcanism in Juan Fernández Ridge, SE Pacific: melting from a low temperature pyroxenite-bearing mantle plume

Abstract

The Juan Fernández Ridge (JFR) is a volcanic chain (~ 800 km) related to a fixed mantle plume in the SE Pacific. New whole-rock geochemical and isotopic data for representative samples of the shield stage in JFR (O'Higgins guyot, Alpha seamount, and Robinson Crusoe, and Alejandro Selkirk islands) are used in a petrogenetic model aimed to understand magmatism over time and space. The shield-building lavas of JFR consist mainly of tholeiitic, transitional, and alkali basalts (more enriched in Robinson Crusoe Island). Their compositional differences are explained by fractional crystallization of olivine + clinopyroxene ± plagioclase, mixing/magmatic recharge, and olivine accumulation. The Sr-Nd-Pb isotopes show a narrow field near to FOZO-A source; with additional participation of DM, especially in Alejandro Selkirk/O'Higgins. These are enriched values compared to MORB, similar in $^{206}Pb/^{204}Pb$ and $^{207}Pb/^{204}Pb$ to other islands of the Nazca Plate (e.g., San Félix and San Ambrosio), and more radiogenic, but in a narrower field compared to Easter Seamount Chain. Geochemical features (e.g. low CaO at given MgO, Ti-Ta-Nb 'TITAN' anomaly, and HREE values) and isotopic signature suggest the presence of pyroxenite (recycled oceanic crust) as a heterogeneity in the mantle source. To quantify plume features, we use the OBS1 software (Kimura and Kawabata, 2015) in primary melts calculated from parental samples estimating some source parameters as potential temperature (values in the range 1290 – 1322 °C for Robinson Crusoe and 1312 – 1362 °C for Alejandro Selkirk), total degree of melting (2.8 – 4.9 vs. 5.2 – 11.4 wt%), and pyroxenite fraction (4 – 8 vs 6 – 12 wt%). These low potential temperatures could be explained by the plume volatile content (high H_2O and probably CO_2). The depth of melting termination (~ 2.4 GPa) is apparently related to the lithosphere-asthenosphere boundary beneath Nazca Plate. Thus, the Juan Fernández Ridge shield stage would have been generated by melting of a low temperature mantle plume with temporal changes in their thermal and lithological features reflected in a relative chemical enrichment in Robinson Crusoe and more marked DM signature in Alejandro Selkirk. This confirms the observation that pyroxenites and heterogeneous mantle plumes are involved in the petrogenesis of many OIB and fuels the discussion about the nature of the plumes and the apparent inconsistence between key geochemical signatures and the absence of geophysical evidence at the same place.

V.1. Introduction

Oceanic intraplate magmatism is characterized by the formation of large basaltic shield volcanoes above an oceanic plate that usually forms remarkable volcanic chains of islands and seamounts. Ascent from deep fixed mantle plumes is the most accepted theory to explain oceanic intraplate magmatism (the so-called 'hotspot hypothesis'; e.g., Morgan, 1971; Morgan, 1972). One of the most evident results of such an origin is the observed age progression of volcanic rocks from oceanic islands and/or seamounts along a chain. However, a number of volcanic alignments do not satisfy this condition, as observed by Clouard and Bonneville (2001) for the Pacific Ocean basin. Alternative ideas

have been proposed as non-fixed plumes (Steinberger and O'Connell, 1988) or tectonically-controlled decompression related to magmatic hydrofractures driven by flexural stresses in presence of a volcanic load (Hieronymus and Bercovici, 2000). More frequent processes as subduction cooling, continental insulation, small-scale convection in presence of ridges, rifts and fracture zones (Anderson, 2000, 2001) or small-scale sublithospheric convections (Ballmer et al., 2007) could also explain the array of hotspot volcanoes on oceanic plates.

The diverse elemental and isotopic compositions of hotspots around the globe suggests that the underlying mantle is heterogeneous in terms of lithologies, compositions and/or mineralogy (Zindler and Hart, 1986 and references therein). The classical sources involved in the OIB genesis are: PM (primitive mantle), DM (depleted mantle), and other components formed by recycling of varied materials: HIMU (high $\mu = {}^{238}U/{}^{204}Pb$; e.g., Zindler and Hart, 1986; Weaver, 1991; Hauri and Hart, 1993; Salters and White, 1998; Stracke et al., 2003; Stracke et al., 2005; Kimura et al., 2016) and EM1/EM2 (enriched mantle 1 and 2; e.g., Blichet-Toft et al., 1999; Willbold and Stracke, 2010; Hoernle et al., 2011; Kimura et al., 2016; Turner et al., 2017). Additionally, a common component recognized in some OIB is called PREMA (Zindler and Hart, 1986), C (Hanan and Grahan, 1996) or FOZO (FOcal ZOne; after Hart et al., 1992), the latter nomenclature adopted in this study. FOZO is interpreted as a relatively uniform mixture of the other components (e.g., Stracke et al., 2005; White, 2015; Kimura et al., 2016) and can be separated in FOZO-A (austral) and FOZO-B (boreal) (Jackson et al., 2007). Based on interpretations about mantle sources and geochemistry of OIB worldwide (e.g., Hawaii: Herzberg, 2006 and Canarias: Day et al., 2009), the existence of recycled lithologies, particularly igneous oceanic crust, as eclogite or pyroxenite in the source of OIB seems to be plausible (e.g., Hofmann and White, 1982; Sobolev et al., 2007).

A still poorly known example is the Juan Fernández Ridge (JFR), an aseismic ridge (around 15 volcanoes: 2 main islands and at least 12 seamounts) emplaced above the Nazca Plate (ca. 27-32 Ma old; Rodrigo and Lara, 2014) in SE Pacific that collides against the South American Plate margin at ~33.4°S (Figure V.1). The JFR was recognized as an expression of a mantle plume (Farley et al., 1993; Devey et al, 2000; Lara et al., 2018b). In the catalogue proposed by Courtillot et al. (2003), JFR satisfies only two of five conditions for primary plumes, in detail: relative high values of buoyancy flux; in the range 1.6 – 1.7 Mg s^{-1} (Davies, 1988; Sleep, 1990); and high values of $^{3}He/^{4}He$, between 7.8 and 18 R_A (Farley et al., 1993; Jackson et al., 2017; Truong et al., 2018). But, new detailed $^{40}Ar/^{39}Ar$ dating (Lara et al., 2018b) show a clear E to W age progression for the shield stage at least in 4 volcanoes of the chain (it would be a new check in the catalogue of Courtillot et al., 2003), confirming the suggested by the previous K-Ar and $^{40}Ar/^{39}Ar$ ages (Booker et al., 1967; Stuessy et al., 1984; von Heune et al., 1997; Reyes et al., 2017; Lara et al., 2018a) and their origin associated to a fixed mantle plume. A controversial topic of the JFR plume is the interpretation of their seismic tomography, while Montelli et al. (2006) propose a plume of intermediate depth, Boschi et al. (2007) did not recognize it. In a recent work, French and Romanowicz (2015) see a vertical conduit beneath JFR, but not clearly continuous.

The JFR is isolated from the nearby active spreading ridges, East Pacific Rise (~ 2500 km to W), and Chile Rise (> 850 km to S; Figure V.1) and thus offers an unrivaled opportunity to study the mantle signatures beneath SE Pacific, their implications in hotspot global view, and the eventual influence of JFR in the geochemistry of the Andean

magmatism. In this contribution we report new geochemical and isotopic analyses of the shield stage magmatism in JFR to unravel its petrogenesis and magmatic evolution in a mantle plume context. With the use of OBS1 model (Kimura and Kawabata, 2015) we establish the plausible physical and chemical conditions of the mantle source.

V.2. Geological background

JFR comprises 2 main islands and at least 12 seamounts with a common base at ca. 3900 m depth (Rodrigo and Lara, 2014). This study is mostly focused on 4 volcanic centers where shield volcanism has been recognized, from E to W: O'Higgins guyot, Alpha seamount, Robinson Crusoe, and Alejandro Selkirk islands (Figure V.1). O'Higgins guyot is a volcanic edifice with geochemical features of shield stage volcanism of ca. 3450 m high with a flat top at ca. 500 m b.s.l. on average, which is overlain by a sequence of fresh rejuvenated (or post-erosional) lavas, gently dipping southward from a vent at ca. 360 m b s l (Lara et al., 2018a).

Some 450 km to the W is located the Alpha seamount (summit at 260-450 m b.s.l.; Farley et al., 1993). Numerous rounded cobbles recovered by dredging suggest a subaerial episode in this seamount. Chemical similarities between Alpha samples and other JFR shield lavas (whole rock geochemistry and isotopic signature; see Farley et al., 1993 and Section 4 of this study) suggest that Alpha would be mostly a shield volcano. The Robinson Crusoe Island (915 m high) and the nearby Santa Clara (375 m high, hereafter considered as part of Robinson Crusoe because of its situation in the same volcanic pedestal) are the main volcanic edifices in JFR (~20 km to W of Alpha). Deep coastal erosion exposes thick sequences representative of the shield stage (Baker et al., 1987; Farley et al., 1993; Reyes et al., 2017). A sharp erosion unconformity separates the shield stage sequence from the upper alkaline rejuvenated stage (Reyes et al., 2017). The reconnaissance of two submerged marine abrasion terraces (at ~ 200 and ~ 500 m b.s.l.; Astudillo, 2014) and sedimentary layers of marine origin at 70 m a.s.l. indicates a complex history of vertical displacement (Sepúlveda et al., 2015). The other emerged volcanic edifice, ~180 km W of Robinson Crusoe, is Alejandro Selkirk Island (1320 m high), a homoclinal asymmetric shield volcano that shows long straight valleys downwards to the east and high cliffs on the west coasts.

In this paper, we focus on the shield stage, and because samples come from the upper slope of O'Higgins guyot and Alpha seamount, and most of them from the subaerial sections in the Alejandro Selkirk and Robinson Crusoe islands, representativeness is restricted to the late shield stage.

The shield stage of O'Higgins guyot has been dated by $^{40}Ar/^{39}Ar$ in the range ~ 8.40 – 9.26 Ma (von Heune et al., 1997; Lara et al., 2018a), and Alpha seamount between ~ 4.58 and 4.63 Ma (Lara et al., 2018b). Robinson Crusoe Island, on the other hand, provided a $^{40}Ar/^{39}Ar$ ages between ~ 3.40 and 4.10 Ma for the shield-building lavas (Reyes et al., 2017; Lara et al., 2018b). Finally, for Alejandro Selkirk there are $^{40}Ar/^{39}Ar$ ages that dating their shield stage in the range ~ 0.83 – 0.94 Ma (Lara et al., 2018b). These progressively younger ages westward are relatively consistent with the eastward Nazca Plate movement of ~70.53 mm/yr (GEODVEL 2010 model; Argus et al., 2010) and are consistent with the fixed mantle plume hypothesis (Lara et al., 2018b), confirming the suggested by old K-Ar data (Booker et al., 1967; Stuessy et al., 1984). In addition to shield volcanism, rejuvenated magmatism has been reported in Robinson Crusoe (Reyes et al.,

2017) and at the summit of O'Higgins seamount (Lara et al., 2018a), but these rocks are not included in this study.

Lavas from the shield stage in JFR are mainly alkaline and subalkaline basalts and picrites with the typical LIL and HFSE enrichment of OIB (e.g., Baker et al., 1987; Reyes et al., 2017; Lara et al., 2018a). Their Sr-Nd-Pb isotopic values show a DUPAL signature (defined by Dupré and Allègre, 1983; Hart; 1984; reported in JFR by Gerlach et al., 1986) concordant with the participation of FOZO-A component (Jackson et al., 2007), with slight differences between volcanic centers. A recognized feature of JFR is their high $^{3}He/^{4}He$ ratios, uncorrelated with Sr-Nd-Pb isotopes. The Robinson Crusoe shield lavas show the highest values of $^{3}He/^{4}He$ in JFR (13.6 – 18 R_A), followed by the rejuvenated stage of the same island (11.2 – 12.5 R_A), and finally the shield stage of Alejandro Selkirk (7.8 – 9.5 R_A; Farley et al., 1993). Truong et al. (2018) suggest additional contribution (in addition to FOZO) of a depleted source in the origin of Alejandro Selkirk and HIMU in Robinson Crusoe. The HIMU component was also proposed in the genesis of Domingo and Friday seamounts, two volcanic edifices located ~80-100 km to the W of Alejandro Selkirk that probably represent the early stages of JFR-volcanism (Devey et al., 2000). Gerlach et al. (1986) recognized differences in JFR relative to other oceanic islands remote from spreading ridges in the Nazca Plate (San Félix and San Ambrosio), which could indicate heterogeneities in the mantle of this region.

V.3. Sampling and analytical procedures

Samples (6) from the O'Higgins guyot were dredged during SO101 CONDOR cruise of the German RV Sonne in 1995 (more details and data in Lara et al., 2018a). 10 samples of dredged rocks from Alpha seamount were provided by Scripps Institution of Oceanography (University of California San Diego, United States), and 2 by professor Hernán Vergara, all of them collected by the HYDROS Expedition (Leg I) in 1988. One sample was collected from surface by means of a biological dredge in 2016 during the CIMAR 22 cruise on board of the AGS61 Cabo de Hornos vessel. 79 samples (lavas and dykes), 48 in Robinson Crusoe and 31 in Alejandro Selkirk, which represent subaerial shield volcanism, were collected during several field campaigns between 2011 and 2013 with strict stratigraphic control. Samples with low-alteration and vesicle content were preferred. In addition, Scripps Institution gave us access to 6 subaerial rocks from Alejandro Selkirk also sampled in the 1993 expedition. Representative samples were analyzed by optical microscopy to unravel their petrographic characteristics. Some samples were also observed in scanning electron microscopy (SEM FEI Quanta 250) at the Centro de Excelencia en Geotermia de Los Andes (CEGA) facilities of Universidad de Chile. Digital modal counts (500 points, recursive grid) were performed in 26 samples (results in Table V.1) using JMicroVision 1.2.7 software.

Whole-rock major and trace elements were analyzed at AcmeLabs, Vancouver, Canada, on different times following the same procedure. Rock chips crushed from field hand samples were pulverized to 85% passed 200 mesh (< 0.074 mm) and separated aliquots fused with lithium metaborate/tetraborate and a dilute nitric acid digestion prior to major element analysis by ICP-ES and trace elements by ICP-MS. In addition, a separate split was digested in Aqua Regia and analyzed by ICP-MS to report the Ni and Pb content. Loss on ignition (LOI) is by weigh difference after ignition at 1000 °C. Based on repeated analysis of standards and duplicated samples, accuracy and precision are better than 2% and 1% (relative) respectively, except for P_2O_5 (<of 4.5 and 2.3%). For trace elements

both values are <7.5% (except for Pb with a precision ~17%). The detections limits vary from 0.01 to 0.04 wt% for major elements, and from 0.01 to 1 ppm in trace elements (details in Table V.2 & Table V.3). Blanks display measured values typically under detection limits for all major and trace elements.

Due to their petrographic, geochemical, and isotopic similarities, the dykes will be considered hereafter as part of the shield-building stage, and consequently referenced simply as lavas.

Sr-Nd-Pb isotope ratios were determined on rock chips for 15 samples (and two replicates). Detailed descriptions for sample preparation and for chemical and mass spectrometry procedures can be found in Hoernle et al. (2011). In summary, Sr, Nd and Pb isotope ratios were determined by thermal ionization mass spectrometry (TIMS) at GEOMAR Helmholtz Center, Kiel, Germany, using a Thermo Fisher Scientific TRITON+ for Sr and Nd isotopic measurements and TRITON+ and a Finnigan MAT 262-RPQ2+ (only for one sample) for Pb isotopic measurements. Prior to acid-digestion, rock chips (100-150 mg of the 0.5-2 mm fraction) was leached in 2N HCl at 70°C for 1-2 hours and then triple-rinsed with 18.2 MΩ water in order to remove possible surface alteration and contamination. All reported errors are at the 2σ confidence level. Strontium and Nd isotope ratios were mass-bias corrected using a within-run value of 0.1194 for $^{86}Sr/^{88}Sr$ and 0.7219 for $^{146}Nd/^{144}Nd$. NBS987 and La Jolla reference materials were measured every 4th to 5th sample to obtain a normalization value for each sample turret relative to our preferred standard values of $^{87}Sr/^{86}Sr = 0.710250$ for NBS987 and $^{143}Nd/^{144}Nd = 0.511850$ for La Jolla. The sample turret normalization value was applied to each sample on the turret. Overall this normalization procedure compensates for inter-machine bias and instrument drift over the course of the study. External 2σ uncertainties (2SD) for NBS987 are ± 0.000009 (n= 102) and for La Jolla, 2SD is ± 0.000006 (n= 114) on the TRITON+. The Pb double-spike (DS) technique of Hoernle et al. (2011) was used for mass bias correction of Pb isotope ratios. DS corrected NBS981 values were $^{206}Pb/^{204}Pb = 16.9412 \pm 12$, $^{207}Pb/^{204}Pb = 15.4983 \pm 13$, $^{208}Pb/^{204}Pb = 36.7208 \pm 31$, $^{207}Pb/^{206}Pb = 0.914832 \pm 27$, $^{208}Pb/^{206}Pb = 2.167549 \pm 82$ (n=22) on the TRITON+ and $^{206}Pb/^{204}Pb = 16.9427 \pm 21$, $^{207}Pb/^{204}Pb = 15.5005 \pm 21$, $^{208}Pb/^{204}Pb = 36.7278 \pm 46$, $^{207}Pb/^{206}Pb = 0.914877 \pm 32$, $^{208}Pb/^{206}Pb = 2.167765 \pm 63$ (n=17) on the MAT262. These NBS981 ratios overlap within 2SD for each instrument and compare well with published double and triple spike data for NBS981 (see Hoernle et al., 2011). Replicate values within the error except for $^{208}Pb/^{204}Pb$. Chemistry blanks were monitored for each batch of samples and are typically < 100 pg for Sr, Nd, and Pb, and thus negligible compared to the amount of sample.

Additionally, 11 samples were analyzed for Sr-Nd isotopes at Laboratoire Magmas and Volcans, Clermont-Ferrand, France, isotope laboratory by TIMS using a Thermo Fischer Triton instrument, corrected for mass fractionation by normalization to $^{86}Sr/^{88}Sr = 0.1194$ and $^{146}Nd/^{144}Nd = 0.7219$ respectively. The Sr-Nd sample decomposition and chemical separation followed the procedure developed by Pin and Zalduegui (1997). The international standards NBS987 and JNd-1 gave $^{87}Sr/^{86}Sr$ and $^{143}Nd/^{144}Nd$ equal to 0.710241 ± 6 (2SD) and 0.512102 ± 4, respectively, during the period of analyses. These values are within error of the accepted standard values. Four samples were analyzed for Sr-Nd isotopes in both laboratories, with variations less than 0.000015 for $^{87}Sr/^{86}Sr$ (except for one sample, LL250711-5 with difference of ~ 0.000050) and 0.000009 for $^{143}Nd/^{144}Nd$.

V.4. Results

Reyes et al. (2017), based on geochemical and mineralogical features, defined for Robinson Crusoe shield stage samples the compositional groups: 'differentiated' (Mg#<58; Mg# = $Mg^{2+}/[Mg^{2+}+Fe^{2+}]$ assuming 90% of total iron is ferrous in all samples, a reasonable estimate used in other oceanic islands like Hawaii, e.g., García, 1996), 'near-primitive' (58<Mg#<68, considering primitive as a magma that underwent minimal differentiation) and 'olivine-rich' (Mg#>68), which we extend to the entire JFR shield sample set. For instance, O'Higgins has compositions that mimic those of the 'differentiated' and 'olivine-rich' groups, while basalts of Alpha are exclusively part of the 'differentiated' lavas. The most variable compositions of Robinson Crusoe and Alejandro Selkirk fall into 'differentiated' and 'olivine-rich' sets, but also in the 'near-primitive' group (Figure V.3).

V.4.1 Petrography

The JFR shield stage is commonly characterized by vesicular lavas (up to ~18 vol%; Table V.1), ranging from porphyritic to aphanitc (highly-vesicular and glassy lavas from the surface of flows were not considered). The mineralogy consists mainly of olivine, clinopyroxene, and plagioclase embedded in an intersertal to intergranular groundmass (subophitic in some basalts and picrites from the 'olivine-rich' group). Olivine is the main mineral phase in JFR with phenocrysts content up to 5% in basalts from the 'differentiated' group, 13% in the 'near-primitive' and 47% in picrites from the 'olivine-rich' group (common values in this set are around 25%; Table V.1). Clinopyroxene and plagioclase phenocrysts are in low abundance (commonly < 3%) or are absent from many samples, with a maximum of 10% for clinopyroxene and 21% for plagioclase (both in the 'differentiated' group; Table V.1). Opaque minerals, presumably Cr-rich spinel, are visible mostly as inclusions in olivines of the 'olivine-rich' group. The groundmass has the same mineralogy but in different proportions: clinopyroxene and plagioclase are the most abundant phases, followed by Fe-Ti oxides (mainly ilmenite and titanomagnetite) and scarce olivine. Submarine samples have a significant content of secondary mineralogy, mainly opaques/clays in the groundmass and iddingsite in olivine, sometimes affecting whole crystals. In subaerial rocks their content is considerably lower, visible as common iddingsite rims of variable width in olivines. Few samples show vesicles partially filled by smectite and clay minerals. Some lavas located to the SW of Robinson Crusoe are strongly altered by smectite, chlorite, calcite and epidote and were not considered in this study.

V.4.2 Major element and Ni geochemistry

The JFR shield-building lavas range between 43.6 – 50.5 wt% SiO_2 and 42.2 – 80.3 Mg# (Table V.2, all major elements of the table recalculated to 100% on a LOI-free total). According to TAS classification diagram (Figure V.2), most samples are subalkaline (tholeiitic by AFM diagram), transitional, and alkali basalts, with subordinated trachy- and picro-basalts (picrites, due to their high olivine, Mg, and Ti content, Table V.1); only two samples are classified as basanites and other as andesitic trachy-basalt, in both cases very close to the fields of more common lithologies. The Ni contents vary between 18 and 1299 ppm (Figure V.3) and show a kink in the correlation with Mg# which allows assigning all of JFR shield lavas into the previously mentioned compositional groups defined by Reyes et al. (2017) for Robinson Crusoe. Submarine samples from O'Higgins and Alpha

are transitional and alkali basalts, but in Robinson Crusoe, and especially in Alejandro Selkirk there is an major proportion of tholeiitic basalts. All the islands/seamounts have the typical OIB major-element features; i.e., high TiO_2 and K_2O contents relative to MORB (Hofmann, 1988) and PM (Lyubetskaya and Korenaga, 2007); although considerable internal differences in TiO_2 and $Fe_2O_3^T$ are observed, slightly depleted for a given Mg# in Alejandro Selkirk (Table V.2). Alpha lavas show enrichment in Al_2O_3, Na_2O, K_2O (highly variable in all volcanoes), and P_2O_5 (Table V.2), possibly as effect of their low-temperature alteration.

V.4.3 Trace elements geochemistry

Lavas from JFR shield stage show a marked enrichment in trace elements relative to DM, PM and MORB, including large-ion lithophile (LILE) and high field strength elements (HFSE), with a range of values broadly correlated to Mg# and SiO_2. The ranges of LILE contents are similar for all volcanoes (e.g., Sr: 181 – 966 ppm for all JFR) (Figure V.3; Table V.3), with low minimum values in O'Higgins and Alpha. Relatively high values of Ti and, most notably, Ta and Nb in all JFR shield, but especially in Robinson Crusoe lavas (e.g., enrichment of Ta 1.53 and Nb 1.38 in Robinson Crusoe and 1.37/1.19 in Alejandro Selkirk considering the definition of Peters and Day, 2014; based on geochemical compatibility) are known as "TITAN" anomalies and have generated interest as a unique feature of OIB magmas (Jackson et al., 2008). The REE patterns of JFR are characterized by La/Yb ratios that vary between 6.76 and 18.54 (average 12.13; Figure V.4), La/Sm between 2.64 and 4.77 (avg. 3.67), and a range of 2.97 – 5.79 (avg. 3.57) for Tb/Lu ratios. Ratios of other HFSE show systematically different values for different volcanoes. For example, Alpha and Robinson Crusoe samples have elevated Nb values (for a given Zr content) relative to O'Higgins and Alejandro Selkirk (Table V.3; Figure V.4). In fact, the average Nb/Zr ratio for O'Higgins is 0.12, 0.16 for Alpha, 0.16 for Robinson Crusoe, and 0.11 for Alejandro Selkirk (Figure V.4). These differences are also visible in ratios of strongly incompatible elements such as Ta/Th (Figure V.4) and less incompatible elements as Ti/Eu, with the lowest values again in Alejandro Selkirk (see also Figure V.S.1).

V.4.4 Radiogenic isotopes

The young age (<9.5 Ma) of the JFR shield-building volcanism allows a direct analysis of the data without the need of an age correction. All isotopic systems considered show a narrow range of values. The ranges of values for lead isotopes are 19.0499 – 19.2874 for $^{206}Pb/^{204}Pb$, 15.6016 – 15.6126 for $^{207}Pb/^{204}Pb$, and 38.9350 – 39.1346 for $^{208}Pb/^{204}Pb$ (Table V.4). These values are very close to the FOZO field (stable mixture of the sources common in OIB, e.g., Stracke et al., 2005; White, 2015; Kimura et al., 2016), particularly to the FOZO-A average value of Jackson et al. (2007), with probable additional participation of DM or EM1 sources, especially recognizable in $^{206}Pb/^{204}Pb$ - $^{207}Pb/^{204}Pb$ trends (Figure V.5). HIMU source does not seem necessary to explain the JFR signature according to their relatively low radiogenic values of Pb compared to Santa Helena or Cook-Austral sources (e.g., Stracke et al., 2005). High values of $^{208}Pb/^{204}Pb$ (for a given $^{206}Pb/^{204}Pb$) relative to DM and MORB, the East Pacific Rise (Macdougall and Lugmair, 1985), and the North Chile Ridge (Bach et al., 1996; Figure V.5) also indicate the presence of DUPAL signature, a classical feature of the southern hemisphere correlated with FOZO-A source (Jackson et al., 2007). The range of $^{87}Sr/^{86}Sr$ values are 0.703496 – 0.703759, and 0.512811 – 0.512899 for $^{143}Nd/^{144}Nd$ (Table V.4), which also suggest a participation

of DM/EM1, but with some differences with respect to lead isotopes. When considering Sr and Nd isotopes, the values are between FOZO-A and FOZO-B; in the mantle array; and the influence of DM is much more evident that EM1. These ambiguities (contribution of DM or EM1) are clarified in Sr-Nd isotopes vs. $^{206}Pb/^{204}Pb$ plots, where it is not possible to visualize a clear pattern in the $^{87}Sr/^{86}Sr$ values, but in the $^{143}Nd/^{144}Nd$ is evident that the trend is toward DM, not to EM1 (Figure V.6).

Internal compositional differences within JFR are best seen if we consider only two groups: Robinson Crusoe plus similar samples from Alpha seamount, and Alejandro Selkirk, which includes a sample of O'Higgins guyot. The Alejandro Selkirk group shows depletions (using DM as a marker of depletion) in $^{206}Pb/^{204}Pb$, $^{208}Pb/^{204}Pb$, and $^{143}Nd/^{144}Nd$. $^{207}Pb/^{204}Pb$ and $^{87}Sr/^{86}Sr$ do not show differences (Table V.4). These isotopic ratios show that Alejandro Selkirk group has a more DM (as North Chile Ridge or East Pacific Rise) signature respect to Robinson Crusoe group, where the values are subtly closer to FOZO-A (Figures V.5 & V.6). Finally, although our JFR samples cover most of the stratigraphic sequence, the ranges of Pb isotopes are narrower than the unleached and picritic-focused analysis of Gerlach et al. (1986) and Truong et al. (2018), but similar for Sr and Nd.

V.5. Discussion

V.5.1 Low-temperature alteration

The petrographic evidence of secondary mineralogy: opaques, clays, iddingiste, and smectite replacing phenocrysts and groundmass or filling vesicles suggests the existence of low-temperature alteration in some lavas from JFR shield stage. In fact, this alteration can explain the few abnormally high values of some mobile elements as Ba (see Figure V.S.1). In detail, some LILE are remobilized in JFR samples, mainly in submarine samples from O'Higgins and Alpha; generating lower or higher values than expected only for the differentiation trend (see Figure V.S.2); a typical behavior observed globally in submarine lava samples. That is why these elements (U, K, Rb and Ba) will not be considered in the analysis and geochemical modeling.

V.5.2 Differentiation and primary melts

Fractional crystallization and gravitational settling or pick-up of primitive olivine antecrysts was proposed to explain the internal geochemical variation of rocks with highest Mg# values in Robinson Crusoe (Reyes et al., 2017). This interpretation can be extended to all JFR shield-building stage lavas, with marked increase in Ni contents in samples with high Mg# ('olivine-rich' group) (Figure V.3) and olivine crystals out of equilibrium with their liquids (Reyes et al., 2017). Rocks of the 'near-primitive' group have experienced little or no olivine fractionation/accumulation, without significant influence of other minerals according to their CaO/Al_2O_3 ratios (Figure V.3). Some samples from this group could be differentiated liquids affected by a magmatic recharge of primitive melts (also observed by Natland, 2003) implying an increase in their MgO content.

Rocks from the 'differentiated' group were formed by fractional crystallization in a shallow magmatic chamber (Reyes et al., 2017), with clinopyroxene, in addition to olivine, playing an important role as suggested by CaO/Al_2O_3 and Sc variations in the evolutionary trend (Figure V.3). The effect of other minerals, such as plagioclase, is not clear (see CaO vs. Sr in Figure V.3), and the negative Eu anomaly is only present in scarce samples of

Alejandro Selkirk (see Figure V.S.1). To accurately determine the phases involved in magma evolution we made a fractional crystallization model in a magmatic reservoir using COMAGMAT 3.72 software (Ariskin, 1999; Ariskin and Barmina, 2004).

The results of the model (see Appendix A for model input details) indicate initial fractionation of olivine on both Robinson Crusoe and Alejandro Selkirk, followed by clinopyroxene in Robinson Crusoe, and by plagioclase in the latter (plagioclase only crystallizes late at Robinson Crusoe). This difference in the crystallization sequence is consistent with the increment in CaO/Al_2O_3 at ~54 Mg# observed in Alejandro Selkirk prior to the descent of the trend (Figure V.7). The model also confirms the suitability of the chosen samples as parental magmas; defined as the most magnesian liquid that can be inferred from a given rock suite (Herzberg et al., 2007); especially LL040213-2 and MF-3, since they satisfy, in general, the geochemistry of major and incompatible elements (REE and La/Yb) of JFR basic lavas (Figure V.7).

All mafic samples of JFR, including parental basalts, come from primary magmas; defined as magma originated as a partial melt of a mantle source (Herzberg et al., 2007); so a critical goal is to infer these compositions for unraveling their source features. For this purpose, we use the PRIMACALC2 software (Kimura and Ariskin, 2014), a program that calls COMAGMAT 3.72 to examine the mantle equilibrium and trace elements calculations of primary basalts with reverse and forward calculations in the parental magmas mentioned above. Conditions are the same used in the fractional crystallization model (see Appendix A) and the results are consistent among them (without significant differences in incompatible elements), especially in Alejandro Selkirk (Table V.5; Figure V.7). The H_2O content is a critical input of PRIMACALC2, but due to the chemical proximity between parental and primary melts in JFR, only very subtle changes are observed in major oxides, whereas trace elements are largely insensitive to water content.

V.5.3 Sources of magmatism and pyroxenites in JFR

Radiogenic isotopes show that JFR shield-building lavas have an enriched signature close to the FOZO-A source, with additional participation of DM, especially in Alejandro Selkirk (Figures V.5 & V.6). Truong et al. (2018) suggest additional participation of HIMU source in the genesis of Robinson Crusoe, but we think that this is not necessary to explain the JFR signature, because the classical values of very radiogenic Pb and unradiogenic Sr for a given Nd isotope ratios of HIMU are not observed in any volcano of JFR. In fact, the $^{206}Pb/^{204}Pb$ values only reach up to ~ 19.29 (Table V.4), and studied samples plot well within the mantle array in Sr-Nd isotope space (Figure V.6). Further contribution of EM1 in JFR shield lavas, additional to its participation in the stable mixture of FOZO-A, is discarded due to the $^{143}Nd/^{144}Nd$ values (see Figures V.5 & V.6), and hence is not considered in this study.

Based on these features, we explore the lithologies likely to be involved in the genesis of JFR magmas. FOZO-A source, a common feature observed in several OIB systems, is interpreted as a stable mixture of the other components (DM, HIMU, EM1 and EM2) (e.g., Hart et al., 1992; Stracke et al., 2005; White, 2015; Kimura et al., 2016). Particularly, HIMU has been classically interpreted as igneous crust recycled back into the mantle in subduction zones, that evolved isotopically over time (e.g., Zindler and Hart, 1986; Weaver, 1991; Hauri and Hart, 1993; Salters and White, 1998; Stracke et al., 2003; Stracke et al., 2005; Kimura et al., 2016). Additionally, the difference between FOZO-A

(southern hemisphere) and FOZO-B (northern hemisphere) is given by the presence of DUPAL anomaly (Jackson et al., 2007), an isotopic enrichment of Pb and Sr restricted to southern hemisphere, probably originated by the influence of recycled slab residues (e.g., Rehkämper and Hofmann, 1997). Thus, to explain the JFR signature, particularly the FOZO-A source (including DUPAL anomaly), seems plausible that recycled material, probably oceanic crust and/or other mafic lithologies plus sediments, would play an important role.

Furthermore, JFR satisfies some first-order geochemical features that have been interpreted as evidence of mafic sources different to peridotite in the source of OIB (considering only samples of 'near-primitive' group). Those are, for example, high TiO_2 content that makes necessary the involvement of a mafic lithology as recycled oceanic crust (high values respect to MORB are distinct in Figure V.8) (Prytulak and Elliot, 2007), values of FC3MS ($FeO/CaO*3MgO/SiO_2$; 0.53 for Robinson Crusoe and 0.60 for Alejandro Selkirk) close to the maximum acceptable for peridotites (0.65) and near to the average value of pyroxenite sources (0.46) (Figure V.8) (Yang and Zhou, 2013), high values of Fe/Mn at a given MnO (Liu et al., 2008), and low CaO to a given MgO (under the boundary of peridotites, only tholeiitic lavas, no clinopyroxene or plagioclase in line of descent) that implies pyroxenitic source (Figure V.8) (Herzberg, 2006; Herzberg and Asimow, 2008). To refine these observations, we run a basic qualitative model of partial melting from lherzolite/garnet peridotite and recycled basalt without involvement of sediments (using parameters of Stracke et al., 2003) to explain the JFR trace geochemistry. We note that TITAN (Jackson et al., 2008) anomaly and HREE values (patterns shown in Figure V.10 that imply the existence of garnet and spinel in the source, see also Figure V.S.1) of JFR cannot be explained exclusively from a garnet or spinel peridotite source and the involvement of a recycled basalt is needed.

When oceanic crust is recycled by subduction becomes dehydrated and metamorphosed to eclogite. Melts originated from eclogites are silica-saturated and do not explain the chemistry of OIBs (Yaxley and Green, 1998; Pertermann and Hirschmann, 2003), but they are capable to react with the surrounding mantle generating refertilization of peridotites (Hauri, 1996; Kogiso et al., 1998; Yaxley and Green, 1998; Spandler et al., 2008) and olivine-free rocks as pyroxenites (Kogiso et al., 2003; Sobolev et al., 2005; Sobolev et al., 2007; Rosenthal et al., 2014) that account for the composition of several OIB-like magmas (e.g., Hauri, 2002, Mallik and Dasgupta, 2012). Thus, the isotopic and chemical evidence allow us to propose the presence of mafic recycled material, particularly pyroxenites, as a minor but relevant component in the source of JFR magmatism and evidence of its heterogeneity.

The involvement of pyroxenites in the JFR source is a reasonable idea considering, in addition to above mentioned evidence, the volume of pyroxenites in the mantle (up to 10%) based on estimations or abundance in orogenic massifs (Pearson and Nixon, 1996; Stracke et al., 2003), and proposed models for other intraplate oceanic islands as Canarias (e.g., Day et al., 2009; Klügel et al., 2017), Hawaii (e.g., Herzberg, 2006; García et al., 2015), Madeira (Gurenko et al., 2013), Mauritius (Paul et al., 2005) and Galápagos (Trela et al., 2015).

V.5.4 Mantle source modeling

Considering the proposed presence of pyroxenite in the source, we would like to quantify its abundance in the heterogeneous mantle plume beneath JFR and the thermodynamic parameters for this combined peridotite/pyroxenite source. Some models have been proposed to constrain the melting of mantle pyroxenites, e.g., OBS1 (Kimura and Kawabata, 2015) or Melt-Px (Lambart et al., 2016), mostly based in the parameterization of Phipps Morgan (2001) and Katz et al. (2003). We decided to use the OBS1 model because it considers both the mixing of melts from peridotite and pyroxenite, and the metasomatic effect that pyroxenitic melts generate in the 'ambient' peridotite (a mix between enriched -PM- and depleted -DM- compositions). The model explores four source parameters (Px_{fr}: pyroxenite fraction; $Per2_{fr}$: enriched peridotite fraction, T_p: potential temperature, P_{mt}: pressure at melting termination). An additional parameter, defined as pyroxenitic 'composition fraction' ($Px\% := Px_{fr}*PxF_{mt}/(PerF_{mt}+Px_{fr}*PxF_{mt})*100$) quantifies the contribution (in wt%) of the pyroxenite component melting in the primary melt.

To make explicit the effect of water in the model (details of input for model in Appendix B), we compared the result of the main parameters (Px_{fr}, Px%, P_{mt}, $TotF_{mt}$) with the most representative samples (LL040213-2 and MF-3) considering 0.025, 0.050 (used in the model) and 0.075 wt% of H_2O. For water increase of 0.025 wt%, the T_p, and P_{mt} decrease (considering the average values, the temperature decreases between 29 and 14 °C, and the pressure in the range 0.05 – 0.09 GPa), and $TotF_{mt}$ remains almost constant with variations lesser than 0.5 wt% (Figure V.9). The behavior of pyroxenite is somewhat surprising because Px_{fr} increases but Px% decreases with higher water content (Figure V.9) due to a progressive lower melting degree of pyroxenite (and constant in peridotite that explain the values observed for $TotF_{mt}$).

Results of the model (details of input for model in Appendix B) are detailed in Table V.7 confirming the presence of pyroxenites in the heterogeneous mantle plume beneath JFR, ranging between 3 and 16 wt% (Px_{fr}), with a relatively low T_p (1262 – 1362 °C), and $TotF_{mt}$ (2.4 – 11.4 wt%) at a P_{mt} between 1.98 and 2.56 GPa.

Considering only the most representative primary melts (from LL040213-2 for Robinson Crusoe and from MF-3 for Alejandro Selkirk), the results of the model show low potential temperatures (values in the range 1290 – 1322 °C for Robinson Crusoe and 1312 – 1362 °C for Alejandro Selkirk), in general, compared to other OIB (e.g., Herzberg et al., 2007; Putirka, 2008) including OBS1 software values (~ 1400 – 1450 °C; Kimura and Kawabata, 2015), but similar to some 'ambient' mantle estimations, e.g., ~ 1396 (Putirka, 2008), 1280 – 1400 (Herzberg et al., 2007), and 1300 – 1310 °C with OBS1 (Kimura and Kawabata, 2015). Our relative low temperatures could be explained by the inclination to cooling that the pyroxenite-bearing mantle plumes have (their density implies low ascent velocity; Herzberg, 2011) and their possible content of volatiles. In fact, the water is included in the model, and was shown that an increment of 0.025 wt% induces an average decrease of 14 to 29 °C (Figure V.9), which is expected because a higher water content reduces the solidus of the mantle (Kushiro et al., 1968; Gaetani and Groove, 1998). In addition, Devey et al. (2000) proposes the existence of a carbonated plume beneath JFR in their study of Domingo and Friday seamounts. The possible presence of CO_2 in the mantle also would cause an increase of the melt generation at a given temperature (decreasing the solidus) in peridotites (Dasgupta et al., 2007) and peridotites hybridized by pyroxenites (e.g., Mallik and Dasgupta, 2014, and references therein). The latter suggests that JFR could be considered as a 'wet spot' rather than a 'hot spot' (if this high volatile content is confirmed),

a mantle plume where the chemical anomaly (including volatiles) predominates over the thermal effect (Bonatti, 1990). The presence of 'wet spots' has been proposed to explain the low potential temperatures obtained in other intraplate systems as Azores (Metrich et al., 2014) and Iceland (Nichols et al., 2002). Furthermore, Mallik and Dasgupta (2012; 2014) demonstrated that near-primitive basalts (MgO > 15 wt%) can be generated at temperatures of ~ 1350 °C from a peridotite hybridized by recycled oceanic crust-derived melts (± CO_2).

Potential temperatures of ~ 1582 °C obtained by Putirka (2008) are ~ 250 °C higher than our results. We consider that these estimations have some methodological problems because GEOROC database (used in his study) includes shield (with numerous 'olivine-rich' samples) and rejuvenated samples from JFR, and thus the use of average values are doubtful due to the contrasting geochemistry, isotopic ratios, and processes (details of differences in Reyes et al., 2017).

The values for the pressure of melt termination (2.34 – 2.54 GPa in Robinson Crusoe and 2.24 – 2.52 GPa in Alejandro Selkirk) are probably related to the lithosphere-asthenosphere boundary, predicted at 60 – 75 km beneath the present position of Robinson Crusoe and Alejandro Selkirk (also for the volcanoes located to the W as Friday and Domingo; Devey et al., 2000), and 75 – 90 km under the E segment of the JFR (including O'Higgins guyot), based on an age-dependent half-space cooling model (Tassara et al., 2006).

Some elements do not satisfy exactly the geochemical features of primary basalts (e.g., Pr, Gd, Tb, Dy). These variations can be explained by subtle differences between the real sources involved and the compositions considered in the model, e.g., enrichment in MREE in the peridotite and/or pyroxenite beneath JFR respect to model sources: DM (Workman and Hart, 2005), PM (Lyubetskaya and Korenaga, 2007), and/or N-MORB (Hofmann, 1988).

On the other hand, notable differences were observed between the results obtained for the most representative samples of Robinson Crusoe and Alejandro Selkirk. In fact, Robinson Crusoe shows lower values of T_p (values of 1290 – 1322 vs. 1312 – 1362 °C in Robinson Crusoe), Px_{fr} (4 – 8 vs 6 – 12 wt%), $PerF_{mt}$ (1.5 – 2.6 vs 2.6 – 5.8 wt%), and PxF_{mt} (24.0 – 33.9 vs 33.2 – 49.8 wt%, reflected in a $TotF_{mt}$ of 2.8 – 4.9 vs 5.2 – 11.4 wt%) (Figure V.10). The higher temperature of Alejandro Selkirk is obviously related with the increase in the degree of melting respect to Robinson Crusoe and explains the geochemical variations observed among these islands. Some features as enrichment in LIL, LREE (visible in Figure V.10, see also Figure V.S.1), and high values of Nb/Zr in Robinson Crusoe are explained by the proportional major extraction of the more incompatible elements at low melting degree, which does not occur in relative more compatible elements as HREE. An apparent inconsistency occurs in the amount of Px_{fr}, since Robinson Crusoe show more 'pyroxenite (or recycled) signature' in terms of geochemistry (e.g., TITAN anomaly and HREE values) and isotopic ratios (closer to FOZO-A), but lower content of pyroxenite in the plume. This inconsistency is not real, since the critical parameter for the primary melt is the participation of pyroxenitic component in the final primary melt (Px%) and not Px_{fr}. Due to their thermodynamic features, the pyroxenite has the solidus at lower temperatures than peridotites, so the melting begin deeper and melts can be extracted from a larger melting column implying a disproportionate contribution (in a fraction from 5 to more than 10) respect to their weight

fraction (e.g., Pertermann and Hirschmann, 2003; Kogiso et al., 2003; Lambart et al., 2016). Then, in terms of Px%, the difference between the islands is negligible (38.6 – 56.4 in Robinson Crusoe vs. 35.8 – 55.6 wt% in Alejandro Selkirk) due to the compensation between higher Px_{fr} (4 – 8 vs. 6 – 12 wt%) and lower PxF_{mt} (24.0 – 33.9 vs. 33.2 – 49.8 wt%) in Robinson Crusoe. This lower melting degree also generates their 'more pyroxenitic' characteristics. The enrichment of DM isotopic signature in Alejandro Selkirk could be explained by subtle temporal changes in the proportion of peridotitic depleted source respect to PM enriched peridotites, that conciliate the isotopic depletion with the conservation of the pyroxenite contribution in the primary melt (Px%). These slight compositional variations through time in the source seem plausible considering the nature of FOZO-A (mixture of other components; e.g., Hart et al., 1992; Stracke et al., 2005; White, 2015; Kimura et al., 2016).

We also modeled two sets of primary melts that represent samples with different values of La/Yb. The high La/Yb group is represented by JR290513-5 and JR170913-18 samples (from Robinson Crusoe and Alejandro Selkirk respectively), and shows lower values of T_p, P_{mt}, and PxF_{mt}; and markedly higher of Px_{fr} respect to the most representative sample of the volcanism from each island (Figure V.10). On the other hand, the low La/Yb group (LL250711-7 from Robinson Crusoe and MF-6 from Alejandro Selkirk) also shows a decrease in T_p, but similar values of Px_{fr} and a notable shallowing with P_{mt} mean of 2.21 and 2.27 GPa respectively (Figure V.10).

V.5.5 Petrogenesis and magmatic evolution

Based on the Farley et al., (1993) scheme, Truong et al. (2018) propose a common but slightly heterogeneous mantle source for the JFR suite as prescribed by Sr-Nd-Pb systematics, although with variable $^{3}He/^{4}He$ pointing to a temporal change over a wide-scale spatial heterogeneity of the mantle. However, with a better geochronology constraint and more precise Pb systematics, we are able to explain the variety of first-order features of the shield stage lavas as a result of melting at different conditions through time and subtle compositional variations in the source.

In fact, the JFR shield stage would be formed by melting of low temperature heterogeneous mantle plume with participation of peridotite (DM and PM) and pyroxenite until to lithosphere-asthenosphere boundary characterized by FOZO-A signature with additional participation of DM (as North Chile Ridge or East Pacific Rise). Isotopic and geochemical differences between Robinson Crusoe/Alpha and Alejandro Selkirk/O'Higgins are explained in terms of temporal changes in the melting degree; generated by an increase of ~ 30 °C; and in proportion of DM in the source.

V.5.6 Mantle compositional variations beneath Nazca Plate

Compared to oceanic volcanism nearby, JFR is clearly enriched in all the analyzed isotopic systems relative to the East Pacific Rise (Macdougall and Lugmair, 1985) and North Chile Ridge (Bach et al., 1996) (Figures V.5 & V.6), two classical examples of MORB. San Félix/San Ambrosio (SF/SA), another example of oceanic intraplate volcanism isolated from spreading ridges in the Nazca plate, is similar to JFR only in $^{206}Pb/^{204}Pb$ and $^{207}Pb/^{204}Pb$ (Figure V.5), but the considerable participation of EM2 in the SF/SA source generates significant differences in the other isotopic systems (data from GEOROC database). Compared with Easter Island and Eastern Seamount Chain

(GEOROC database), JFR is clearly more radiogenic, but in a more limited field (Figures V.5 & V.6). The large variation of isotopic ratios in Easter Island would be a result of the mixing of a mantle plume source with depleted upper mantle (DM) component due to their proximity to East Pacific Rise (i.e., plume-ridge interaction). These observations confirm a pioneer idea by Gerlach et al. (1986) about the mantle beneath the Nazca plate and its notable heterogeneities.

V.6. Conclusions

O'Higgins guyot, Alpha seamount, Robinson Crusoe and Alejandro Selkirk islands are large volcanic edifices of JFR in the Nazca Plate that mainly consist of tholeiitic, transitional, and alkali basalts representatives of the shield-building stage of volcanism. Their differentiation is controlled by fractional crystallization (including accumulation) and mixing/magmatic recharge. Whole-rock geochemical and Sr-Nd-Pb isotopic features (e.g., low CaO at given MgO, and TITAN anomaly, with FOZO-A and DM sources involved) suggest the existence of lithological heterogeneities in the mantle source, particularly pyroxenites (as reflect of recycled oceanic crust). A petrogenetic model (for the most representative primary melts calculated from Robinson Crusoe and Alejandro Selkirk parental samples) based in incompatible elements patterns indicates low potential temperature (< ~1360 °C), notable contribution of pyroxenite (up to 56.4 wt% of the final melt), and depth of melting termination coherent with the lithosphere-asthenosphere boundary. The more marked chemical enrichment of Robinson Crusoe respect to Alejandro Selkirk is related to some changes in the plume beneath JFR as potential temperature (~ 30 °C on average) and total degree of melting (average values of 3.8 vs. 8.0 wt%) at similar pyroxenite contribution in the primary melt. Thus, the isotopic depletion of Alejandro Selkirk is explained by temporal changes in the DM proportion in peridotites of FOZO-A source. This implies that a low temperature heterogeneous mantle plume is involved in the petrogenesis of shield volcanism in JFR.

Acknowledgments

This research was supported by FONDECYT 1110966, 1141303 (both granted to L.E. Lara) and FONDAP 15090013 projects. Main results presented in this manuscript are part of the first author's doctoral thesis also supported by a CONICYT fellowship. Authors are grateful to X and Y for providing constructive reviews that improved this paper. We also acknowledge to Scripps Institution of Oceanography the samples from Alpha seamount and Alejandro Selkirk Island, and to Clermont-Ferrand staff: J-L. Paquette, Delphine Auclair, and Chantal Bosq who performed some Sr-Nd analysis. CONAF authorized scientific research in this protected area and DIFROL provided logistical support during the 2013 field campaign.

Appendix A. Fractional crystallization model

The starting compositions for COMAGMAT 3.72 (Ariskin and Barmina, 2004) fractional crystallization model are 3 samples from Robinson Crusoe and 3 from Alejandro Selkirk in order to cover some internal variations in La/Yb ratios observed in each volcano. The starting compositions were selected as parental candidates from the 'near-primitive' or 'olivine-rich' groups based on their chemical characteristics (e.g., high Mg#, moderate enrichment in Ni and Cr). The most representative samples (with medium values of La/Yb) are LL040213-2 of Robinson Crusoe (similar to Alpha seamount) and MF-3 of Alejandro

Selkirk (similar to O'Higgins guyot). Other selected samples (JR290513-5 and LL250711-7 for Robinson Crusoe, and JR170913-18 and MF-6 for Alejandro Selkirk) represent groups constituted by few samples with La/Yb values higher or lower than the most representative trend. Pressure of fractionation was fixed in 2.0 kbar (taken from Reyes et al., 2017), and redox conditions were set at the QFM buffer as recommended for OIB by Kimura and Ariskin (2014), with a crystallization increment of 0.1 %. Magmatic water contents are more problematic since there are no direct measurements of H_2O content in JFR lavas. Putirka (2008) estimated 1.91 wt% H_2O based on his calculated partial melting degree (F) and typical H_2O/Ce ratios for the ocean island sources (Dixon et al., 2002). This value, however, inherits potential problems in the estimation of F and temperature because the data considered in the calculations were taken from the GEOROC database, with data mainly from Farley et al. (1993) and, although the latter included samples from different stages of the volcanism, sampling was skewed towards the picrites because their goal was the analysis of $^3He/^4He$ retained in mafic phenocrysts. Then, using the same estimation of Dixon et al. (2002) (H_2O/Ce of 200 in Pacific-FOZO), but only in the best candidates for parental magmas (LL040213-2 for Robinson Crusoe, and MF-3 for Alejandro Selkirk) we obtain a value of ~0.80 H_2O wt% for JFR, which we used as input in the model. This amount seems to be reasonable considering other estimations, e.g., 0.9 – 1.0 wt% for the plume source end-member in Eastern Seamount Chain (a source more enriched than JFR) (Simons et al., 2002).

Appendix B. OBS1 mantle source modeling

The input parameters of the model are: primary melt, melting model, pyroxenite, and enriched peridotite composition, additional depletion of DM and H_2O content in the source. We submit to OBS1 the primary melts calculated by PRIMACALC2 (see section 5.2) considering that LL040213-2 and MF-3 are the most representative samples of Robinson Crusoe/Alpha and Alejandro Selkirk/O'Higgins, respectively. Respect to the melting model, metasomatic parameterization appears to be more realistic (Kimura and Kawabata, 2015) and was selected in this study. The absence of direct evidence of pyroxenite or their residues (e.g., as xenoliths) in JFR also supports this choice. The different sources compositions were taken from the literature, specifically, the average depleted mantle of Workman and Hart (2005) was considered to DM (additional depletion is not necessary in OIB), primitive mantle of Lyubetskaya and Korenaga (2007) for PM, and N-MORB of Hofmann (1988) for pyroxenite. According to the discussion in section 5.3, pyroxenites come from oceanic recycled crust (classically N-MORB). Taking into account that the effect of alteration is limited to the top of the crust (Staudigel et al., 1996) and subduction modification is difficult to estimate, but less than 5% for REE and HFSE (Porter and White, 2009; Kimura et al., 2014), we consider reasonable the simplification of considering N-MORB as the pyroxenite source, particularly because the analysis is based mostly on Nb, Zr, La, and Yb concentrations (in general immobile elements). Regarding the water content, there are not yet studies about that for JFR, and then this parameter must be estimated. Dixon et al. (2002) proposed 0.075 H_2O wt% in Pacific FOZO mantle, but JFR has DM additional contribution (a source with considerably less water). Similarly, Simons et al. (2002) measured the same concentration (0.075 wt%) in the plume end-member of Easter, that is more enriched (chemical and isotopically) than JFR. We propose a content of 0.050 wt% for the model, a value lower than estimations for more enriched sources, similar to the 0.053 wt% average value of Kovalenko et al. (2006) for their Type III magmas (which share some similarities with JFR, e.g., $K_2O > 0.2$

wt% and H_2O > 0.2 wt%), and higher than the primitive mantle value of 0.033 wt% (Dixon and Clague, 2001).

Finally, the fitting window is fixed in 200 % for LILE (Rb, Ba, Th, U); 60 % for Ta, K, Ce, Pr, Sr, and 30 % for Nd, Sm, Hf, Eu, Gd, Tb, Dy, Y, Ho, Er, Tm, Lu. The model is focused on the behavior of Nb/Zr and La/Yb ratios (distinctive features among the JFR volcanoes) and hence for these ratios and for Nb, Zr, La, and Yb the fitting window is only 15 %. A summary of the input parameters is shown in Table V.6. After an exploratory modeling, we ran 100,000 iterations or more until completing at least 50 successful results.

Bibliography

Anderson, D.L., 2000. The thermal state of the upper mantle; no role for mantle plumes. Geophys. Res. Lett. 27, 3623–3626. doi:10.1029/2000GL011533

Anderson, D.L., 2001. Top-down tectonics? Science 293, 2016–2018. doi:10.1126/science.1065448

Argus, D.F., Gordon, R.G., Heflin, M.B., Ma, C., Eanes, R.J., Willis, P., Peltier, W.R., Owen, S.E., 2010. The angular velocities of the plates and the velocity of Earth's centre from space geodesy. Geophys. J. Int. 180, 913–960. doi.org/10.1111/j.1365-246X.2009.04463.x

Ariskin, A.A., 1999. Phase equilibria modeling in igneous petrology: use of COMAGMAT model for simulating fractionation of ferro-basaltic magmas and the genesis of high-alumina basalt. J. Volcanol. Geotherm. Res. 90, 115–162. doi.org/10.1016/S0377-0273(99)00022-0

Ariskin, A.A., Barmina, G.S., 2004. COMAGMAT: Development of a magma crystallization model and its petrological applications. Geochemistry Int. 42, s1–s157. doi.org/scopus/2-s2.0-5444237530

Astudillo, V., 2014. Geomorfología y evolución geológica de la isla Robinson Crusoe, Archipiélago Juan Fernández. Universidad de Chile (154 pp.).

Bach, W., Erzinger, J., Dosso, L., Bollinger, C., Bougault, H., Etoubleau, J., Sauerwein, J., 1996. Unusually large NbTa depletions in North Chile ridge basalts at 36°50′ to 38°56′S: major element, trace element, and isotopic data. Earth Planet. Sci. Lett. 142, 223–240. doi.org/10.1016/0012-821X(96)00095-7

Baker, P.E., Gledhill, A., Harvey, P.K., Hawkesworth, C.J., 1987. Geochemical evolution of the Juan Fernandez Islands, SE Pacific. J. Geol. Soc. London. 144, 933–944. doi.org/10.1144/gsjgs.144.6.0933

Ballmer, M.D., van Hunen, J., Ito, G., Tackley, P.J., Bianco, T. a., 2007. Non-hotspot volcano chains originating from small-scale sublithospheric convection. Geophys. Res. Lett. 34. doi:10.1029/2007GL031636

Blichert-Toft, J., 1999. Hf isotope evidence for pelagic sediments in the source of hawaiian basalts. Science 285 (5429), 879–882. doi.org/10.1126/science.285.5429.879

Bonatti, E., 1990. Not So hot "hot spots" in the oceanic mantle. Science 250 (4977), 107–111. doi.org/10.1126/science.250.4977.107

Booker, J., Bullard, E.C., Grasty, R.L., 1967. Palaeomagnetism and age of rocks from Easter Island and Juan Fernandez. Geophys. J. Int. 12, 469–471. doi.org/10.1111/j.1365-246X.1967.tb03127.x

Boschi, L., Becker, T.W., Steinberger, B. 2007. Mantle plumes: Dynamic models and seismic images, Geochem. Geophys. Geosyst., 8, Q10006, doi: 10.1029/2007GC001733

Clouard, V., Bonneville, A., 2001. How many Pacific hotspots are fed by deep-mantle plumes? Geology 29(8), 695–698. doi:10.1130/0091-7613(2001)029<0695:HMPHAF>2.0.CO;2

Courtillot, V., Davaille, A., Besse, J., Stock, J., 2003. Three distinct types of hotspots in the Earth's mantle. Earth Planet. Sci. Lett. 205, 295–308. doi.org/10.1016/S0012-821X(02)01048-8

Dasgupta, R., Hirschmann, M.M., Smith, N.D., 2007. Water follows carbon: CO2 incites deep silicate melting and dehydration beneath mid-ocean ridges. Geology 35, 135–138. doi.org/10.1130/G22856A.1

Davies, G.F. 1988. Ocean bathymetry and mantle convection: 1. Large-scale flow and hotspots. J. Geophys. Res. 93(B9), 467–480. doi.org/10.1029/JB093iB09p10467

Day, J.M.D., Pearson, D.G., Macpherson, C.G., Lowry, D., Carracedo, J.-C., 2009. Pyroxenite-rich mantle formed by recycled oceanic lithosphere: Oxygen-osmium isotope evidence from Canary Island lavas. Geology 37, 555–558. doi.org/10.1130/G25613A.1

Devey, C.W., Hémond, C., Stoffers, P., 2000. Metasomatic reactions between carbonated plume melts and mantle harzburgite: the evidence from Friday and Domingo Seamounts (Juan Fernandez chain, SE Pacific). Contrib. to Mineral. Petrol. 139, 68–84. doi.org/10.1007/s004100050574

Dixon, J.E., Clague, D. a., 2001. Volatiles in basaltic glasses from Loihi Seamount, Hawaii: Evidence for a relatively dry plume component. J. Petrol. 42, 627–654. doi.org/10.1093/petrology/42.3.627

Dixon, J.E., Leist, L., Langmuir, C., Schilling, J.-G., 2002. Recycled dehydrated lithosphere observed in plume-influenced mid-ocean-ridge basalt. Nature 420, 385–389. doi.org/10.1038/nature01215

Dupré, B., Allègre, C.J. 1983. Pb-Sr isotope variation in Indian Ocean basalts and mixing phenomena. Nature 303, 142–146. doi.org/10.1038/303142a0

Farley, K.A., Basu, A.R., Craig, H., 1993. He, Sr and Nd isotopic variations in lavas from the Juan Fernandez Archipelago, SE Pacific. Contrib. to Mineral. Petrol. 115, 75–87. doi.org/10.1007/BF00712980

French, S.W., Romanowicz, B., 2015. Broad plumes rooted at the base of the Earth's mantle beneath major hotspots. Nature 525, 95–99. doi.org/10.1038/nature14876

Gaetani, G.A., Grove, T.L., 1998. The influence of water on melting of mantle peridotite. Contrib. to Mineral. Petrol. 131, 323–346. doi.org/10.1007/s004100050396

Garcia, M.O., 1996. Petrography and olivine and glass chemistry of lavas from the Hawaii Scientific Drilling Project. Journal of Geophysical Research: Solid Earth 101, 11701–11713. doi:10.1029/95JB03846

Garcia, M.O., Smith, J.R., Tree, J.P., Weis, D., Harrison, L., Jicha, B.R., 2015. Petrology, geochemistry, and ages of lavas from Northwest Hawaiian Ridge volcanoes. Geological Society of America Special Papers 511 . doi:10.1130/2015.2511(01)

Gerlach, D.C., Hart, S.R., Morales, V.W.J., Palacios, C., 1986. Mantle heterogeneity beneath the Nazca plate: San Felix and Juan Fernandez islands. Nature 322, 165–169. doi.org/10.1038/322165a0

Gurenko, A.A., Geldmacher, J., Hoernle, K.A., Sobolev, A. V., 2013. A composite, isotopically-depleted peridotite and enriched pyroxenite source for Madeira magmas: Insights from olivine. Lithos 170–171, 224–238. doi.org/10.1016/j.lithos.2013.03.002

Hanan, B.B., Graham, D.W., 1996. Lead and helium isotope evidence from cceanic basalts for a common deep source of mantle plumes. Science 272 (5264), 991–995. doi:10.1126/science.272.5264.991

Hart, S.R., 1984. A large-scale isotope anomaly in the Southern Hemisphere mantle. Nature 309, 753–757. doi.org/10.1038/309753a0

Hart, S.R., 1988. Heterogeneous mantle domains: signatures, genesis and mixing chronologies. Earth Planet. Sci. Lett. 90, 273–296. doi.org/10.1016/0012-821X(88)90131-8

Hart, S.R., Hauri, E.H., Oschmann, L.A., Whitehead, J.A., 1992. Mantle Plumes and Entrainment: Isotopic Evidence. Science 256 (5056), 517–520. doi.org/10.1126/science.256.5056.517

Hauri, E.H., Hart, S.R., 1993. Re-Os isotope systematics of HIMU and EMII oceanic island basalts from the south Pacific Ocean. Earth Planet. Sci. Lett. 114, 353–371. doi.org/10.1016/0012-821X(93)90036-9

Hauri, E.H., 1996. Major-element variability in the Hawaiian mantle plume. Nature 382, 415–419. doi.org/10.1038/382415a0

Hauri, E.H., 2002. Osmium isotopes and mantle convection. Philos. Trans. R. Soc. A Math. Phys. Eng. Sci. 360, 2371–2382. doi.org/10.1098/rsta.2002.1073

Herzberg, C., 2006. Petrology and thermal structure of the Hawaiian plume from Mauna Kea volcano. Nature 444, 605–609. doi.org/10.1038/nature05254

Herzberg, C., Asimow, P.D., Arndt, N., Niu, Y., Lesher, C.M., Fitton, J.G., Cheadle, M.J., Saunders, A.D., 2007. Temperatures in ambient mantle and plumes: Constraints from basalts, picrites, and komatiites. Geochemistry, Geophys. Geosystems 8, Q02006. doi.org/10.1029/2006GC001390

Herzberg, C., Asimow, P.D., 2008. Petrology of some oceanic island basalts: PRIMELT2.XLS software for primary magma calculation. Geochemistry, Geophys. Geosystems 9, Q09001. doi.org/10.1029/2008GC002057

Herzberg, C., 2011. Identification of source lithology in the Hawaiian and Canary Islands: implications for origins. J. Petrol. 52, 113–146. doi.org/10.1093/petrology/egq075

Hieronymus, C.F., Bercovici, D., 2000. Non-hot spot formation of volcanic chains: Controls of tectonic stresses on magma transport. Earth Planet. Sci. Lett. 181, 539–554. doi:10.1016/S0012-821X(00)00227-2

Hoernle, K., Hauff, F., Werner, R., van den Bogaard, P., Gibbons, A.D., Conrad, S., Müller, R.D., 2011. Origin of Indian Ocean Seamount Province by shallow recycling of continental lithosphere. Nat. Geosci. 4, 883–887. doi.org/10.1038/ngeo1331

Hofmann, A.Q., White, W.M. 1982. Mantle plumes from ancient oceanic crust. Earth Planet. Sci. Lett. 57(2), 421–436. doi.org/10.1016/0012-821X(82)90161-3

Hofmann, A.W., 1988. Chemical differentiation of the Earth: the relationship between mantle, continental crust, and oceanic crust. Earth Planet. Sci. Lett. 90, 297–314. doi.org/10.1016/0012-821X(88)90132-X

Jackson, M.G., Kurz, M.D., Hart, S.R., Workman, R.K., 2007. New Samoan lavas from Ofu Island reveal a hemispherically heterogeneous high $^{3}He/^{4}He$ mantle. Earth Planet. Sci. Lett. 264, 360–374. doi.org/10.1016/j.epsl.2007.09.023

Jackson, M.G., Hart, S.R., Saal, A.E., Shimizu, N., Kurz, M.D., Blusztajn, J.S., Skovgaard, A.C., 2008. Globally elevated titanium, tantalum, and niobium (TITAN) in ocean island basalts with high 3He/4He. Geochemistry, Geophys. Geosystems 9, Q04027. doi.org/10.1029/2007GC001876

Jackson, M.G., Konter, J.G., Becker, T.W., 2017. Primordial helium entrained by the hottest mantle plumes. Nature 542, 340–343. doi.org/10.1038/nature21023

Katz, R.F., Spiegelman, M., Langmuir, C.H., 2003. A new parameterization of hydrous mantle melting. Geochemistry, Geophys. Geosystems 4, 1073. doi.org/10.1029/2002GC000433

Kimura, J.-I., Ariskin, A.A., 2014. Calculation of water-bearing primary basalt and estimation of source mantle conditions beneath arcs: PRIMACALC2 model for WINDOWS. Geochemistry, Geophys. Geosystems 15, 1494–1514. doi.org/10.1002/2014GC005329

Kimura, J.-I., Kawabata, H., 2015. Ocean Basalt Simulator version 1 (OBS1): Trace element mass balance in adiabatic melting of a pyroxenite-bearing peridotite. Geochemistry, Geophys. Geosystems 16, 267–300. doi.org/10.1002/2014GC005606

Kimura, J.-I., Gill, J.B., Skora, S., van Keken, P.E., Kawabata, H., 2016. Origin of geochemical mantle components: Role of subduction filter. Geochemistry, Geophys. Geosystems 17, 3289–3325. doi.org/10.1002/2016GC006343

Klügel, A., Galipp, K., Hoernle, K., Hauff, F., Groom, S., 2017. Geochemical and volcanological evolution of La Palma, Canary Islands. J. Petrol. 58, 1227–1248. doi.org/10.1093/petrology/egx052

Kogiso, T., Hirschmann, M.M., Frost, D.J., 2003. High-pressure partial melting of garnet pyroxenite: possible mafic lithologies in the source of ocean island basalts. Earth Planet. Sci. Lett. 216, 603–617. doi.org/10.1016/S0012-821X(03)00538-7

Kovalenko, V.I., Naumov, V.B., Girnis, a. V., Dorofeeva, V. a., Yarmolyuk, V. V., 2006. Composition and chemical structure of oceanic mantle plumes. Petrology 14, 452–476. doi.org/10.1134/S0869591106050031

Kushiro, I., Syono, Y., Akimoto, S., 1968. Melting of a peridotite nodule at high pressures and high water pressures. J. Geophys. Res. 73, 6023–6029. doi.org/10.1029/JB073i018p06023

Lambart, S., Baker, M.B., Stolper, E.M., 2016. The role of pyroxenite in basalt genesis: Melt-PX, a melting parameterization for mantle pyroxenites between 0.9 and 5 GPa. J. Geophys. Res. Solid Earth 121, 5708–5735. doi.org/10.1002/2015JB012762

Lara, L.E., Díaz-Naveas, J., Reyes, J., Jicha, B., Orozco, G., Kay, S.M., 2018a. Unraveling short-lived rejuvenated volcanism and a rapid transition from shield stage at O ' Higgins guyot , Juan Fernández Ridge , Pacific SE. Submitted to Deep Sea Research Part I.

Lara, L.E., Reyes, J., Jicha, B., Díaz-Naveas, J. 2018b. $^{40}Ar/^{39}Ar$ constraints for the age progression along the Juan Fernández Ridge, SE Pacific: insights into deep mantle processes. Submitted to Frontiers in Volcanology.

Le Maitre, R.W., 2002. Igneous rocks – a classification and glossary of terms. Cambridge University Press, Cambridge (236 pp.). doi.org/10.1017/CBO9780511535581

Liu, Y., Gao, S., Kelemen, P.B., Xu, W., 2008. Recycled crust controls contrasting source compositions of Mesozoic and Cenozoic basalts in the North China Craton. Geochim. Cosmochim. Acta 72, 2349–2376. doi.org/10.1016/j.gca.2008.02.018

Lyubetskaya, T., Korenaga, J., 2007. Chemical composition of Earth's primitive mantle and its variance: 1. Method and results. J. Geophys. Res. 112, B03211. doi.org/10.1029/2005JB004223

Macdougall, J.D., Lugmair, G.W., 1985. Extreme isotopic homogeneity among basalts from the southern East Pacific Rise: mantle or mixing effect? Nature 313, 209–211. doi.org/10.1038/313209a0

Mallik, A., Dasgupta, R., 2014. Effect of variable CO 2 on eclogite-derived andesite and lherzolite reaction at 3 GPa-Implications for mantle source characteristics of alkalic ocean island basalts. Geochemistry, Geophys. Geosystems 15, 1533–1557. doi.org/10.1002/2014GC005251

Mallik, A., Dasgupta, R., 2014. Effect of variable CO 2 on eclogite-derived andesite and lherzolite reaction at 3 GPa-Implications for mantle source characteristics of alkalic ocean island basalts. Geochemistry, Geophys. Geosystems 15, 1533–1557. doi.org/10.1002/2014GC005251

Métrich, N., Zanon, V., Créon, L., Hildenbrand, A., Moreira, M., Marques, F.O., 2014. Is the "Azores hotspot" a wetspot? Insights from the geochemistry of fluid and melt inclusions in olivine of Pico basalts. J. Petrol. 55, 377–393. doi.org/10.1093/petrology/egt071

Montelli, R., Nolet, G., Dahlen, F.A., Masters, G., 2006. A catalogue of deep mantle plumes: New results from finite-frequency tomography. Geochemistry, Geophys. Geosystems 7, Q11007. doi.org/10.1029/2006GC001248

Morgan, W.J., 1971. Convection plumes in the lower mantle. Nature 230, 42–43. doi.org/10.1038/230042a0

Morgan, W.J., 1972. Deep mantle convection plumes and plate motions. Am. Assoc. Pet. Geol. Bull. 56, 203–213. doi.org/10.1306/819A3E50-16C5-11D7-8645000102C1865D

Natland, J.H., 2003. Capture of helium and other volatiles during the growth of olivine phenocrysts in picritic basalts from the Juan Fernandez Islands. J. Petrol. 44, 421–456. doi.org/10.1093/petrology/44.3.421

Nichols, A.R.L., Carroll, M.R., Höskuldsson, Á., 2002. Is the Iceland hot spot also wet? Evidence from the water contents of undegassed submarine and subglacial pillow basalts. Earth Planet. Sci. Lett. 202, 77–87. doi.org/10.1016/S0012-821X(02)00758-6

Paul, D., White, W.M., Blichert-Toft, J., 2005. Geochemistry of Mauritius and the origin of rejuvenescent volcanism on oceanic island volcanoes. Geochemistry, Geophys. Geosystems 6, Q06007. doi.org/10.1029/2004GC000883

Pearson, D.G., Nixon, P.H., 1996. Diamonds in young orogenic belts: graphitised diamonds from Beni Bousera, N. Morocoo, a comparison with kimberlite-derived diamond occurences and implications for diamond genesis and exploration. Africa Geosci. Rev. 3, 295–316.

Pertermann, M., Hirschmann, M.M., 2003. Partial melting experiments on a MORB-like pyroxenite between 2 and 3 GPa: Constraints on the presence of pyroxenite in basalt

source regions from solidus location and melting rate. J. Geophys. Res. Solid Earth 108, 1–17. doi.org/10.1029/2000JB000118

Peters, B.J., Day, J.M.D., 2014. Assessment of relative Ti, Ta, and Nb (TITAN) enrichments in ocean island basalts. Geochemistry, Geophys. Geosystems 15, 4424–4444. doi.org/10.1002/2014GC005506

Phipps Morgan, J., 2001. Thermodynamics of pressure release melting of a veined plum pudding mantle. Geochemistry, Geophys. Geosystems 2. doi.org/10.1029/2000GC000049

Pin, C., Zalduegui, J.S., 1997. Sequential separation of light rare-earth elements, thorium and uranium by miniaturized extraction chromatography: Application to isotopic analyses of silicate rocks. Anal. Chim. Acta 339, 79–89. doi.org/10.1016/S0003-2670(96)00499-0

Porter, K.A., White, W.M., 2009. Deep mantle subduction flux. Geochemistry, Geophys. Geosystems 10, Q12016. doi.org/10.1029/2009GC002656

Prytulak, J., Elliott, T., 2007. TiO2 enrichment in ocean island basalts. Earth Planet. Sci. Lett. 263, 388–403. doi.org/10.1016/j.epsl.2007.09.015

Putirka, K., 2008. Excess temperatures at ocean islands: Implications for mantle layering and convection. Geology 36, 283–286. doi.org/10.1130/G24615A.1

Reyes, J., Lara, L.E., Morata, D., 2017. Contrasting P-T paths of shield and rejuvenated volcanism at Robinson Crusoe Island, Juan Fernández Ridge, SE Pacific. J. Volcanol. Geotherm. Res. 341, 242–254. doi.org/10.1016/j.jvolgeores.2017.05.035

Rehkämper, M., Hofmann, A.W., 1997. Recycled ocean crust and sediment in Indian Ocean MORB. Earth Planet. Sci. Lett. 147, 93–106. doi.org/10.1016/S0012-821X(97)00009-5

Rodrigo, C., Lara, L.E., 2014. Plate tectonics and the origin of the Juan Fernandez Ridge: analysis of bathymetry and magnetic patterns. Lat. Am. J. Aquat. Res. 42, 907–917. doi.org/10.3856/vol42-issue4-fulltext-15

Rosenthal, A., Yaxley, G.M., Green, D.H., Hermann, J., Kovács, I., Spandler, C., 2015. Continuous eclogite melting and variable refertilisation in upwelling heterogeneous mantle. Sci. Rep. 4, 6099. doi.org/10.1038/srep06099

Salters, V.J., White, W.M., 1998. Hf isotope constraints on mantle evolution. Chem. Geol. 145, 447–460. doi.org/10.1016/S0009-2541(97)00154-X

Sepúlveda, P., Le Roux, J.P., Lara, L.E., Orozco, G., Astudillo, V., 2015. Biostratigraphic evidence for dramatic Holocene uplift of Robinson Crusoe Island, Juan Fernández Ridge, SE Pacific Ocean. Biogeosciences 12, 1993–2001. doi.org/10.5194/bg-12-1993-2015

Simons, K., Dixon, J., Schilling, J.-G., Kingsley, R., Poreda, R., 2002. Volatiles in basaltic glasses from the Easter-Salas y Gomez Seamount Chain and Easter Microplate: Implications for geochemical cycling of volatile elements. Geochemistry, Geophys. Geosystems 3, 1–29. doi.org/10.1029/2001GC000173Sleep, N.H., 1990. Hotspots and mantle plumes: Some phenomenology. J. Geophys. Res. 95, 6715. doi.org/10.1029/JB095iB05p06715

Sobolev, A. V., Hofmann, A.W., Sobolev, S. V., Nikogosian, I.K., 2005. An olivine-free mantle source of Hawaiian shield basalts. Nature 434, 590–597. doi.org/10.1038/nature03411

Sobolev, A. V, Hofmann, A.W., Kuzmin, D. V, Yaxley, G.M., Arndt, N.T., Chung, S.-L., Danyushevsky, L. V, Elliott, T., Frey, F.A., Garcia, M.O., Gurenko, A.A., Kamenetsky, V.S., Kerr, A.C., Krivolutskaya, N.A., Matvienkov, V. V, Nikogosian, I.K., Rocholl, A., Sigurdsson, I.A., Sushchevskaya, N.M., Teklay, M., 2007. The Amount of Recycled Crust in Sources of Mantle-Derived Melts. Science 316 (5823), 412–417. doi.org/10.1126/science. 1138113

Steinberger, B., O'Connell, R.J., 1998. Advection of plumes in mantle flow: implications for hotspot motion, mantle viscosity and plume distribution. Geophys. J. Int. 132, 412–434. doi.org/10.1046/j.1365-246x.1998.00447.x

Spandler, C., Yaxley, G., Green, D.H., Rosenthal, A., 2008. Phase relations and melting of anhydrous K-bearing eclogite from 1200 to 1600 C and 3 to 5 GPa. J. Petrol. 49, 771–795. doi.org/10.1093/petrology/egm039

Stracke, A., Bizimis, M., Salters, V.J.M., 2003. Recycling oceanic crust: Quantitative constraints. Geochemistry, Geophys. Geosystems 4 (3). 8003 doi.org/10.1029/2001GC000223

Stracke, A., Hofmann, A.W., Hart, S.R., 2005. FOZO, HIMU, and the rest of the mantle zoo. Geochemistry, Geophys. Geosystems 6, Q05007. doi.org/10.1029/2004GC000824

Stuessy, T.F., Foland, K.A., Sutter, J.F., Sanders, R.W., Silva., M., 1984. Botanical and geological significance of potassium-argon dates from the Juan Fernandez Islands. Science 225 (4657), 49–51. doi.org/10.1126/science.225.4657.49

Tassara, A., Götze, H.-J., Schmidt, S., Hackney, R., 2006. Three-dimensional density model of the Nazca plate and the Andean continental margin. J. Geophys. Res. 111, B09404. doi.org/10.1029/2005JB003976

Trela, J., Vidito, C., Gazel, E., Herzberg, C., Class, C., Whalen, W., Jicha, B., Bizimis, M., Alvarado, G.E., 2015. Recycled crust in the Galápagos Plume source at 70 Ma: Implications for plume evolution. Earth Planet. Sci. Lett. 425, 268–277. doi.org/10.1016/j.epsl.2015.05.036

Truong, T.B., Castillo, P.R., Hilton, D.R., Day, J.M.D., 2018. The trace element and Sr-Nd-Pb isotope geochemistry of Juan Fernandez lavas reveal variable contributions from a high- $^{3}He/^{4}He$ mantle plume. Chem. Geol. 476 280–291. doi.org/10.1016/j.chemgeo.2017.11.024

Turner, S.J., Langmuir, C.H., Dungan, M.A., Escrig, S., 2017. The importance of mantle wedge heterogeneity to subduction zone magmatism and the origin of EM1. Earth Planet. Sci. Lett. 472, 216–228. doi.org/10.1016/j.epsl.2017.04.051

von Huene, R., Corvalán, J., Flueh, E.R., Hinz, K., Korstgard, J., Ranero, C.R., Weinrebe, W., 1997. Tectonic control of the subducting Juan Fernández Ridge on the Andean margin near Valparaiso, Chile. Tectonics 16, 474–488. doi.org/10.1029/96TC03703

Weaver, B.L., 1991. The origin of ocean island basalt end-member compositions: trace element and isotopic constraints. Earth Planet. Sci. Lett. 104, 381–397. doi.org/10.1016/0012-821X(91)90217-6

White, W.M., 2015. Isotopes, DUPAL, LLSVPs, and Anekantavada. Chem. Geol. 419, 10–28. doi.org/10.1016/j.chemgeo.2015.09.026

Willbold, M., Stracke, A., 2010. Formation of enriched mantle components by recycling of upper and lower continental crust. Chem. Geol. 276, 188–197. doi.org/10.1016/j.chemgeo.2010.06.005

Workman, R.K., Hart, S.R., 2005. Major and trace element composition of the depleted MORB mantle (DMM). Earth Planet. Sci. Lett. 231, 53–72. doi.org/10.1016/j.epsl.2004.12.005

Yang, Z.-F., Zhou, J.-H., 2013. Can we identify source lithology of basalt? Sci. Rep. 3, 1856. doi.org/10.1038/srep01856

Yaxley, G.M., Green, D.H., 1998. Reactions between eclogite and peridotite: Mantle refertilisation by subduction of oceanic crust. Schweizerische Mineral. Und Petrogr. Mitteilungen 78, 243–255.

Zindler, A., Hart, S., 1986. Chemical Geodynamics. Annu. Rev. Earth Planet. Sci. 14, 493–571. doi.org/10.1146/annurev.ea.14.050186.002425

Table V.1. Petrography of representative shield samples from O'Higgins, Alpha, Robinson Crusoe, and Alejandro Selkirk based on 500 points count using JMicroVision 1.2.7 software. Mineralogy reported as vesicle-free volume percent for pheno- and microphenocrysts (>0.2 mm in diameter). Rock type according mineralogy and chemistry. (GM: groundmass. Ves: vesicle content. Ol: olivine. Cpx: clinopyroxene. Plg: plagioclase. Op: opaques).

			GM	Mineralogy				Ves
Sample		Rock type	(%)	Ol	Cpx	Plg	Op	(%)
O'Higgins guyot								
'olivine-rich'	D10-5	picrite	70	29	-	<1	<1	-
	D10-7	picrite	75	25	-	-	-	<1
'differentiated'	D10-42	alkali basalt	92	7	-	1	-	18
Alpha seamount								
'differentiated'	D11-03	alkali basalt	98	<1	-	2	-	-
	D11-04	alkali basalt	99	<<1	-	1	-	-
	D11-14	alkali basalt	93	2	4	1	-	4
Robinson Crusoe Island								
'olivine-rich'	LL250711-5	tholeiitic basalt	75	25	<<1	<<1	-	-
	MP270112-5B	picrite	76	24	-	-	-	6
'near-primitive'	JR290513-2	tholeiitic basalt	92	7	-	-	1	-
	JR290513-5	alkali basalt	93	2	3	2	-	3
	LL250711-7	tholeiitic basalt	92	6	1	1	-	5
'differentiated'	JR160913-13	tholeiitic basalt	99	<<1	1	<<1	-	1
	LL220112-3	tholeiitic basalt	94	2	2	2	-	5
	LL240711-1	alkali basalt	98	<1	<<1	2	-	12
	LL250711-1	alkali basalt	64	5	10	21	-	4
	LL250711-9	tholeiitic basalt	98	<1	1	1	-	4
Alejandro Selkirk Island								
'olivine-rich'	JR170913-4	picrite	52	47	<<1	-	1	-
	MF-6	tholeiitic basalt	82	17	<<1	1	-	17
	MF-C2	tholeiitic basalt	64	25	6	5	-	1
'near-primitive'	JR170913-5	tholeiitic basalt	80	13	4	3	-	11
	JR170913-16	tholeiitic basalt	90	6	-	4	-	4
	MF-16	tholeiitic basalt	88	10	-	2	-	17
'differentiated'	JR170913-7	alkali basalt	100	<1	-	<1	-	1
	JR180913-1	trachy-basalt	93	3	<<1	4	-	<1
	LL250112-1	alkali basalt	75	4	<<1	21	-	4
	LL260112-4	alkali basalt	99	<1	-	1	-	1

Table V.2. Major element (wt%) and Ni (ppm) concentrations of samples from Alpha seamount, Robinson Crusoe, and Alejandro Selkirk islands. $Fe_2O_3^T$: total iron as ferric. Loss-on-ignition (LOI) (wt%) is included.

Sample		SiO_2	TiO_2	Al_2O_3	$Fe_2O_3^T$	MgO	MnO	CaO	Na_2O	K_2O	P_2O_5	Ni	LOI	Sum
Det. limit		*0.01*	*0.01*	*0.01*	*0.04*	*0.01*	*0.01*	*0.01*	*0.01*	*0.01*	*0.01*	*0.1*	*0.1*	
Alpha seamount														
D11-02	Dredged	46.80	3.60	15.02	11.80	5.75	0.17	10.07	3.13	1.02	0.46	48.0	1.8	99.62
D11-03	Dredged	45.28	4.02	16.09	12.37	5.82	0.20	9.32	3.37	1.29	0.59	46.5	1.2	99.55
D11-04	Dredged	45.22	3.72	15.63	12.16	4.64	0.18	10.22	3.53	1.19	0.61	49.3	2.5	99.60
D11-07	Dredged	46.16	4.17	15.41	12.77	5.45	0.15	8.07	3.62	1.32	0.56	25.7	1.9	99.58
D11-08	Dredged	46.09	3.51	15.38	11.71	5.80	0.15	9.74	3.11	1.06	0.51	61.3	2.6	99.66
D11-10	Dredged	45.61	3.73	15.61	12.05	4.97	0.18	9.72	3.58	1.20	0.57	49.1	2.4	99.62
D11-12	Dredged	44.36	3.49	15.08	11.74	5.80	0.17	10.82	3.12	0.97	0.52	47.5	3.5	99.57
D11-14	Dredged	45.62	3.08	15.63	11.33	6.33	0.14	10.99	2.70	0.78	0.53	61.3	2.5	99.63
D11-15	Dredged	44.65	3.16	15.60	11.72	6.15	0.15	10.55	2.64	0.88	0.60	69.1	3.5	99.60
D11-17	Dredged	46.04	3.55	16.11	12.26	5.05	0.23	8.35	3.77	1.41	0.72	94.7	2.1	99.59
BM220588-1	Dregded	45.88	3.75	15.63	12.03	4.91	0.19	9.66	3.49	1.18	0.62	86.0	2.0	99.34
BM220588-2	Dregded	45.16	3.91	15.76	12.40	6.05	0.22	9.62	3.17	1.19	0.59	101.0	1.4	99.47
JF1A-1	Dregded	43.23	3.55	14.28	13.60	7.30	0.24	10.49	2.52	0.85	0.75	196.0	2.7	99.51
Robinson Crusoe Island														
JR260112-1	Dyke	47.05	3.42	14.05	12.83	5.96	0.18	9.42	3.02	0.84	0.42	127.7	2.5	99.69
JR260112-3	Dyke	48.10	3.08	14.36	11.12	6.33	0.23	10.70	3.03	0.65	0.35	67.3	1.7	99.65
JR160913-4	Dyke	48.69	3.69	15.59	10.00	4.01	0.11	10.10	3.03	0.72	0.43	81.0	3.3	99.67
JR160913-6	Dyke	46.09	3.31	14.00	12.51	6.03	0.18	10.55	2.89	0.82	0.40	43.1	2.9	99.68
JR160913-7	Dyke	47.76	3.69	14.73	11.02	5.06	0.16	9.46	3.18	1.08	0.57	41.9	2.9	99.61
LL040213-3	Clast	46.60	3.37	14.64	11.46	6.40	0.13	10.57	2.66	0.87	0.43	70.3	2.5	99.63
LL240711-3	Dyke	46.84	3.47	14.80	12.94	5.14	0.16	9.96	2.82	0.45	0.41	39.8	2.7	99.69
LL240711-4	Dyke	46.36	3.38	15.45	12.32	6.50	0.16	8.36	3.50	1.29	0.68	85.2	1.6	99.60
LL240711-5D	Dyke	46.49	3.39	15.53	12.22	6.25	0.15	8.35	3.46	1.26	0.67	83.9	1.8	99.57
LL240711-7	Dyke	47.84	4.07	14.15	13.00	4.54	0.14	9.01	3.28	1.12	0.56	24.6	2.0	99.71
JR220112-1	Dyke	47.37	3.46	15.20	12.51	6.84	0.16	10.16	3.15	0.74	0.40	64.9	-0.3	99.72
JR140913-1	Dyke	47.73	3.38	15.85	13.59	4.78	0.20	7.09	4.13	1.68	0.77	29.6	0.5	99.70
JR160913-11	Dyke	48.79	2.92	15.97	10.49	4.15	0.15	7.37	4.52	1.87	0.70	26.3	2.7	99.63
JR160913-12	Sill	47.27	3.48	14.73	11.27	6.22	0.15	10.81	3.13	0.96	0.43	48.2	1.2	99.65
MP270112-5A	Dyke	44.53	3.75	15.54	12.86	6.39	0.17	9.87	2.24	0.41	0.42	56.8	3.5	99.68
MP270112-5B	Dyke	42.58	2.50	10.80	13.85	18.64	0.18	6.46	1.47	0.38	0.31	737.4	2.1	99.27
Alejandro Selkirk Island														
LL250112-1	Lava	49.01	3.26	15.48	11.14	5.39	0.15	10.10	3.66	1.22	0.57	43.6	-0.3	99.71
LL250112-2	Lava	48.01	2.52	14.97	12.54	5.91	0.17	10.78	2.91	0.52	0.27	55.5	1.0	99.60
LL260112-1	Lava	46.39	3.25	13.31	12.58	10.29	0.16	8.74	2.99	1.02	0.47	269.4	0.3	99.50
LL260112-2	Lava	47.10	3.72	14.90	13.44	5.87	0.17	9.11	3.25	0.72	0.51	26.5	0.9	99.69
LL260112-4	Lava	49.03	3.43	15.43	11.70	5.51	0.16	9.03	3.53	1.10	0.54	35.6	0.2	99.66
LL270112-1	Lava	47.16	2.90	16.43	11.46	6.30	0.16	10.20	2.74	0.43	0.33	92.4	1.6	99.71
MF-20	Lava	46.47	3.72	14.35	12.55	8.54	0.15	9.36	3.14	1.24	0.55	153.8	-0.6	99.53
MF-C2	Lava	45.69	2.39	12.31	13.95	15.01	0.17	7.03	2.39	0.63	0.37	508.0	-0.6	99.40
MF-6	Lava	46.52	1.95	12.34	12.91	14.42	0.17	8.50	2.24	0.52	0.23	469.8	-0.4	99.44
MF-16	Lava	47.18	2.17	13.44	12.48	11.35	0.16	9.27	2.52	0.58	0.26	326.0	0.1	99.51
MF-3	Lava	43.79	1.82	11.61	13.25	15.92	0.17	7.78	2.70	0.34	0.18	531.0	1.8	99.36
MF-C4	Lava	46.92	2.59	12.99	13.54	12.54	0.17	7.34	2.59	0.75	0.34	375.2	-0.3	99.50
JR170913-1	Lava	48.96	2.80	14.51	11.62	7.05	0.16	11.10	2.56	0.60	0.31	45.8	0.0	99.67
JR170913-5	Lava	46.70	2.46	13.80	11.68	10.70	0.15	9.39	2.53	0.51	0.31	302.6	1.3	99.53
JR170913-4	Cobble	43.84	1.19	6.10	14.55	26.91	0.18	4.28	1.04	0.28	0.13	1298.8	0.6	99.10
JR170913-8	Lava	46.60	3.04	16.04	12.31	7.01	0.16	9.78	2.76	0.33	0.40	111.0	1.2	99.63
JR170913-9	Lava	46.47	2.94	14.94	12.59	7.23	0.16	10.39	2.81	0.47	0.37	106.1	1.2	99.57
JR170913-10	Lava	49.98	2.77	14.71	12.18	5.82	0.17	10.30	2.63	0.59	0.29	21.9	0.3	99.74
JR170913-12	Lava	49.38	3.07	14.01	11.52	5.48	0.19	11.00	2.92	0.85	0.34	28.8	0.9	99.66
JR170913-14	Lava	46.80	2.40	13.86	13.15	10.48	0.17	9.24	2.71	0.54	0.29	248.2	-0.1	99.55
JR170913-16	Lava	47.28	2.89	14.40	11.56	8.88	0.12	8.31	2.97	1.01	0.44	191.2	1.7	99.56
JR170913-18	Lava	46.46	2.80	13.33	12.24	11.33	0.16	9.12	2.77	0.97	0.40	302.5	-0.1	99.49
JR170913-19	Lava	47.99	2.43	14.08	12.50	8.97	0.17	10.04	2.30	0.42	0.20	138.6	0.5	99.60
JR180913-1	Lava	50.33	3.13	16.54	11.59	4.18	0.17	6.60	4.32	1.89	0.92	33.8	0.0	99.67
JR180913-2	Lava	47.17	3.48	17.17	12.48	4.14	0.16	6.03	3.56	1.74	0.88	37.6	2.9	99.71
JR170913-7	Dome	48.78	4.06	14.68	13.39	4.49	0.16	7.84	3.54	1.24	0.62	18.4	0.9	99.70
LL250112-3	Dyke	47.25	3.11	14.22	11.63	5.24	0.15	9.84	3.37	0.91	0.44	45.0	3.5	99.66
LL250112-4	Dyke	48.26	2.96	14.97	11.06	6.02	0.14	10.97	2.86	0.72	0.35	58.4	1.3	99.61
LL270112-2	Dyke	46.32	3.46	13.61	12.62	9.60	0.16	8.83	2.99	1.13	0.54	234.6	0.3	99.56

JR170913-2	Dyke	48.85	3.26	15.29	11.05	5.78	0.15	10.28	3.02	0.94	0.41	48.9	0.6	99.63
JR170913-6	Dyke	48.46	3.32	15.25	11.25	5.59	0.22	10.82	2.95	0.84	0.35	111.1	0.6	99.65
JR170913-11	Dyke	49.06	3.37	15.48	11.21	4.67	0.26	11.11	2.84	0.74	0.34	41.7	0.6	99.68
JR170913-13	Dyke	47.68	3.31	15.05	10.85	6.14	0.14	9.65	2.92	1.00	0.44	66.4	2.5	99.68
JR170913-15	Dyke	48.23	2.93	14.97	11.95	5.56	0.17	10.77	2.84	0.69	0.34	36.5	1.2	99.65
JR170913-17	Dyke	48.69	3.41	14.96	11.09	6.80	0.15	10.00	3.09	0.98	0.48	94.3	0.0	99.65
JR170913-20	Dyke	48.55	2.96	14.94	11.71	6.28	0.16	10.68	3.09	0.89	0.39	58.2	0.0	99.65
JR170913-22	Sill	48.77	2.89	15.21	11.63	6.20	0.15	10.76	3.15	0.88	0.39	62.3	-0.4	99.67

Table V.3. Trace element data (ppm, Cr_2O_3 in wt%) for lavas and dykes from Alpha seamount, Robinson Crusoe, and Alejandro Selkirk islands.

Sample	Cr_2O_3	Sc	Ba	Co	Ga	Hf	Nb	Rb	Sr	Ta	Th	U	V	Zr	Y
Det. limit	*0.002*	*1*	*1*	*0.2*	*0.5*	*0.1*	*0.1*	*0.1*	*0.5*	*0.1*	*0.2*	*0.1*	*8*	*0.1*	*0.1*
Alpha seamount															
D11-02	0.014	27	273	58.2	27.2	6.9	45.3	22.3	639.3	2.9	3.4	0.9	416	289.3	35.6
D11-03	0.003	19	369	61.9	28.8	7.5	60.1	30.2	902.8	3.7	4.1	1.2	379	338.9	35.5
D11-04	0.016	24	310	50.5	27.7	8.0	54.8	27.3	957.7	3.4	4.2	1.2	402	345.1	43.1
D11-07	0.007	22	317	46.2	29.3	8.5	57.8	32.0	670.0	3.7	4.3	1.1	400	386.8	43.2
D11-08	0.021	25	255	51.1	25.5	7.1	45.5	19.7	664.1	2.9	3.5	0.5	373	297.1	36.0
D11-10	0.016	24	298	49.7	26.8	7.6	52.0	26.1	824.9	3.3	4.0	1.0	377	350.1	39.4
D11-12	0.017	28	246	55.0	27.0	6.4	41.9	21.0	637.4	2.8	3.2	1.4	400	277.3	32.1
D11-14	0.037	31	197	45.9	24.9	6.2	34.0	11.0	587.5	2.3	2.5	1.5	396	238.6	31.7
D11-15	0.037	31	191	44.8	24.0	6.5	35.4	12.1	667.6	2.3	2.7	1.7	395	242.6	37.8
D11-17	0.018	21	364	62.5	28.4	8.6	64.4	34.6	762.5	4.1	5.2	1.6	368	400.5	44.4
BM220588-1	0.018	24	231	49.4	21.7	6.6	41.2	20.7	609.7	2.6	3.3	1.2	293	275.7	32.7
BM220588-2	0.011	21	267	60.5	21.1	6.5	44.2	21.7	627.5	2.7	3.2	1.0	307	253.2	29.5
JF1A-1	0.020	29	193	63.6	22.0	5.7	36.2	11.8	966.2	2.4	2.6	1.4	346	233.4	29.1
Robinson Crusoe Island															
LL230711-7	0.008	27	127	36.6	21.0	5.0	32.1	5.4	514.8	2.2	2.3	0.6	378	205.5	28.4
LL230112-1	0.032	24	336	54.7	29.7	7.8	56.5	27.4	787.7	3.4	4.2	1.1	434	332.8	38.1
JR260112-1	0.010	28	512	33.3	22.3	5.2	35.8	13.4	454.8	2.2	2.4	0.7	319	207.7	27.8
JR260112-3	0.034	29	202	44.7	19.7	5.2	27.7	12.0	444.8	1.7	2.1	0.6	287	198.1	32.6
JR160913-4	0.020	30	249	35.6	24.5	6.4	37.8	6.4	576.3	2.6	3.0	0.9	298	255	42.6
JR160913-6	0.013	28	211	42.4	20.7	5.2	33.9	15.0	513.7	2.0	2.9	0.7	313	222.8	29.0
JR160913-7	0.018	26	233	42.5	22.7	7.1	41.5	18.9	549.6	2.8	3.5	1.1	310	298	32.1
JR300513-3	0.030	28	212	44.1	21.7	5.8	36.2	20.0	472.1	2.3	3.0	0.7	299	233.1	28.5
LL040213-3	0.032	26	211	42.8	23.5	5.9	33.4	11.3	527.8	2.1	2.8	0.3	312	236.4	29.4
JR290513-5	0.066	25	245	46.7	17.8	4.5	35.4	29.0	634.1	2.3	2.8	0.6	301	203.7	24.5
LL240711-1	0.012	28	242	42.5	22.0	5.5	38.7	19.7	564.0	2.4	3.1	0.7	369	231	31.5
LL240711-2	0.030	29	221	43.2	20.3	4.8	34.5	15.9	535.2	2.2	2.7	0.6	344	188.7	26.4
LL240711-6	0.021	25	239	42.3	22.7	5.6	36.7	16.0	608.8	2.4	2.9	0.7	351	217.2	43.3
LL260711-2	0.010	27	229	43.2	23.5	6.2	39.3	20.1	586.6	2.5	2.8	0.8	385	230.1	30.1
JR270513-2	0.130	21	199	71.7	15.7	4.2	30.1	16.3	412.3	1.9	2.4	0.4	286	195.8	24.3
JR270513-1	0.018	27	320	41.0	24.4	6.4	44.5	12.8	584.3	2.8	3.7	0.8	354	257.7	35.1
JR290513-2	0.187	25	177	59.5	15.5	3.6	20.7	12.4	416.6	1.3	1.7	0.4	264	145.6	18.3
LL250711-1	0.038	25	345	39.2	23.1	6.7	46.3	16.6	738.8	3.0	3.6	0.6	345	258.1	30.9
LL250711-3	0.028	25	307	43.9	24.7	6.9	47.0	19.7	707.4	3.0	3.4	0.5	370	274.2	49.9
LL250711-5	0.145	20	75	88.1	15.0	2.5	13.0	7.3	267.2	0.9	0.9	0.3	243	102.8	17.7
LL250711-7	0.075	28	197	50.9	20.5	4.7	29.7	7.7	486.3	1.8	2.2	0.3	343	176	28.9
LL220112-2	0.014	30	254	34.5	23.1	6.5	38.4	13.9	518.8	2.4	2.9	0.5	298	244.3	38.7
LL220112-3	0.041	30	196	39.8	19.8	5.4	33.3	15.1	495.6	2.1	2.1	0.5	313	211.5	26.6
LL220112-5	0.004	23	334	57.5	32.5	9.6	61.3	36.0	850.0	3.5	4.6	1.2	435	375.3	46.1
JR220112-2	0.007	25	227	37.9	22.9	5.3	40.4	21.5	544.8	2.4	2.8	0.7	299	223.5	25.1
JR250513-1	0.242	18	235	118.6	11.6	3.1	18.3	10.2	248.6	1.0	1.3	0.4	183	128.2	17.5
JR250513-2	0.019	29	225	44.0	19.2	4.2	26.2	11.9	454.8	1.6	2.0	0.5	292	170.3	27.7
JR250513-4	0.027	29	221	37.9	20.1	5.2	30.7	13.8	520.7	1.8	2.4	0.5	291	200.7	25.2
JR250513-5	0.019	21	309	34.1	21.3	6.4	46.5	23.5	689.9	2.8	3.9	0.9	309	278.7	29.6
JR160913-1	0.044	31	3789	45.5	22.2	5.6	33.3	7.2	751.1	2.1	3.3	0.5	277	226.4	37.6
JR160913-10	0.050	30	176	34.3	22.1	5.4	30.6	19.8	542.3	1.9	2.6	0.7	313	212.8	27.0
JR160913-13	0.028	29	223	36.4	21.7	5.8	40.9	16.2	613.3	2.6	3.6	0.7	319	238.4	29.0
LL240711-3	0.010	29	190	38.2	22.5	5.5	29.5	2.5	469.1	1.8	2.3	0.3	356	206.7	31.2
LL240711-4	0.027	18	352	43.8	22.7	7.8	50.6	40.3	704.0	3.2	4.1	1.1	256	308	31.1
LL240711-5D	0.024	18	329	42.4	22.0	7.4	51.8	35.6	693.3	3.2	4.4	1.2	262	313	33.7
LL240711-7	0.003	27	233	34.1	23.0	6.8	41.9	21.7	526.9	2.7	3.1	0.7	405	272	32.8
JR220112-1	0.032	25	161	37.1	21.0	4.9	27.5	14.4	492.9	1.8	2.1	0.4	267	193.3	26.1
JR140913-1	0.006	19	334	34.9	26.2	8.3	53.6	28.7	556.7	3.0	4.8	0.6	303	364.3	38.6
JR160913-11	0.007	15	355	28.6	26.6	9.5	60.6	40.0	563.3	3.6	6.0	1.6	216	424.2	37.8
JR160913-12	0.025	29	220	40.8	21.7	5.6	39.3	19.1	554.4	2.4	3.4	0.8	325	231	27.2
LL250711-8	0.017	29	253	48.4	22.2	6.0	38.8	17.4	539.5	2.5	2.5	0.6	379	230.8	26.8
LL250711-9	0.019	30	222	47.3	23.0	5.1	36.2	17.2	524.8	2.2	2.6	0.7	378	202.9	32.4
LL040213-2	0.130	23	143	72.3	17.7	3.6	23.8	12.0	370.8	1.4	1.7	0.2	267	161.3	20.9
LL300113-1	0.071	28	162	54.7	19.6	4.0	26.9	11.0	393.5	1.4	1.8	0.2	305	176.5	22.0
LL250711-4	0.027	25	275	47.7	23.6	7.6	44.8	18.0	590.0	2.9	3.5	0.8	330	277.5	36.5
MP270112-4	0.023	21	270	42.3	21.1	7.1	40.4	23.7	640.4	2.8	3.1	0.9	256	274.4	30.7
MP270112-5A	0.026	31	196	43.0	21.8	6.2	37.2	2.4	454.6	2.1	2.4	0.1	343	228.3	23.9
MP270112-5B	0.151	23	156	81.6	16.4	3.7	25.1	3.0	261.5	1.6	1.6	0.2	228	160.1	16.3

Alejandro Selkirk Island

LL250112-1	0.020	22	268	32.8	22.5	7.1	37.2	26.3	680.2	2.3	3.6	0.8	228	283.5	26.8
LL250112-2	0.035	28	166	58.5	26.5	6.1	29.5	15.5	515.1	1.7	2.7	0.5	373	217.8	34.6
LL260112-1	0.063	21	214	51.1	19.7	6.4	32.7	19.2	560.5	2.1	2.8	0.8	216	258.1	25.3
LL260112-2	0.007	25	216	40.2	23.8	6.7	31.4	6.2	472.1	1.9	2.8	0.5	240	262.7	32.1
LL260112-4	0.020	23	212	37.1	24.4	7.3	30.6	16.5	561.7	2.1	2.8	0.8	214	299.6	29.6
LL270112-1	0.050	27	132	37.4	21.7	4.6	20.5	1.9	471.5	1.4	1.9	0.1	229	194.6	24.4
MF-20	0.047	21	306	58.3	26.6	8.6	43.6	28.3	820.1	2.9	3.6	0.9	291	367.4	30.6
MF-C2	0.104	18	149	85.6	21.8	6.7	25.9	8.4	430.8	1.6	2.6	0.6	194	259.8	30.0
MF-6	0.110	22	108	81.5	19.4	4.4	17.9	11.5	406.4	1.1	1.4	0.4	240	178.8	23.8
MF-16	0.081	25	119	69.2	21.4	4.3	19.4	12.7	446.2	1.2	1.5	0.5	265	194.8	27.1
MF-3	0.129	22	116	97.1	18.7	4.5	16.4	6.4	363.2	1.1	1.8	0.4	226	185	22.2
MF-C4	0.079	19	184	78.8	23.4	6.7	24.5	19.2	430.1	1.8	2.5	0.8	216	289.1	35.2
JR170913-1	0.037	30	145	44.2	20.3	4.6	23.4	12.3	474.9	1.5	2.2	0.5	278	189.6	26.0
JR170913-5	0.097	24	181	57.0	18.6	4.7	25.4	9.8	481.5	1.7	2.4	0.4	219	184	22.8
JR170913-4	0.229	14	67	120.5	9.8	2.0	11.4	6.6	181.2	0.6	1.1	0.3	129	81.3	11.1
JR170913-8	0.047	26	158	45.4	22.5	5.8	24.8	1.6	486.8	1.6	2.2	0.4	247	236	28.8
JR170913-9	0.051	27	147	45.7	21.8	5.7	24.9	4.7	512.1	1.7	2.2	0.4	272	223.5	28.4
JR170913-10	0.029	29	110	40.0	20.8	4.8	20.6	11.3	399.8	1.4	1.9	0.4	277	179.9	27.9
JR170913-12	0.021	29	168	40.1	21.6	5.4	26.6	18.7	425.6	1.7	2.7	0.7	284	209.7	30.3
JR170913-14	0.083	23	118	61.3	20.4	4.4	18.2	9.5	416.2	1.2	1.7	0.4	227	182.1	24.6
JR170913-16	0.048	19	179	49.4	20.4	6.4	28.4	24.1	552.0	1.8	2.6	0.7	202	251.2	24.6
JR170913-18	0.083	24	226	57.7	21.0	5.5	28.7	21.4	523.7	1.7	2.6	0.8	240	247.8	25.1
JR170913-19	0.065	28	97	53.0	21.4	4.5	19.2	9.2	375.2	1.3	1.6	0.4	258	172.4	25.3
JR180913-1	0.004	16	351	27.1	26.0	9.7	45.9	39.4	524.9	3.0	5.6	1.5	202	432	45.6
JR180913-2	0.008	17	320	33.9	28.6	10.3	46.9	30.2	402.6	3.0	5.1	1.2	224	445	40.3
JR170913-7	0.008	24	218	36.2	25.8	9.0	36.7	26.2	497.6	2.1	3.7	0.9	285	369.9	53.9
LL250112-3	0.023	27	180	37.5	19.6	6.5	29.3	15.3	462.8	1.9	2.6	0.5	247	233.1	30.0
LL250112-4	0.034	28	216	52.2	27.8	7.3	34.6	25.3	672.8	2.2	3.0	0.8	381	280.9	39.1
LL270112-2	0.060	22	218	50.6	20.3	7.2	34.8	27.9	605.7	2.1	2.9	0.5	227	283.4	29.3
JR170913-2	0.030	27	164	36.2	22.0	6.0	25.8	17.5	506.8	1.8	2.3	0.7	272	246.8	30.5
JR170913-6	0.036	27	146	47.2	21.8	5.5	24.7	16.2	517.2	1.5	2.2	0.8	285	216.2	28.1
JR170913-11	0.034	30	135	42.8	22.4	5.7	23.5	14.2	501.7	1.7	1.9	1.1	291	212.9	28.4
JR170913-13	0.030	26	213	37.5	21.0	6.6	31.4	30.6	536.4	2.1	2.7	0.6	267	257.3	29.9
JR170913-15	0.022	27	149	41.3	21.0	5.3	23.8	11.6	483.3	1.6	2.2	0.6	268	209.7	28.6
JR170913-17	0.044	26	191	38.7	23.7	6.8	31.7	21.3	552.2	1.8	2.6	0.7	263	278.2	29.8
JR170913-20	0.031	27	194	42.6	23.8	5.8	29.2	18.2	567.9	1.8	2.6	0.5	262	236.4	27.8
JR170913-22	0.033	27	218	41.5	22.5	5.6	27.5	14.9	573.9	2.0	2.6	0.4	262	223.4	25.0

Table V.3. (continued)

Sample	Pb	La	Ce	Pr	Nd	Sm	Eu	Gd	Tb	Dy	Ho	Er	Tm	Yb	Lu
Det. limit	*0.1*	*0.1*	*0.1*	*0.02*	*0.3*	*0.05*	*0.02*	*0.05*	*0.01*	*0.05*	*0.02*	*0.03*	*0.01*	*0.05*	*0.01*
Alpha shield															
D11-02	1.9	34.4	74.2	9.46	41.1	9.28	3.01	9.54	1.32	7.59	1.24	3.34	0.46	2.88	0.37
D11-03	2.9	43.6	91.5	11.51	48.6	10.69	3.40	10.50	1.34	7.94	1.30	3.41	0.44	2.91	0.40
D11-04	1.6	41.3	92.0	11.47	49.1	10.83	3.43	11.01	1.50	8.56	1.49	3.94	0.54	3.53	0.46
D11-07	0.7	44.6	96.6	12.28	49.8	11.51	3.65	11.72	1.53	9.22	1.53	4.00	0.53	3.61	0.45
D11-08	2.3	36.5	75.0	9.55	43.0	9.30	3.11	9.89	1.30	7.55	1.30	3.32	0.44	2.88	0.39
D11-10	1.4	42.4	87.1	11.15	48.0	10.55	3.40	11.09	1.42	8.65	1.38	3.86	0.50	3.47	0.41
D11-12	2.4	32.7	71.9	9.11	39.2	9.02	2.94	9.45	1.27	7.35	1.19	3.18	0.43	2.69	0.37
D11-14	1.0	25.8	58.9	7.73	34.7	7.81	2.64	8.54	1.15	7.13	1.21	3.13	0.41	2.36	0.34
D11-15	1.2	34.1	73.2	9.56	45.0	9.78	3.10	10.24	1.36	8.15	1.39	3.69	0.49	2.88	0.41
D11-17	2.5	49.5	105.7	13.33	57.3	12.31	3.86	12.35	1.63	9.61	1.63	4.39	0.54	3.99	0.50
BM220588-1		34.3	73.3	9.19	38.5	8.47	2.84	8.40	1.24	6.86	1.22	3.34	0.43	2.77	0.38
BM220588-2		33.1	70.4	9.04	37.9	7.94	2.69	8.02	1.14	6.21	1.16	3.05	0.38	2.26	0.33
JF1A-1		26.5	56.0	7.72	33.6	7.13	2.32	7.55	1.08	6.00	1.15	3.05	0.38	2.35	0.33
Robinson Crusoe shield															
LL230711-7	1.6	25.9	54.8	6.97	29.3	6.90	2.28	6.93	1.11	5.57	1.10	2.93	0.39	2.37	0.32
LL230112-1	0.8	43.2	91.0	11.44	50.4	10.69	3.54	11.32	1.41	8.70	1.31	3.40	0.45	2.51	0.36
JR260112-1	0.7	25.6	53.4	6.86	29.5	6.70	2.26	7.25	1.11	5.97	1.03	2.89	0.42	2.38	0.36
JR260112-3	0.4	26.0	50.0	7.11	32.8	7.53	2.45	7.51	1.23	6.47	1.20	3.18	0.44	2.60	0.34
JR160913-4	1.4	33.3	60.7	9.12	39.5	9.37	3.18	9.68	1.47	7.92	1.62	4.14	0.55	3.43	0.48
JR160913-6	1.0	28.0	56.9	7.44	30.6	6.94	2.25	6.83	1.09	6.09	1.07	2.71	0.39	2.24	0.32
JR160913-7	0.7	35.1	75.3	9.62	41.2	8.85	2.90	9.03	1.35	7.05	1.31	3.34	0.42	2.47	0.37
JR300513-3	1.4	30.9	63.9	8.35	35.9	7.80	2.53	7.52	1.12	6.30	1.18	2.98	0.40	2.36	0.32
LL040213-3	0.5	27.3	60.4	8.02	34.3	7.54	2.51	7.62	1.11	6.49	1.17	2.81	0.38	2.41	0.33
JR290513-5	1.0	28.0	59.3	7.56	30.6	6.39	2.13	6.25	0.97	5.35	0.95	2.39	0.33	1.87	0.26
LL240711-1	0.5	32.1	67.6	8.92	38.4	8.15	2.72	8.14	1.28	6.44	1.24	3.11	0.44	2.47	0.33
LL240711-2	0.8	27.8	57.6	7.07	29.6	6.63	2.24	6.59	1.05	5.39	1.04	2.71	0.38	2.27	0.30
LL240711-6	24.2	34.8	69.6	9.23	42.0	8.98	3.05	9.84	1.52	7.71	1.58	4.09	0.56	3.20	0.44
LL260711-2	0.5	30.6	65.5	8.27	36.0	7.77	2.56	7.74	1.22	5.97	1.20	3.11	0.42	2.45	0.34
JR270513-2	0.9	24.1	51.5	6.80	27.2	6.19	1.99	6.17	0.95	5.30	0.89	2.25	0.30	1.71	0.25
JR270513-1	2.2	38.7	70.6	10.11	42.8	8.82	2.90	8.63	1.29	6.85	1.26	3.22	0.42	2.33	0.33
JR290513-2	0.6	18.0	38.5	4.88	20.8	4.75	1.55	4.83	0.78	4.12	0.70	1.74	0.25	1.50	0.20
LL250711-1	1.9	36.2	75.0	9.78	42.6	9.00	2.98	8.57	1.33	6.21	1.16	2.94	0.37	2.15	0.30
LL250711-3	1.0	38.8	77.7	10.90	48.8	10.84	3.67	11.24	1.81	9.04	1.83	4.65	0.64	3.67	0.51
LL250711-5	0.3	9.8	22.8	3.17	15.3	3.71	1.22	3.91	0.65	3.42	0.67	1.82	0.25	1.45	0.21
LL250711-7	0.4	24.6	52.2	6.86	30.0	6.83	2.25	6.90	1.15	5.62	1.11	2.82	0.42	2.46	0.34
LL220112-2	0.5	41.6	85.8	11.36	48.6	10.57	3.44	10.36	1.53	8.58	1.46	3.69	0.48	2.73	0.37
LL220112-3	0.5	27.0	57.0	7.74	31.4	7.48	2.41	7.57	1.12	6.29	1.15	2.79	0.39	2.33	0.31
LL220112-5	1.2	44.4	96.1	12.21	53.1	11.52	3.84	12.07	1.60	9.26	1.62	4.44	0.58	3.39	0.47
JR220112-2	0.9	29.3	59.9	7.72	32.9	7.08	2.26	6.83	1.04	5.53	0.97	2.61	0.37	2.00	0.28
JR250513-1	0.7	17.8	34.3	4.76	19.9	4.24	1.49	4.56	0.67	3.64	0.63	1.52	0.21	1.32	0.21
JR250513-2	0.9	22.4	47.7	6.46	26.9	6.06	2.06	6.52	0.99	5.42	1.00	2.63	0.36	2.06	0.30
JR250513-4	0.7	24.9	52.4	6.84	28.4	6.23	2.12	6.74	0.99	5.44	0.94	2.49	0.35	1.98	0.28
JR250513-5	0.8	38.3	81.1	10.01	39.4	8.42	2.68	7.90	1.24	6.42	1.11	2.90	0.38	2.25	0.31
JR160913-1	1.1	49.6	85.5	13.34	56.1	12.15	3.73	11.23	1.63	8.92	1.57	3.79	0.51	2.78	0.38
JR160913-10	0.7	25.6	54.2	6.97	31.9	6.89	2.34	7.22	1.03	5.69	1.00	2.65	0.37	2.24	0.31
JR160913-13	0.8	32.3	65.7	8.33	34.8	7.26	2.47	7.43	1.12	6.12	1.09	2.79	0.40	2.41	0.33
LL240711-3	1.4	24.6	50.9	7.01	30.7	7.10	2.36	7.31	1.17	5.93	1.16	2.99	0.43	2.40	0.35
LL240711-4	1.5	42.0	86.2	10.48	42.9	9.03	2.83	8.23	1.25	6.07	1.17	2.89	0.41	2.41	0.33
LL240711-5D	1.6	41.9	87.6	10.71	43.9	9.04	2.92	8.60	1.32	6.68	1.26	3.23	0.44	2.55	0.37
LL240711-7	1.6	31.2	67.1	8.94	38.3	8.59	2.80	8.46	1.33	6.76	1.30	3.34	0.47	2.66	0.39
JR220112-1	0.4	22.0	47.2	6.02	26.7	6.45	2.21	6.51	1.01	5.15	1.00	2.75	0.34	2.22	0.34
JR140913-1	1.7	44.2	96.7	12.56	51.9	11.02	3.63	10.80	1.60	8.62	1.59	3.84	0.52	3.10	0.43
JR160913-11	2.4	50.9	103.3	12.95	52.3	10.66	3.45	9.96	1.48	7.88	1.47	3.69	0.53	3.11	0.45
JR160913-12	0.9	32.3	68.5	8.38	34.6	7.53	2.48	7.06	1.14	6.10	1.08	2.80	0.38	2.16	0.33
LL250711-8	1.1	29.3	64.4	8.05	34.0	7.64	2.53	7.10	1.15	5.66	1.05	2.67	0.37	2.16	0.30
LL250711-9	1.3	31.6	59.2	8.09	34.2	7.72	2.59	7.49	1.24	6.29	1.25	3.26	0.45	2.61	0.37
LL040213-2	0.6	19.1	40.5	5.40	22.9	5.24	1.82	5.32	0.77	4.45	0.83	1.98	0.27	1.59	0.24
LL300113-1	0.6	20.3	45.0	5.86	26.7	5.43	1.97	5.80	0.82	5.40	0.84	2.13	0.31	1.48	0.25
LL250711-4	0.5	35.9	75.9	9.68	40.6	8.86	2.90	8.62	1.40	6.94	1.41	3.67	0.50	2.95	0.42
MP270112-4	1.2	36.0	72.0	9.67	42.5	8.72	2.92	8.90	1.31	7.21	1.31	3.16	0.44	2.57	0.34
MP270112-5A	1.3	20.4	49.4	6.40	29.5	6.86	2.31	6.63	0.99	5.44	1.15	2.57	0.29	2.15	0.25
MP270112-5B	0.6	14.8	34.3	4.40	20.7	4.38	1.49	4.48	0.68	4.16	0.73	1.73	0.21	1.36	0.19

Alejandro Selkirk shield															
LL250112-1	1.7	35.9	74.8	9.27	38.2	8.56	2.76	8.38	1.20	6.21	1.07	2.82	0.35	2.04	0.29
LL250112-2	0.5	24.9	52.6	6.93	30.8	7.43	2.67	8.43	1.20	7.16	1.18	3.30	0.46	3.11	0.39
LL260112-1	1.1	28.8	60.8	8.13	34.5	8.05	2.59	8.29	1.13	6.14	1.06	2.54	0.36	1.97	0.27
LL260112-2	0.6	28.4	61.1	8.26	36.3	8.58	2.78	9.08	1.32	7.60	1.29	3.18	0.40	2.62	0.34
LL260112-4	0.5	31.9	71.4	9.50	39.3	9.25	3.11	9.01	1.34	7.60	1.24	3.11	0.40	2.33	0.31
LL270112-1	0.5	18.1	42.5	5.50	27.8	6.13	2.21	7.00	1.00	4.99	0.94	2.50	0.32	2.01	0.32
MF-20	1.1	38.0	85.2	11.01	50.5	11.06	3.65	10.71	1.39	7.32	1.14	2.81	0.33	2.05	0.24
MF-C2	0.5	22.7	50.5	6.89	30.2	7.60	2.43	8.05	1.12	6.26	1.04	2.94	0.36	2.19	0.29
MF-6	<0,1	15.7	35.2	4.90	23.8	5.59	1.86	6.00	0.85	5.03	0.94	2.42	0.31	1.84	0.25
MF-16	0.1	17.6	40.0	5.42	24.4	6.17	2.08	7.11	0.99	5.60	0.98	2.82	0.35	2.39	0.30
MF-3	0.7	17.2	37.8	5.24	23.5	5.79	1.92	6.39	0.88	5.17	0.82	2.19	0.31	1.71	0.24
MF-C4	0.3	25.1	55.2	7.59	34.6	8.59	2.78	9.20	1.28	7.03	1.26	3.28	0.44	2.47	0.33
JR170913-1	0.4	20.9	45.6	5.96	26.9	6.32	2.16	6.55	0.98	5.49	0.99	2.66	0.37	2.24	0.31
JR170913-5	0.9	23.5	46.5	5.91	24.7	5.67	1.94	5.69	0.88	4.83	0.88	2.28	0.31	1.76	0.25
JR170913-4	0.4	9.5	20.1	2.63	12.2	2.66	0.91	2.64	0.40	2.36	0.42	1.06	0.15	0.87	0.13
JR170913-8	1.1	25.5	52.7	8.26	37.4	8.46	2.90	8.26	1.31	7.25	1.19	3.02	0.38	2.24	0.31
JR170913-9	0.9	22.5	49.2	6.72	29.7	6.91	2.38	7.44	1.09	6.11	1.09	2.70	0.39	2.27	0.33
JR170913-10	0.4	18.6	39.4	5.31	23.8	6.06	2.04	6.32	1.02	5.76	1.09	2.80	0.38	2.20	0.33
JR170913-12	0.4	24.2	51.1	6.56	29.3	6.80	2.34	7.26	1.18	6.93	1.23	3.24	0.44	2.61	0.36
JR170913-14	0.4	16.9	37.7	5.00	22.4	5.49	1.99	5.92	0.93	5.00	0.95	2.37	0.34	2.01	0.27
JR170913-16	0.8	26.0	55.9	7.49	33.2	7.58	2.52	7.02	1.14	5.60	0.96	2.30	0.30	1.75	0.26
JR170913-18	0.6	26.9	57.6	7.47	32.9	7.10	2.17	6.43	1.03	5.34	0.98	2.32	0.32	1.92	0.28
JR170913-19	0.5	15.6	35.8	4.60	20.4	5.25	1.80	5.70	0.97	5.23	0.95	2.49	0.33	2.06	0.31
JR180913-1	26.0	53.9	106.9	14.88	62.1	13.30	4.16	12.81	1.92	10.34	1.76	4.55	0.63	3.73	0.48
JR180913-2	2.4	46.7	101.0	12.93	55.7	12.18	3.86	12.20	1.75	9.11	1.53	4.00	0.56	3.22	0.43
JR170913-7	1.0	45.2	84.9	13.98	61.7	14.69	4.74	14.27	2.19	11.87	2.04	5.38	0.73	4.32	0.60
LL250112-3	1.1	27.3	57.4	7.16	33.3	7.08	2.36	7.79	1.16	6.16	1.16	3.06	0.40	2.44	0.34
LL250112-4	0.8	30.1	68.2	8.71	39.9	9.38	3.08	10.17	1.36	8.03	1.28	3.49	0.47	3.02	0.40
LL270112-2	1.5	31.5	67.5	9.03	36.9	8.62	2.80	8.69	1.21	6.58	1.15	2.44	0.32	1.91	0.26
JR170913-2	0.3	23.2	51.6	6.85	31.3	7.17	2.46	7.43	1.22	6.54	1.20	3.09	0.41	2.35	0.35
JR170913-6	0.5	22.2	46.8	6.25	27.7	6.95	2.33	7.07	1.08	5.96	1.04	2.76	0.36	2.23	0.32
JR170913-11	0.3	20.7	45.1	6.12	27.5	6.57	2.25	7.33	1.17	6.43	1.09	2.93	0.40	2.44	0.34
JR170913-13	1.0	27.5	60.7	7.79	34.1	7.86	2.63	7.75	1.25	6.77	1.16	2.86	0.40	2.43	0.36
JR170913-15	1.0	21.8	47.9	6.31	29.1	6.83	2.38	7.14	1.13	6.24	1.12	2.90	0.40	2.32	0.32
JR170913-17	1.2	27.9	63.2	8.34	35.3	8.35	2.61	7.84	1.27	6.68	1.21	2.83	0.39	2.35	0.34
JR170913-20	0.9	25.7	54.9	7.33	31.6	7.26	2.43	7.23	1.10	5.92	1.02	2.82	0.36	2.20	0.32
JR170913-22	1.3	25.8	54.7	7.14	31.7	6.95	2.25	6.70	1.11	5.91	1.04	2.59	0.34	1.97	0.30

Table V.4. Radiogenic isotopic composition of whole-rock representative samples from O'Higgins, Alpha, Robinson Crusoe, and Alejandro Selkirk shield stages. Standard error (2σ) and laboratory of analysis are indicated (a: GEOMAR Helmholtz Center, Kiel, Germany. b: Laboratoire Magmas and Volcans, Clermont-Ferrand, France).

Sample	$^{87}Sr/^{86}Sr$	±	$^{143}Nd/^{144}Nd$	±	$^{206}Pb/^{204}Pb$	±	$^{207}Pb/^{204}Pb$	±	$^{208}Pb/^{204}Pb$	±	Lab
O'Higgins guyot											
D10-5	-		0.512885	7	-		-		-		b)
D10-7	0.703496	5	0.512899	4	19.0957	8	15.6059	9	38.9466	30	a)
Alpha seamount											
D11-04	0.703522	5	0.512864	4	19.2218	13	15.6100	11	39.0569	31	a)
D11-14	0.703595	4	0.512848	5	19.2211	13	15.6064	12	39.0652	38	a)
D11-14 rep	0.703590	5	0.512846	4	19.2213	16	15.6064	16	39.0641	34	a)
Robinson Crusoe Island											
LL230711-7	0.703612	8	0.512843	5	-		-		-		b)
LL230711-6	0.703693	6	0.512830	6	-		-		-		b)
JR290513-5	0.703676	5	0.512825	4	19.1698	14	15.6078	12	39.0166	31	a)
MP260112-1	0.703693	5	0.512821	5	19.2607	9	15.6110	8	39.1346	21	a)
JR290513-2	0.703520	5	0.512858	5	19.1667	11	15.6016	9	38.9915	23	a)
LL250711-5	0.703508	4	0.512843	4	19.2874	8	15.6126	7	39.1133	18	a)
LL250711-5 rep	0.703516	5	0.512848	3	-		-		-		a)
LL250711-5 *	0.703564	8	0.512842	6	-		-		-		b)
JR220112-2	0.703616	4	0.512844	3	19.1639	7	15.6023	8	39.0122	26	a)
JR220112-2 *	0.703632	6	0.512836	6	-		-		-		b)
JR220112-1	0.703648	6	0.512823	3	19.1820	11	15.6045	9	39.0558	25	a)
JR220112-1 *	0.703647	5	0.512815	6	-		-		-		b)
LL250711-8	0.703567	4	0.512858	4	19.1680	11	15.6045	9	39.0033	23	a)
LL250711-9	0.703684	6	0.512827	6	-		-		-		b)
LL250711-4	0.703759	7	0.512811	6	-		-		-		b)
MP270112-4	0.703714	6	0.512815	6	-		-		-		b)
Alejandro Selkirk Island											
LL250112-1	0.703596	5	0.512832	5	-		-		-		b)
LL260112-4	0.703577	4	0.512880	4	19.1602	10	15.6093	11	39.0245	31	a)
LL260112-4 *	0.703594	5	0.512870	5	-		-		-		b)
MF-6	0.703582	5	0.512875	4	19.0635	17	15.6071	14	38.9350	37	a)
JR170913-16	0.703667	4	0.512872	5	19.0499	9	15.6075	8	38.9592	22	a)
JR170913-21	0.703561	5	0.512888	4	19.1104	11	15.6086	9	39.0102	26	a)
JR180913-1	0.703663	4	0.512864	4	19.0893	6	15.6091	7	39.0008	22	a)

Table V.5. Major (wt%) and trace element (ppm) composition of primary melts obtained by PRIMACALC2 model (Kimura and Ariskin, 2014) from parental samples of Robinson Crusoe and Alejandro Selkirk islands.

	Robinson Crusoe		Alejandro Selkirk			
Sample	LL040213-2	JR290513-5	LL250711-7	MF-3	JR170913-18	MF-6
SiO_2 (wt%)	47.50	46.35	47.03	45.46	46.70	47.20
TiO_2	2.51	2.97	2.67	1.88	2.61	1.97
Al_2O_3	11.27	12.04	12.07	11.96	12.44	12.47
FeO^T	11.49	11.44	12.02	12.37	11.21	11.79
MgO	15.39	14.76	14.09	16.82	14.51	14.78
MnO	0.18	0.17	0.15	0.18	0.16	0.18
CaO	8.74	8.32	8.75	8.02	8.51	8.59
Na_2O	2.05	2.40	2.34	2.78	2.59	2.27
K_2O	0.59	1.17	0.57	0.35	0.90	0.53
P_2O_5	0.28	0.37	0.30	0.19	0.36	0.23
K (ppm)	4795	9355	4600	2836	7248	4282
Ni	632	662	815	594	594	498
Ba	138.78	204.83	164.70	113.71	202.57	106.93
Hf	3.49	3.77	3.93	4.41	4.93	4.36
Nb	23.10	29.60	24.83	16.08	25.73	17.72
Rb	11.65	24.25	6.44	6.27	19.18	11.39
Sr	360	530	407	356	469	402
Ta	1.36	1.92	1.50	1.08	1.52	1.09
Th	1.65	2.34	1.84	1.76	2.33	1.39
U	0.19	0.50	0.25	0.39	0.72	0.40
Zr	156.56	170.53	147.36	181.37	222.28	177.04
Y	20.29	20.53	24.22	21.77	22.53	23.57
Pb	0.58	0.84	0.33	0.69	0.54	0.00
La	18.54	23.45	20.60	16.86	24.13	15.55
Ce	39.31	49.63	43.69	37.06	51.66	34.85
Pr	5.24	6.33	5.74	5.14	6.70	4.85
Nd	22.23	25.60	25.10	23.04	29.50	23.56
Sm	5.09	5.34	5.71	5.68	6.37	5.53
Eu	1.77	1.78	1.88	1.88	1.95	1.84
Gd	5.16	5.23	5.77	6.26	5.77	5.94
Tb	0.75	0.81	0.96	0.86	0.92	0.84
Dy	4.32	4.48	4.70	5.07	4.79	4.98
Ho	0.81	0.80	0.93	0.80	0.88	0.93
Er	1.92	2.01	2.37	2.15	2.08	2.40
Tm	0.26	0.28	0.35	0.30	0.29	0.31
Yb	1.54	1.57	2.07	1.68	1.73	1.82
Lu	0.23	0.22	0.28	0.24	0.25	0.25

Table V.6. Main parameters used in the OBS1 model (Kimura and Kawabata, 2015).

Parameter	Value
Primary melts	Robinson Crusoe (Alpha):
	LL040213-2 (medium La/Yb, most representative)
	JR290513-5 (high La/Yb)
	LL250711-7 (low La/Yb)
	Alejandro Selkirk (O'Higgins):
	MF-3 (medium La/Yb, most representative)
	JR170913-18 (high La/Yb)
	MF-6 (low La/Yb)
Melting model	Metasomatic
DM composition	Workman and Hart, 2005
Pyroxenite composition	Hofmann, 1988 (N-MORB)
Enriched peridotite comp.	Lyubetskaya and Korenaga, 2007
Additional DM depletion	0%
H_2O in the source	0.050 wt%
Fitting window	15% (Nb/Zr, La/Yb, Nb, Zr, La, Yb)
	30% (Nd, Sm, Hf, Eu, Gd, Tb, Dy, Y, Ho, Er, Tm, Lu)
	60% (Ta, K, Ce, Pr, Sr)
	200% (Rb, Ba, Th, U)

Table V.7. Results of the OBS1 model (Kimura and Kawabata, 2015) for samples from Robinson Crusoe and Alejandro Selkirk, volcanoes representatives of shield stage in Juan Fernández Ridge. Main parameters are shown: pyroxenite fraction (Px_{fr}), potential temperature (T_p), pyroxenitic composition fraction (Px%), pressure at melting termination (P_{mt}), and degree of melting (total: $TotF_{mt}$, pyroxenite: PxF_{mt}, peridotite: $PerF_{mt}$).

Sample	Px_{fr} (wt%)	T_p (°C)	PX% (wt%)	P_{mt} (GPa)	$TotF_{mt}$ (wt%)	$PerF_{mt}$ (wt%)	PxF_{mt} (wt%)
Robinson Crusoe Island							
LL040213-2	4.5 – 8.1	1290 – 1322	38.6 – 56.4	2.34 – 2.54	2.8 – 4.9	1.5 – 2.6	24.0 – 33.9
	6.1	1306	47.1	2.45	3.8	2.0	29.1
JR290513-5	3.9 – 9.9	1282 – 1316	30.7 – 63.4	2.30 – 2.56	2.9 – 5.1	1.4 – 2.7	21.3 – 30.2
	7.4	1297	48.1	2.40	3.9	2.0	25.6
L250711-7	3.3 – 8.1	1262 – 1296	24.1 – 52.3	1.98 – 2.34	2.4 – 4.2	1.4 – 2.7	19.2 – 26.3
	5.9	1280	40.0	2.21	3.3	2.0	22.6
Alejandro Selkirk Island							
MF-3	6.3 – 12.3	1312 – 1362	35.8 – 55.6	2.24 – 2.52	5.2 – 11.4	2.6 – 5,8	33.2 – 49.8
	9.0	1336	46.8	2.40	8.0	4.2	41.1
JR170913-18	9.6 – 16.2	1298 – 1344	47.1 – 65.5	2.20 – 2.52	5.3 – 10.5	2.2 – 4.3	27.4 – 40.2
	12.8	1318	57.3	2.37	7.3	3.1	32.7
MF-6	4.8 – 11.4	1296 – 1340	28.0 – 55.1	2.08 – 2.44	4.4 – 9.1	2.3 – 5.1	28.7 – 42.5
	7.8	1315	42.9	2.27	6.3	3.6	34.9

Figure V.1. Bathymetric map of the Juan Fernández Ridge (JFR) and seafloor around it (GEBCO, SHOA and data from Astudillo, 2014). The location of O'Higgins guyot, Alpha seamount, Robinson Crusoe, Santa Clara, and Alejandro Selkirk islands; the main volcanoes of JFR; is showed. Inset also show the location of main oceanic features and islands (Eas: Easter, SyG: Salas y Gomez, SF-SA: San Félix and San Ambrosio) around JFR.

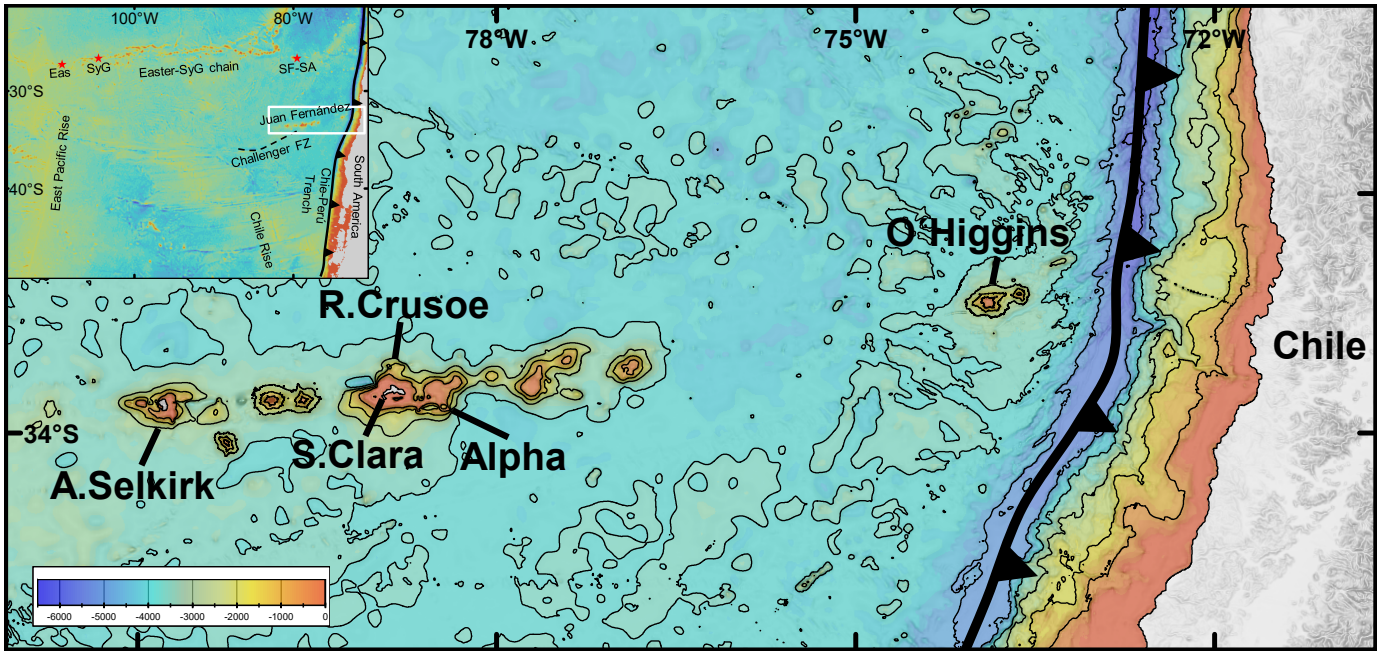

Figure V.2. Total-alkali vs. silica (TAS) classification diagram for lavas and dykes from shield-building stage in O'Higgins, Alpha, Robinson Crusoe, and Alejandro Selkirk volcanoes (after Le Maitre, 2002). The field of alkaline JFR rejuvenated lavas (from O'Higgins and Robinson Crusoe) is also showed. Published data from Reyes et al. (2017) and Lara et al. (2018a) are also included.

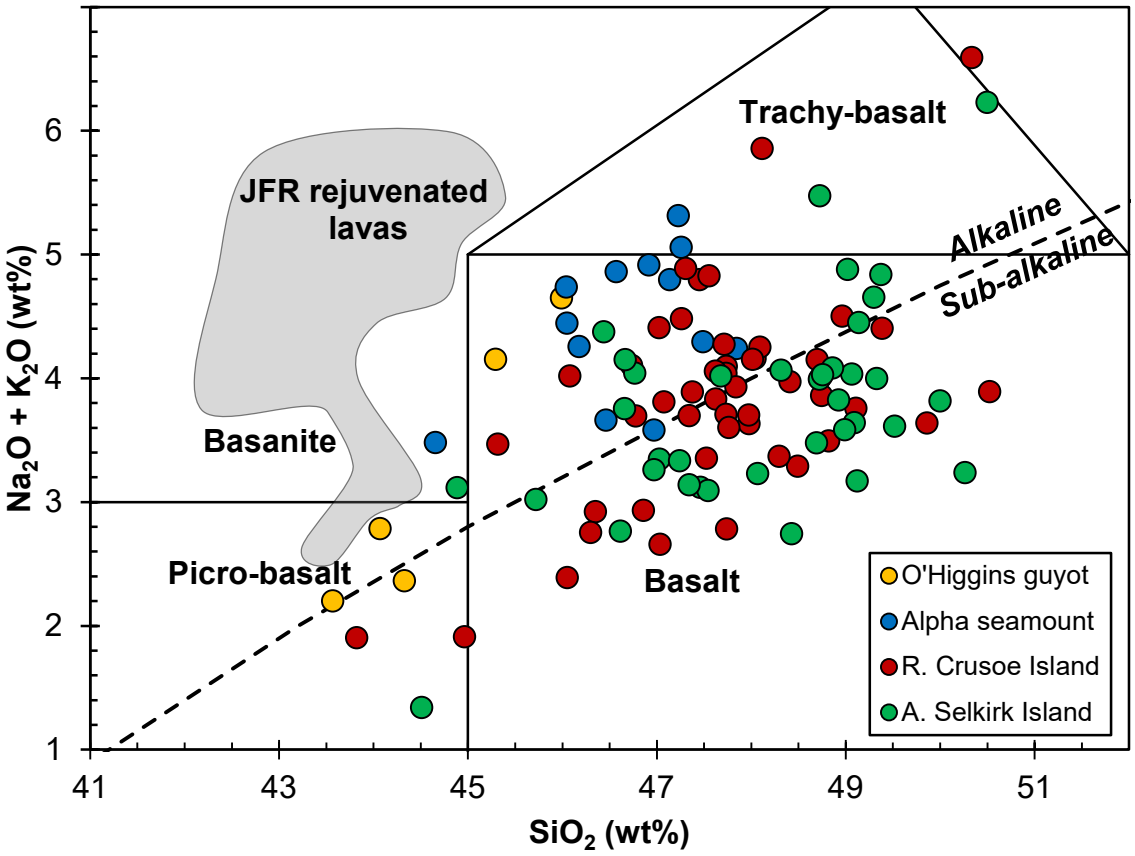

Figure V.3. Mg-number (Mg#) vs. major (CaO/Al2O3) and trace elements (Sc, Ni and Sr in ppm) plots for lavas from O'Higgins, Alpha, Robinson Crusoe, and Alejandro Selkirk shield stages. Dashed line in Ni plot marks the boundaries between compositional groups defined in Reyes et al., 2017. Mg# = Mg2+/[Mg2++Fe2+] assuming 90% of total iron is ferrous in all samples.

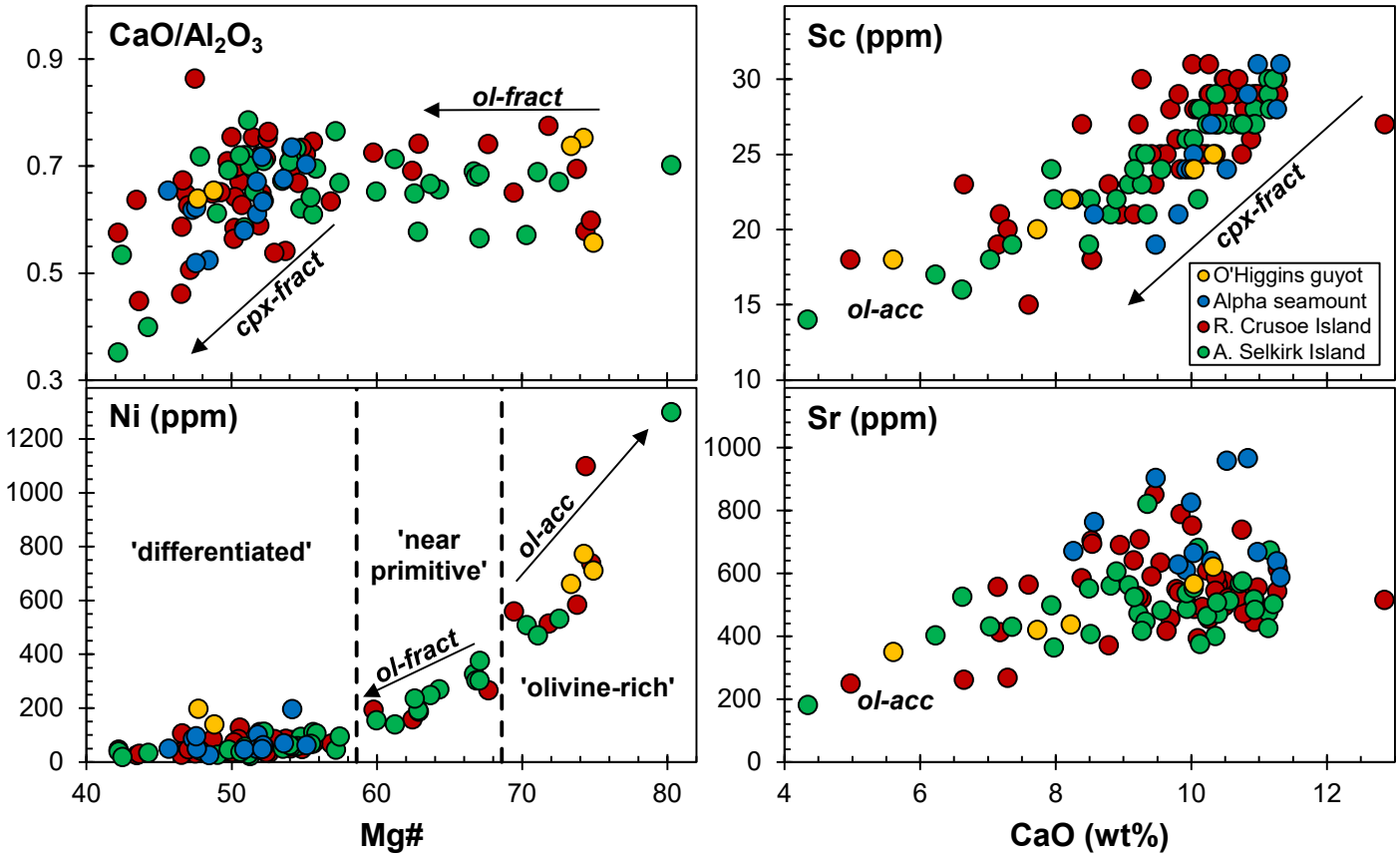

Figure V.4. Trace element variations plots for new ICP-MS data of lavas from O'Higgins, Alpha, Robinson Crusoe, and Alejandro Selkirk shield stages. Incompatible element enrichment is evident for Robinson Crusoe and Alpha reflected in a Nb/Zr ratio of 0.16 vs. 0.11 in Alejandro Selkirk/O'Higgins, and in higher values of Ta/Th. La/Yb does not vary significantly.

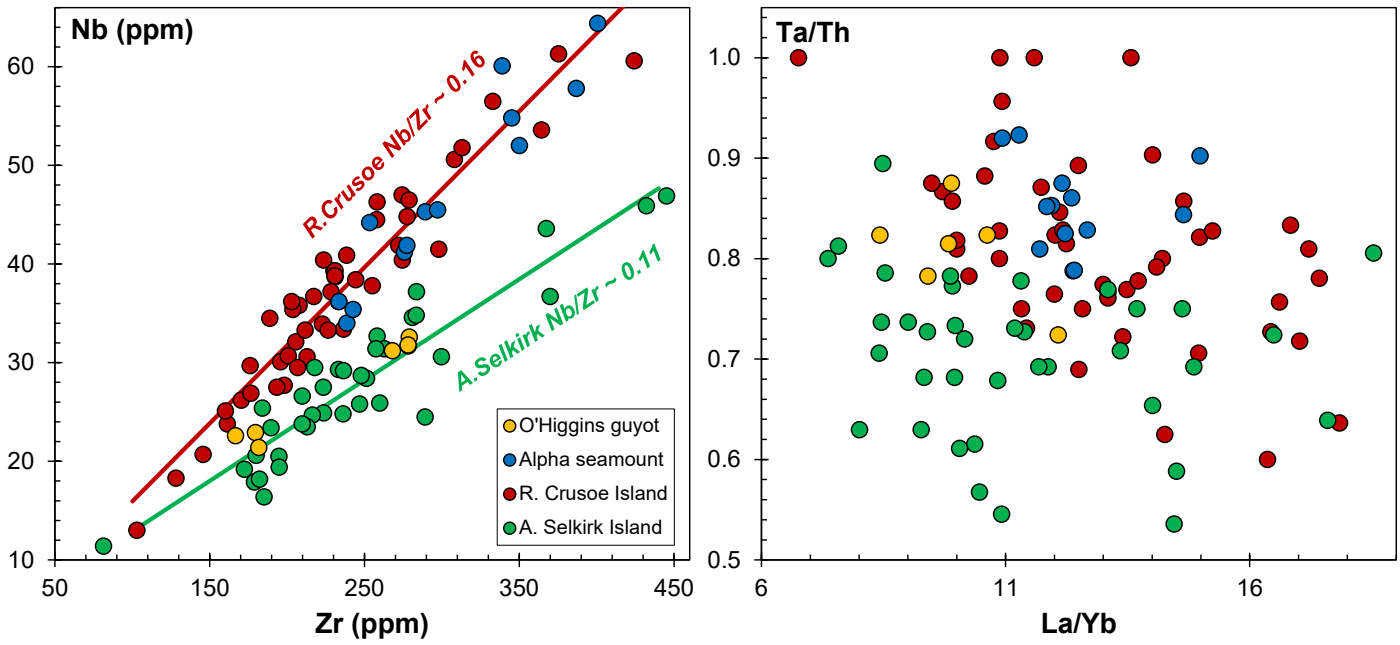

Figure V.5. Isotopic variation plots of the shield stage in JFR. a) $^{206}Pb/^{204}Pb$ vs. $^{207}Pb/^{204}Pb$, and $^{208}Pb/^{204}Pb$ show values near to FOZO-A with additional participation of DM or EM1. b) $^{87}Sr/^{86}Sr$ vs. $^{143}Nd/^{144}Nd$ show signature away of FOZO-A, and more evident DM contribution.

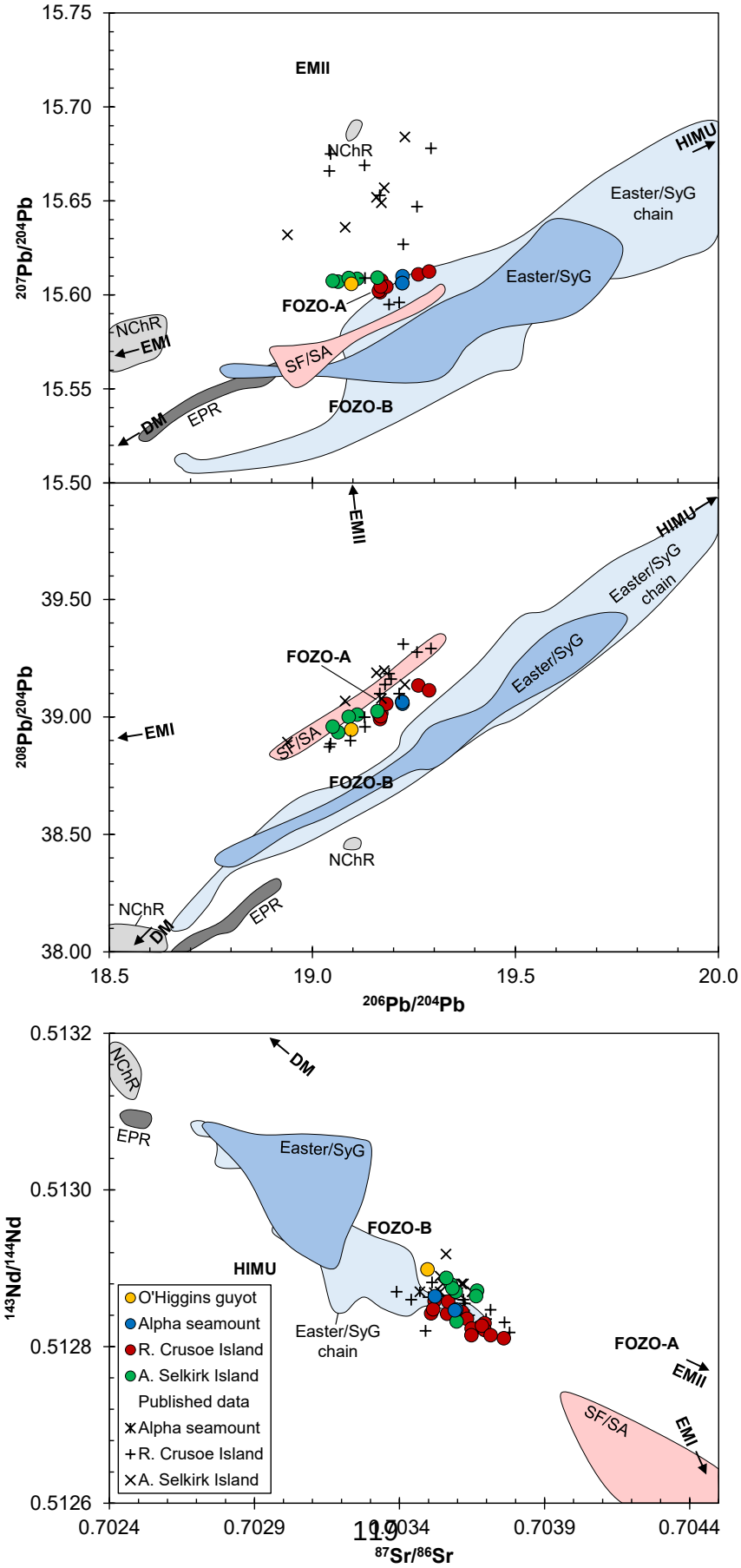

Figure V.6. Isotopic variation plots of $^{206}Pb/^{204}Pb$ vs. $^{87}Sr/^{86}Sr$ and $^{143}Nd/^{144}Nd$ for shield lavas in JFR. DM contribution is clear and discards the alternative of EM1 participation (additional to involvement in the stable mixture of FOZO-A), especially in $^{143}Nd/^{144}Nd$. The 'approach' to FOZO-B source is given only for $^{87}Sr/^{86}Sr$, $^{143}Nd/^{144}Nd$ values are near to FOZO-A (as for the lead isotopes).

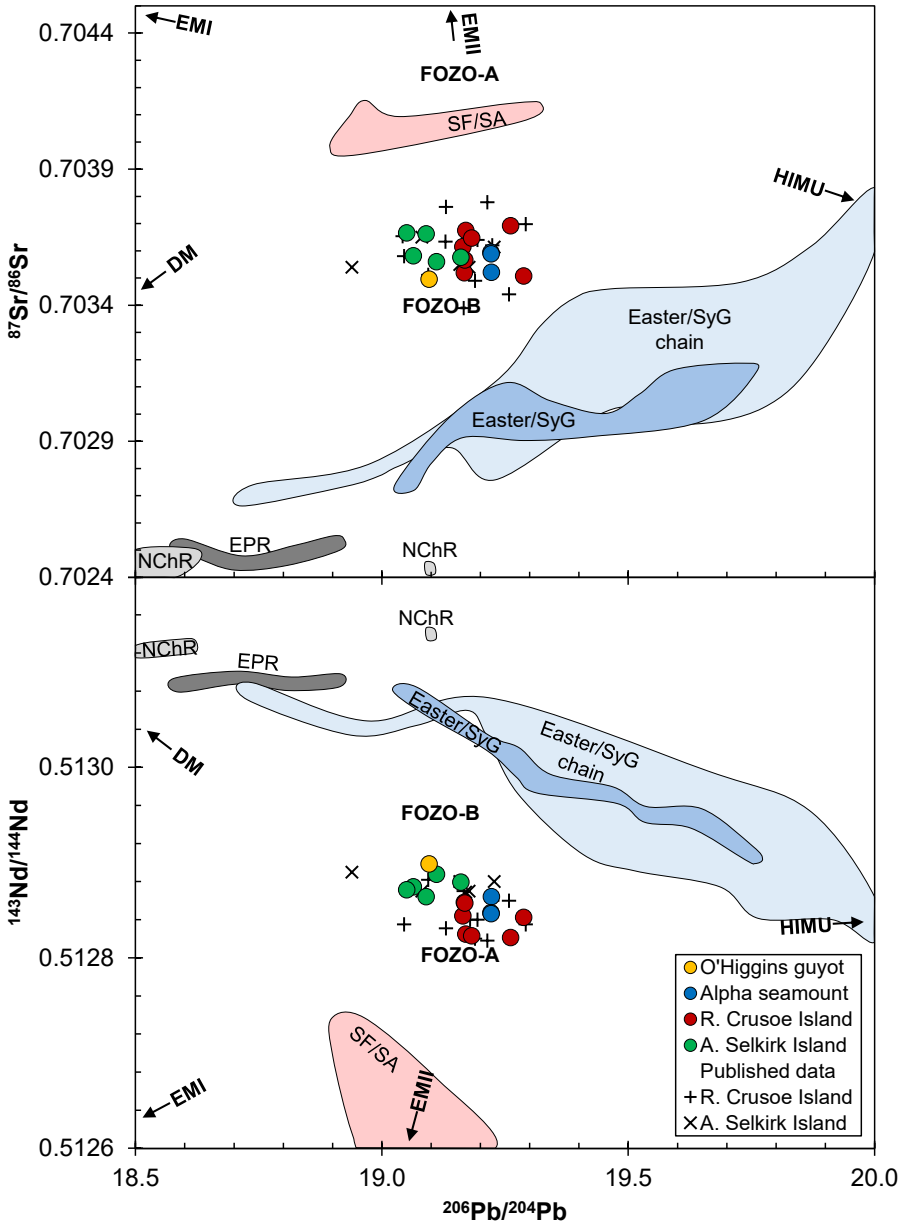

Figure V.7. Mg-number (Mg#) vs. CaO/Al_2O_3, La/Yb, La and Yb plots for shield lavas from Robinson Crusoe and Alejandro Selkirk showing the results of COMAGMAT 3.72 (Ariskin and Barmina, 2004) fractional crystallization (2 kbar, 0.8 wt% H_2O, QFM buffer, details in text) confirming the features of parental samples (from 'near-primitive' or 'olivine-rich' groups) in each volcano. Stars indicate the primary melts according PRIMACALC2 model (Kimura and Ariskin, 2014) applied in parental samples, yellow represents the most representative sample in each case. Blue and black represent little groups with high and low La/Yb (respect to main trend) ratios respectively.

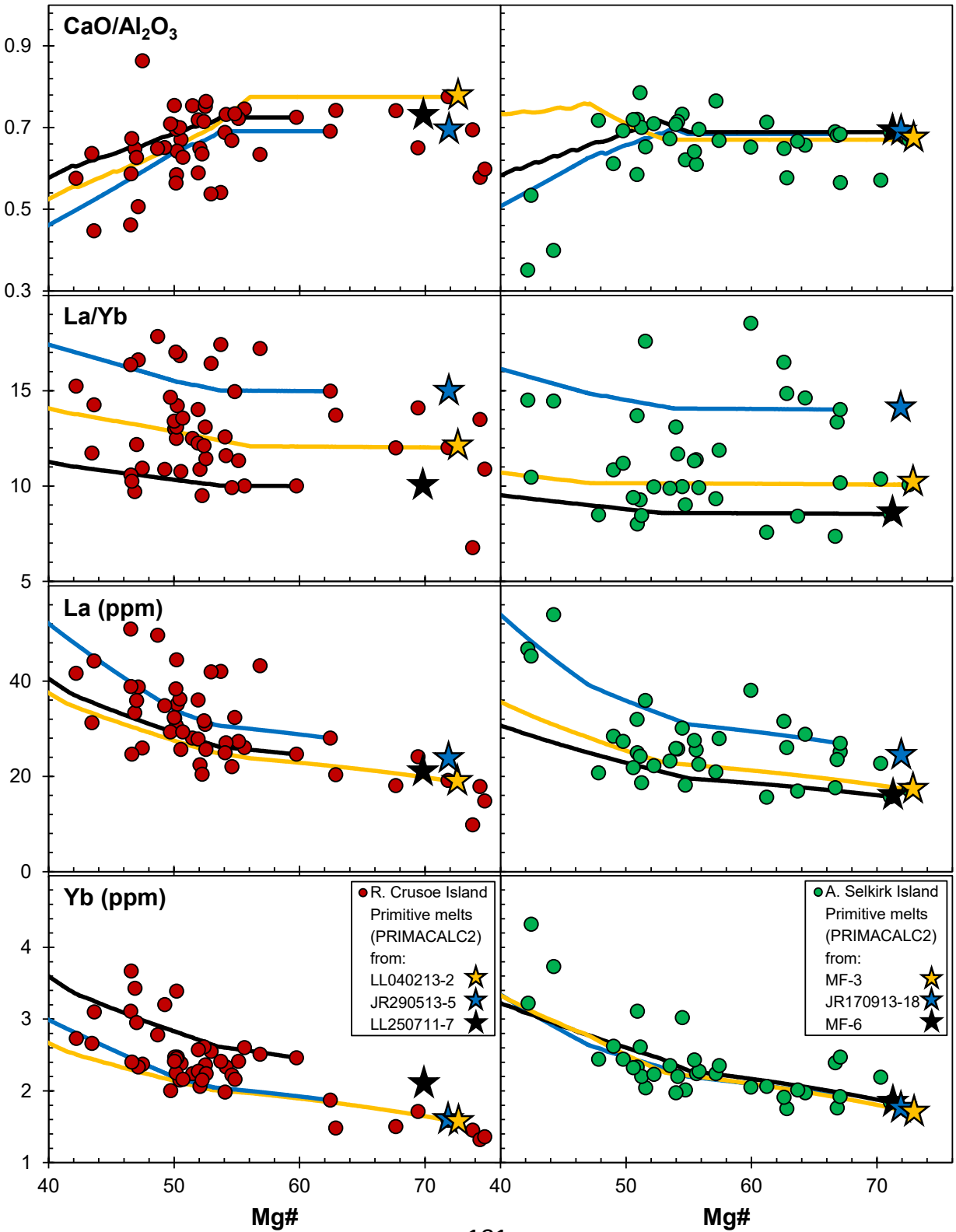

Figure V.8. Geochemical evidences of pyroxenite involvement in the source of JFR shield stage. Only 'near-primitive' samples are plotted to avoid fractionation and accumulation effect. a) MgO (wt%) vs. CaO (wt%) shows low CaO content to a given MgO in the field of pyroxenite partial melts (only tholeiitic samples, no clinopyroxene or plagioclase in line of descent; according Herzberg, 2006). b) TiO_2 (wt%) vs. FC3MS (FeO/CaO – $3MgO/SiO_2$) exhibit values near to pyroxenite melts average (0.46) and in some cases above the maximum value of FC3MS (0.65) for peridotite melts (Yang and Zhou, 2013). High values of TiO_2 respect to EPR (MORB), considered as pyroxenitic evidence (Prytulak and Elliot, 2007), are also showed.

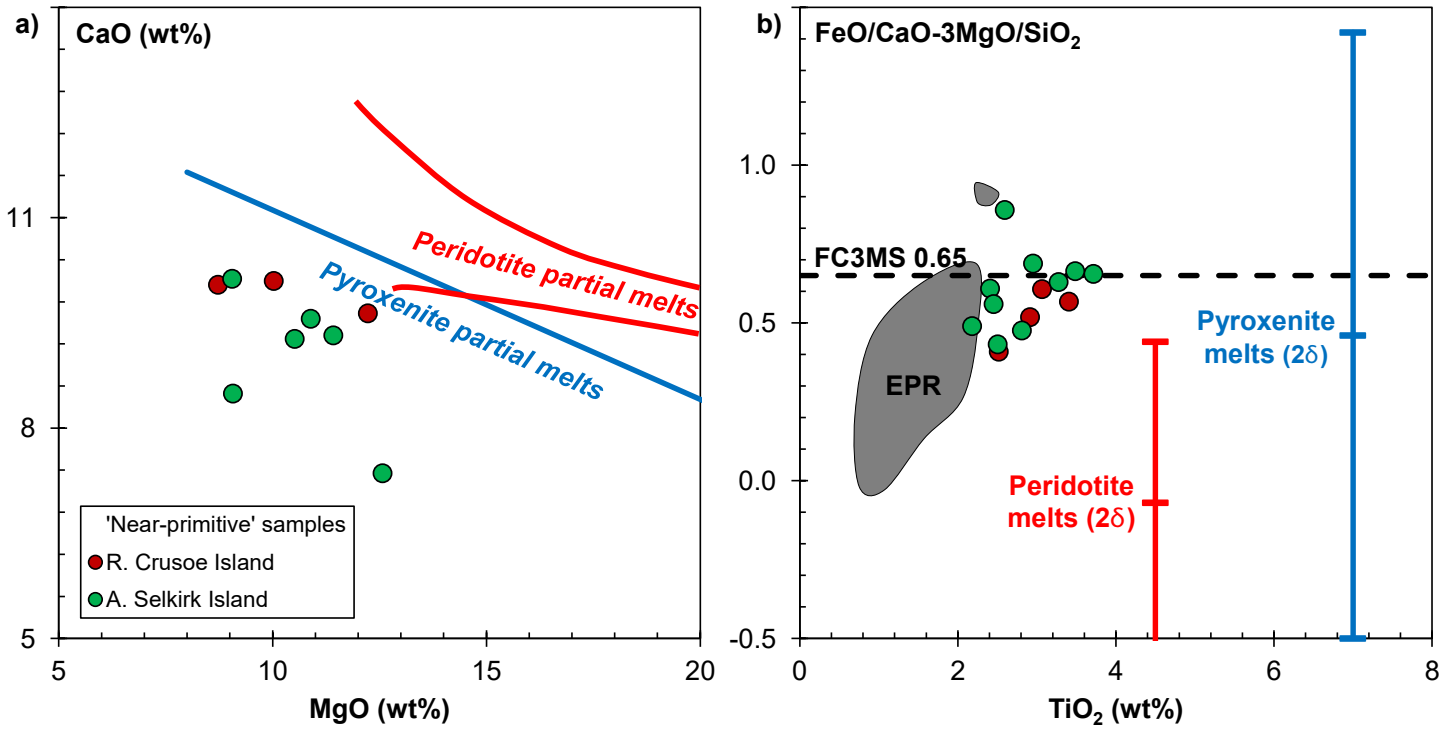

Figure V.9. OBS1 model results for the most representative samples (LL040213-2 for Robinson Crusoe, and MF-3 for Alejandro Selkirk) exhibiting the influence of water content (0.025, 0.050, and 0.075 wt%) of the mantle source in each parameter. Potential temperature (T_p; °C), pyroxenitic composition fraction (Px%; wt%), and pressure at melting termination (P_{mt}; GPa) decreases with water increment, but pyroxenite fraction (Px_{fr}; wt%) increases.

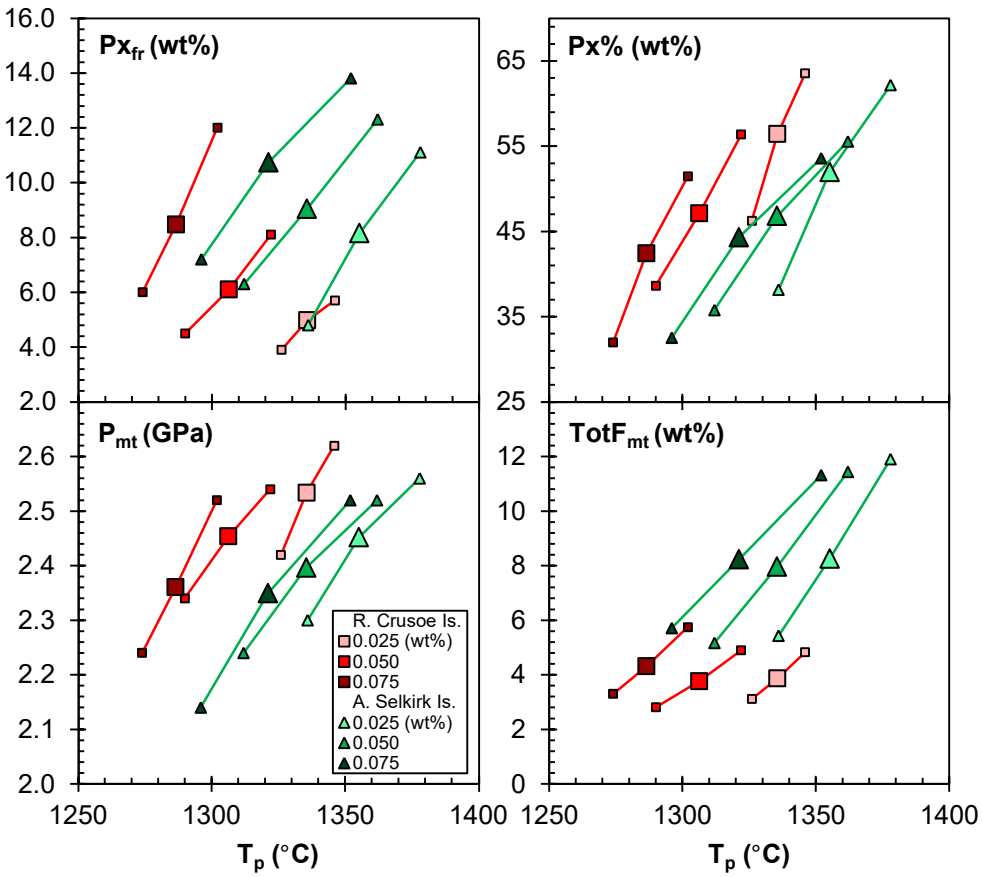

Figure V.10. Primitive mantle-normalized (PM from Lyubetskaya and Korenaga, 2007) trace element content patterns of primitive melts (modeled from parental samples) from Robinson Crusoe (a: red) and Alejandro Selkirk (b: green) showing the results of OBS1 mode (Kimura and Kawabata, 2015) in each case. The more pyroxenitic signature of Robinson Crusoe is evidenced by the values of some incompatible elements (e.g., Ti, Ta, Nb, and HREE). Average, minimum, and maximum values obtained by the model are compared with the target (primary melts). Values of potential temperature (Tp), pressure at melting termination (Pmt), pyroxenite fraction (Pxfr), and degree of melting at melting termination: total (TotFmt), of pyroxenite (PxFmt), and peridotite (PerFmt); that satisfies the model conditions are also showed. A good fit is visible for the majority of elements analyzed, only some mobile elements (e.g., U and K) and MREE (Eu, Gd, Tb, Dy) are slightly away from the model (details in text). n indicates the number of OBS1 successful results and stars are showed to facilitate the link with Figure 7.

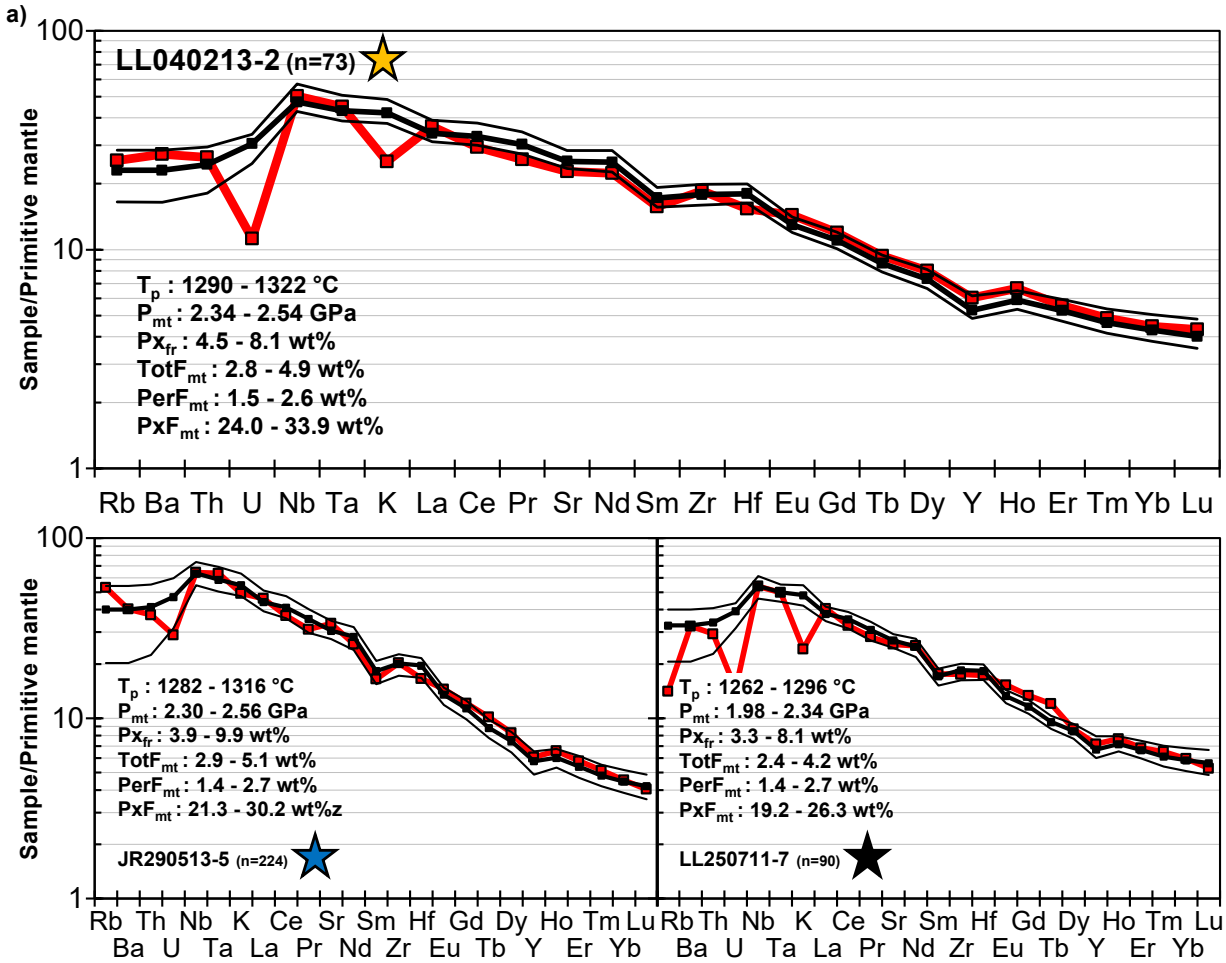

Figure V.10. (continued).

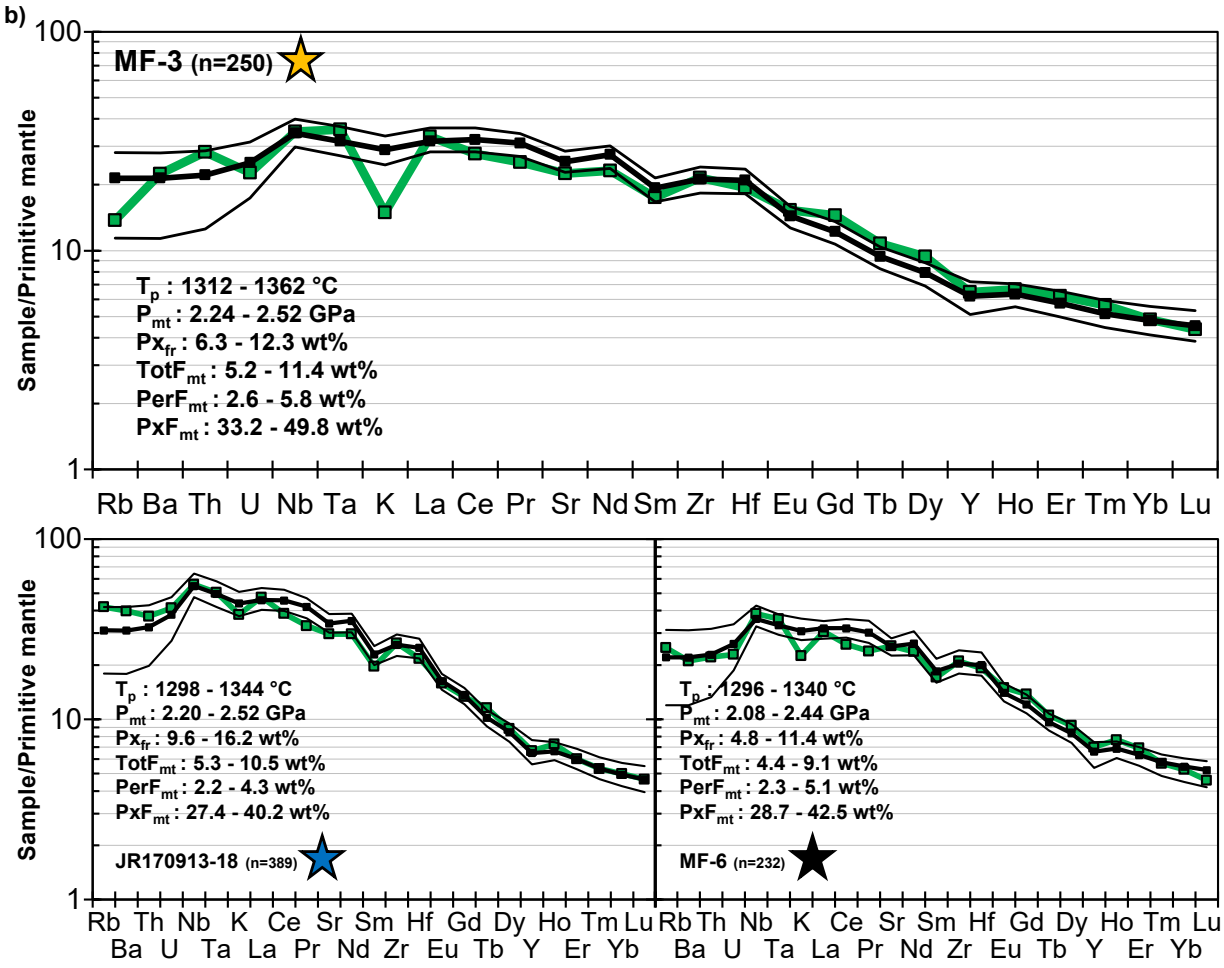

Figure V.S.1. Primitive mantle-normalized (PM from Lyubetskaya and Korenaga, 2007) trace element content patterns of samples from O'Higgins (yellow), Alpha (blue), Robinson Crusoe (red), and Alejandro Selkirk (green) showing the relative chemical enrichment of Robinson Crusoe/Alpha relative to Alejandro Selkirk/O'Higgins.

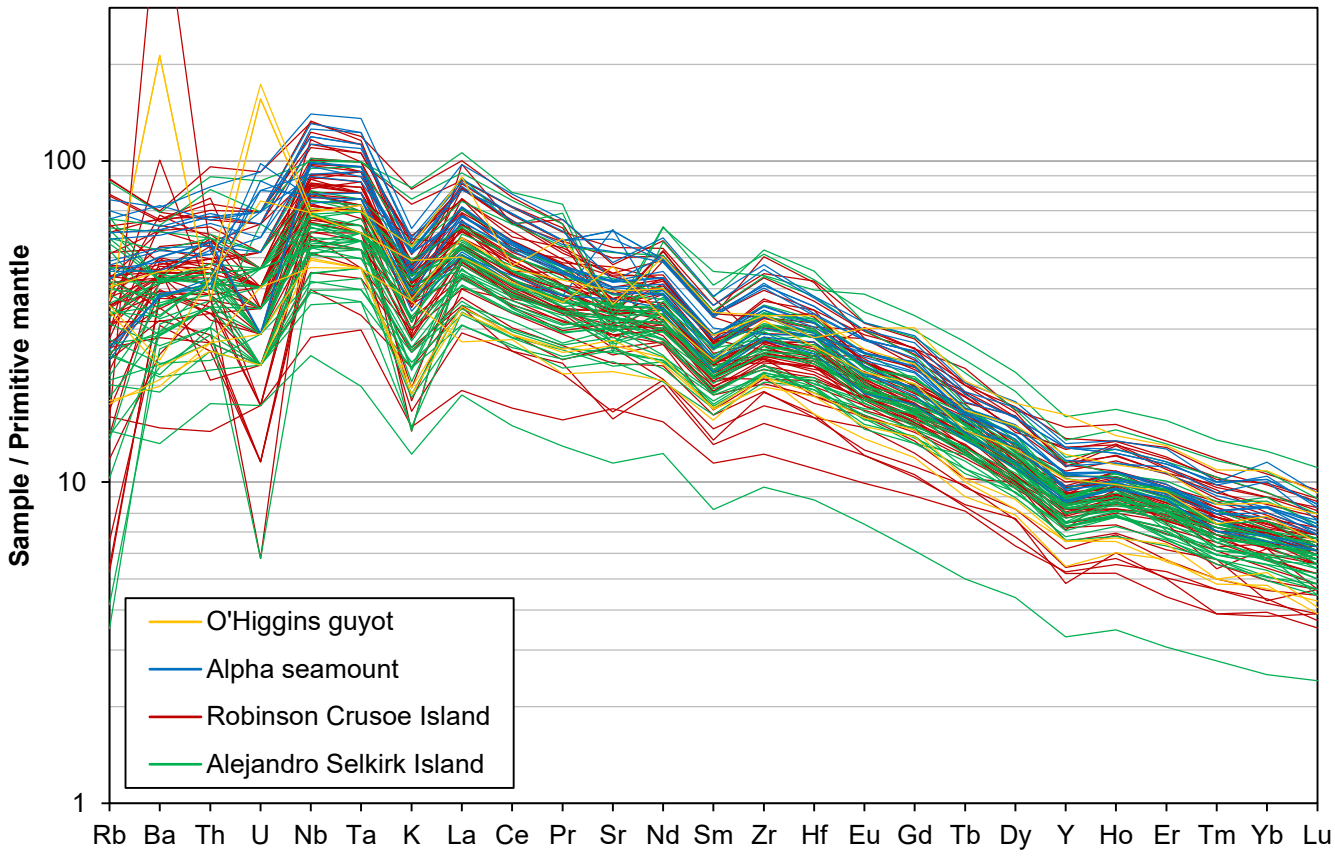

Figure V.S.2. Mobile elements: K_2O (wt%) and U (ppm) vs. immobile element (Nb) for lavas from O'Higgins guyot, Alpha seamount, Robinson Crusoe, and Alejandro Selkirk islands. K_2O and U are remobilized in JFR subaerial samples (Robinson Crusoe and Alejandro Selkirk) and enriched in submarine lavas (O'Higgins and Alpha) related to low-temperature alteration.

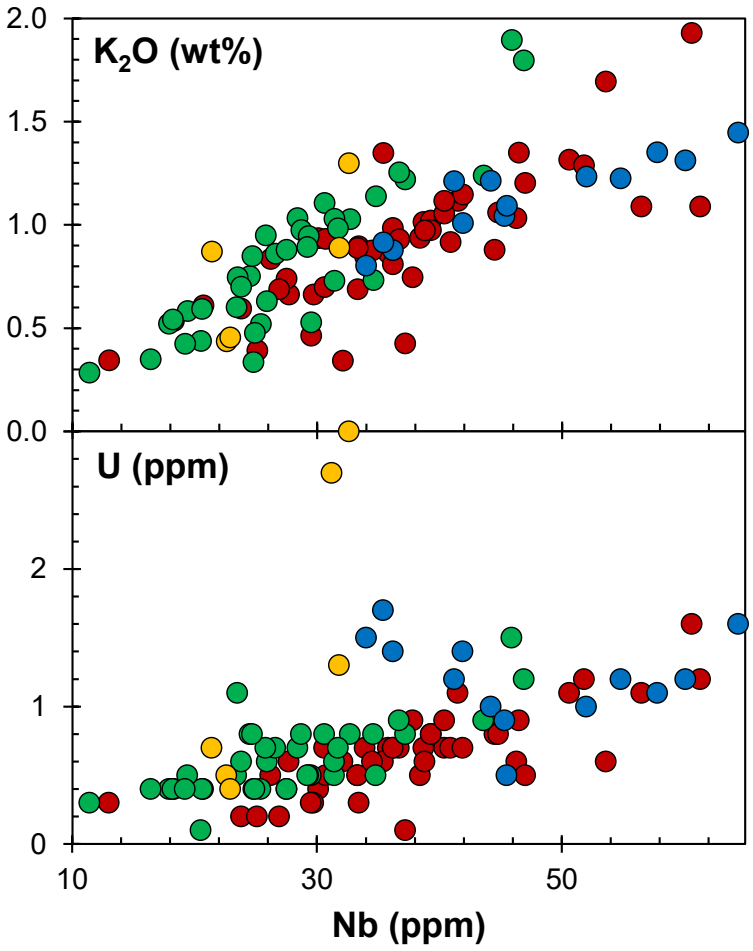

Capítulo VI

Geochemistry and isotopic features of the rejuvenated volcanism in Juan Fernández Ridge, SE Pacific

VI.1. Introduction

The rejuvenated volcanism (before called post-erosional) is a common feature in many oceanic intraplate systems generally expressed by relatively primitive alkaline magmatism (Ozawa et al., 2005) after a variable time of volcanic quiescence (from near zero to millions of years), and erosion next to the shield-building stage (Ribe and Christensen, 1999; Garcia et al., 2010) recognized in Hawaii (e.g., Ozawa et al., 2005; Garcia et al., 2010), Samoa (Wright and White, 1987; Konter and Jackson, 2012), Marquesas (Woodhead, 1992), Canary (e.g., Hoernle and Schmincke, 1993), Society (White and Duncan, 1996), Kerguelen (Weis et al., 1998), Madeira (Geldmacher and Hoernle, 2000), Mauritius (Paul et al., 2005), Fieberling-Guadalupe (Konter et al., 2009) and Juan Fernández (Reyes et al., 2017; Lara et al., 2018).

Different models have been proposed to explain this volcanism: melt of oceanic lithosphere around plume due to their thermal effect in the ambient mantle (Gurriet, 1987); secondary melting zone in the plume as a reflect of internal processes and lateral spreading beneath oceanic lithosphere (Ribe and Christensen, 1999); uplift of the oceanic plate generated by flexure effect due to the charge of a new volcano in the chain, and subsequent decompression melting (Bianco et al., 2005); and small-scale sublithospheric convection in the ambient mantle and lateral spreading plume (Ballmer et al., 2011). These models must be critically evaluated depending on the available data (geochemistry, isotopic and geophysics) in each intraplate system.

In this short contribution, new geochemical and isotopic data are presented for rejuvenated stage volcanism in O'Higgins guyot and Robinson Crusoe Island, two main volcanoes in Juan Fernández Ridge (JFR), and contrasted with the shield stage (see Chapter V) to suggest hypotheses to explain the observed differences.

VI.2. Analytical methods

Petrographic was made by optical microscopy at Centro de Excelencia en Geotermia de Los Andes (CEGA) facilities with modal count (500 points) in 9 samples using JMicroVision 1.2.7 software (Table 1). Whole-rock trace element chemistry was analyzed by ICP-MS for 22 samples at AcmeLabs, Vancouver, Canada (major elements are published in Reyes et al., 2017; and Lara et al., 2018). Isotopic ratios measurements were measured by TIMS (Triton Plus) for 13 samples at GEOMAR Helmholtz Center, Kiel, Germany; and Laboratoire Magmas and Volcans, Clermont-Ferrand, France. More details about methods and analytical procedures are available in Chapter V.

VI.3. Geology and $^{40}Ar/^{39}Ar$ geochronology

In O'Higgins guyot, the rejuvenated volcanism is represented by basanitic flows of ~ 8.16 Ma at the top of the guyot (~ 0.25 Ma younger) apparently fed from a low relief vent (Lara et al., 2018, and Chapter III). On the other hand, rejuvenated sequence in Robinson Crusoe is composed by pyroclastic successions that contain juvenile basanite material embedded in a palagonitic matrix covered by basanite lava flows (~ 0.77 to ~

1.67 Ma). This sequence fills the eroded morphology of the shield after a hiatus in the volcanism (< ~ 1.73 Ma) (Reyes et al., 2017 and Chapter III). In both cases, the mineralogy consists of olivine (> 5 vol%) and subordinated clinopyroxene (generally < 2 vol%) phenocrysts (Table VI.1) immersed in a clinopyroxene, plagioclase, olivine and Fe-Ti oxides groundmass with occasional presence of analcime and natrolite.

VI.4. Whole-rock geochemistry

The basanites (and subordinate picrites) of the rejuvenated volcanism of Robinson Crusoe are characterized by relative low SiO_2 (41.6 – 45.4 wt%) (Figure VI.1), and high Mg# (55.9 – 69.9) with a marked enrichment in MnO, Na_2O, K_2O, and P_2O_5 content relative to shield stage (Reyes et al., 2017). Data for O'Higgins show that basanites have values within the range reported for Robinson Crusoe (Figure VI.1) (Table A.1) (Table A.2). In addition, many trace elements show typical features of ocean island volcanoes (e.g., TITAN anomaly; Jackson et al. 2008; Peters and Day, 2014), and are notably enriched respect to shield volcanism. In fact, LILE (e.g., Rb and Ba), LREE (La, Ce, Pr, Nd), Nb and Ta, show values clearly higher than shield (Figure VI.2). Other REE (Sm, Eu, Gd, Tb, Dy, Ho, Er, Tm, Yb and Lu), Zr, Hf, and Y do not show significantly differences respect to shield (except with 'olivine-rich' group, affected by olivine accumulation) (Figure VI.2). This different behavior is reflected in some incompatible element ratios, e.g., the relatively enriched values of Nb and La in rejuvenated stage generate high Nb/Zr (0.22 – 0.28 in rejuvenated vs. 0.08 – 0.18 in shield) and La/Yb (19.5 – 24.7 vs. 6.8 – 18.5) that allow a discrimination between evolutionary stages based on trace element geochemistry (Figure VI.3).

VI.5. Sr-Nd-Pb isotopes

The rejuvenated lavas of JFR (O'Higgins and Robinson Crusoe) show a narrow field for isotopic ratios with values for lead in the ranges 19.1016 – 19.2404 for $^{206}Pb/^{204}Pb$, 15.5845 – 15.5965 for $^{207}Pb/^{204}Pb$, and 39.0716 – 39.1562 for $^{208}Pb/^{204}Pb$ (Table VI.3). These values are slightly depleted in $^{207}Pb/^{204}Pb$ and enriched in $^{208}Pb/^{204}Pb$ respect to the JFR shield stage (Chapter V), but also close to a stable mixture of FOZO-A source (Jackson et al., 2007) with additional participation of DM component (after Zindler and Hart, 1986), very closer to San Felix/San Ambrosio field (from GEOROC database), and influenced by DUPAL anomaly (Hart, 1984). In the Sr-Nd system, the rejuvenated stage also shows values near to JFR shield stage between 0.703386 and 0.703551 for $^{87}Sr/^{86}Sr$, and 0.512830 and 0.512873 for $^{143}Nd/^{144}Nd$. There is not clear evidence about additional participation of HIMU, EM1 and/or EM2 sources.

VI.6. Discussion

The geochemical, isotopic, and mineral chemistry (Chapter III) similarities between rejuvenated stages in O'Higgins and Robinson Crusoe allow considering as a result of equivalent (or very similar) petrogenetic mechanisms. The chemical internal differences of these basanites can be explained by differentiation through fractional crystallization of olivine and clinopyroxene, forming sub-parallel enrichment of incompatible elements and the expected trends as decrease of Sc.

The incompatible elements pattern of rejuvenated lavas has the same shape and anomalies that JFR shield, but more enriched in the most incompatible elements (e.g. LILE, LREE and Nb), and similar values in more 'compatible' elements (HREE) (Figure

VI.2). This behavior can be explained by lower melting degrees of the same (or similar) mantle source involved in shield petrogenesis, because the more incompatible elements are preferentially incorporated in the melt increasing their content and some ratios as La/Yb or Nb/Zr (Figure VI.3). If this is true, it would be expected to find the same (or similar) isotopic ratios in both stages. In fact, the rejuvenated and shield stages of JFR have a very similar isotopic signature, with only small differences principally in $^{207}Pb/^{204}Pb$ and $^{87}Sr/^{86}Sr$, and away from the MORB values of southern East Pacific Rise (Macdougall and Lugmair, 1985) and North Chile Ridge (Bach et al., 1996) (Figure VI.4), confirming their origin from a mantle plume (see Chapter IV and V), and discarding the exclusive lithospheric participation in the genesis of the rejuvenated magmatism. Additionally, the more marked FOZO-A signature (Figure VI.4) and some geochemical features as TITAN anomaly and LILE enrichment (higher than shield), imply the presence of pyroxenite in the plume beneath JFR, probably with a major participation in the final primary melt (Px% defined in Chapter V) at lower degrees of melting.

A physical model for rejuvenated volcanism (with variable period of volcanic inactivity) at JFR is beyond the scope of this study. However, some preliminary ideas can be assessed in a more global context. The model of Gurriet (1987) implies the melting of the lithospheric mantle due to the thermal effect of the ascending plume that previously generated the shield volcanism. This model is discarded due to the enriched isotopic signature of JFR, far to the DM field representative of depleted lithosphere, implying the direct participation of the plume in the origin of rejuvenated volcanism. The effect of flexural deformation prescribed by a distant load (new volcano) has also been proposed for the secondary volcanism in Hawaii (Bianco et al., 2005). However, due to the low elastic thickness of Nazca Plate (Manríquez et al., 2015), the flexure induced by the formation of a new shield volcano only affects the vicinity of the volcanic edifice (< 80 km) (Orozco, 2016). In the JFR case study, rejuvenated stage in Robinson Crusoe (~ 0.77 – 1.67 Ma) is coeval with the shield stage in Alejandro Selkirk (~ 0.83 – 0.94 Ma) (Chapter III), but the distance between them (~ 180 km) discard the flexural mechanism. Thus, the late-stage volcanism remains an enigmatic process (Homrighausen et al., 2018), but melting of the plume in a secondary zone (Ribe and Christensen, 1999) and maybe the plume spreading because of the small-scale sublithospheric convection (Ballmer et al., 2011) would be suitable candidates that could be taken into account in presence of new geophysical data. Recently, Lara et al. (2018) propose that the rapid transition between the summit erosion of the shield stage in O'Higgins and the subsequent rejuvenated volcanism (with a slightly different magma source) could be explained in terms of isostatic rebound and flexural deformation due to partial collapse of the shield volcano. Their model must be evaluated in Robinson Crusoe, where the volcanic gap is apparently longer, but the similarities between rejuvenated volcanism in both volcanoes call for a recurrent and hence geodynamically-controlled process.

Bibliography

Bach, W., Erzinger, J., Dosso, L., Bollinger, C., Bougault, H., Etoubleau, J., Sauerwein, J., 1996. Unusually large NbTa depletions in North Chile ridge basalts at 36°50′ to 38°56′S: major element, trace element, and isotopic data. Earth Planet. Sci. Lett. 142, 223–240. doi.org/10.1016/0012-821X(96)00095-7

Ballmer, M.D., Ito, G., van Hunen, J., Tackley, P.J., 2011. Spatial and temporal variability in Hawaiian hotspot volcanism induced by small-scale convection. Nat. Geosci. 4, 457–460. doi:10.1038/ngeo1187

Bianco, T.A., Ito, G., Becker, J.M., Garcia, M.O., 2005. Secondary Hawaiian volcanism formed by flexural arch decompression. Geochemistry, Geophys. Geosystems 6, 1–24. doi:10.1029/2005GC000945

Garcia, M.O., Swinnard, L., Weis, D., Greene, a. R., Tagami, T., Sano, H., Gandy, C.E., 2010. Petrology, geochemistry and geochronology of Kaua'i lavas over 4-5 Myr: Implications for the origin of rejuvenated volcanism and the evolution of the Hawaiian plume. J. Petrol. 51, 1507–1540. doi:10.1093/petrology/egq027

Geldmacher, J., Hoernle, K., 2000. The 72 Ma geochemical evolution of the Madeira hotspot (eastern North Atlantic): Recycling of Paleozoic (<500 Ma) oceanic lithosphere. Earth Planet. Sci. Lett. 183, 73–92. doi:10.1016/S0012-821X(00)00266-1

Gurriet, P., 1987. A thermal model for the origin of post-erosional alkalic lava, Hawaii. Earth Planet. Sci. Lett. 82, 153–158. doi:10.1016/0012-821X(87)90115-4

Hart, S.R., 1984. A large-scale isotope anomaly in the Southern Hemisphere mantle. Nature 309, 753–757. doi.org/10.1038/309753a0

Hoernle, K., Schmincke, H.U., 1993. The petrology of the tholeiites through melilite nephelinites on Gran Canaria, Canary Islands: Crystal fractionation, accumulation, and depths of melting. J. Petrol. 34, 573–597. doi:10.1093/petrology/34.3.573

Homrighausen, S., Hoernle, K., Geldmacher, J., Wartho, J.-A., Hauff, F., Portnyagin, M., Werner, R., van den Bogaard, P., Garbe-Schönberg, D., 2018. Unexpected HIMU-type late-stage volcanism on the Walvis Ridge. Earth Planet. Sci. Lett. 492, 251–263. doi.org/10.1016/j.epsl.2018.03.049

Irvine, T.N., Baragar, R.A., 1971. A guide to the chemical classification of the common volcanic rocks. Can. J. Earth Sci. 8 (5), 523–548. doi:10.1139/e71-055

Jackson, M.G., Kurz, M.D., Hart, S.R., Workman, R.K., 2007. New Samoan lavas from Ofu Island reveal a hemispherically heterogeneous high $^{3}He/^{4}He$ mantle. Earth Planet. Sci. Lett. 264, 360–374. doi.org/10.1016/j.epsl.2007.09.023

Jackson, M.G., Hart, S.R., Saal, A.E., Shimizu, N., Kurz, M.D., Blusztajn, J.S., Skovgaard, A.C., 2008. Globally elevated titanium, tantalum, and niobium (TITAN) in ocean island basalts with high $^{3}He/^{4}He$. Geochemistry, Geophys. Geosystems 9, Q04027. doi.org/10.1029/2007GC001876

Konter, J.G., Staudigel, H., Blichert-Toft, J., Hanan, B.B., Polvé, M., Davies, G.R., Shimizu, N., Schiffman, P., 2009. Geochemical stages at Jasper seamount and the origin of intraplate volcanoes. Geochemistry, Geophys. Geosystems 10. doi:10.1029/2008GC002236

Konter, J.G., Jackson, M.G., 2012. Large volumes of rejuvenated volcanism in Samoa: Evidence supporting a tectonic influence on late-stage volcanism. Geochemistry, Geophys. Geosystems 13. doi:10.1029/2011GC003974

Macdougall, J.D., Lugmair, G.W., 1985. Extreme isotopic homogeneity among basalts from the southern East Pacific Rise: mantle or mixing effect? Nature 313, 209–211. doi.org/10.1038/313209a0

Manríquez, P., Contreras-Reyes, E., Osses, A., 2014. Lithospheric 3-D flexure modelling of the oceanic plate seaward of the trench using variable elastic thickness. Geophys. J. Int. 196, 681–693. doi.org/10.1093/gji/ggt464

Lara, L.E., Díaz-Naveas, J., Reyes, J., Jicha, B., Orozco, G., Kay, S.M., 2018. Unraveling short-lived rejuvenated volcanism and a rapid transition from shield stage at O ' Higgins guyot , Juan Fernández Ridge , Pacific SE. Submitted to Deep-Sea Research Part I.

Le Maitre, R.W., 2002. Igneous rocks – a classification and glossary of terms. Cambridge University Press, Cambridge (236 pp.). doi:10.1017/CBO9780511535581

Orozco, G., 2016. Evolución estructural y tectónica de la Isla Robinson Crusoe, Dorsal de Juan Fernández. Universidad de Chile (96 pp.).

Ozawa, A., Tagami, T., Garcia, M.O., 2005. Unspiked K–Ar dating of the Honolulu rejuvenated and Ko'olau shield volcanism on O'ahu, Hawai'i. Earth and Planetary Science Letters 232, 1–11. doi:10.1016/j.epsl.2005.01.021

Paul, D., White, W.M., Blichert-Toft, J., 2005. Geochemistry of Mauritius and the origin of rejuvenescent volcanism on oceanic island volcanoes. Geochemistry, Geophys. Geosystems 6. doi:10.1029/2004GC000883

Peters, B.J., Day, J.M.D., 2014. Assessment of relative Ti, Ta, and Nb (TITAN) enrichments in ocean island basalts. Geochemistry, Geophys. Geosystems 15, 4424–4444. doi.org/10.1002/2014GC005506

Reyes, J., Lara, L.E., Morata, D., 2017. Contrasting P-T paths of shield and rejuvenated volcanism at Robinson Crusoe Island, Juan Fernández Ridge, SE Pacific. J. Volcanol. Geotherm. Res. 341, 242–254. https://doi.org/10.1016/j.jvolgeores.2017.05.035

Ribe, N.M., Christensen, U.R., 1999. The dynamical origin of Hawaiian volcanism. Earth Planet. Sci. Lett. 171, 517–531. doi:10.1016/S0012-821X(99)00179-X

Sun, S., McDonough, W.F., 1989. Chemical and isotopic systematics of oceanic basalts: implications for mantle composition and processes. Geol. Soc. London, Spec. Publ. 42, 313–345. doi.org/10.1144/GSL.SP.1989.042.01.19

Weis, D., Frey, F.A., Giret, A., Cantagrel, J.M., 1998. Geochemical characteristics of the youngest volcano (Mount Ross) in the Kerguelen Archipelago: Inferences for magma flux, lithosphere assimilation and composition of the Kerguelen plume. J. Petrol. 39, 973–994. doi:10.1093/petroj/39.5.973

White, W.M., Duncan, R.A., 1996. Geochemistry and geochronology of the Society Islands: New evidence for deep mantle recycling, in: Earth Processes: Reading the Isotopic Code. American Geophysical Union, pp. 183–206. doi:10.1029/GM095p0183

Woodhead, J.D., 1992. Temporal geochemical evolution in oceanic intra-plate volcanics: A case study from the Marquesas (French Polynesia) and comparison with other hotspots. Contrib. to Mineral. Petrol. 111, 458–467. doi:10.1007/BF00320901

Wright, E., White, W.M., 1987. The origin of Samoa: New evidence from Sr, Nd, and Pb isotopes. Earth Planet. Sci. Lett. 81, 151–162. doi:10.1016/0012-821X(87)90152-X

Zindler, A., Hart, S., 1986. Chemical Geodynamics. Annu. Rev. Earth Planet. Sci. 14, 493–571. doi.org/10.1146/annurev.earth.14.1.493

Table VI.1. Petrography of representative rejuvenated samples from O'Higgins and Robinson Crusoe based on 500 points count using JMicroVision 1.2.7 software. Mineralogy reported as vesicle-free volume percent for pheno- and microphenocrysts (>0.2 mm in diameter). Rock type according mineralogy and chemistry. (GM: groundmass. Ves: vesicle content. Ol: olivine. Cpx: clinopyroxene. Plg: plagioclase. Op: opaque).

			GM	Mineralogy				Ves
Volcanic unit	Sample	Rock type	(%)	Oli	Cpx	Plg	Op	(%)
O'Higgins guyot								
'low-Mg'	2D-1	basanite	94	6	<1	-	-	7
	2D-2	basanite	94	5	1	-	-	1
Robinson Crusoe Island								
'high-Mg'	JR220112-3	basanite	88	12	<1	-	-	3
	JR250112-3	picrite	87	12	1	-	-	2
'low-Mg'								
	LL230711-2	basanite	81	10	9	-	<1	<1
	JR020613-3	basanite	93	5	1	-	1	2
	JR160913-2	basanite	87	6	7	-	-	2
	LL010213-6	basanite	94	6	<1	-	<1	-
	LL220112-4	basanite	90	8	2	-	-	-

Table VI.2. Trace element data (ppm, Cr_2O_3 in wt%) for rejuvenated lavas from O'Higgins guyot and Robinson Crusoe Island. Major elements are published in Reyes et al. (2017) and Lara et al. (submitted).

Sample	Cr_2O_3	Sc	Ba	Co	Ga	Hf	Nb	Rb	Sr	Ta	Th	U	V	Zr	Y
Det. limit	*0.002*	*1*	*1*	*0.2*	*0.5*	*0.1*	*0.1*	*0.1*	*0.5*	*0.1*	*0.2*	*0.1*	*8*	*0.1*	*0.1*
O'Higgins guyot															
2D-1	0.031	21	542	47.8	17.5	6.9	70.5	33.8	1029	4.3	5.4	1.5	291	321	30.8
2D-2	0.031	21	558	47.9	19.1	7.4	73	40.9	1057.4	4.6	5.5	1.7	295	335.6	31.9
Robinson Crusoe Island															
LL230711-2	0.07	27	652	54.7	17.6	6.4	75.2	5.3	880.9	4.5	7	1.5	311	279.8	30.4
LL230711-8	0.052	25	542	57	17.7	6.1	70.2	13.7	843.3	4.3	5.9	1.3	334	260.6	27.9
JR250112-2	0.064	24	497	55.5	17.5	5.9	68.2	25.6	793.6	4.1	5.4	1.3	290	261.2	25.2
JR250112-3	0.107	29	417	51.4	17.4	4.3	59.5	5.2	671.5	3.2	4.5	1	270	219.1	22.8
LL060213-4	0.052	23	706	46.3	19.9	7.9	85	55.9	997.9	5.5	8.1	1.9	287	344.8	34.9
LL230112-2	0.072	25	678	82.4	22.4	7.6	88.5	47.4	1038	5.3	7.8	1.9	385	326.9	36.7
LL230112-4	0.104	30	644	76.7	24.6	7.4	84.1	7.9	999	5.1	7	1.6	441	324.9	36
JR230112-1	0.058	28	535	53.9	18.8	6.5	72.1	38.3	813.3	3.8	5.5	1.2	312	262.3	28.1
JR230112-2	0.056	28	530	54.9	18.5	5.8	71.9	46.9	807.8	4	5	1.5	278	257.2	28.6
JR230112-3	0.048	22	625	46.4	18.6	8	86.4	50.7	974.5	5.1	7.6	2	231	345.5	32.5
JR160913-2	0.049	25	762	49.5	18.1	6.9	76.1	11.4	962.5	4.8	7	1.5	276	299.6	30.8
MP270112-3	0.065	22	604	45.7	17.1	8.1	86.6	52.3	944.2	5.3	7.6	1.8	212	344.5	32.5
JR020613-3	0.065	23	649	49.5	19.7	7.8	80.2	51.5	973.6	4.9	7.8	1.8	229	347.9	32.5
LL010213-6	0.04	20	654	51.9	20.5	8.2	83.4	56.7	971.8	5	6.8	1.7	275	343.4	32.9
JR220112-4A	0.044	24	525	47.9	18.3	6.1	70.8	40	857.5	4.3	5.9	1.1	254	286.1	29.8
LL220112-1	0.068	26	491	51.9	19.6	6.1	66.9	33.9	830.5	3.8	5	1.3	267	256.1	28.6
JR220112-3	0.075	28	411	58.7	17.4	5.4	57.4	31.6	672	3.6	4.8	1	266	222.3	24.6
JR250513-3	0.059	26	609	55.9	17	5.9	69.8	11.4	885.4	3.9	6.7	1.6	297	275.4	28.1
LL220112-4	0.04	21	644	46.6	19.4	7.8	87.6	58	986.4	5.5	8.2	1.8	217	357.2	33.3
JR250513-9	0.048	17	700	44.3	17.1	7.8	85.6	51.4	1032.3	4.8	8.4	2.1	212	366.1	33.3

Table VI.2. (continued)

Sample	Pb	La	Ce	Pr	Nd	Sm	Eu	Gd	Tb	Dy	Ho	Er	Tm	Yb	Lu
Det. limit	*0.1*	*0.1*	*0.1*	*0.02*	*0.3*	*0.05*	*0.02*	*0.05*	*0.01*	*0.05*	*0.02*	*0.03*	*0.01*	*0.05*	*0.01*
O'Higgins guyot															
2D-1	11.7	50.1	103.2	12.16	50.3	9.34	3	8.76	1.24	6.66	1.08	3.09	0.41	2.3	0.36
2D-2	5.2	51.2	107.8	12.81	52.2	9.93	2.97	9.3	1.28	6.46	1.17	3.11	0.41	2.56	0.33
Robinson Crusoe Island															
LL230711-2	3	64.1	116.9	13.35	48.6	9.25	2.87	7.86	1.2	6.09	1.17	3.17	0.47	2.88	0.42
LL230711-8	2.7	52.2	102.5	11.7	46.5	8.6	2.74	7.63	1.17	5.67	1.09	2.76	0.39	2.19	0.32
JR250112-2	2	47	91.4	10.77	40.5	7.95	2.6	7.18	1.07	5.83	1.05	2.74	0.37	2.04	0.31
JR250112-3	1.6	39.9	76.1	9.22	37.4	6.96	2.31	6.57	0.93	5.24	0.91	2.3	0.33	2.01	0.26
LL060213-4	3.1	67.3	127.5	15.04	55.4	10.17	3.1	8.55	1.28	6.96	1.25	3.36	0.46	2.72	0.45
LL230112-2	2.1	62	118.3	14.13	58.4	10.48	3.39	10.58	1.29	7.87	1.35	3.2	0.45	2.79	0.41
LL230112-4	1.9	58.7	117.4	13.54	56.4	10.9	3.43	10.77	1.3	7.67	1.31	3.23	0.44	2.92	0.4
JR230112-1	1.2	49.4	93.8	11.14	45.4	8.16	2.61	7.77	1.14	6.48	1.08	2.97	0.39	2.54	0.32
JR230112-2	0.4	48	91.2	10.81	42.4	8.18	2.5	7.59	1.11	5.84	1.06	2.75	0.4	2.4	0.33
JR230112-3	3	61.3	118.3	13.63	52	9.94	3.16	9.19	1.28	7	1.3	3.31	0.47	2.83	0.39
JR160913-2	2.6	59.8	113.8	13.24	51.2	9.26	2.87	8.25	1.23	6.48	1.27	3.21	0.46	2.81	0.41
MP270112-3	2.4	64.1	121.4	13.82	52.7	9.46	3	8.62	1.24	7.05	1.23	3.58	0.49	2.99	0.45
JR020613-3	3.8	64.2	120.2	13.94	54	9.8	3.01	8.41	1.19	6.65	1.27	3.38	0.48	2.73	0.42
LL010213-6	1	62.7	122	14.56	54.1	10.36	3.25	9.34	1.28	6.99	1.33	3.36	0.43	2.63	0.41
JR220112-4A	1.3	50.7	98.3	11.75	47.9	8.97	2.79	7.76	1.17	6.56	1.15	2.83	0.42	2.47	0.35
LL220112-1	2.2	48.5	91.1	10.63	45	8.26	2.8	7.85	1.26	6.42	1.15	2.88	0.37	2.34	0.32
JR220112-3	1.3	39.1	76.8	8.79	35.5	6.78	2.16	6.74	0.97	5.14	0.91	2.44	0.33	1.94	0.27
JR250513-3	2.3	51.2	97.7	11.27	41.6	8.05	2.55	7.85	1.12	5.95	1.02	2.59	0.37	2.3	0.33
LL220112-4	0.8	65.7	122.4	13.75	52.5	9.59	2.97	8.53	1.25	6.98	1.21	3.27	0.47	2.83	0.45
JR250513-9	3.1	67.5	127.8	14.74	54.8	10.17	3.18	9	1.28	6.6	1.19	3.14	0.45	2.74	0.4

Table VI.3. Radiogenic isotopic composition of whole-rock representative samples from O'Higgins and Robinson Crusoe rejuvenated stages. Standard error (2σ) and laboratory of analysis are indicated (a: GEOMAR Helmholtz Center, Kiel, Germany. b: Laboratoire Magmas and Volcans, Clermont-Ferrand, France). (rep: replicate. *: sample analyzed in both laboratories).

Sample	$^{87}Sr/^{86}Sr$	±	$^{143}Nd/^{144}Nd$	±	$^{206}Pb/^{204}Pb$	±	$^{207}Pb/^{204}Pb$	±	$^{208}Pb/^{204}Pb$	±	Lab
O'Higgins guyot											
2D-1	-		0.512830	5	19.2249	17	15.5965	14	39.1345	36	(a)
2D-2	0.703544	5	0.512831	5	19.2211	13	15.5924	10	39.1230	27	(a)
Robinson Crusoe Island											
LL230711-2	0.703537	6	0.512842	6	-		-		-		(b)
LL230711-8	0.703501	6	0.512850	5	-		-		-		(b)
JR250112-3	0.703477	4	0.512873	5	19.1684	17	15.5888	13	39.0716	33	(a)
LL230112-4	0.703469	5	0.512868	3	19.1394	6	15.5902	5	39.1037	16	(a)
JR230112-1	0.703414	5	0.512869	4	19.2210	7	15.5942	8	39.1562	28	(a)
JR230112-1 rep	0.703402	5	0.512869	3	19.2200	7	15.5935	9	39.1538	29	(a)
JR230112-3	0.703508	6	0.512851	6	-		-		-		(b)
JR160913-2	0.703466	5	0.512861	4	19.1866	14	15.5893	12	39.1392	34	(a)
MP270112-3	0.703551	6	0.512854	4	-		-		-		(b)
JR020613-3	0.703520	5	0.512870	2	19.1016	8	15.5845	8	39.0787	28	(a)
LL010213-6	0.703488	5	0.512865	5	19.1351	8	15.5888	8	39.1004	26	(a)
JR220112-3	0.703386	4	0.512871	3	19.2404	6	15.5961	7	39.1372	22	(a)
JR220112-3 *	0.703411	4	0.512866	5	-		-		-		(b)

Figure VI.1. Total-alkali vs. silica (TAS) classification diagram for lavas and dykes from shield and rejuvenated stages in Juan Fernández Ridge (O'Higgins, Alpha, Robinson Crusoe and Alejandro Selkirk volcanoes) (after Le Maitre, 2002; alkali-subalkali boundary is from Irvine and Baragar, 1971).

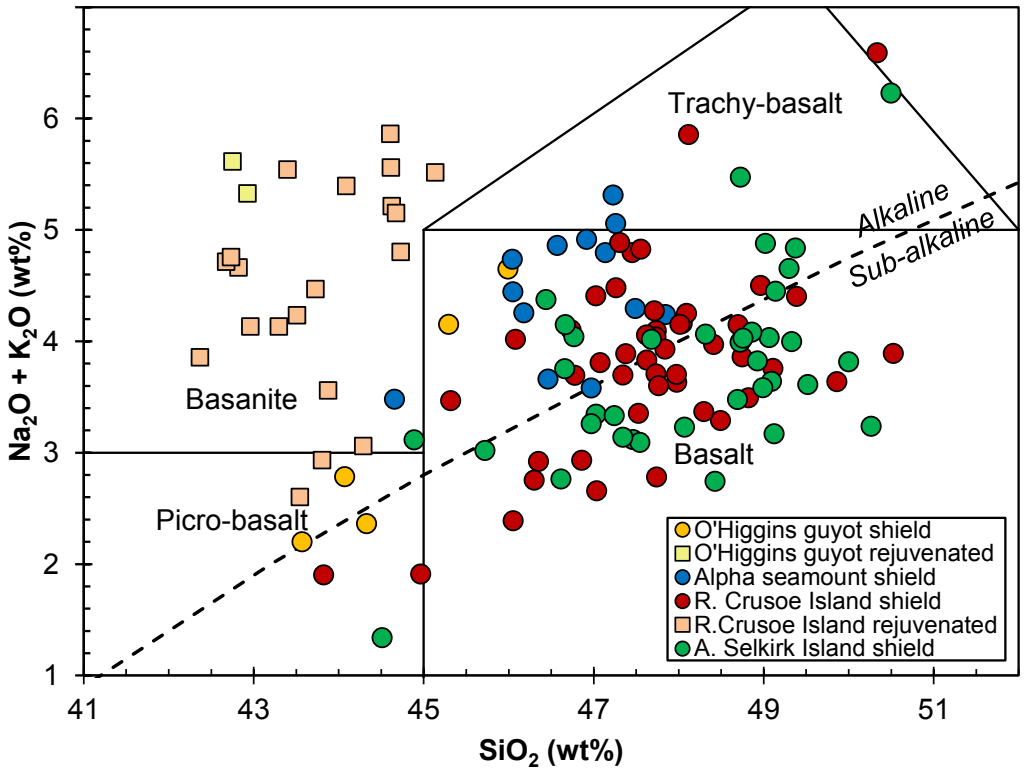

Figure VI.2. Primitive mantle-normalized (PM from Sun and McDonough, 1989) trace element content patterns of lavas from rejuvenated volcanism in O'Higgins and Robinson Crusoe volcanoes. Average values of shield stage compositional groups ('olivine-rich', 'near-primitive' and 'differentiated') are also showed.

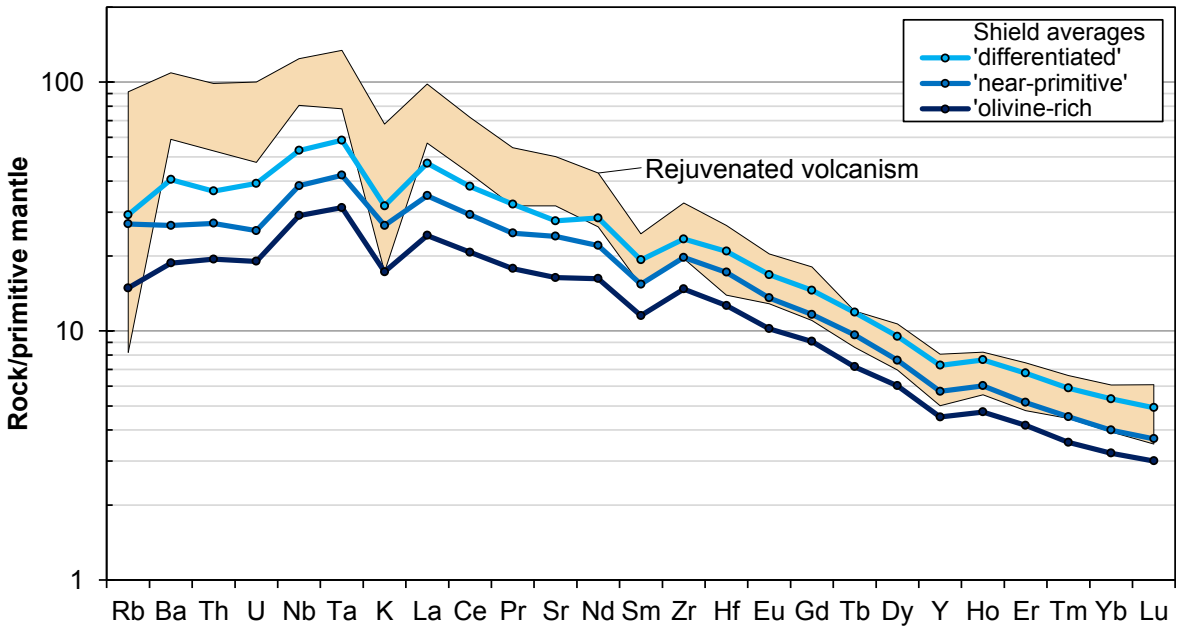

Figure VI.3. Trace element ratios La/Yb vs. Nb/Zr as discriminant between lavas from shield and rejuvenated stages in Juan Fernández Ridge (O'Higgins, Alpha, Robinson Crusoe and Alejandro Selkirk).

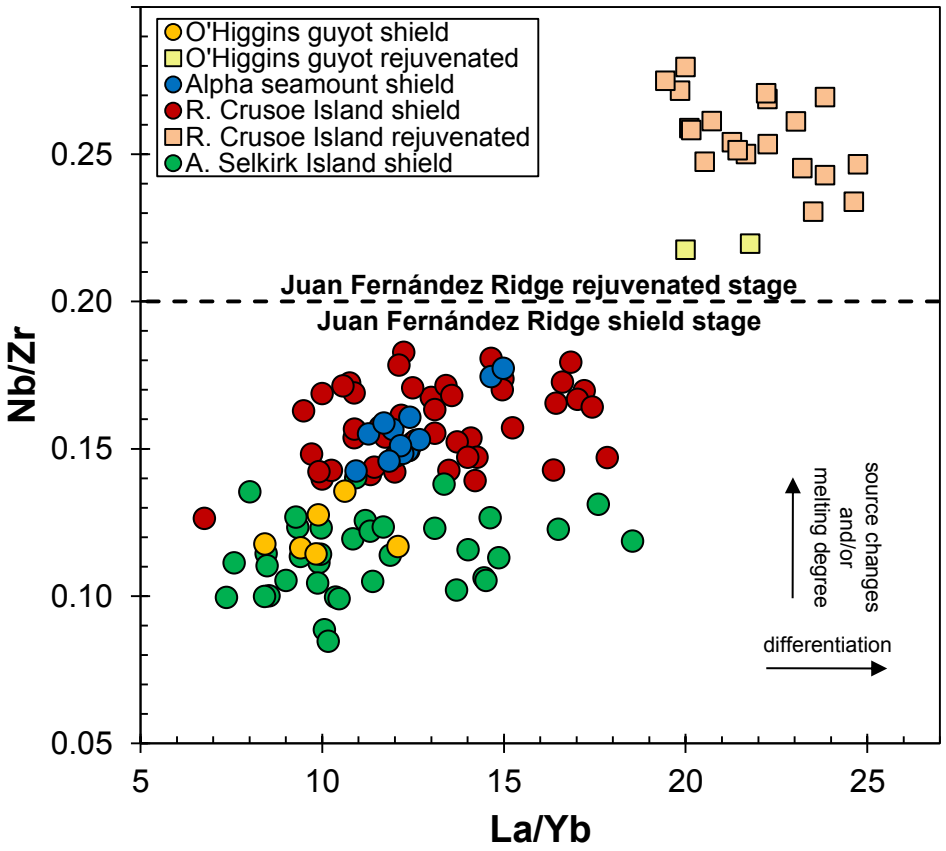

Figure VI.4. Isotopic variation plots of the shield and rejuvenated stages in Juan Fernández Ridge. a) $^{206}Pb/^{204}Pb$ vs. $^{207}Pb/^{204}Pb$ and $^{208}Pb/^{204}Pb$ show values near to FOZO-A with additional participation of HIMU and EMI sources. b) $^{87}Sr/^{86}Sr$ vs. $^{143}Nd/^{144}Nd$ also show HIMU signature (more evident in rejuvenated volcanism), but away of FOZO-A.

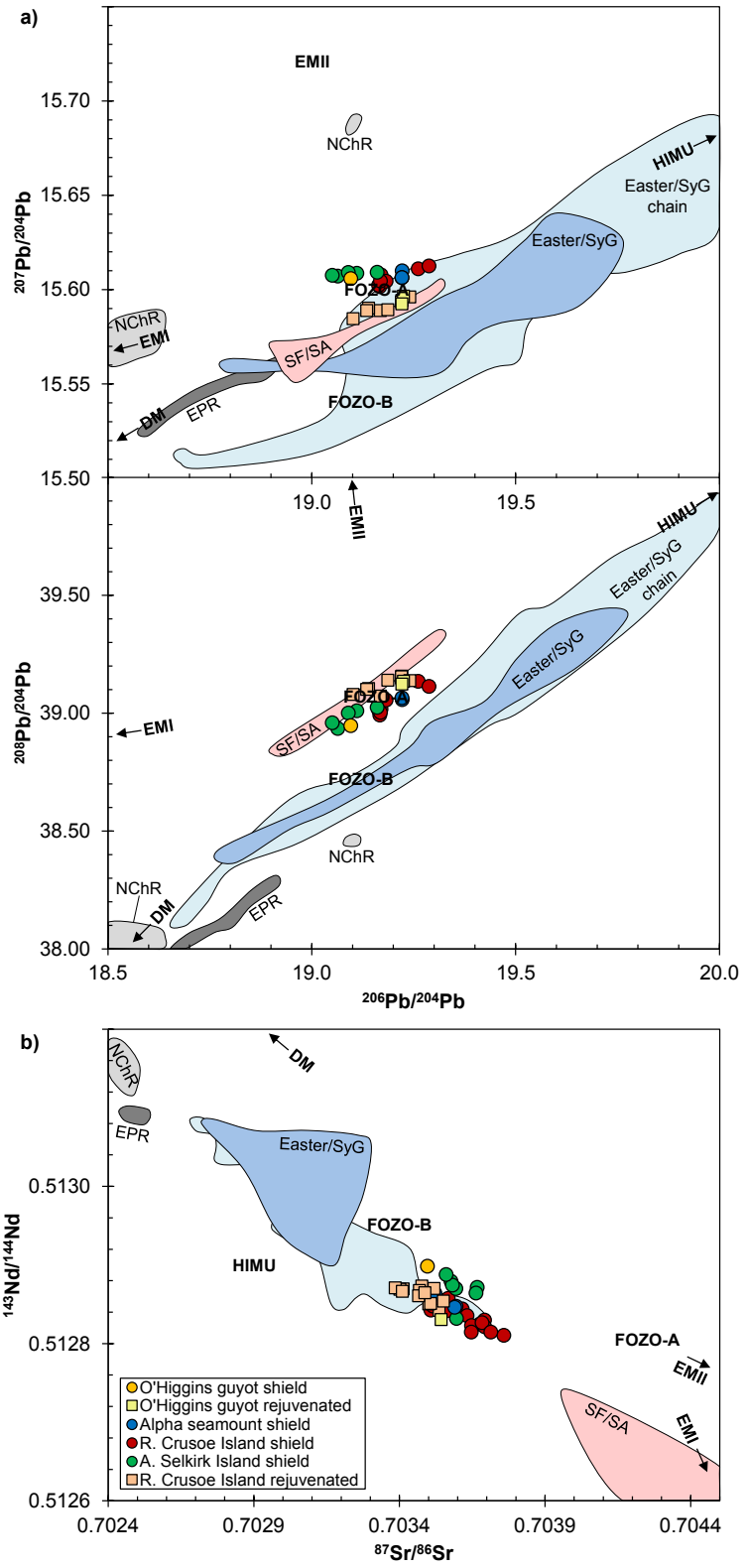

Capítulo VII

Discusión general

VII.1. Etapas del volcanismo en la Dorsal de Juan Fernández y su patrón de ascenso y almacenamiento magmático

En base a observaciones de campo y datos geocronológicos (confirmado con signatura geoquímica e isotópica), es posible establecer la presencia de lavas representativas de dos etapas de volcanismo diferentes en la Dorsal de Juan Fernández (JFR) (en base a la evolución típica observada en Hawaii; e.g., García et al., 2015; y en otros sistemas de intraplaca oceánicos; e.g., Konter et al*.,* 2012): la etapa de escudo, y la de volcanismo rejuvenecido (o post-erosional). El escudo se constituye principalmente de volumétricas secuencias de basaltos (toleíticos, transicionales y alcalinos) y picritas reconocidas en O'Higgins, Alpha, Robinson Crusoe y Alejandro Selkirk. En tanto, la secuencia rejuvenecida se desarrolla tras un periodo de inactividad volcánica, y está formada por basanitas intercaladas con depósitos piroclásticos de la misma composición que se han reportado en el techo del guyot O'Higgins, y en torno a diversos centros de emisión poco volumétricos en Robinson Crusoe. Las basanitas rejuvenecidas se caracterizan por un notable enriquecimiento (respecto al volcanismo de escudo) en elementos incompatibles (reflejado, por ejemplo, en altos valores de Nb/Zr y La/Yb), y en la razón isotópica de $^{208}Pb/^{204}Pb$; junto a empobrecimiento en $^{207}Pb/^{204}Pb$ y $^{87}Sr/^{86}Sr$.

Mediante análisis texturales, y cálculos geotermobarométricos (Nimis y Ulmer, 1998; Herzberg y O'Hara, 2002; Putirka et al., 2003) a partir de datos EPMA de química mineral (en olivino y clinopiroxeno) se pueden establecer patrones de ascenso contrastantes para las lavas que formaron el volcanismo de escudo, y el rejuvenecido en JFR. En efecto, la etapa de escudo se caracteriza por la formación de cámaras magmáticas someras (< 3.2 kbar), donde los magmas basálticos pueden diferenciarse; principalmente por cristalización fraccionada de olivino, clinopiroxeno y plagioclasa (y disminuir su temperatura hasta 1156 – 1181 °C); ser parcialmente mezclados con magmas menos evolucionados, o sufrir procesos de acumulación cristalina, lo que explica la variedad de rocas muestreadas en cada edificio volcánico. En tanto, el volcanismo rejuvenecido se caracteriza por el ascenso mucho más directo, con ocasional captura de xenocristales (mantélicos y corticales) y cristalización polibárica (e.g., 1.7 – 10.3 kbar en un mismo cristal), de magmas más primitivos y con mayor temperatura (en torno a 1300 °C), que pueden formar pequeñas cámaras magmáticas con cortos periodos de residencia.

VII.2. Origen del magmatismo intraplaca de JFR

El origen del magmatismo intraplaca es un tema controversial en ciencias de la Tierra. Básicamente existen dos visiones extremas que explican su génesis: la teoría de plumas mantélicas de origen profundo (e.g., Morgan, 1972), y la de origen somero asociado a variaciones normales en el contexto de tectónica de placas (e.g., Anderson, 2005). En el caso de JFR, su puntuación en catálogos de eventuales plumas del manto es relativamente alto (Courtillot et al., 2003; Anderson, 2005; Jackson et al., 2017), principalmente debido a los altos valores de la razón $^{3}He/^{4}He$ (Farley et al., 1993) que sugieren un origen en manto profundo. En tanto, los análisis de tomografías sísmicas muestran interpretaciones dispares. Boschi et al. (2007) no reconoce a Juan Fernández

como pluma, sino más bien asociado a procesos someros, mientras que Montelli et al. (2006) si lo incluye como pluma, pero de profundidad media, y French and Romanowicz (2015) como un conducto vertical, pero no claramente continuo.

Dos aspectos claves utilizados como argumento a favor de un origen asociado a pluma mantélica son la existencia de LIP ('large igneous provinces') al inicio de la cadena, y progresión de edades concordante al movimiento de la placa oceánica subyaciente en los edificios volcánicos alineados (e.g., Niu et al., 2017). JFR no tiene LIP asociado, o bien este pudo ser subductado en el pasado, por lo que es un aspecto imposible de evaluar. La progresión de edades fue evaluada en esta tesis mediante geocronología $^{40}Ar/^{39}Ar$ en 4 volcanes de JFR que cubren ~650 km (Capítulo IV), y muestran una progresión concordante al movimiento calculado para la placa de Nazca, aspecto que resulta clave en asignar el origen de JFR a una pluma del manto, probablemente de temperatura relativamente baja (Capítulo V). Otros mecanismos propuestos como origen del volcanismo intraplaca, por ejemplo, hidrofracturas magmáticas formadas por stress flexural en presencia de una carga volcánica (Hieronymus and Bercovici, 2000), fracturas inducidas por cambios en la dirección de movimiento una placa respecto a la fosa (propuesto por Anderson, 2005 para JFR) y convecciones sublitosféricas de pequeña escala (Ballmer et al., 2007) no son capaces de explicar la progresión de edades observada en JFR, ni se reflejan en estructuras (observadas o inferidas) en la placa de Nazca.

Un aspecto interesante de desarrollar en estudios futuros sería revisitar la isotopía de $^{3}He/^{4}He$, incluyendo nuevos volcanes de JFR y siguiendo un riguroso control estratigráfico. Altos valores como los reportados por Farley et al. (1993) para Robinson Crusoe y Alejandro Selkirk suelen ser asociados con fuentes del manto profundas, pero dicho estudio se centra principalmente en rodados recolectados desde las costas de las islas. Nuevos estudios permitirían caracterizar en detalle la isotopía de cada etapa evolutiva, y aportar al conocimiento global sobre el comportamiento del helio en fuentes del manto tipo FOZO-A, HIMU y DM.

VII.3. Características de la pluma mantélica bajo JFR

Si bien es complejo determinar la profundidad del origen de la pluma bajo JFR, si es posible cuantificar algunas de sus características y comprender las características del manto bajo la placa de Nazca en el Pacífico SE a partir de la composición de las rocas volcánicas representativas de la etapa de escudo en JFR. En base a su signatura geoquímica se determina la presencia de fuente tipo FOZO-A en la petrogénesis, junto a participación (adicional a la que ya tiene en la mezcla relativamente homogénea que constituye FOZO-A) de fuentes HIMU y DM. HIMU preferencialmente muestreada en Robinson Crusoe y Alpha, y DM en Alejandro Selkirk y O'Higgins, lo que sugiere la existencia de leves heterogeneidades mantélicas en la pluma. Adicionalmente, en base a la isotopía, geoquímica y resultados del modelo OBS1 (Kimura y Kawabata, 2015; parámetros detallados en Capítulo V) se propone la presencia de piroxenitas como heterogeneidad en la pluma, con presencia relativamente baja (en promedio 6 a 9 wt%), pero importante participación en el volcanismo debido a su mayor facilidad para fundirse (e.g., Pertermann y Hirschmann, 2003). Dicha pluma también se caracteriza por una temperatura potencial baja (en promedio levemente superior a 1300 °C), similar al manto ambiente (e.g., Herzberg et al., 2007) y a algunas otras plumas donde se ha propuesto un alto contenido de volátiles (Nichols et al., 2002; Metrich et al., 2014),

situación que podría repetirse en JFR. Variaciones en la fracción de piroxenitas (4 – 8 vs 6 – 12 wt%), temperatura potencial de la pluma heterogénea (1290 – 1322 vs. 1312 – 1362 °C), y en la tasa de fusión parcial (2.8 – 4.9 vs 5.2 – 11.4 wt%) bajo Robinson Crusoe (y Alpha) respecto a Alejandro Selkirk (y O'Higgins) explican las variaciones geoquímicas e isotópicas observadas.

Las bajas temperaturas estimadas para el manto que genera los magmas de JFR (parecidas al manto ambiente) complican la explicación del origen de la buoyancia en la pluma mantélica. De hecho, estas bajas temperaturas, junto a las condiciones de presión estimadas, de cierta manera argumentan a favor de un origen diferente al de pluma (por ejemplo, asociado a procesos más superficiales). Sin embargo, la progresión de edades observada (Capítulo III) a lo largo de la cadena implica un origen a partir de una fuente estática tipo pluma. Una posible explicación para la buoyancia sería considerar la posibilidad de que JFR se genera a partir de una pluma termoquímica (del tipo secundaria), con probable buoyancia baja, y temperatura levemente superior al manto ambiente (Dannberg y Sobolev, 2015). Esta opción implica un origen de profundidad media, lo que ha sido sugerido para JFR en base a estudios de tomografía sísmica (Montelli et al., 2006; French and Romanowicz, 2015). Los alcances de este estudio pueden ser de importancia para entender el volcanismo intraplaca con progresión de edades sin temperaturas potenciales demasiado superiores a las reportadas para el manto ambiente, y contribuyen al conocimiento de la situación térmica de la astenosfera bajo la placa de Nazca.

En tanto, el volcanismo rejuvenecido, reportado en O'Higgins y Robinson Crusoe, posee una signatura isotópica similar (solo muy sutilmente diferente) al volcanismo de escudo, lo que sugiere que su fuente es básicamente la misma, probablemente con leves variaciones composicionales esperables dada la naturaleza heterogénea de la pluma. La notable alcalinidad de los magmas rejuvenecidos se explica por una tasa de fusión parcial considerablemente menor que en la etapa de desarrollo del escudo, posiblemente a una temperatura potencial aún menor, y muestreo selectivo proporcionalmente mayor de fuente tipo DM (con leve enriquecimiento en $^{207}Pb/^{204}Pb$). Las razones que permiten la fusión parcial de la pluma tras un periodo variable de inactividad volcánica (de al menos ~ 0.25 Ma en O'Higgins, y ~ 1.73 Ma en Robinson Crusoe) son enigmáticas, pero los modelos propuestos en la literatura pueden ser evaluados para el caso de JFR. El modelo térmico de Gurriet (1987) se descarta debido a que implica la participación exclusiva de litósfera, lo que es descartado dada la signatura isotópica notablemente enriquecida del volcanismo rejuvenecido en JFR. El modelo de alzamiento por respuesta flexural a la formación de un nuevo edificio volcánico (Bianco et al., 2005) no aplica en el caso de JFR, ya que el bajo espesor elástico de la placa de Nazca (Manríquez et al., 2015) genera deformación flexural con baja longitud de onda (< 80 km; Orozco, 2016), considerablemente menor a la distancia entre Robinson Crusoe y Alejandro Selkirk (que tienen volcanismo rejuvenecido y de escudo coetáneo). Las otras teorías planteadas, es decir, segunda zona de fusión en la pluma (que implica una región de generación magmática levemente más profunda; Ribe y Christensen, 1999), y pequeñas celdas convectivas sub-litosféricas que generan regiones con leves descompresiones capaces de generar fusión (Ballmer et al., 2011) deben ser críticamente evaluadas, idealmente en presencia de datos geofísicos de alta resolución.

Una característica enigmática de JFR es el gap de estructuras volcánicas por ~250 km existente al W del guyot O'Higgins. Una explicación especulativa radica en la baja temperatura potencial de la pluma bajo JFR. Luego, un leve descenso en ella podría impedir las condiciones apropiadas para la generación de fusión parcial, lo que podría ocurrir al W de O'Higgins. Esta condición es interrumpida por un eventual aumento de la temperatura en la formación de Alpha y Robinson Crusoe, estructuras volcánicas emplazadas sobre la zona de fractura de Challenger, una estructura de primer orden de la placa de Nazca, que podría facilitar las condiciones para restituir los procesos de fusión parcial.

Estudios de inclusiones fundidas y fluidas permitirían caracterizar el contenido de volátiles en las distintas etapas evolutivas de JFR, lo que posibilitaría evaluar la hipótesis de un alto contenido relativo de estos en la pluma del manto asociada a su petrogénesis, y establecer comparaciones con los valores reportados de volátiles para el manto en otras regiones bajo Nazca (e.g., en la cadena volcánica de Pascua, Simons et al., 2002). Los estudios geoquímicos sugeridos, junto a los aportados por esta tesis, permitirían clarificar la signatura isotópica y geoquímica de JFR, lo que facilitaría la evaluación de su eventual impacto en el magmatismo de arco existente en el margen Sudamericano.

Bibliografía

Anderson, D.L. 2005. Scoring hotspots: The plume and plate paradigms. In: Plates, plumes and paradigms, Foulger, G.R., Natland, J.H., Presnall, D.C., Anderson, D.L. doi.org/10.1130/SPE388

Ballmer, M.D., van Hunen, J., Ito, G., Tackley, P.J., Bianco, T. a., 2007. Non-hotspot volcano chains originating from small-scale sublithospheric convection. Geophys. Res. Lett. 34. doi:10.1029/2007GL031636

Ballmer, M.D., Ito, G., van Hunen, J., Tackley, P.J., 2011. Spatial and temporal variability in Hawaiian hotspot volcanism induced by small-scale convection. Nat. Geosci. 4, 457–460. doi:10.1038/ngeo1187

Bianco, T.A., Ito, G., Becker, J.M., Garcia, M.O., 2005. Secondary Hawaiian volcanism formed by flexural arch decompression. Geochemistry, Geophys. Geosystems 6, 1–24. doi:10.1029/2005GC000945

Boschi, L., Becker, T.W., Steinberger, B. 2007. Mantle plumes: Dynamic models and seismic images, Geochem. Geophys. Geosyst., 8, Q10006, doi: 10.1029/2007GC001733

Courtillot, V., Davaille, A., Besse, J., Stock, J., 2003. Three distinct types of hotspots I the Earth's mantle. Earth Planet. Sci. Lett. 205, 295–308. doi.org/10.1016/S0012-821X(02)01048-8

Dannberg, J., Sobolev, S.V. 2015. Low-buoyancy thermochemical plumes resolve controversy of classical mantle plume concept. Nature Communication 6 (6960). doi.org/10.1038/ncomms7960

Farley, K.A., Basu, A.R., Craig, H., 1993. He, Sr and Nd isotopic variations in lavas from the Juan Fernandez Archipelago, SE Pacific. Contrib. to Mineral. Petrol. 115, 75–87. doi:10.1007/BF00712980

French, S.W., Romanowicz, B., 2015. Broad plumes rooted at the base of the Earth's mantle beneath major hotspots. Nature 525, 95–99. doi.org/10.1038/nature14876

Garcia, M.O., Smith, J.R., Tree, J.P., Weis, D., Harrison, L., Jicha, B.R., 2015. Petrology, geochemistry, and ages of lavas from Northwest Hawaiian Ridge volcanoes. Geological Society of America Special Papers 511 . doi:10.1130/2015.2511(01)

Gurriet, P., 1987. A thermal model for the origin of post-erosional alkalic lava, Hawaii. Earth Planet. Sci. Lett. 82, 153–158. doi:10.1016/0012-821X(87)90115-4

Herzberg, C., O'Hara, M.J., 2002. Plume-associated ultramafic magmas of Phanerozoic age. J. Petrol. 43, 1857–1883. doi:10.1093/petrology/43.10.1857

Herzberg, C., Asimow, P.D., Arndt, N., Niu, Y., Lesher, C.M., Fitton, J.G., Cheadle, M.J., Saunders, A.D., 2007. Temperatures in ambient mantle and plumes: Constraints from basalts, picrites, and komatiites. Geochemistry, Geophys. Geosystems 8, Q02006. doi.org/10.1029/2006GC001390

Hieronymus, C.F., Bercovici, D., 2000. Non-hot spot formation of volcanic chains: Controls of tectonic stresses on magma transport. Earth Planet. Sci. Lett. 181, 539–554. doi:10.1016/S0012-821X(00)00227-2

Jackson, M.G., Konter, J.G., Becker, T.W., 2017. Primordial helium entrained by the hottest mantle plumes. Nature 542, 340–343. doi.org/10.1038/nature21023

Kimura, J.-I., Kawabata, H., 2015. Ocean Basalt Simulator version 1 (OBS1): Trace element mass balance in adiabatic melting of a pyroxenite-bearing peridotite. Geochemistry, Geophys. Geosystems 16, 267–300. doi.org/10.1002/2014GC005606

Konter, J.G., Jackson, M.G., 2012. Large volumes of rejuvenated volcanism in Samoa: Evidence supporting a tectonic influence on late-stage volcanism. Geochemistry, Geophys. Geosystems 13. doi:10.1029/2011GC003974

Manríquez, P., Contreras-Reyes, E., Osses, A., 2014. Lithospheric 3-D flexure modelling of the oceanic plate seaward of the trench using variable elastic thickness. Geophys. J. Int. 196, 681–693. doi.org/10.1093/gji/ggt464

Métrich, N., Zanon, V., Créon, L., Hildenbrand, A., Moreira, M., Marques, F.O., 2014. Is the “Azores hotspot” a wetspot? Insights from the geochemistry of fluid and melt inclusions in olivine of Pico basalts. J. Petrol. 55, 377–393. doi.org/10.1093/petrology/egt071

Montelli, R., Nolet, G., Dahlen, F.A., Masters, G., 2006. A catalogue of deep mantle plumes: New results from finite-frequency tomography. Geochemistry, Geophys. Geosystems 7, Q11007. doi.org/10.1029/2006GC001248

Morgan, W.J., 1972. Deep mantle convection plumes and plate motions. Am. Assoc. Pet. Geol. Bull: 56(2), 203–213. doi:10.1306/819A3E50-16C5-11D7-8645000102C1865D

Nichols, A.R.L., Carroll, M.R., Höskuldsson, Á., 2002. Is the Iceland hot spot also wet? Evidence from the water contents of undegassed submarine and subglacial pillow basalts. Earth Planet. Sci. Lett. 202, 77–87. doi:10.1016/S0012-821X(02)00758-6

Nimis, P., Ulmer, P., 1998. Clinopyroxene geobarometry of magmatic rocks Part 1: An expanded structural geobarometer for anhydrous and hydrous, basic and ultrabasic systems. Contrib. to Mineral. Petrol. 133, 122–135. doi:10.1007/s004100050442

Niu, Y., Shi, X., Li, T., Wu, S., Sun, W., Zhu, R. 2017. Testing the mantle plume hypothesis: an IODP effort to drill into the Kamchatka-Okhotsk Sea basement. Science Bulletin 62 (21): 1464–1472. doi.org/10.1016/j.scib.2017.09.019

Pertermann, M., Hirschmann, M.M., 2003. Partial melting experiments on a MORB-like pyroxenite between 2 and 3 GPa: Constraints on the presence of pyroxenite in basalt source regions from solidus location and melting rate. J. Geophys. Res. Solid Earth 108, 1–17. doi.org/10.1029/2000JB000118

Putirka, K.D., Mikaelian, H., Ryerson, F., Shaw, H. 2003. New clinopyroxene-liquid thermobarometers for mafic, evolved, and volatile-bearing lava compositions, with applications to lavas from Tibet and the Snake River Plain, Idaho. Am. Mineral. 88, 1542–1554. doi:10.2138/am-2003-1017

Ribe, N.M., Christensen, U.R., 1999. The dynamical origin of Hawaiian volcanism. Earth Planet. Sci. Lett. 171, 517–531. doi:10.1016/S0012-821X(99)00179-X

Simons, K., Dixon, J., Schilling, J.-G., Kingsley, R., Poreda, R., 2002. Volatiles in basaltic glasses from the Easter-Salas y Gomez Seamount Chain and Easter Microplate: Implications for geochemical cycling of volatile elements. Geochemistry, Geophys. Geosystems 3, 1–29. doi.org/10.1029/2001GC000173

Sleep, N.H., 1990. Hotspots and mantle plumes: Some phenomenology. J. Geophys. Res. 95, 6715. doi.org/10.1029/JB095iB05p06715

Capítulo VIII

Conclusiones

La Dorsal de Juan Fernández (JFR) es un clásico ejemplo de magmatismo intraplaca alejado de márgenes activos, lo que supone una oportunidad única para estudiar las características del manto en el Pacífico SE. En efecto, sus características composicionales en conjunto a la geocronología $^{40}Ar/^{39}Ar$ muestran una progresión de edades concordante con el movimiento estimado para la Placa de Nazca, validando su formación mediante el ascenso de una pluma mantélica.

El guyot O'Higgins (~ 9.26 – 8.41 Ma), monte submarino Alpha (~ 4.63 – 4.58 Ma), islas Robinson Crusoe (~ 4.10 – 3.40 Ma) y Alejandro Selkirk (~ 0.94 – 0.83 Ma) son los principales edificios volcánicos constituyentes de JFR. Están formados principalmente por basaltos (toleíticos, transicionales y alcalinos) representativos de una etapa de volcanismo de escudo. Características geoquímicas (alto contenido de TiO_2, alto FC3MS, anomalía TITAN y empobrecimientos en CaO, Rb y U) e isotópicas (participación de fuentes asociadas a litologías recicladas como FOZO-A) sugieren la presencia de piroxenitas en la fuente mantélica asociada a este volcanismo como una heterogeneidad en un medio dominado por peridotitas. Mediante modelos basados en el comportamiento de elementos incompatibles se cuantifican diversos parámetros de la pluma mantélica, estableciendo una baja temperatura potencial (< 1360 °C, similar al manto ambiente), probablemente debido a la importante concentración de volátiles; una presión de término de fusión (~ 2.4 GPa) correlacionable al límite litósfera-astenósfera; y confirmando una importante contribución al melt final de fundidos provenientes de piroxenita (hasta de 56.4 wt%) pese a su baja presencia como litología (< 12 wt%).

La signatura geoquímica de las lavas de escudo en Robinson Crusoe y Alpha es más enriquecida que en Alejandro Selkirk y O'Higgins, estos últimos además están caracterizados por una mayor presencia de fuente DM en su génesis. Dichas diferencias se explican por sutiles variaciones en la temperatura potencial (~ 30 °C mayor, en promedio, en Alejandro Selkirk) del manto bajo cada conjunto volcánico (y sus consecuentes variaciones en la tasa de fusión parcial), y diferencias temporales sutiles en la proporción de peridotitas empobrecidas y enriquecidas. Las variaciones geoquímicas internas se explican por cristalización fraccionada de olivino + clinopiroxeno ± plagioclasa (generando un descenso de temperatura hasta ~ 1156 – 1181 °C), mezcla parcial entre magmas primitivos (formados a ~ 1321 °C) y diferenciados, y acumulación de cristales de olivino. Estos procesos ocurren en una cámara magmática superficial (~1 a 3 kbar), que a la vez es responsable del rápido crecimiento, por ejemplo, de Robinson Crusoe.

Además, algunos volcanes de JFR, en particular O'Higgins y Robinson Crusoe, exhiben secuencias volcánicas con características de campo (e.g., relleno de paleo-valles) que indican una edad inferior al ya mencionado volcanismo de escudo. En efecto, estas coladas son a lo más ~ 0.25 Ma más jóvenes que el escudo en O'Higgins y ~ 1.73 Ma en Robinson Crusoe y corresponden a la etapa de volcanismo rejuvenecido en JFR. Se componen de basanitas marcadamente enriquecidas en elementos incompatibles con signatura isotópica parecida al escudo, pero con leve empobrecimiento en $^{207}Pb/^{204}Pb$ y $^{87}Sr/^{86}Sr$. Se propone que estas características se explican por sutiles variaciones en la participación de piroxenitas y un menor grado de fusión parcial en una pluma mantélica

muy similar a la que originó el magmatismo de escudo. Estas basanitas ascienden rápidamente experimentando cristalización polibárica, y capturando ocasionalmente xenocristales de diversos orígenes (mantélico y cortical), algunos de estos magmas son almacenados por poco tiempo en pequeños reservorios magmáticos superficiales (~ 1256 – 1295 °C), mientras que otros ascienden directo (~ 1316 – 1354 °C) antes de alimentar erupciones de poco volumen. Esta profundización en la cristalización de lavas pertenecientes a volcanismo posterior a la etapa de escudo también ha sido reconocida en otros ambientes de intraplaca y parece ser un patrón a escala global.

Luego, las diferencias químicas e isotópicas entre los distintos edificios volcánicos y sus etapas evolutivas se explican por sutiles variaciones composicionales en la fuente, y fundamentalmente, por cambios en la tasa de fusión para cada volcán, diferencias en la temperatura potencial del manto, y variaciones en el patrón de ascenso y almacenamiento magmático en el contexto de una pluma mantélica heterogénea con baja temperatura y presencia de fuente FOZO-A con contribución adicional de DM.

Anexo

Las tablas A.1 y A.2 incluyen los datos aún no publicados (en revision) para el guyot O'Higgins.

Table A.1. Contenido de elementos mayores (wt%) y Ni (ppm) en lavas del guyot O'Higgins (etapas de escudo y rejuvenecida) incluidas en Lara et al. (submitted).

Sample	SiO_2	TiO_2	Al_2O_3	$Fe_2O_3^T$	MgO	MnO	CaO	Na_2O	K_2O	P_2O_5	Ni	LOI	Sum
Det. limit	*0.01*	*0.01*	*0.01*	*0.04*	*0.01*	*0.01*	*0.01*	*0.01*	*0.01*	*0.01*	*0.1*	*0.1*	
Shield stage													
D10-2	39.72	2.72	13.80	14.87	4.21	0.47	11.89	3.06	1.12	2.82	130.3	4.80	99.48
D10-5	42.95	1.97	10.13	14.30	18.73	0.28	7.62	1.74	0.43	0.43	772.0	0.70	99.28
D10-7	43.88	2.15	11.04	13.74	17.21	0.18	8.14	1.89	0.45	0.31	661.0	0.30	99.29
D10-10	43.92	2.93	15.01	13.01	5.39	0.67	9.59	3.20	1.24	0.54	196.8	4.10	99.60
D10-18	42.54	1.99	9.72	14.33	19.45	0.19	5.41	1.85	0.84	0.21	711.2	2.70	99.23
D10-42	43.29	3.06	15.09	13.33	5.77	0.15	9.87	3.12	0.85	1.05	139.4	4.00	99.58
Rejuvenated stage													
2D-1	41.90	4.24	13.08	14.23	8.75	0.19	9.24	3.54	1.66	0.78	136.4	1.90	99.51
2D-2	41.66	4.15	13.12	13.82	9.00	0.19	9.24	3.43	2.04	0.80	124.1	2.00	99.45

Table A.2. Contenido de elementos traza (ppm, Cr_2O_3 en wt%) para lavas del guyot O'Higgins (etapas de escudo y rejuvenecida) incluidas en Lara et al. (submitted).

Sample	Cr_2O_3	Sc	Ba	Co	Ga	Hf	Nb	Rb	Sr	Ta	Th	U	V	Zr	Y
Det. limit	*0.002*	*1*	*1*	*0.2*	*0.5*	*0.1*	*0.1*	*0.1*	*0.5*	*0.1*	*0.2*	*0.1*	*8*	*0.1*	*0.1*
Shield stage															
D10-2	0.055	22	1083	92.0	24.3	6.0	31.2	16.8	742.3	1.8	2.3	2.7	380	268.0	34.4
D10-5	0.181	20	101	123.8	17.0	4.2	22.6	8.2	420.0	1.4	1.7	0.5	258	166.6	22.1
D10-7	0.158	22	106	102.0	18.1	4.3	22.9	8.0	437.1	1.4	1.6	0.4	251	179.4	22.0
D10-10	0.047	24	230	81.6	25.5	6.4	32.6	18.5	565.7	2.1	2.9	3.0	347	278.8	54.6
D10-18	0.172	18	116	111.5	13.6	3.7	21.4	15.5	349.0	1.4	1.7	0.7	192	181.7	18.4
D10-42	0.057	25	122	65.5	25.9	7.5	31.8	16.2	620.5	2.2	2.7	1.3	361	278.1	41.1
Rejuvenated stage															
2D-1	0.031	21	542	47.8	17.5	6.9	70.5	33.8	1029.0	4.3	5.4	1.5	291	321.0	30.8
2D-2	0.031	21	558	47.9	19.1	7.4	73	40.9	1057.4	4.6	5.5	1.7	295	335.6	31.9

Table A.2. (continuación)

Sample	Pb	La	Ce	Pr	Nd	Sm	Eu	Gd	Tb	Dy	Ho	Er	Tm	Yb	Lu
Det. limit	*0.1*	*0.1*	*0.1*	*0.02*	*0.3*	*0.05*	*0.02*	*0.05*	*0.01*	*0.05*	*0.02*	*0.03*	*0.01*	*0.05*	*0.01*
Shield stage															
D10-2	1.8	25.5	56.1	7.36	32.4	7.76	2.70	8.74	1.16	6.84	1.19	3.22	0.40	2.71	0.35
D10-5	0.5	17.1	38.5	5.15	24.3	5.46	1.83	5.97	0.80	4.45	0.79	1.95	0.27	1.61	0.23
D10-7	0.6	17.9	38.6	5.27	23.2	5.52	1.95	6.29	0.82	4.76	0.81	2.22	0.27	1.81	0.22
D10-10	1.9	45.3	63.1	11.64	49.9	10.95	3.70	13.06	1.65	9.51	1.69	4.50	0.59	3.75	0.50
D10-18	1.8	13.9	37.2	4.41	20.6	5.05	1.68	5.15	0.72	4.27	0.73	1.99	0.26	1.65	0.21
D10-42	1.5	29.3	61.9	8.65	39.8	9.28	3.19	10.05	1.34	8.09	1.37	3.72	0.46	2.98	0.43
Rejuvenated stage															
2D-1	11.7	50.1	103.2	12.16	50.3	9.34	3.00	8.76	1.24	6.66	1.08	3.09	0.41	2.30	0.36
2D-2	5.2	51.2	107.8	12.81	52.2	9.93	2.97	9.3	1.28	6.46	1.17	3.11	0.41	2.56	0.33